Engineering Development of Coal-Fired High Performance Power Systems Phase II and III

DE-AC22-95PC95144

Quarterly Progress Report

April 1 - June 30, 1996

Prepared for

Pittsburgh Energy Technology Center
Pittsburgh, Pennsylvania

United Technologies Research Center
411 Silver Lane, East Hartford, Connecticut 06108

MASTER

DISCLAIMER

Portions of this document may be illegible
in electronic image products.   Images are
produced from the best available original
document.

DOE/PC/95144 -- T1

CONTENTS

DISCLAIMER

CONTENTS (CONTINUED)

Executive Summery

This report presents work carried out under contract DE-AC22-95PC95144 "Engineering Development of Coal-Fired High Performance Systems Phase II and III." The goals of the program are to develop a coal-fired high performance power generation system (HIPPS) by the year 2000 that is capable of:

- >47% thermal efficiency (HHV)

- NO_x, SO_x, and particulates $\geq$ 10% NSPS

- coal providing $\geq$ 65% of heat input

- all solid wastes benign

- cost of electricity 90% of present plant

Work reported herein is from Task 1.3 HIPPS Commercial Plant Design, Task 2.2 HITAF Air Heater; Task 2.3 Ash Management; Task 2.4 Duct Heater Design; and Task 2.6 Operations and Controls.

The impact on cycle efficiency from the integration of various technology advances is presented. The criteria associated with a commercial HIPPS plant design as well as possible environmental control options are presented.

The design of the HITAF air heaters, both radiative and convective, is the most critical task in the program. In this report, a chronology of the different radiative air heater designs that have been considered is provided. The primary testing of the air heater design will be carried out in the UND/EERC pilot-scale furnace; progress to date on the design and construction of the furnace is a major part of this report. The results of laboratory and bench scale activities associated with defining slag properties are presented. Correct material selection is critical for the success of the concept; the materials, both ceramic and metallic, being considered for radiant air heater are presented.

Removal of slag forming particulates and proper handling of any resulting slag is another critical element of the concept. The ongoing work addressing slag viscosity, the design of a slag screen, and the design of the quench zone is presented.

The activities associated with the duct heater and system operations and controls are also presented.

Task 1.3 HIPPS Commercial Plant Design

Cycle Analysis

A series of advanced HIPPS power cycles were evaluated to develop estimates of the performance potential of each configuration type. The technology used varies from that available in today's state-of-the-art (SOA) machinery to that projected to be available in the 2010 time frame.

The cycles investigated are:

- Aeroderivative combined cycle with standard steam system
- Aeroderivative combined cycle with advanced steam system
- Advanced aeroderivative with advanced steam
- Aeroderivative HAT cycle
- Advanced aeroderivative HAT cycle
- Advanced aeroderivative HAT cycle with reheat
- Heavy frame with advanced steam

Aeroderivative Combined Cycle With Standard Steam System

The HIPPS with the aeroderivative combined cycle with standard steam system is shown in Exhibit 1.3-1. The gas turbine technology is representative of current SOA and the steam system
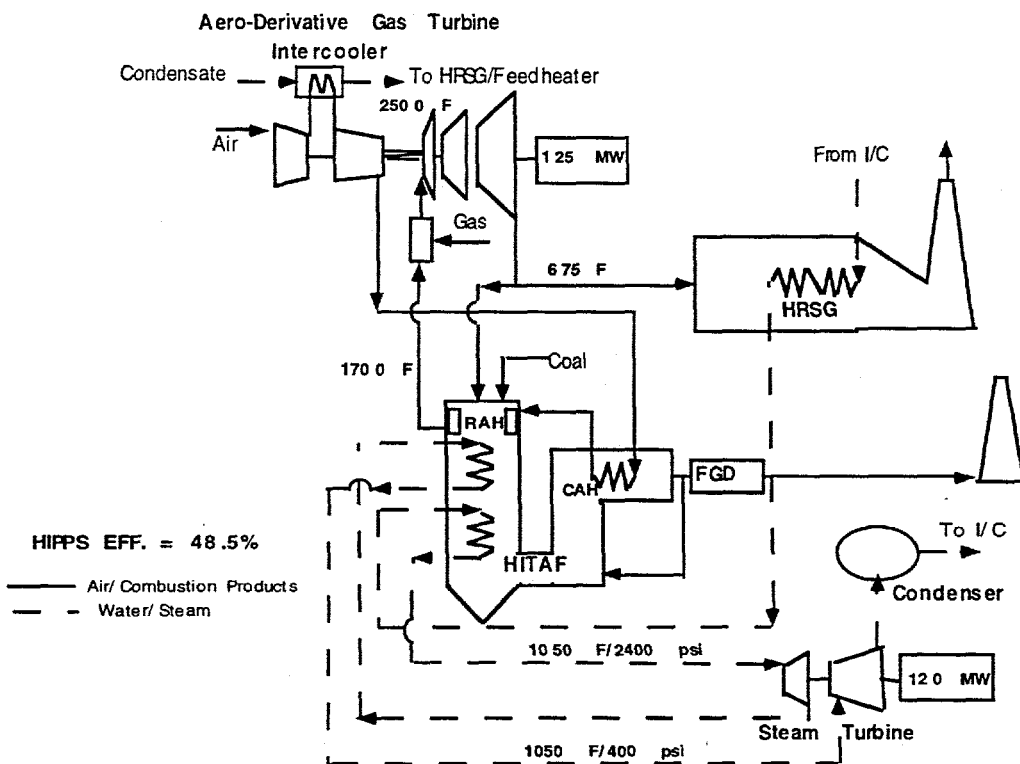
HIPPS WITH AERO-DERIVATIVE GAS TURBINE/STANDARD STEAM SYSTEM

Exhibit 1.3-1

SOA and the steam system is typical for coal-fired plants, but somewhat above the conditions usually encountered in combined cycles. The estimated performance, 48.5% (HHV) is approximately one percentage point higher than that estimated for the Phase I Commercial Plant Design using a heavy frame gas turbine.

Aeroderivative Combined Cycle With Advanced Steam System

The same gas turbine is used in a cycle (Exhibit 1.3-2) which has a ultra high pressure and temperature steam system (5500 psi/1300 F). This system is one being developed by Innovative Steam Technologies/Performance Steam International, one of the companies spun off from SOLAR Turbine, Inc. They have demonstrated a 1500 psi/1500 F turbine and have designed the 6000 psi/1300 F machine. The advanced steam turbine exhaust directly into the 2400 psi/1050 F /1050 F system used as the base combined cycle steam system. Use of the advanced steam conditions gains approximately 3 points over the HIPPS with the aeroderivative and standard steam cycle giving an estimated efficiency of 51.4%.
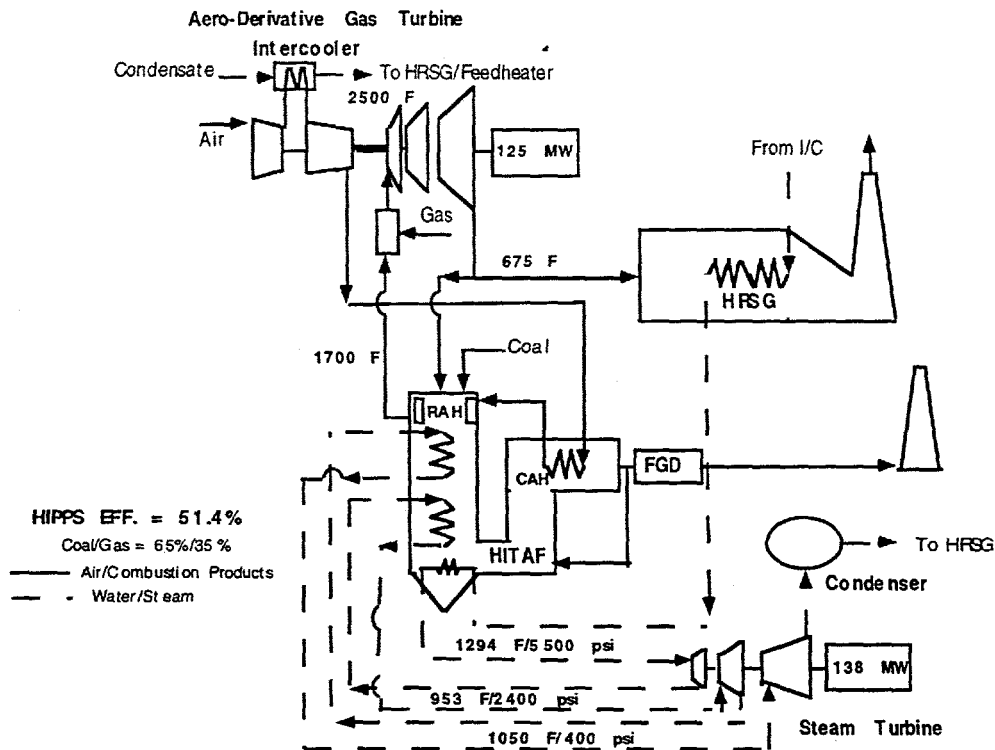
HIPPS WITH AERO-DERIVATIVE GAS TURBINE/ADVANCED STEAM SYSTEM

Exhibit 1.3-2

Advanced Aeroderivative With Advanced Steam

The system in Exhibit 1.3-2 has been changed by increasing the combustor exit temperature and adding a reheater before the power turbine (Exhibit 1.3-3). Projections for aeroderivative gas turbines indicate that turbine inlet temperatures will climb as improvements in cooling and materials occur. Currently, aircraft engines operate several hundred degrees above their industrial derivatives. Thus, the 2900 F temperature is a real possibility. The limiting factor may not be turbine capabilities but NO_x emissions.

The use of a reheater has been demonstrated on a heavy frame machine by ABB. The reheat combustor for aeroderivative use will require some development, but the temperature level is similar to the ABB machine. Materials and cooling of power turbine airfoils will also require additional development. The reheat cycle at 53%, would be about 1.5 points more efficient than the previous aeroderivative cycle, but the reheater requires additional gas fuel and the 65% coal/35% gas split is not maintained.
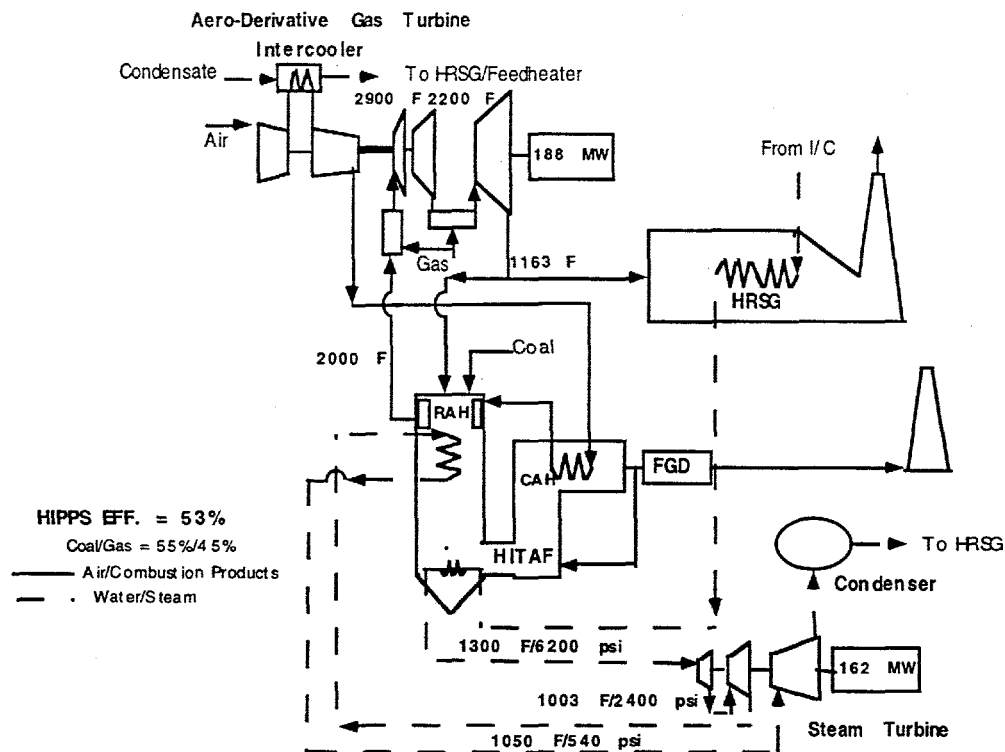
HIPPS WITH AERO-DERIVATIVE GAS TURBINE/ADVANCED STEAM SYSTEM

Exhibit 1.3-3

Aeroderivative HAT Cycle

The Humid Air Turbine (HAT) cycle offers the potential for higher efficiency and power for the same GT operating conditions. The system shown in Exhibit 1.3-4 produces 198 MW versus the 125 MW for the same GT in non-HAT application. The additional power is from the approximately 20% more mass flow of the humidified flow to the combustor. This flow requires more gas (and coal) to heat to desired outlet conditions. With the desired 65% coal/35% gas fuel split, the cycle efficiency would be about one point (at 49.3%) over the non-HAT version.

Aero-Derivative Gas Turbine

HIPPS/HAT EFF. = 49.3%

Coal/Gas = 65%/35%
——— Air/Saturated Air
— — Water

HIPPS WITH HAT GAS TURBINE
Exhibit 1.3-4
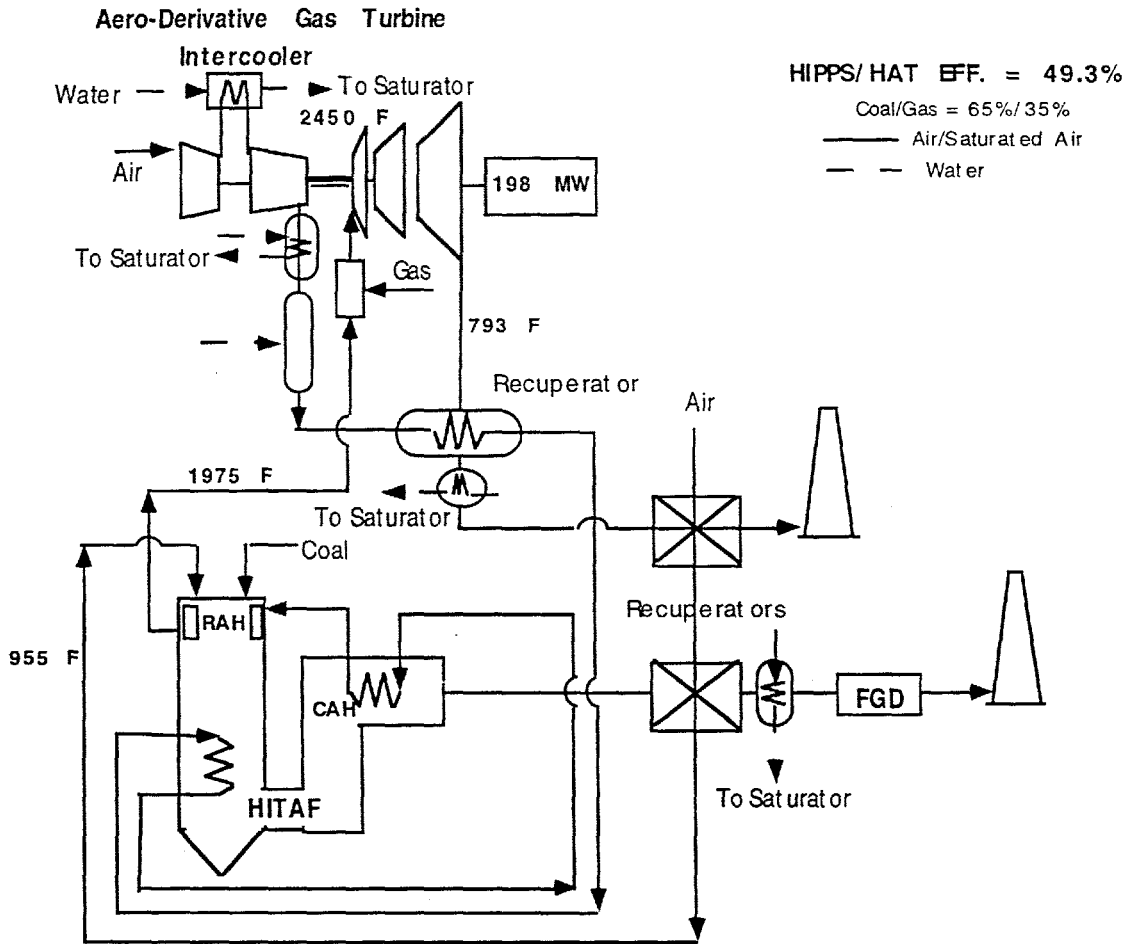
Advanced Aeroderivative HAT Cycle

The advanced turbine conditions of the Exhibit 1.3-3 configuration have been applied to the HAT cycle. An advanced HAT cycle based on a 2900 F version of the aeroderivative is shown in Exhibit 1.3-5. It is not known at this time how the presence of water vapor will affect NOx production in gas turbine combustors. Tests are planned as part of a forthcoming DoE program, which could provide answers to this question. The efficiency is estimated to be over 54% (54.3%) and the power is estimated to be 352 MW.
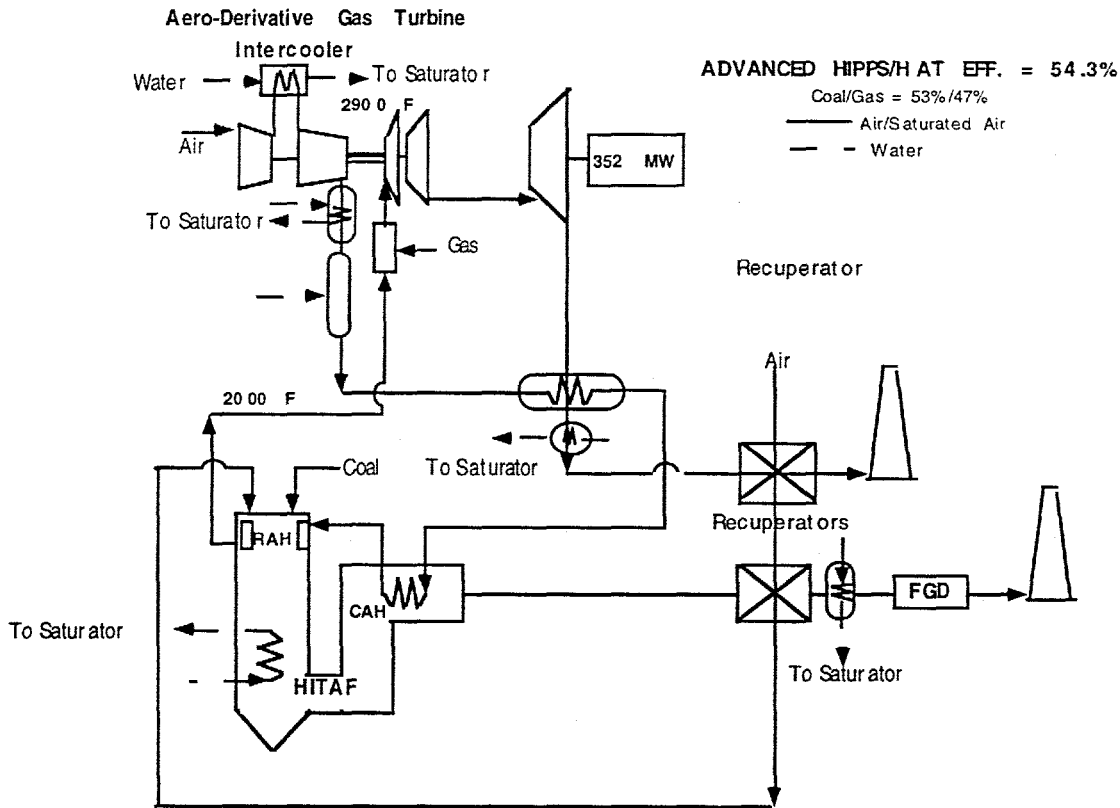
ADVANCED HIPPS WITH HAT GAS TURBINE
Exhibit 1.3-5

Advanced Aeroderivative HAT Cycle with Reheat

The advanced turbine conditions and the reheat combustor approach of Exhibit 1.3-3 has been applied to the HAT cycle (Exhibit 1.3-6). In order to keep the reheat temperature at desired levels, the combustor exit temperature has been reduced to 2780 F from the 2900 F value in the Exhibit 1.3-4 configuration. The turbine power output is increased to 395 MW. Additional coal (and gas) would be required for the reheater, but the fuel split (62% coal/38% gas) still is beyond the DoE guideline. The efficiency is estimated to be over 54%, highest of all the cycles considered.
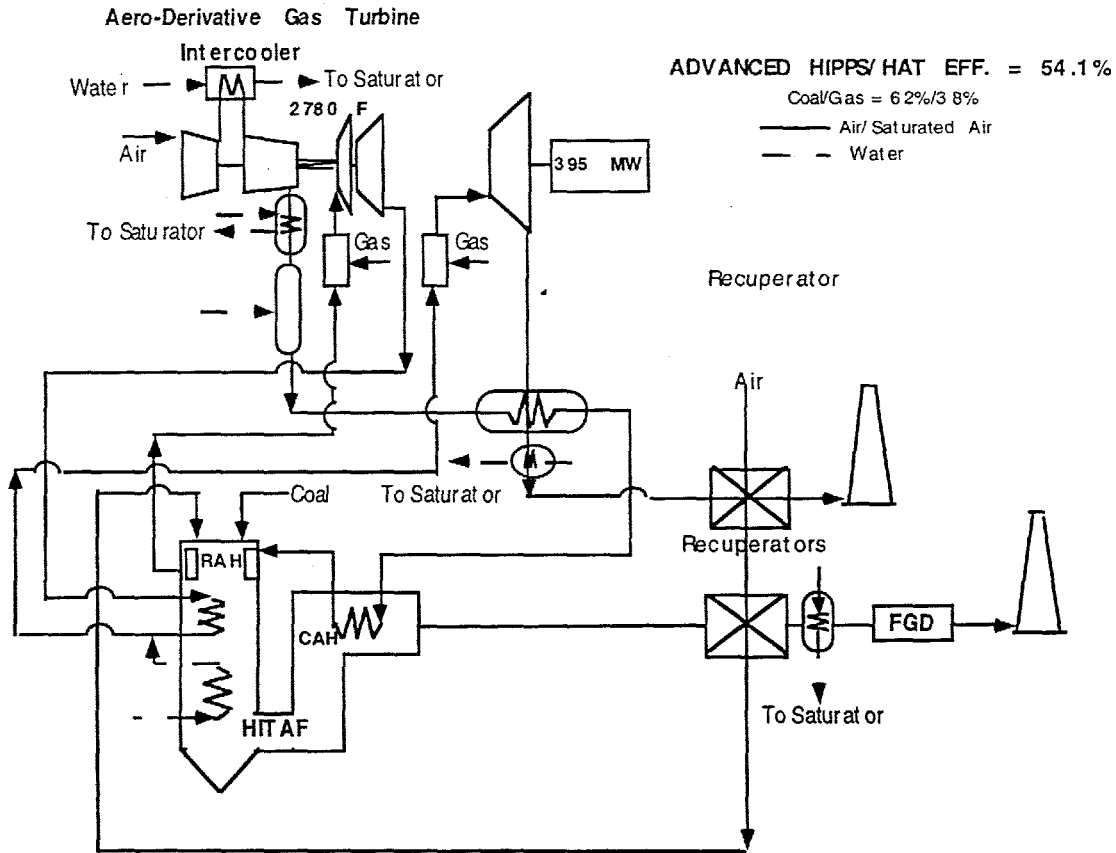
ADVANCED HIPPS WITH HAT GAS TURBINE

Exhibit 1.3-6

Heavy Frame with Advanced Steam

In order to evaluate the benefits of the advanced steam conditions of the Exhibit 1.3-2 configuration, the heavy frame machine used in the Phase I Commercial Plant Design was mated with the 5500 psi/1300 F steam system. this configuration is shown in Exhibit 1.3-7. The system has an estimated efficiency of 50.4%, a two point increase over the base system. The advanced steam appears to be well worth developing.
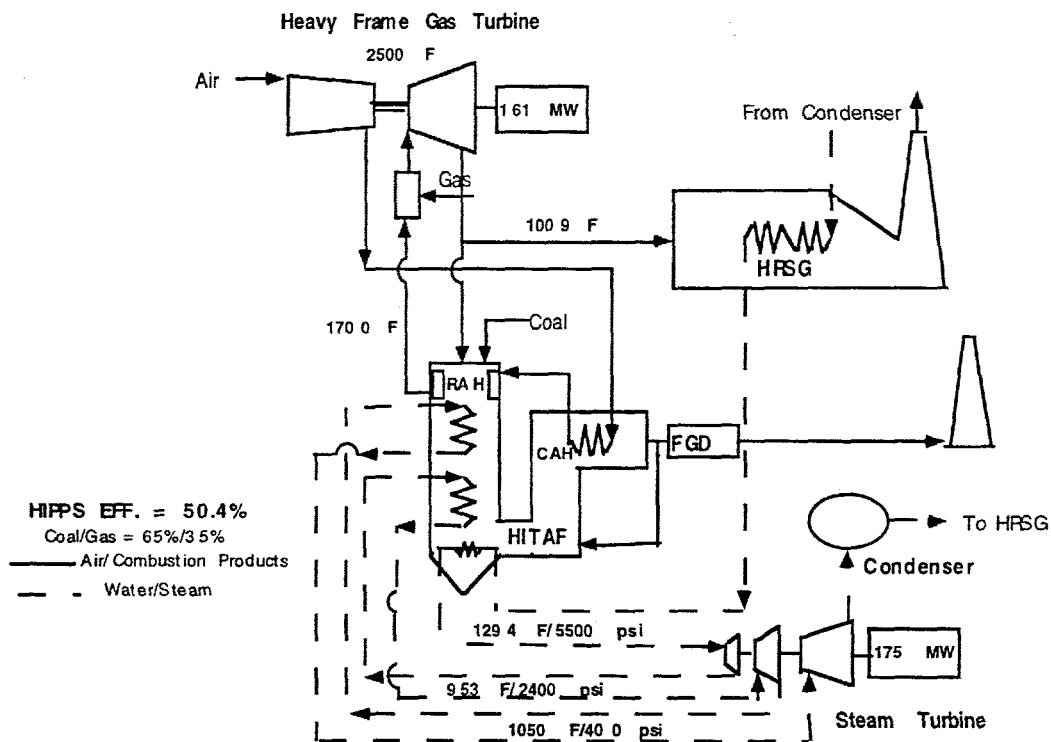
HIPPS WITH HEAVY FRAME GAS TURBINE/ ADVANCED STEAM SYSTEM

Exhibit 1.3-7

Concluding Remarks

The analyses presented here indicate the trends in cycle efficiency as various technology advances are integrated. It must be noted that the cycles presented are not necessarily the optimum for each type; however, they are close. There could be configuration changes due to operating requirements. For example, the GT exhaust may have its own HRSG with no bypass allowing use as combustion air. A more or less conventional air preheater would be used on the HITAF. Other changes allowing easier startup or faster load following may be required.

Even with all these caveats, it appears that a HIPPS with efficiencies (HHV) of over 53% and possibly near 55% could be proposed within the next decade. If the HIPPS plants were to have emissions measured at the stack, versus at the GT exhaust of the power turbine, it could be possible to circumvent the perceived requirement for a 9 ppm NOx machine. A SCR, or other NOx stack gas device could be used. This could allow the gas turbine to run at its highest potential, and probably still meet a 9 ppm level after the treatment device. This would reduce the emissions/MWh, which should be the ultimate goal.

The analyses of the advanced cycles will continue. Economic considerations will be introduced and the cost of electricity will become a figure of merit. The changes in the US utility industry as it moves towards deregulation may make some of these high performance cycles even more attractive, especially if they can be used in repowering of urban sites.

HIPPS Commercial Plant Design Criteria

Background

The High Performance Power Systems (HIPPS) electric power generation plant integrates a combustion gas turbine and heat recovery steam generator (HRSG) combined cycle arrangement with an advanced coal-fired boiler. The unique feature of the HIPPS plant is the partial heating of gas turbine (GT) compressor outlet air using energy released by firing coal in the high temperature advanced furnace (HITAF). The compressed air is additionally heated prior to entering the GT expander section by burning natural gas. Thermal energy in the gas turbine exhaust and in the HITAF flue gas are used in a steam cycle to maximize electric power production. The HIPPS plant arrangement is thus a combination of existing technologies (gas turbine, heat recovery boilers, conventional steam cycle) and new technologies (the HITAF design including the air heaters, and especially the heater located in the radiant section).

Exhibit 1.3-8 illustrates the HIPPS concept. The HITAF provides heat to the compressor outlet air using two air heaters, a convective air heater (CAH), and a radiant air heater (RAH). The HITAF is a slagging furnace which contains the radiant air heater, as well as waterwalls and steam drum for the high pressure (HP) steam system. Hot flue gas leaving the HITAF furnace passes over the CAH prior to entering heat recovery steam generator (HRSG) #2. Hot exhaust gas from the gas turbine is ducted to HRSG #1 in a typical combined cycle arrangement. The HITAF, gas turbine and HRSGs are configured to achieve the required high efficiency of the HIPPS plant.

HIPPS Powerplant
Exhibit 1.3-8

Design Scope and Assumptions

The conceptual commercial plant design scope is a non-site specific, greenfield power generation plant and includes all facilities required for power production. Consistent with the June, 1993 EPRI TAG[TM], the HIPPS plant boundaries for design and cost estimates include all the major operating systems such as the HITAF unit, heat recovery steam generators, gas turbine, environmental control equipment, auxiliary equipment and all support facilities needed to operate the plant (shops, offices, cafeteria, fuel handling and storage equipment, water intake structures, and waste treatment facilities). The plant includes the high voltage bushing of the generator step-up transformer, but not the switchyard and transmission lines. The switchyard and lines are generally influenced by transmission system specific conditions and in compliance with the EPRI TAG[TM] are not included with the cost or design.

In addition to the unique HITAF equipment, the commercial power plant design includes a single modern frame-type gas turbine and a Rankine cycle steam bottoming turbine. The nominal generating capacity of the HIPPS plant is 300 Mwe. The plant is planned for a baseloaded duty cycle with limited cycling capability. The present set of design criteria will be expanded as Phase II proceeds. Criteria and specifications for major equipment will be developed as part of the process design engineering for use in the major equipment list, and for requesting budget price data from suppliers.

In many areas, technical and economic criteria prepared for the study use the EPRI TAG[TM], Volume 1: Rev. 7; June, 1993 as a basis.

Site Location and Conditions

For design calculations, the plant location and site conditions are taken from the TAG, and are as follows:

Site related:

- Plant site   Central USA[1]
- Site elevation (above mean sea level)   600 feet
- Seismic zone   0 (UBC)[2]
- Water transportation   Lake Michigan
- Water makeup source[3]   Lake Michigan
- Electric power source for startup   Grid
- Fuel Storage Capacity   60 Days at 100%
- Unit train coal delivery with rotary dump cars
    1. EPRI identified region: E/W Central US (Kenosha, WI)
    2. Uniform Building Code.
    3. Representative analysis is shown in Exhibit 1.3-9

Meteorological:

- Average annual conditions
  - dry bulb temperature   60°F
  - wet bulb temperature   52°F
  - atmospheric pressure   14.4 psia
  - rainfall   31 inch/yr
- Other meteorological data
  - max. dry bulb temperature   95°F
  - max. wet bulb temperature   75°F
  - minimum temperature   20°F for performance
  - minimum temperature   -20°F for freeze protection

Exhibit 1.3-9
Representative Water Analysis

	mg/l	mg/l as CaCO3
Silica (SiO2)	6.8	--
Calcium (Ca)	76.01	89.0
Magnesium (Mg)	16.0	68.0
Sodium (Na)	20.0	44.0
Potassium (K)	2.9	3.7
Bicarbonate (HCO3)	246.0	202.0
Sulfate (SO4)	56.0	58.0
Chloride (Cl)	26.0	37.0
Nitrate (NO3)	6.9	5.6
Total dissolved solids	457.0	--
Total hardness	--	255.0
pH	8.0	
Temperature range (°F)	40 - 80	

Plant Performance Criteria

The following are the major criteria specified for the design and cost assessments.

- Service conditions: The plant is to be designed for baseload operation. Also, in recent years an important market aspect has surfaced in the power generation business. Load profiles are increasingly indicating a need for flexible plant operations, and new plant designs that account for daily output requirement swings. Thus, a minimum turndown of 50% and operational flexibility are very desirable features.

- Design life: The nominal design life is 30 years.

- Target efficiency: The net efficiency of the reference commercial plant is to be 47 percent or higher (maximum heat rate 7,260 Btu/kWh, HHV) at ISO conditions.

- Design basis fuel: The plant burns Illinois No. 6 bituminous coal as the primary fuel. Coal is burned to supply 65 percent or more of the total heat input to the HITAF system. Properties of the design coal are listed in Exhibit 1.3-10.

- Environmental criteria: In general, the Phase I study limited environmental impacts of the HIPPS plant to 25 percent of New Sources Performance Standards (NSPS). However, Phase II requires more restrictive limits for the commercial plant design.

- Environmental limits are:

	New Source Performance	Phase I	Phase II
Sulfur Oxides (lb/MMBtu)	0.40*	0.10	0.06
Nitrogen Oxides (lb/MMBtu)	0.50	0.125	0.06
Particulate (lb/MMBtu)	0.03	0.008	0.003
Solid Wastes	Benign	Benign	Benign

* *Based on 90% reduction of the total sulfur in the fuel with the design coal (5.98 pounds of SO_2 per MMBtu) and a 65/35 ratio of coal and natural gas.*

Liquid discharges are treated to meet NSPS requirements.

Solid wastes (ash and FGD sludges) are to be stabilized and shipped for off site disposal.

Exhibit 1.3-10
Design Coal Properties

(Illinois No. 6 Bituminous Coal from 1993 EPRI TAG)

Proximate analysis	Average
Higher heating value (Btu/lb)	10,982
Sulfur %wt	3.28
SO_2/MMBtu	5.98
Grindability index (Hardgrove)	51

	% wt
Moisture	12.25
Ash	10.97
Fixed carbon	41.48
Volatile matter	35.30
TOTAL	100.00

Ultimate analysis (%wt)	
Moisture	12.25
Carbon	61.00
Hydrogen	4.25
Nitrogen	1.25
Chlorine	0.07
Sulfur	3.28
Ash	10.97
Oxygen	6.93
TOTAL	100.00

Ash analysis (%wt)	
SiO_2	50.66
Al_2O_3	19.00
TiO_2	0.83
Fe_2O_3	20.30
CaO	2.24
MgO	0.89
Na_2O	0.67
K_2O	2.54
P_2O_3	0.17
SO_3	1.90
Undetermined	0.58
TOTAL	100.00

Ash fusion temperature (°F)	Reducing	Oxidizing
Initial deformation	1,950	2,250
Softening (H=Q)	2,030	2,300
Fluid	2,150	2,450

(Ash fusion data from 1989 TAG)

Natural gas will serve as auxiliary and warm-up fuel. Natural gas may provide up to 35 percent of the energy requirements at the HITAF system design point. Composition and properties of natural gas are listed in Exhibit 1.3-11.

Exhibit 1.3-11
Natural Gas Composition

Ultimate analysis (%wt)

C		73.25
H		24.26
N		1.87
O		0.62
	TOTAL	100.00

Composition (mole %)

CH_4		96.67
C_2H_6		1.80
C_3H_8		0.11
CO_2		0.32
H_2S		0.0004
N_2		balance
	TOTAL	100.00

Average molecular weight 16.55

Higher heating value
(dry gas at 60 °F, 30 inches Hg)

Btu/scf	1,013
Btu/lb	23,171

Code of Accounts

Exhibit 1.3-12 presents the code of accounts, or identification system employed with the HIPPS plant. The account numbers are used on the block flow diagram and cost estimate to ensure consistency and understanding of the plant's technical and cost estimating scope. The code is consistent with other parts of the DoE Combustion 2000 program.

Exhibit 1.3-12
HIPPS Commercial Plant Code of Accounts

(Exhibit 1.3-12 will be revised and expanded as Phase II work proceeds.)

CODE OF ACCOUNTS FOR COMBUSTION
HITAF POWER GENERATION COMMERCIAL PLANT DESIGN

Account	Code of Accounts	Account	Code of Accounts
POWER		**BALANCE OF**	
1.0	SOLIDS FEEDING AND REMOVAL	10.0	SOLID MATERIAL SHANDLING
1.1	• Coal Warming/Drying	10.1	• Coal Receiving, Storage and Handling
1.2	• Coal Preparation and Feeding	10.2	• Limestone Receiving, Storage and Handling
1.3	• Transport Air Heating	10.3	• Ash Handling and Disposal
1.4	• Limestone (FGD) Preparation and Feeding		
		11.0	WATER SYSTEMS
2.0	STEAM GENERATION ISLAND	11.1	• Cooling Water and Heat Rejection System
2.1	• High Temperature Furnace	11.2	• Raw Water Supply and Treatment
2.2	• Slag, Burnout Quench and Water Wall Systems	11.3	• Process and Plant Effluent Treatment
2.3	• Heat Recovery Steam Generator		
2.4	• Stack and Low Temperature Ducting	12.0	SUPPORT SYSTEMS
2.5	• Inducted Draft Fan	12.1	• Service and Instrument Air
		12.2	• Natural Gas Supply
3.0	HIGH TEMPERATURE HEAT EXCHANGERS	12.3	• Electrical Distribution
3.1	• Radiant Air Heater	12.4	• Instrumentation and Controls
3.2	• Convective Air Heater	12.5	• Interconnecting Piping
		12.6	• Fire Protection
4.0	HIGH TEMPERATURE PIPING AND DUCTING	12.7	• General Services
5.0	PROCESS SYSTEMS	13.0	CIVIL STRUCTURAL
5.1	• In-duct Gas Fired Burner	13.1	• Site Preparation and Facilities
		13.2	• Buildings and Structures
6.0	GAS TURBINE- GENERATOR		
7.0	STEAM TURBINE AND BOILER FEED WATER		
8.0	EMISSION CONTROL SYSTEMS		
8.1	• Particulate Control		
8.2	• Flue Gas Desulfurization SOx Control		
8.3	• Selective NonCatalytic Reduction (SNCR) NOx Control		
8.4	• Selective Catalytic Reduction (SCR) NOx Control		

Criteria and Specifications for Major Equipment

High Temperature Advanced Furnace

The HITAF is still being defined, and its major specifications determined during Phase II. In Phase I of the project, the HIPPS plant contained two identical HITAF units, each with a capacity of about 685 million Btu per hour of fuel input to the combustor.

For the near-term HITAF design, the temperature of the air being heated for the gas turbine is planned to be 1,700°F or less. Thus, the HITAF radiant heater can be designed using a special metal alloy that can be more easily obtained, fabricated and installed than could a ceramic exchanger. The lower temperature heat exchanger in the furnace convective zone is designed using more common nickel-alloy metals. Both exchangers are protected from corrosion and erosion in the fire side of the HITAF by suitable refractory materials.

It is also planned that NO_x control equipment such as non-selective catalytic reduction (SNCR), or selective catalytic reduction (SCR), or some combination will be designed as integral parts of the HITAF.

Gas Turbine-Generator

It is currently planned to use a single heavy frame industrial gas turbine (GT) in the HIPPS plant. Units are available with a wide range of capacities from several suppliers, and will be well suited to the conceptual plant capacity of 300 MW and operating schedule. As the current plan is for the HITAF to preheat the GT air to 1,700°F, an in-duct natural gas burner will boost the air temperature to the required GT inlet temperature, or about 2,450°F.

GT Exhaust (Clean) Heat Recover Steam Generator

The exhaust gases from the GT are clean of SO_2, particulate and other controlled emission elements, compared to the HITAF flue gas. Thus for several reasons, but mainly to avoid mixing the gases prior to the stack, separate HRSGs are planned. Steam conditions are 1,000°F and 2,400 psia with single reheat to 1,000°F and 480 psia.

HITAF Flue Gas (Dirty) Heat Recovery Steam Generator

The HITAF flue gas HRSGs --there are two identical HRSGs, one for each HITAF units-- have the same steam conditions as in the GT exhaust HRSG. Steam from all the HRSGs is sent to a single steam turbine. The steam generation system shares a single feedwater and condensate system.

Steam Turbine-Generator

Steam at 2,400 psia and 1,000°F, with reheat to 480 psia and 1,000°F is used in a multiple pressure turbine to generate electric power. For most scenarios examined for the conceptual commercial plant, the steam turbine and gas turbine power generation is split about equally or 150 MW each.

Flue Gas Desulfurization

The FGD system's criteria and equipment specifications will be driven by the project emission control requirements. A separate topical report was prepared to examine the FGD options available to the project. With such information as background, and other input form project team members a FGD system will be defined and selected early in Phase II.

Nitrogen Oxide Control

The topical report noted above also examined NO_x control options for the project team to select for use in the conceptual design.

Particulate Removal

Additionally, the topical report examined particulate control options which will be selected in Phase II for the design.

Other Code of Account Equipment and Systems

The remaining items on the code of accounts, and major equipment grouped as part of the code of account's items will be selected and specifications prepared early in Phase II work. This will occur soon after the basic power cycle, and major conditions i.e. temperature, pressure, flow rates are determined by the project team.

Recommendations for Future Cost and Economic Evaluations

Currently, the HIPPS project's statement of work requires the use of the June, 1993 EPRI TAG^{TM} as a basis for cost and economic evaluations. Some of the data and methodology in the TAG ^{TM} may no longer provide the best approach for assessing the HIPPS technology.

The TAG has the advantage of historical consistency. However, the HIPPS project's credibility can be enhanced by the use of more current data and methodology more closely reflecting the state of the industry. While the TAG^{TM} data for site conditions, fuel characteristics and some cost factors are still valid, estimates of power generation capital costs and especially fuel prices have changed significantly from the 93 TAG. EPRI TAG ^{TM} criteria such as a 60 day inactive coal storage and the EPRI system for adding contingencies to cost estimates should also be reviewed.

Other items to be discussed with the DoE to improve the project's performance may include:

- Other coals, such as bituminous and low rank coals, should be considered in addition to Illinois Basin coal for HIPPS plants.

- The base case concept for a commercial plant should include production of byproduct gypsum.

- The plant should utilize the coal ash product.

- The bituminous coals for HIPPS should be physically cleaned to minimize hazardous air pollutants. Cleaning may even be a beneficial action for some low rank coals.

- The plant should be a zero release water system design.

- On-line coal analysis should be used ahead of the pulverizer day bins to monitor and control coal quality.

- A supercritical steam cycle should be considered.

These are issues that will need to be approved by the US DoE before any changes are implemented. It is suggested that a discussion be initiated, and if DoE is open to new ideas, that a methodology and data be prepared for use in the HIPPS Combustion 2000 program.

As a preliminary effort in this area, the work described below was completed, and could be the basis for continuing cost and economic assessments in the Combustion 2000 program.

Economic Forecasts Basis

It is proposed that the DoE/EIA Publication 0383(96), *Annual Energy Outlook, 1996, with Projections to 2015*, be the source for coal and natural gas prices, and forecasts of escalation for labor, material and other cost inputs. As this is an annual publication, data can be updated to reflect the most recent estimates as the Combustion 2000 project proceeds.

Exhibit 1.3-13 shows the EIA prices for delivered pipeline natural gas (PNG), coal, and electricity. At the present time, we do not have access to the broad EIA data base, and are working with tables in the Annual Report. Thus, the coal price uses a recent price for Illinois Basin high sulfur coal similar to the project's design coal, and applies the escalation factors from EIA to give the price over time. As shown on the Exhibit, coal prices are nearly constant, and actually decline slightly in the 1994 to 2015 timeframe. The EIA estimates are calculated in 1994 dollars. For the project these can be escalated to 1996 price levels to serve as our basis.
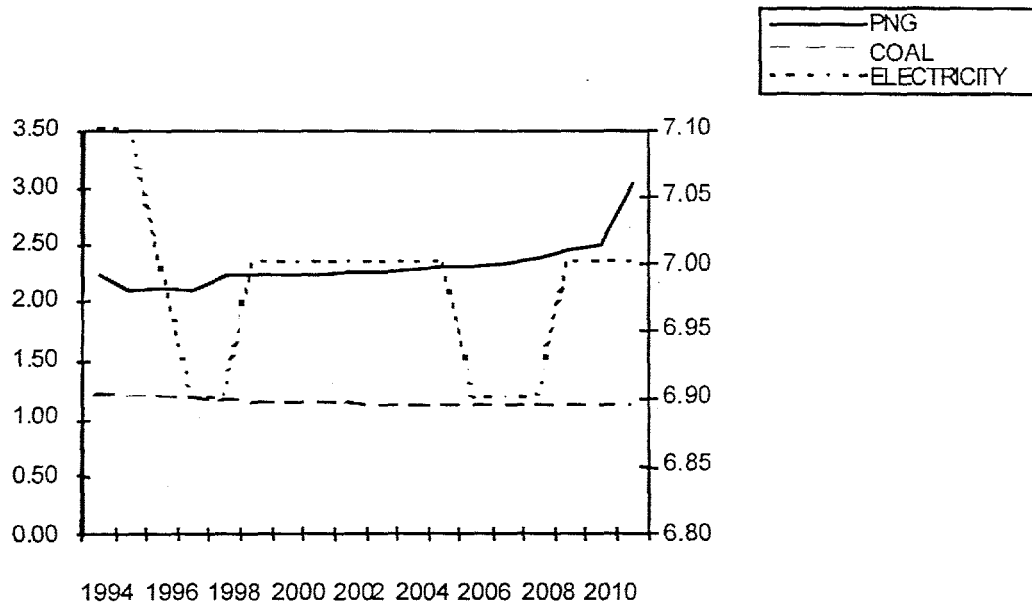
Delivered Fuel Prices --EIA Annual Report 1996
Exhibit 1.3.-13

Economic Assessment Methodology

To possibly better reflect changes in the power generation industry originating from various degrees of deregulation and competition, a cash flow type of analysis showing revenues minus expenses for an investment period i.e. much less time than the operating life of the plant has been examined. The cash flow methodology provides a simple, widely understood way to compare the HIPPS conceptual commercial plant with pulverized coal-fired power plants or other power generation options. Also, if other comparison standards are desired; rate of return, annualized cost, present worth, these can be calculated from the cash flow data.

Exhibit 1.3-14 shows the results of one cash flow comparison for a 300 MW gas turbine combined cycle, a pulverized coal-fired, and the HIPPS plant. This is only an example, because costs for the HIPPS plant will not be determined until later in Phase II. For the example, the following assumptions have been made.

Cash Flow Example Assumptions	Heat Rate	Capital Cost	Capacity	Cost of	Power Price
300 MW Power Plants	BTU/kWh	$/kW	Factor	Funds	$/kWh
Gas Turbine Combined Cycle with Selective Catalytic Reduction	7,150	600	80%	12%	0.07
Subcritical Pulverized Coal with Flue Gas Desulfurization and SCR	9,850	1,300	80%	12%	0.07
HIPPS Commercial Plant	7,200	1,105	80%	12%	0.07
Note: HIPPS capital cost is taken as 85% of the pulverized coal plant cost.					

Exhibit 1.3-14
Example of Reference Case Cash Flows for Three, 300 MW Power Plants

(Costs in 1,000s of Dollars)

	Year	Fuel $/MMBTU	$/kWh	Fuel Cost	O&M Cost	Total	Capital Expenses	Revenues	Net Income
				Gas Turbine Combined Cycle (GTCC) with SCR					
	1994	$2.24	0.0160	0	0	0			
	1995	$2.09	0.0149	0	0	0			
	1996	$2.14	0.0153	0	0	0			
	1997	$2.10	0.0150	0	0	0			
	1998	$2.23	0.0159	0	0	0			
1	1999	$2.24	0.0160	0	0	0	201,600	0	(201,600)
2	2000	$2.24	0.0160	0	0	0	21,600	0	(21,600)
3	2001	$2.26	0.0162	33,973	5,942	39,915	31,857	147,168	75,396
4	2002	$2.27	0.0162	34,123	5,942	40,065	31,857	147,168	75,246
5	2003	$2.27	0.0162	34,123	5,942	40,065	31,857	147,168	75,246
6	2004	$2.29	0.0164	34,424	5,942	40,366	31,857	147,168	74,945
7	2005	$2.31	0.0165	34,724	5,942	40,666	31,857	147,168	74,644
8	2006	$2.31	0.0165	34,724	5,942	40,666	31,857	147,168	74,644
9	2007	$2.35	0.0168	35,326	5,942	41,268	31,857	147,168	74,043
10	2008	$2.38	0.0170	35,777	5,942	41,719	31,857	147,168	73,592
11	2009	$2.45	0.0175	36,829	5,942	42,771	31,857	147,168	72,540
12	2010	$2.49	0.0178	37,430	5,942	43,372	31,857	147,168	71,939
	2015	$3.02							519,035

Exhibit 1.3-14
Example of Reference Case Cash Flows for Three, 300 MW Power Plants

(Costs in 1,000s of Dollars)

	Year	Fuel $/MMBTU	$/kWh	Fuel Cost	O&M Cost	Total	Capital Expenses	Revenues	Net Income
		Pulverized Coal-Fired Subcritical Boiler with FGD and SCR							
	1994	$1.20	0.0118	0	0	0			
	1995	$1.19	0.0117	0	0	0			
	1996	$1.17	0.0115	0	0	0			
	1997	$1.16	0.0114	0	0	0			
	1998	$1.14	0.0113	0	0	0			
1	1999	$1.13	0.0111	0	0	0	436,800		(436,800)
2	2000	$1.12	0.0110	0	0	0	46,800		(46,800)
3	2001	$1.12	0.0110	23,091	24,850	47,941	69,024	147,168	30,203
4	2002	$1.11	0.0110	23,068	24,850	47,918	69,024	147,168	30,226
5	2003	$1.11	0.0110	23,045	24,850	47,895	69,024	147,168	30,249
6	2004	$1.11	0.0110	23,022	24,850	47,872	69,024	147,168	30,272
7	2005	$1.11	0.0109	22,999	24,850	47,849	69,024	147,168	30,295
8	2006	$1.11	0.0109	22,976	24,850	47,826	69,024	147,168	30,318
9	2007	$1.11	0.0109	22,953	24,850	47,803	69,024	147,168	30,341
10	2008	$1.11	0.0109	22,930	24,850	47,780	69,024	147,168	30,364
11	2009	$1.11	0.0109	22,907	24,850	47,757	69,024	147,168	30,387
12	2010	$1.11	0.0109	22,884	24,850	47,734	69,024	147,168	30,410
	2015	$1.10							(180,534)

Exhibit 1.3-14
Example of Reference Case Cash Flows for Three, 300 MW Power Plants

(Costs in 1,000s of Dollars)

|	Year	Fuel $/MMBTU	$/kWh	Fuel Cost	O&M Cost	Total	Capital Expenses	Revenues	Net Income
				HIPPS	**Conceptual**	**Plant**	**Design**		
	1994	$1.56	0.0113	0	0	0			
	1995	$1.50	0.0108	0	0	0			
	1996	$1.51	0.0109	0	0	0			
	1997	$1.49	0.0107	0	0	0			
	1998	$1.52	0.0110	0	0	0			
1	1999	$1.52	0.0109	0	0	0	371,280	0	(371,280)
2	2000	$1.51	0.0109	0	0	0	39,780	0	(39,780)
3	2001	$1.52	0.0109	22,945	15,290	38,235	58,670	147,168	50,263
4	2002	$1.52	0.0109	22,987	15,290	38,277	58,670	147,168	50,221
5	2003	$1.52	0.0109	22,976	15,290	38,266	58,670	147,168	50,232
6	2004	$1.52	0.0110	23,071	15,290	38,361	58,670	147,168	50,137
7	2005	$1.53	0.0110	23,166	15,290	38,456	58,670	147,168	50,042
8	2006	$1.53	0.0110	23,155	15,290	38,445	58,670	147,168	50,053
9	2007	$1.54	0.0111	23,356	15,290	38,646	58,670	147,168	49,852
10	2008	$1.55	0.0112	23,504	15,290	38,794	58,670	147,168	49,704
11	2009	$1.58	0.0114	23,864	15,290	39,154	58,670	147,168	49,344
12	2010	$1.59	0.0114	24,065	15,290	39,355	58,670	147,168	49,143
	2015	$1.77	0.0128						87,932

On Exhibit 1.3-14 in the capital expenses column, a midpoint for capital and interest on capital to that point is shown in year 1, or 1999. (The Year 1999 is too early for the final design scenario, especially if this scenario is for a "Nth plant of its kind" cost estimate.) There is more interest during construction in year 2, and operations and revenues begin in year 3 and continue for the 10 year investment period selected for the example. Fuel prices are from the EIA annual energy report noted above. Revenues are the same for all the plants operating at 80% capacity and a nominal 300 MW size.

Even though Exhibit 1.3-14 is only a methodology example, the results are interesting. The GTCC show a large net income because of the forecast low cost of pipeline natural gas and minimum capital costs. The pulverized coal plant has a negative income in the time period examined. HIPPS has a positive income and with this set of assumptions is clearly favored over the pulverized coal plant. The Exhibit also confirms how a major future goal of the project must be to reduce capital costs where possible to be competitive.

Exhibit 1.3-15 uses the tabular data for net income in plots of the cumulative income cash flow for the three power plants.

The cross-overs from negative to positive income are also of interest.
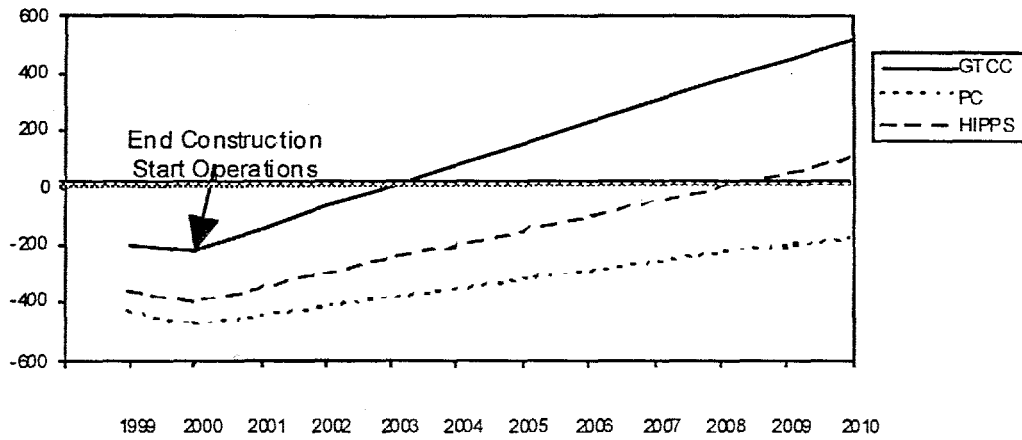
Example of Cumulative Net Incomé Cash Flows for Three Power Plants
Exhibit 1.3-15

(Millions of dollars)

Exhibit 1.3-16 summarizes six cases tested for sensitivity to the major economic variables, again to illustrate the methodology.

Exhibit 1.3-16
Example of Case Results for Net Income Calculations

	GTCC Plant	PC Plant	HIPPS Plant
Case A	$519,035	($180,534)	$87,932
Case B	$431,172	($180,534)	$56,964
Case C	$519,035	($180,534)	$159,820
Case D	$519,035	($180,534)	$264,007
Case E	$519,035	($180,534)	$335,896
Case F	$431,172	($180,534)	$327,048

LEGEND:

A   Base Case

B   PNG Price 25% above estimate

C   90 % coal used in HIPPS

D   HIPPS capital cost is 70% of PC

E   HIPPS capital cost is 70% of PC, and 90% coal is used

F   Case E plus PNG price rise of 25%

- Case A is uses the conditions noted for Exhibit 1.3-14 and is the reference case.
- Case B uses a natural gas price that is 25% higher than forecast by EIA.
- Case C uses 90% coal and 10% natural gas in the HIPPS furnace.
- Case D the HIPPS plant cost is taken as 70% of the pulverized coal plant.
- Case E combines Cases C and D by reducing capital cost and increasing coal use.
- Case F uses the Case E values for HIPPS capital cost and coal use, and adds 25% to the EIA gas prices.

The results confirm that reducing capital cost is very important, and significant improvements are possible too, by increasing the amount of coal burned in the HIPPS, if all other factors are kept constant.

HIPPS Environmental Control Options

Background

The HIPPS electric power generation plant integrates a combustion gas turbine/HRSG combined cycle arrangement with an advanced coal-fired boiler. The unique feature of the HIPPS plant is the partial heating of gas turbine (GT) compressor outlet air using energy released by firing coal in the high temperature advanced furnace (HITAF). The compressed air is additionally heated prior to entering the GT expander section by burning natural gas. Thermal energy in the gas turbine exhaust and in the HITAF flue gas are used in a steam cycle to maximize electric power production. The HIPPS plant arrangement is thus a combination of existing technologies (gas turbine, heat recovery boilers, conventional steam cycle) and new technologies (the HITAF design, including the air heaters, and especially the heater located in the radiant section).

Exhibit 1.3-8 illustrates the HIPPS concept. The HITAF provides heat to the compressor outlet air using two air heaters, a convective air heater (CAH), and a radiant air heater (RAH). The HITAF is a slagging furnace which contains the radiant air heater, as well as waterwalls and steam drum for the high pressure (HP) steam system. Hot flue gas leaving the HITAF furnace passes over the CAH prior to entering heat recovery steam generator (HRSG) #2. Hot exhaust gas from the gas turbine is ducted to HRSG #1 in a typical combined cycle arrangement. The HITAF, gas turbine and HRSGs are configured to achieve the required high efficiency of the HIPPS plant.

Exhibit 1.3-8 reflects the conceptual commercial plant design as it was configured at the end of the project's first phase. For Phase I, the environmental control requirements specified that NO_x, SO_x and particulate emissions were not to exceed 25% of the Federal New Source Performance Standards. For the second phase of the project the limits are about 1/10 of the NSPS.

	New Source Performance	Phase I	Phase II
Sulfur Oxides (lb/MMBtu)	0.40*	0.10	0.06
Nitrogen Oxides (lb/MMBtu)	0.50	0.125	0.06
Particulate (lb/MMBtu)	0.03	0.008	0.003
Solid Wastes	Benign	Benign	Benign

* *Based on 90% reduction of the total sulfur in the fuel with the design coal (5.98 pounds of SO_2 per MMBtu) and a 65/35 ratio of coal and natural gas.*

Thus, for Phase I, relatively well proven commercial control equipment could be used in the design. However, with the Phase II requirements, the installation of more advanced technologies may benefit the environmental control operation and the overall plant efficiency and economic performance.

Other major criteria of the commercial plant design are:

- Plant efficiency of 47% or more based on the fuel higher heating value (HHV).

- Cost of electricity at least 10% lower than for a modern pulverized coal plant with controls to meet NSPS.

Topical Report Objectives

The work performed and reported here will be used to screen and select, with others on the UTRC team, the environmental control technologies for the conceptual commercial HIPPS plant.

To summarize, the air emission limits for Phase II designs used to screen control technologies are:

- SO_x 0.06 lb/MMBtu measured as SO_2
- NO_x 0.06 lb/MMBtu measured as NO_2
- Particulate   0.003 lb/MMBtu

The limits are based on total energy input to the system, i.e. both the coal and natural gas fuels.

Sulfur Dioxide

The flue gas desulfurization (FGD) process will be designed for 105% of the calculated gas flow. For the design coal higher heating value, SO_2 capture from the flue gas needs to be 99% if the emissions requirement is 0.06 lb/MMBtu. This would be for an all coal plant, which is the ultimate plan for the HIPPS system. However, in the near term for HIPPS plants, as much as 35% of the total plant fuel can be natural gas burned to raise the GT inlet air temperature to GT inlet conditions. For the 65%/35% coal and gas scenario, a SO_2 capture of 98.5% is sufficient to meet the Phase II standard.

Nitrogen Oxide

In the Phase I commercial plant configuration, NO_2 is only formed in the coal combustion process, and not in the GT operation. Thus, post combustion controls will be needed only for the coal flue gas stream. To obtain the required NO_2 control, commercial and developing NO_2 capture processes are examined.

Particulate

With the control limit of 0.003 lb per MMBtu, or an order of magnitude increase of the current regulations, the particulate control system will require capture efficiencies of 99.9 to 99.99%. This is consistent with the project objective to minimize the release of potentially hazardous trace elements or heavy metals. A variety of systems are examined in the report.

Phase I Commercial Plant Design

The conceptual design created for Phase I used the following environmental control technologies.

Flue Gas Desulfurization

A wet limestone forced oxidation process with a limestone-water slurry and throw-away product system is used for the commercial plant design. The FGD is a generic version of several available systems. There are two identical HITAF units in the design. Each furnace has its own FGD.

Only the coal combustion flue gas is cleaned. Exhaust gas from the gas turbine heat recovery steam generator is sent to the stack where it mixes with the scrubbed flue gas and is released to the atmosphere. The estimated temperature of the mixed stack gas is 157 °F at the stack exit.

NO_x Control

The HITAF design includes low NO_x burners. For post combustion control, a selective non-catalytic reduction (SNCR) reactor is installed downstream of the radiant heating section, where the temperatures range from 1,600 to 1,900 °F, and a selective catalytic reduction (SCR) reactor is placed in a lower temperature zone of the HRSG. By using SNCR as the primary NO_x control, the SCR unit can be relatively small and less costly. The combined controls are designed to reduce the NO_x to 0.125 lb per million BTU of total energy input to the plant

The HITAF emission control combination of SNCR and SCR can limit NO_x to 0.06 lb/MMBtu. As part of Phase II, SNCR/SCR process suppliers, and alternative process developers will be contacted to update and collect new data so that NO_x control system(s) can be selected and recommended for Phase II design.

Particulate Control Process Description

The HITAF Phase I design has a baghouse located between the HRSG and the FGD system. To meet the strict limits for particulate in Phase II, the system's dust capture capabilities will have to be improved.

Phase II Environmental Control Process Screening

Processes are required to control SO_2, NO_x, and particulate. A summary of the information collected for the different control technologies is shown in Exhibit 1.3-17, and other details are discussed in the following sections.

Exhibit 1.3-17
Summary of Emissions Control Options
for the HITAF Commercial Plant

Emissions Control Options Examined	DEVELOPMENT STATUS	EMISSION CONTROL PERFORMANCE Pct Removed			PLANT SIZE	AUXILIARY POWER REQUIREMENT	CAPITAL COST (Adjusted to 1996 dollars)	OPERATING COST (Adjusted to 1996 dollars)
		SO2	NOX	PART	MW	Pct of Plant Capacity	$millions	$ Millions
Wet Limestone FGD	Commercial	98.5%				1.2%	34	6
Chiyoda CT-121 JBR System	Commercial outside of U.S.	98%+		99%	300	1.3%	159	8
Saarberg-Holter System	Commercial outside of U.S.	90%			300	1.1%	154	7
Pure Air Forced Oxidation	Commercial outside of U.S.	98%			300	1.7%	180	8
ABB Low Cost FGD (LS-2)	130 MW demo plant scale	95%			---	not available	Note 1	Note 1
Tung FGD Process	No recent progress in development	n.a.			---	not available	not available	not available
Union Carbide CANSOLV	pilot scale; CCT project was canceled for variety of reasons.	98%		75%	---	not available	Note 2	Note 2
Ammonia Scrubbing -GE Environmental Systems	Demo scale; economics dependent on byproduct sales	98%+			---	not available	Note 3	Note 3
Wet FGD with Metal Chelates -Dravo	pilot scale	99.5%	75%	99%	300	not available	23	10
NOXSO Process -NOXSO Corp./PETC	pilot scale	98%	85%		500	1.6%	127	18
SNOX Process -Haldor Topsoe	commercial in Europe; demo in U.S.	95%+	95%+	99.9%+	385	2.4%	124	5
Activated Coke Process	commercial in Japan for medium to low sulfur coal	98%+	80%+	0.998	300	1.1%	373	12
Parsons Process	pilot scale	98%+	96%		---	not available	recent costs not available	
SOXAL Process - AQUALYTICS	pilot scale. No longer being developed for U.S. utilities.	98%+	70%		300	3.1%	200	11
ESP followed by FGD System i.e. CT121	could be commercial	98%+		99.8%	---	not available	not available	not available
Hybrid SNCR/SCR -NALCO	could be commercial		90%+		---	not available	not available	not available
Selective NonCatalytic Reduction (SNCR)	Commercial		60%		500	not available	Note 4	Note 4
Selective Catalytic Reduction (SCR)	Commercial		90%		500	not available	Note 5	Note 5
Low Temperatue Baghouse	Commercial			99.9%	---	not available		

Notes

1. 25 to 30% less than wet limestone FGD at 500 MW scale, or $150 to $250 levelized cost per ton of SO2 removed. About $350/ton SO2 at 300 MW.

2. Capital cost is about the same as for wet limestone FGD. Operating cost is claimed to be 40% less than wet limestone FGD.

3. Capital cost is about 1.4 times wet limetone FGD. Overall levelized cost is claimed to be $160/ ton of SO2 removed.

4. 1995 cost of $15 per kW for retrofit capital and $1,100 (levelized cost) for operations per ton of NOX removed, or total levelized cost per ton of NOX removed of about $1,600.

5. 1995 retrofit capital cost of $60 per kW, operating cost (levelized) of about $300 per ton of NOX removed, or total levelized cost per ton of NOX removed of $900.

Sulfur Dioxide Control Processes

As one of the results for the Clean Air Act Phase I regulations, many of the wet FGD systems in the US are being designed with the following criteria.

- Limestone based units are designed for between 90 and 95% sulfur dioxide removal, with the potential to increase the removal rate by 3 to 5 points if an organic acid is added to the FGD system. There are technical and economic questions for utilities that are planning to use organic acids to increase SO_2 removal. There is a lack of experience with using the acids to increase removal rates to high values, and the long term economics are uncertain.

- Magnesium enhanced lime FGD systems makeup about 1/3 of the Phase I units, and are designed for 95 to 98% removal. The Mg enhanced lime system is considered the most efficient commercially available. SO_2 removal rates of 98% are easily obtained at low liquid to gas ratios. The cost for the sorbent has been a deterrent to wide use of the technology, but the supply base for the material may be broadening and that could reduce the cost.

- Most of the limestone units will be forced oxidation with a throw-away gypsum product.

- Many designs still include spare absorber capacity or multiple trains, but not to past design concept levels where nearly all the equipment was spared.

- Construction materials are alloy steels, as opposed to carbon steel, for the corrosive environment.

- Reheat is usually not included in the designs, and wet stack operations are favored.

As a brief summary, the designs are in-between those of the earlier US systems and the more advanced systems being used in Japan and Europe. The higher sulfur coals at US stations where FGDs are most likely to be built is one reason for the more conservative design basis.

The base case HITAF plant design uses a generic wet limestone FGD system for 98.5% SO_2 reduction. The conventional counter-current spray tower design uses high liquid to gas ratios (L/G=100 to 120 gpm/1000 acfm), and moderate superficial gas velocities (8 to 10 fps). Such FGD systems are offered by suppliers including General Electric Environmental Systems Inc., ABB Environmental Systems, Bischoff, Hitachi and others. To get 99% removal, modifications are made to the basic FGD system by some suppliers. Testing by PETC to demonstrate "High SO_2 Removal Efficiency" has shown this level of removal can be achieved. The large unknown is whether units can be operated at very high SO_2 removal rates for extensive periods without excursions to conditions where emission limits are exceeded, and if the high efficiencies are economical in a competitive power market.

The Mg enhanced lime FGD systems were not considered in the previous conceptual design because of their cost. The Mg enhanced systems should be reexamined for the conceptual design updates.

Second generation wet limestone FGD systems are possible alternatives to the base case and are discussed below. Some of the "second generation" technologies have existed, or even operated for 10-20 years. Most of the recent (10 years) experience with FGD design, construction and operations has been in Europe and Asia, especially Japan.

- Chiyoda CT-121 system

- Saarberg-Holter system

- Pure Air Advanced FGD system

- ABB's LS-2 FGD system

Chiyoda CT-121

The Chiyoda Thoroughbred 121 FGD process was developed by Chiyoda Corporation in 1975. The CT-121 system employs a unique absorber, referred to as a jet bubbling reactor (JBR). The JBR contains limestone slurry as a continuous phase. Flue gas is bubbled into the JBR through vertical sparger pipes and the SO_2 is absorbed in the slurry. The absorbed SO_2 is completely oxidized to sulfate by air injection at the bottom of the JBR. Calcium sulfate is precipitated as gypsum. The cleaned flue gas is released from the JBR through gas risers to the upper deck and through a mist eliminator to the stack.

Also inherent to the JBR operation, fly ash particulate removal is accomplished with efficiencies approaching 99%.

The CT-121 limestone slurry is divided into two zones. The jet bubbling zone and the reaction zone. This concept is an important design feature because the following four processes are occurring simultaneously within the JBR vessel.

- Absorption of SO_2

- Oxidation of sulfites to sulfates

- Neutralization of sulfuric acid by limestone

- Gypsum precipitation, followed by crystal growth to increase strength and facilitate dewatering

The absorption of SO_2 occurs in the jet bubbling slurry zone where gas bubbles are continually forming and collapsing. The bubbling zone is formed by the untreated flue gas entering the JBR at normal duct velocity, and being accelerated through the sparger pipes into the liquid slurry. SO_2 capture occurs at the gas/liquid interface. Sulfur removal efficiency is a function of the following.

- Height of the liquor above the bottom of the sparger pipes

- Operating pH

- Inlet SO_2 concentration.

The JBR is designed for low superficial gas velocities (5 to 6 fps) and has no liquor recirculation. However, the energy saved by avoiding liquid pumping is consumed by the gas-side pressure drop. Thus, the CT-121 system's energy consumption is about the same as for a conventional wet limestone system.

The CT-121 operates at a low pH (3.5 to 5) which provides:

- Complete oxidation of sulfite to sulfate

- Essentially 100 percent limestone utilization

- Minimum scaling and plugging

SO$_2$ removal efficiencies range from 90 to 99 percent in commercial units in Japan. The system is being demonstrated as part of the DoE Clean Coal Technology program at Georgia Power's Plant Yates (100 MW). A high sulfur coal is used (inlet SO$_2$ is from 1,950 to 2,550 ppm). Preliminary results indicate 93-98% SO$_2$ removal; fly ash removal is 99%; the unit availability has been 96+%.

Saarberg-Holter Umwelttechnik (SHU)

The SHU process is a wet limestone scrubbing process with formic acid enhancement. SHU has an absorber with both co-current and counter-current flow areas for SO$_2$ capture. The flue gas first enters the co-current section where it is contacted with liquor from multiple levels of spray nozzles. Scrubber liquor is collected in a sump. The flue gas continues to the counter-current flow section of the scrubber where additional SO$_2$ is captured. The second stage scrubbing is recommended for SO$_2$ removal requirements in excess of 90 percent.

Formic acid is added to the makeup slurry stream to enhance SO$_2$ removal with a pH range of 4.2 to 5.2. Formic acid buffering increases limestone solubility and SO$_2$ removal; it improves process responses to SO$_2$ concentration and operational load variations and reduces L/G requirements by about 15% for a given SO$_2$ removal. Lower power consumption is direct result of the lower L/G requirement.

Air is injected into the sump, producing a bisulfite oxidation of greater than 99%. Commercial grade gypsum can be formed by cake washing to control chloride and dewatering to 90+% solids. Dewatering also minimizes the formic acid losses from cake entrainment.

Pure Air Advanced FGD

The Pure Air Advanced FGD system is a wet limestone, co-current flow, in situ forced oxidation process. The system features a high velocity (15 to 20 fps), open grid-packing absorber for SO$_2$ capture. It uses an air rotary sparger in the sump for in situ oxidation to produce gypsum.

The co-current flow allows a higher superficial gas velocity compared to counter-current flow (15 to 20 fps versus. 8 to 10 fps). The absorption grids provide a high gas/liquid contact area and contribute to uniform distribution of the flue gas. This allows for an absorber with a smaller diameter and less height than counter-current systems. The scrubbing liquor recirculation rate is similar to other advanced wet limestone systems.

The Pure Air system is being demonstrated as part of the DoE Clean Coal Technology program at NIPSCO's Bailly station. The coal has up to 4.5 % sulfur. A single absorber module, nominally 600 MW, is installed. SO$_2$ removal is greater than 95%, and availability has also been 95+%.

ABB Environmental Systems LS-2 FGD System

The LS-2 FGD unit is based on traditional open spray tower technology with new developments by ABB. A demonstration of the system is being conducted at the Niles Station of Ohio Edison. The nominal rating is 130 MW. Startup was in August, 1995 and wallboard grade gypsum is produced and sold locally.

The LS-2 is an advanced, compact wet FGD which is claimed to have superior performance and lower costs than state of the art wet FGD systems. The LS-2 system is based on several unique design features:

- Dry limestone grinding
- High velocity spray zone
- High mass transfer header
- Compact reaction tank
- Integrated dewatering system
- Compact and integrated regenerative reheat system

While the LS-2 system estimates for SO_2 reduction are less than the required 98.5 to 99% specified in the Combustion 2000 criteria, there may be applications for repowering or retrofit cases with the HITAF concept.

Other Developing FGD Systems

Other FGD systems may become competitive in the next 5 to 10 years. Three such systems are briefly described below although they may not be available in time for use with the HITAF system.

Tung FGD Process. The Tung FGD process is a regenerable sulfur recovery process. SO_2 is scrubbed from the flue gas with a sodium sulfite solution in a packed tower operation, yielding a sodium bisulfite solution. The bisulfite solution is extracted with a organic solvent, thus regenerating the sodium sulfite. The spent organic solvent is the steam stripped in a stripper column, which produces a concentrated SO_2 gas stream. The organic solvent is recycled to the extraction system. The SO_2 can be converted to elemental sulfur or sulfuric acid byproducts.

The Tung FGD process utilizes an innovative liquid/liquid extraction system to regenerate a sodium based aqueous scrubbing liquor. Steam stripping of the solvent recovers SO_2 as a byproduct, and requires only a fraction of the energy that would be needed to steam strip SO_2 from an aqueous solution.

Discussions with the process developers indicate that little progress has been made toward commercialization. The Tung process can be screened out of the study at this point.

Union Carbide CANSOLV System. The CANSOLV system uses a thermally regenerable organic amine as the absorbent in a recovery type SO_2 scrubbing process. Counter-current, multiple stage scrubbing is used to take advantage of the absorbent's high reactivity and SO_2 capture capacity. An in-duct water prescrubber is used to remove particulate and acid gases. A packed tower amine scrubber is needed for high SO_2 removal. Up to 99% SO_2 removal is achievable in a very compact and energy efficient system. Induct amine scrubbing can be used for lower SO_2 removals. The SO_2 laden absorbent is heated to liberate the SO_2. The water saturated SO_2 is dried and liquefied for storage. Byproduct possibilities include the manufacture of sulfuric acid or elemental sulfur. Landfill wastes can be avoided.

The CANSOLV process was successfully tested at a pilot plan treating 6000 acfm of flue gas from boilers burning 7% sulfur petroleum coke. SO_2 removal of >95% was achieved at low L/G ratios and scrubber residence times of less than 1 second. A DoE Clean Coal demonstration was planned at the Warrick Power Plant operated by the Alcoa Generating Corporation. The unit was sized at 75 MW. Demonstration of the process did not proceed and is stalled for lack of investment funds.

The CANSOLV system can also be screened out of the emission control options for the HIPPS plant.

Ammonia Scrubbing -General Electric Environmental Systems. Ammonia as a scrubbing agent has been a known art since the 1960s. GE and the Dakota Gasification Company tested a 3 MW pilot plant in 1992-93 using ammonia and limestone as sorbents for the boiler flue gas. The test results included:

- SO_2 removal of more than 99%.
- Ammonia slip of 1-5 ppm.
- Ammonium sulfate byproduct 99+% pure.
- Limestone and ammonia were used with the same equipment and process.

The pilot plant test results have led to contracts for a first-of-a-kind commercial scrubbing system (300 MW steam equivalent) with operations planned for June, 1996.

GE estimates capital costs to be 40% more than for a wet limestone system, but with lower operating costs and byproduct sales, the levelized cost per ton of SO_2 removed is $160 compared to $270 for a limestone system. Two points in favor of the process are that costs are reduced as the flue gas sulfur content increases, and the byproduct price is closely tied to the natural gas market.

This process will continue to be observed for possible application in Phase II commercial plant designs.

Nitrogen Oxides Emissions Control

The Phase I HITAF design includes low NO_x burners in the coal combustor and both SNCR and SCR for post combustion NO_x reduction. These units should be able to meet the NO_x limit of .06 lb per MMBtu. Developing combined SO_2 and NO_x removal technologies are examined in a later section, and could compete with the conventional SNCR and SCR combination.

Hybrid SNCR/SCR - NALCO

There is in fact a similar process proposed and tested by NALCO FUEL TECH and Public Service Electric & Gas. The "Hybrid" term is used to differentiate between the process and an installation with SNCR and SCR installed in series and operated independently of each other. The hybrid process uses the ammonia slip from the SNCR as the sole NO_x reductant for the downstream SCR.

The process objective is to minimize costs at a required NO_x limit. Especially for retrofit cases, the SCR capital cost would be minimized, and the SNCR reagent cost would be minimized. This would give the system the lowest life cycle cost. Tests of a hybrid system sized for 320 MW were conducted at a Public Service Electric and Gas Station. Use of the ammonia slip to drive the SCR reaction worked. Overall NO_x reduction for the test was 90%.

Particulate Control

The HITAF design uses a baghouse located between the HRSG and the FGD system for particulate control. This scheme was adequate.for Phase I. However, there are alternatives to the baghouse and these are discussed below.

Combined SO_2 and Particulate Removal

This process uses a medium efficiency electrostatic precipitator (ESP) with 95-98% particulate removal, followed by an FGD system with an efficient particulate removing absorber (such as JBR of the CT-121 FGD system). Gypsum produced by this system is only suited for landfill. A JBR can remove 99% of the particulate, giving an overall removal efficiency of close to 100%. The cost of a 95-98% efficiency ESP should be less than a baghouse.

Hot Gas Cleanup

Hot gas cleanup systems are generally more expensive than cold cleanup processes. The hot systems may be justified if immediate downstream processing requires a clean hot gas. The Phase I HITAF design does not require hot gas cleaning, and the technology will only be reexamined if the broad HITAF concept changes to make hot gas cleaning more attractive.

Combined SO_2-NO_x-Particulate Processes

Several processes are being developed for combined SO_2 and NO_x emissions control. Some processes, by their nature also remove particulate from the flue gas.

Wet FGD with Metal Chelates -Dravo

The process is being developed by Dravo and several others in the US and aboard. An iron chelate additive, such as aminopolycarboxlic acid (EDTA or HMTA) is added to conventional wet thiosorbic lime scrubbing. The iron chelates collect and remove NO_x in the FGD spray tower as the ferrous ion reacts with NO in the flue gas. Maintaining the required chemical conditions, and purging the system of soluble sulfur and nitrogen compounds are two areas of continuing research.

A 1.5 MW pilot plant was operated in 1991. NO_x reduction was 60% and SO_2 reduction was basically 100%. For a conceptual commercial system, an ESP would likely be used ahead of the scrubber for particulate removal.

NO_xSO Process - NO_xSO Corp./PETC

The NOXSO process has been under development since 1979. A 5 MW proof-of-concept pilot plant test was recently completed. A commercial scale demonstration, under the DoE Clean Coal Technology Program, is under construction at Alcoa Generating Corporation's Warrick Power Plant near Newburgh, Indiana.

The NOXSO process is a dry, post combustion flue gas treatment technology which uses a regenerable sorbent, high surface area gamma alumina impregnated with an alkali material, to simultaneously adsorb both SO_2 and NO_x from the flue gas. The adsorption process is performed in a two stage fluidized bed. The sorbent is heated to 1,150 °F for regeneration in a moving bed regenerator. During the heating process, NO_x and loosely bound SO_2 are desorbed and transported away in the heating gas. The NO_x is recycled to the boiler. In the regenerator, sorbent is contacted with natural gas, which reduces sulfur compounds on the sorbent (mainly sodium sulfate) to primarily SO_2 and H_2S with some COS. The offgas from the regenerator is sent to a sulfur byproduct plant.

The process may be capable of 98% SO_2 removal, and 95% NO_x removal at economical operating conditions, but this has not been demonstrated: Results to date indicate a SO_2 removal of 95% and NO_x reduction of 80%. The capital requirement will be higher than for a simple wet limestone process. Credit for the simultaneous removal of NO_x and byproduct sales are possible economic benefits for the system.

The process may be especially attractive for retrofit cases because the reaction for SO_2 and NO_x are carried out at a relatively low temperature of about 250 °F.

SNOX Process - Haldor Topsoe

The SNOX process is a catalytic process that removes both SO_2 and NO_x, and produces sulfuric acid byproducts. Haldor Topsoe is the process developer and the technology is offered, under license by ABB Environmental Systems. Performance has been demonstrated at two commercial plants in Europe and a demonstration plant in the US SO_2 and NO_x reduction rates are above 95% and 90% respectively. As with other SCR systems, the costs are sensitive to catalyst cost, quantity and life. The assumed sulfuric acid byproduct sales price is another important cost variable.

Activated Coke Process - Mitsui Mining Company

The process is developed and tested for smaller scale operations by Mitsui and others in Japan and Europe. The process is a dry, regenerable operation using one or two stages of vertical cross-flow, moving bed absorber containing activated coke or char. Ammonia is injected for NO_x reduction. The process has been used with low sulfur (less than 1.3% S) fuels. For higher sulfur coals, the capital and operating costs are not as competitive.

Mitsui and Bergbau-Forschung GmbH (BF) claim to have developed a low cost char that will work economically with higher sulfur coals. In the Mitsui-BF process, SO_2 and NO_x removals are

98% or more, and 80% or more respectively. Thermal regeneration is used to reactivate the carbon material, and produce a concentrated SO_2 stream. Commercial processes (RESOX, Claus) can then be used to produce elemental sulfur.

Parsons Process

The process is based on simultaneous catalytic reduction of SO_2 and NO_x in a hydrogenation reaction with steam-methane reformer gas. Sulfur can be produced from the resulting H_2S. Pilot scale tests have been run with high sulfur coals at the St. Mary's Municipal Power Plant in Ohio. Test results show a SO_2 and NO_x reduction of 98%+ and 92-96%. A number of key process factors require better understanding and optimization. Parsons has been contacted for more information.

SOXAL Process - AQUALYTICS

The process is a regenerable sodium based scrubber combined with urea-methanol injection. Goals for the process are 90% SO_2 and NO_x removal. A pilot scale 3 MW test was completed in 1993 by Allied Signal. The process has been acquired by AQUALYTICS, a division of Graver Company, for SO_2 control possibilities. AQUALYTICS is not currently actively marketing the process.

For those combined removal processes that continue to develop, and have economic and performance promise to meet the HIPPS requirements, the project should continue to collect data and evaluate the processes application for the commercial plant design.

Recommendations

The following items are recommended as action items for completion in the early part of Phase II.

- The emission control technologies examined here should be reviewed. Any new processes should be added to the list of candidate technologies.

- From the review process, a short-list of control technologies that are thought best suited to the commercial plant design will be prepared.

- For the short-list of candidates, a request for technical performance data and budget-level costs will be prepared. The request will include requirements for the commercial plant design, the design coal and other specifics to assist technology developers to provide their data.

- The short-listed process developers will be contacted and the requests for data presented for their action.

- Finally, the request for and receipt of data will be documented for UTRC and the commercial plant design updates. Emission control technologies for SO_2, NO_x, and particulate, or combinations, will be selected by the team for use in the commercial plant design.

Appendix Task 1.3

List of Literature and Personal Contacts

Wet Limestone FGD (Generic)

1. Radian Corporation, "High SO_2 Removal Efficiency Testing", DE-AC22-92PC91338, prepared for Janice Murphy, US Department of Energy, Pittsburgh Energy Technology Center, Pittsburgh, PA, 10 March 1995

2. Proposal to Bechtel, Yosick, Paul J., ABB Environmental Systems, 8/21/95.

3. Design and Operational Results of the Advanced FGD System for a 1,000 MW Coal Fired Boiler (Paper), T. Katsube, Babcock-Hitachi, 1995 SO_2 Control Symposium, March 28 - 31, 1995, Miami

4. Design of 4 x 550 MW Wet FGD Systems for Taiwan Power Company's Taichung Units 5 - 8 (Paper), M. Polster, Babcock & Wilcox, 20 S. Van Buren Ave., Barberton, OH 44203, 1995 SO_2 Control Symposium, March 28 - 31, 1995, Miami, Phone: 216.753.4511 Fax: 216.860.1886

Commercial NO_x Removal Technology

1. Helping the Utility Compete and Comply: Lessons Learned to Informed Decision Making for NOx Emission Reductions, J.R. Cochran and M.G. Gregory, Black & Veatch; V. Rummenhohl, STEAG AG, Presented at Power-Gen Americas, Anaheim, California, 12/5-7/95.

Chiyoda Thoroughbred 121 (CT-121)

1. Operational Highlights of the Chiyoda CT-121 FGD Demonstration at Georgia Power Plant Yates (Paper) - D.B. Burford, Southern Company Services, Birmingham, Alabama, 1995 SO_2 Control Symposium, March 28 - 31, 1995, Miami; Phone: 205.870.6329 Fax: 205.877.7535

2. Economic Evaluation of FGD Systems, Vols. 1 & 2, EPRI GS-7193-L, Feb. 1991 & Jan 1992 (also used for data on several other technologies).

Saarberg-Holter System

1. Developer: Saarberg-Holter Umweltteechnik GmbH, Hafenstr. 6, Saarbrucken, Germany Erhard Gillessen and Paul Schmidt Phone: 011.49.201.896.8746

2. In USA: Saarberg-Holter, Houston; John Glamser, Phone: 713.297.8860; Fax: -8864

Forced Oxidation Limestone FGD

1. Developer: Mitsubishi Heavy Industries, Tokyo, Japan; Licensee: Pure Air, 7540 Windsor Dr., Allentown, PA 18195; Tom Sarkus, PETC, Phone: 412.892.5981

2. Owensboro Municipal Utilities Commercial Grade Gypsum Forced Oxidation Limestone FGD System project Upgrade (Paper) - J.T. Morris, Jr. & J.L. Murphy, Wheelabrator Air Pollution

Control, 441 Smithfield Street, Pittsburgh, PA 15222; SO_2 Control Symp., March 28 - 31, 1995, Miami   Phone: 412.562.7300 Fax: .7254

ABB Low Cost FGD (LS-2)

1. Next Generation Low Cost Wet FGD System (Paper)
   - J.S. Klingspor, ABB Environmental Systems
   - B.E. Bresowar, ABB Environmental Systems
   - D.E. Gray, Ohio Edison
   - POWER-GEN '95, December 5 - 7, 1995, Anaheim

Tung FGD Process

1. Dr. Shao E Tung (ex-MIT professor), 91 Blake Road, Brookline MA 02146; Private Communication.   Phone: 617.731.6367

2. Economic Comparisons of Emerging SO_2 Technologies (Paper) - Robert Martinelli, B & W, Barberton, OH; 1993 SO_2 Control Symposium, August 24 - 27, 1993, Boston

3. Phone: 216.753.4511

4. Tung FGD Plant Performance (Paper) - Peter Strangway, Niagara Mohawk Power Corp., Syracuse, NY; 1993 SO_2 Control Symposium, August 24 - 27, 1993, Boston. Also Private Communication.   Phone: 315.428.6532

Union Carbide CANSOLV Process

1. Demonstration of the Union Carbide CANSOLV System Process At The Alcoa Generating Corporation Warrick Power Plant, A.B. Barnett and L.E. Kahha, Union Carbide, US DoE Clean Coal Technology Conference, Cleveland, Sept. 22-24, 1992.

2. Leo Hakka, Private Communication, Phone: 514.493.2617; Fax: 514.645.5121

Combined SO_x NO_x Particulate Systems

1. Alternative Flue Gas Treatment Technologies for Integrated SO_2 and NO_x Control (Paper) - Joanna M. Markussen, PETC, DoE, C. David Livengood, ANL, 57th Annual Meeting, American Power Conference, April 18 - 20, 1995, Chicago.

2. Technical Evaluation of Simultaneous SO_2/NO_x Control Technologies, RP-3004-1,2, Prepared by Sargent & Lundy for EPRI, December 1991.

Wet FGD With Metal Chelates

1. Dravo Lime Company, Pittsburgh, PA; Shiaw Tseng Phone: 412.777.0713   Fax: 412.777.0727

NOXSO Process

1. NOXSO Corporation, Bethel Park, PA, Private Communication
   - John Haslbeck   Phone: 412.854.1200; Fax: 412.854.5729

SNOX Process - Haldor Topsoe

1. ABB Environmental Systems, Birmingham, Alabama. Also Private Communication, J.S. Klingsport, Knoxville, Phone: 423.694.5300 Fax: 423.694.5201

Activated Coke Process

1. Technical Evaluation of Simultaneous SO_2/NO_x Control Technologies, RP-3004-1,2, Prepared by Sargent & Lundy for EPRI, December 1991.

Parsons Process

1. Kwang, K. Vincent, Ralph M. Parsons, 100 W. Walnut St., Pasadena, CA Ph: 818.440.2000. (Called, but no response yet)

SOXAL Process

1. Ms. Caroline Byszewski, AQUALYTICS Division, Private Communication, March 1996.

Hot Gas Cleanup System

1. Overview of METC's Gas Stream Cleanup Program

   - R.K. Staubly; R.A. Dennis; D.C. Cicero, Morgantown Energy Tech.Center

   - Annual International Pittsburgh Coal Conference, 12 - 16 Sept. 1994

   - Ron K. Staubly: 304.285.4991; Larry Rath (Div. Dir.) x4094

2. Development of Novel Copper-Based Sorbents for Hot-Gas Cleanup: Technical Report, 1 March - 31 May, 1994.

   - J. Abbasian, Institute of Gas Technology, Chicago, IL

Task 2.2 HITAF Air Heaters

Design Chronology of the Radiant Air Heater

As described in the last quarterly report, many design options have been considered for the Radiant Air Heater (RAH). The "tubes-in-a-cage" design was selected as most promising. This design was found to have the following advantages:

- Since the tubes and refractory are not mechanically coupled, they need not be constrained with respect to each other. This results in

  ⇒ lower thermal stresses, and

  ⇒ easier assembly with less clamping required.

- The alloy tubes receive heat from all sides by radiation, reducing the thermal gradient and partially compensating for the heat transfer loss due to the tube spacing.

Work during this quarter involved more detailed analysis of the RAH "tubes-in-a-box" design (Exhibit 2.2.-1) with respect to:

1. heat transfer in the radiation cavity,
2. overall sizing of the RAH,
3. support strategies for the outer refractory wall including:

   a) support rails,

   b) anchors,

   c) brick mating surfaces,

1. thermal insulation, and
2. stresses in the tubes and outer refractory wall.

Cross-Section of RAH
Exhibit 2.2-1

Heat Transfer

The local heat transfer in this design is more complex than for the panel design in that the radiative transfer from the refractory to the alloy tubes is multi-dimensional. In order to size and optimize the RAH, the original RAH program was modified, and a new program was developed to solve the radiative heat transfer within the box.

Modification to RAH Sizing Program

Panel Design
Exhibit 2.2-2a

Tubes-In-A-Box Design
Exhibit 2.2-2b

The RAH program is used to size the RAH with respect to heat exchange. The program has been described in previous reports. It was originally developed for the panel design. In order to use the RAH program for the tubes-in-a-box design, the following modifications were made to the code:

- The alloy layer of the original program is redefined to be the inner refractory layer (B) in the new design. The gap resistance is now the gap between refractories A and B (Exhibit 2.2-2b).

- For the original design, a fin effectiveness calculation is used to reduce the dimension of the problem from 3 to 2. The same must be done for this design, but the radiation heat transfer within the box is too complex to be included in this code. A method has been devised to parameterize the amount of heat transfer per unit RAH area.

The parameterization is derived from data provided by the Radiation Program described in the next section.

The code can accommodate a double refractory layer with a gap between them. This construction has been suggested in order to make the design more fail safe, and better optimized to various refractory properties.

With a single layer refractory wall, the preferred material currently is

Jagal M: with $k \cong 7$ (W/m-k), and a thickness of $\cong 1.5$ inch.

With the double wall, the outer layer could be the best for corrosion resistance

Monofrax E: with $k \cong 3.3$ (W/m-k), and a thickness of $\cong 0.5$ inch.

and an inner layer for support of the highly conductive

Dimox: with $k \cong 30$ (W/m-k), and a thickness of $\cong 1.5$ inch.

The ratio of the resistance of the double layer wall to the single layer wall would be

$$\frac{1.5/30 + 0.5/3.3}{1.5/7} = 0.94$$

or approximately unity, provided that the gap resistance between the refractories is small.

Radiation Program

A radiation program has been created to determine and optimize the heat transfer from the outer refractory wall to the air in the tubes. The total heat transfer per unit RAH surface area is represented as a function of:

1. temperature of the hot surface facing the top of the tubes,

2. geometry parameters,

3. the air-side convection coefficients, and

4. the air temperature.

From this an effective convective coefficient is expressed as a function of the hot refractory surface temperature and the air temperature for a given geometry and material properties, and air-side convection coefficient.
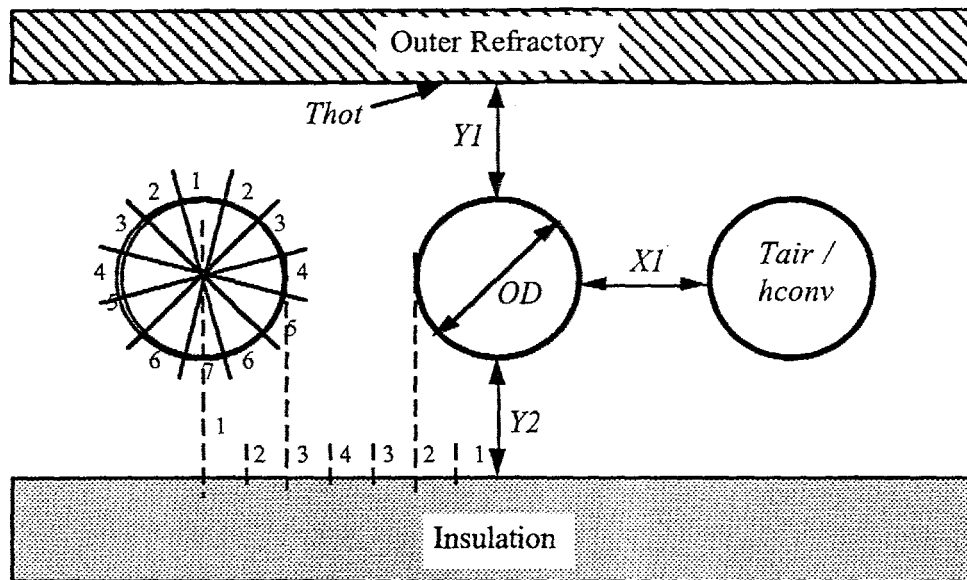
**Schematic of Radiation Transfer Sub-Problems
Exhibit 2.2-3**

The following parameters define the geometry of the radiation problem:

Y1:   space between tubes and hot refractory

Y2:   space between tubes and refractory insulation (re-radiating surface)

X1:   space between tubes

OD: the diameter of the tubes

The boundary conditions are specified as:

Thot: temperature of the hot surface facing the top of the tubes,

Tair: temperature of the air inside the tubes,

hc: convection coefficient from the inside of the tube to the air,

the net radiative heat flux to the insulation (re-radiating wall) is zero, and

the net radiative heat flux to the tube wall elements is equal to that which convects to the air.

the tube wall thickness and conductivity is entered as an added resistance to heat transfer.

The tube is broken into a total of 12 elements of equal circumference. The top element is #1, and the bottom element is #7. A symmetry plane exists vertically through each tube, and therefore only 7 independent elements need to be defined. Each tube element may have its own temperature and emittance.

The re-radiating plane is also broken into elements. There are 4 equally sized elements under each tube, and 3 equally sized elements in the space between the tubes. Again due to symmetry, only 4 independent elements need to be defined. Each refractory element may have its own temperature and emittance. The hot surface is treated as a single element.

Method of Solution

For each element, radiation shape factors are determined as functions of the geometry parameters, defined from the element's center. Since there are many interactions, an iterative method of solution was developed where the following sub problems are solved separately:

- The re-radiating plane temperature distribution is found assuming that the tube temperature distribution is known and fixed.

- A single tube temperature distribution is found assuming that the other tubes and the re-radiating plane is known and fixed.

Within each sub-problem, the temperature of each element is relaxed until the prescribed boundary heat flux is obtained. Iteration is required at each sub-problem level, and between the two sub-problems. The temperature distribution of the neighboring tubes is taken as the previous iteration solution.

Results

The results of the analysis are:

- Increasing the tube spacing (X1) increases the temperature (or radiosity) of the re-radiating surface, which increases the transfer to the "cold" side of the tubes. As the tube spacing increases, the amount of heat transfer per tube increases, but the number of tubes per RAH area decreases. Overall, it was found that the heat transfer per unit RAH decreases with increasing space between the tubes, but the tube temperature profile became more uniform, and therefore resulted in less thermal stresses and deflections.

- With increasing RAH size, and decreasing normal heat flux, the refractory can provide more insulation, and therefore can be thicker.

- Increasing the tube to wall spacings (Y1, Y2) increases the uniformity of the refractory temperature profile. It was found that a spacing of approximately 1 tube diameter is sufficient.

- The emittance of both the hot surface and the tubes determines (together with the geometry) the effective gap resistance. The emittance of the re-radiating surface (assuming negligible heat loss) does not. The lowest gap resistance is for black surfaces ($\varepsilon = 1$). This will allow for the thickest refractory for a given geometry.

- The emittance of the tube can be varied to even out its temperature distribution by providing a low emissivity coating on the top surface, and a high emissivity coating on the lower surface. The total heat transfer per unit tube can be maximized by then raising the hot refractory surface temperature. Although this leads to smallest RAH size and minimizes the tubes stresses and deflections, the increased gap resistance requires a thinner refractory.

Exhibit 2.2-4 shows the temperature profiles of the tube (black body) for various tube spacings.

Black body / Thot = 2050 / Tair = 1700 / hc = {

Legend: X1 = 1, X1 = 2, X1 = 3

X-axis: Circum. Position (deg from top)
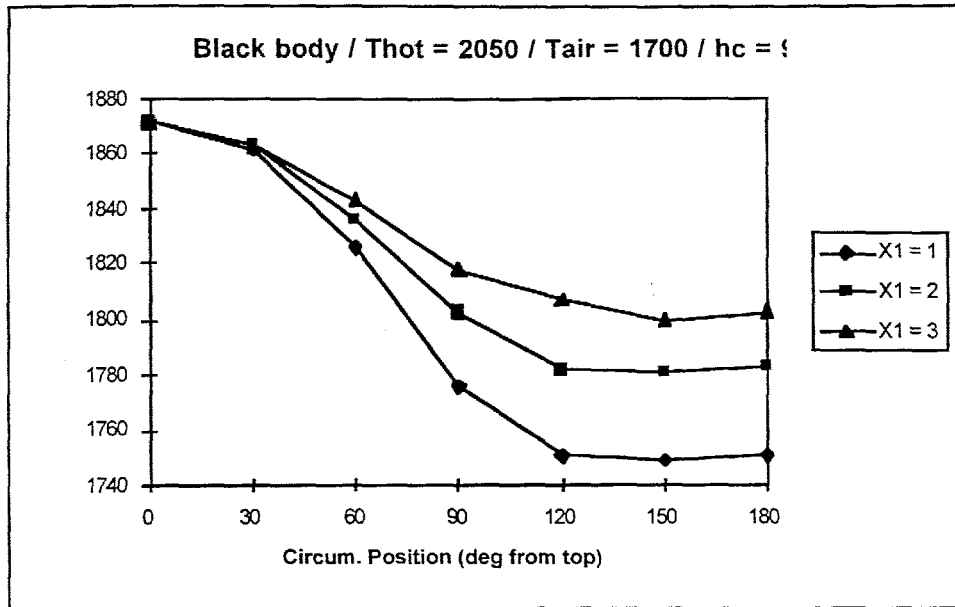
Temperature Distribution Around Single Alloy Tube
Exhibit 2.2-4

In the RAH design, various material constraints must be considered. Since the "tubes-in-a-box" design relieves the stress problem in the alloy tubes, the tube properties no-longer constrain the problem. The current design is being constrained by the minimum allowable refractory thickness. Because of this it is not expedient to vary the emissivity of the tubes since it leads to higher overall gap resistance.

Parameterization of the Radiation Program Results

The radiation program has been run with

- the emittance of the tubes uniform = 0.85
- the emittance of the hot refractory surface = 0.85, and
- the emittance of the re-radiating surface = 0.40.

for

- Tair = 1300, 1500, 1700 F
- Twall = Tair + (300 → 600), and
- hc = 70, 100, 130 (btu/hr-F-ft^2)

It was found that the effective heat transfer conductance between the hot refractory and the air (through the tubes) could be well represented as a function of

- geometry,
- air side convection coefficient, and
- a single temperature function => $T\_avg = 0.65\ T\_hot + 0.35\ T\_air$.

Exhibit 2.2-5 shows this relation.
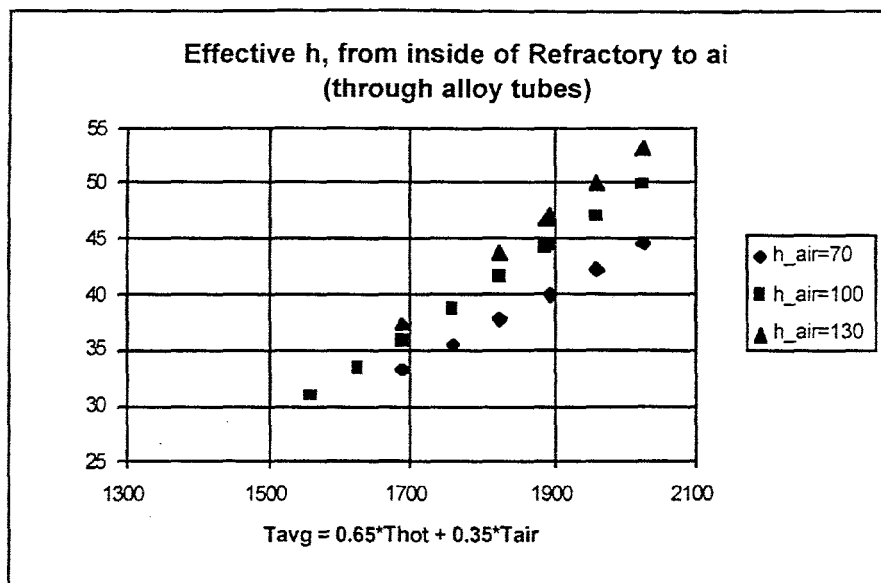
**Heat Transfer Conductance
Exhibit 2.2-5**

Combining the two codes for sizing and optimization studies

Since the radiation program results could be easily parameterized, the two codes were combined by:

1. converting the radiation code to a subroutine, and
2. inserting a call to this subroutine before each iteration, after the geometries have been set by the Optimizer, and the convection coefficient calculated.

Optimization studies have not yet been performed, but will be after more design details and material properties are finalized.

Preliminary Sizing

A preliminary sizing of the RAH was performed. The following geometry assumptions were used:

- thick of Jargal M ($k = 7$ W/m-K) was used for the refractory wall.
- Each refractory brick was 30 inches wide by 18 inches tall.
- Support rails (each 4 inches wide) occurred every 30 inches to support the bricks.
- The width of each box was therefore 26 inches.
- No credit was taken for extra heat transfer that might occur to the tubes at the end of each box (since the support rails will be hotter than the neighboring brick).
- Tube wall thickness = 1/8 inch.

The results of this sizing were:

- Overall size of (1/2) RAH = 60 ft tall, by 36 ft diameter. This is ~30% larger than the flat plate design studied earlier (but this design has not been fully optimized).

- The tube size is ~2 inch ID, OD = 2.25.

- With 6 tubes in a box, tube spacing = 26 / 6 = 4.33 inch, this allows for ~2 inches between tubes (which is sufficient).

Other RAH Calculations

Insulation thickness, and supports

Exhibit 2.2-1 shows a schematic of the RAH cross-section. The radiation box must be insulated from the steel support structure, and the steel support structure must be insulated from the outside world. The refractory support rails are dense, and have a relatively high thermal conductivity, and therefore must be thermally isolated from the steel support (by hollow metal-alloy spacers). The total heat transfer, and required insulation values were calculated by assuming:

T   radiation box = 2000 F

T   steel support structure = 700 F

T   outside surface = 175 F (OK to touch), and

T   outside air = 75 F.

The outside convection coefficient was calculated to be 1.2 btu/hr-ft^2-F.

The heat flux per unit area is then 120 btu/hr-ft^2 (less than 1% of the total heat transfer through the hot refractory).

The required resistance value for the refractory insulation

= (2000 - 700) / 120 = 10.8 (hr-ft^2-F/btu).

Low density refractory can have conductivity values of between 0.1 and 0.2 W/m-K. Assuming 0.15 W/m-K (or 0.086 btu/hr-F-ft), the required thickness is 10.8 * 0.086 = .93 ft or 11 inches.

The Wedge-Shaped Brick:

To align the bricks with the support rails, and to minimize the number of support rails, it is necessary to stack the bricks so that they are aligned directly on top of the brick below, with no horizontal overlap. This situation was cause for concern, since a failed brick would result in a collapse of an entire vertical section. Various schemes for staggering were investigated, but were ultimately rejected. The primary concern was that due to the large amount of thermal bending expected for each brick, it would not be possible to maintain a seal at each vertical brick interface (at each side) where there was no support rail.

An alternate idea for preventing catastrophic failure was proposed: supporting each brick individually by shelves on the support rail This idea was pursued with the following criteria:

- The effective thermal conductance of the design must be maintained.

- The horizontal brick interfaces (top and bottom) must create a slag seal.

Two designs have emerged.

1. Winged: The active part of the brick is unchanged. A wing is added to each side which mates with the shelves cut into the support rails. The design is a manufacturing concern since a large amount of material may need to be "hogged out."

2. Wedge: The entire brick is wedge shaped (nominal 1 to 2 inches thickness variation). The thick part of the wedge is down, and rests on the support shelf. This design creates large thermal variations over the height of each brick, the implications of which need to be investigated.

Finite-Element is being used to study the heat transfer and thermal stresses of the bricks. A three-dimensional model is currently being constructed. Issues of concern are:

1. How much heat transfer can be counted on from each end of the box, through the support rails.

2. How do edge variations (at the support rails, and at each horizontal brick interface) affect the thermal stresses.

3. How does the wedge shape affect the temperature profiles and stresses.

The thermal boundary conditions on each side of the brick were developed as:

Hot side: T coal gas = 2800 F, h coal gas = radiative function of temperatures.

Cold side: T air = 1300 to 1700 F, h effective = function of temperatures which is determined from the RAH computer programs described in the previous sections.

Pilot-Scale Testing

This activity consists of three subtasks involving the design and procurement, construction and shakedown, and operation, respectively, of the pilot-scale high-temperature slagging furnace system along with the analytical support required to evaluate performance thoroughly. A more detailed discussion of each subtask is presented in the following paragraphs.

Design/procurement and construction/shakedown activities began in 1995. These activities have been and will continue to be performed in accordance with appropriate Occupational Safety and Health Administration (OSHA) standards and codes concerning pressure piping, structural steel, and electrical standards.

As of December 31, 1995, structural steel design was well under way, and procurement and fabrication activities had begun. A draft preliminary system design was prepared and reviewed in early January 1996. As a result of that review process, the final design of the fuel feed system, including the primary and auxiliary burners, the slagging furnace, four tube-and-shell heat exchangers, and the pulse-jet baghouse was started. System components requiring further conceptual development include the slag screen, the dilution/quench zone, and the convective air heater (CAH) section.

The final preliminary design package for the overall system will include a process flow diagram, process and instrument diagrams (P&IDs), a list of instrumentation, and a test unit layout (elevation and plan views). Once the overall preliminary system design is approved, overall final system design will be completed.

The final system design will include detailed component designs for the pilot-scale high-temperature slagging furnace system (including support systems), specifications for purchased components, instruments, piping and electrical specifications, basic engineering design data, utility and raw material requirements, and lists of fabrication materials and equipment.

Primary slagging furnace system components include

1. combustion air system (Area 100),
2. fuel feed system (Area 200),
3. slagging furnace (Area 300),
4. slag screen–quench zone–convective pass (Area 400),
5. flue gas system–baghouse (Area 500),
6. cooling air system (Areas 600 and 700),
7. system instrumentation, and
8. data acquisition system.

The pilot-scale high-temperature slagging furnace will be a downfired, vertically oriented unit with a nominal firing rate of 2.5 million Btu/hr using pulverized coal. Critical design features include firing rate, temperature control, furnace access for the radiant air heater (RAH) panels (four 1-ft^2 panels and one panel approximately 6 ft tall by 1 ft wide), the slag tap and quench, system access for slag screen installation, the flue gas dilution/quench zone, system access for the CAH panel, sootblowing capabilities, ash removal, and optical access.

Design and procurement, began in 1995 and will be completed in 1996. Construction and shakedown, also began in December 1995 and will continue through mid-1997. Operation of the pilot-scale slagging furnace system, in support of the HITAF development effort, will begin following completion of shakedown activities in 1997 and continue through June 1999.

During the past quarter, design activities were completed for the baghouse, four tube-and-shell heat exchangers, primary and auxiliary burners, and the slagging furnace and slag pot shells. Procurement and fabrication activities have been initiated for these system components. The remainder of this section will discuss the design, procurement, fabrication, and installation activities completed in the past quarter concerning the pilot-scale slagging furnace system.

Structural Steel Design, Procurement, Fabrication, and Erection

Structural steel design, drafting, and procurement activities were essentially completed in April; fabrication and erection were completed in May; and priming and painting continued through June. Remaining structural steel activities will address supports specific to the installation of individual process components (slagging furnace, refractory-lined duct sections, heat exchangers, baghouse, and system fans). These supports will be factored into the final design of the individual components. Further priming and painting will be completed as individual system components are installed and area touch-up is required. Photographs documenting the status of the structural steel as of June 30, 1996, are presented in Exhibit 2.2-6.

Preliminary Design of the Pilot-Scale Slagging Furnace System

The primary purpose of the pilot-scale slagging furnace is to evaluate heat transfer and material and slag/ash issues related to the performance of the RAH, slag screen, and CAH components.

In a review the conceptual design for the pilot-scale slagging furnace system held in January 1996, it was determined that further work on the conceptual design of the slag screen, dilution/quench zone, and CAH sections was necessary.

Based on recommendations resulting from modeling of the dilution/quench zone and slag screen, respectively, a modified process illustration (Exhibit 2.2-7) of the overall slagging furnace system was prepared for review. The modified layout orients the circular dilution/quench zone vertically, maintains a 1-ft diameter in the area of the flue gas recirculation nozzles, and then expands the duct diameter to 2 ft to provide adequate residence time within duct length constraints. The duct section containing the flue gas recirculation nozzles will be a spool piece in order to accommodate potential changes to the size, number, and orientation of the flue gas recirculation nozzles. Changes to the slag screen were minimal and primarily involved changing the geometric layout of the tubes to reduce pressure drop. Following a review of the design, the final design and construction of the slag screen and dilution/quench zone sections of the system was initiated.

Photograph Illustrating the Progress of the Structural Steel
Exhibit 2.2-6
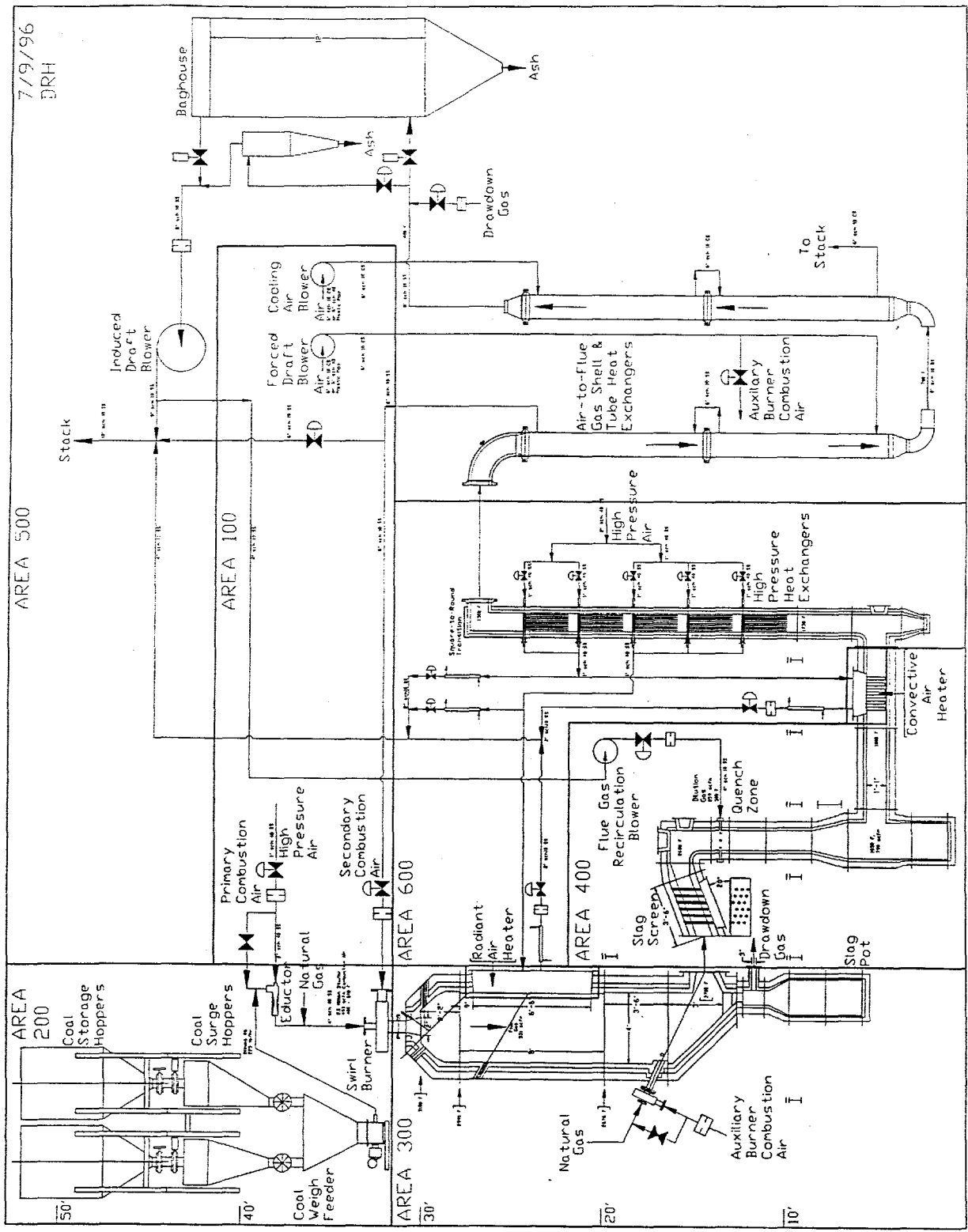
Combustion 2000 Slagging Furnace and Support Systems
Exhibit 2.2-7

A draft set of P&IDs has been prepared and reviewed. A detailed list of system instrumentation and data acquisition system components has been completed, along with an initial cost estimate. This list was compared with system P&IDs in early June. Minor changes to the P&IDs and instrument list are being made as a result. A draft set of plan and elevation view drawings has also been prepared.

Work was initiated in June concerning the development of the final fan specifications. The pilot-scale slagging furnace system will require four fans: a combustion air-forced draft fan, a cooling air-forced draft fan, an induced-draft fan, and a flue gas recirculation fan. Vendor recommendations are currently being assembled. At this time, it appears that all four fans will be centrifugal-type fans. Details concerning motor size and the potential use of speed controllers are currently under review. The remainder of this section presents the current design assumptions and the status of the preliminary system design and final component designs.

Pilot-Scale Slagging Furnace

The pilot-scale slagging furnace design is intended to be as fuel-flexible as possible, with maximum furnace exit temperatures of 2700E to 2900EF in order to maintain desired slag flow. It will have a nominal firing rate of 2.5 million Btu/hr and a range of 2.0 to 3.0 million Btu/hr using a single burner. The design is based on a bituminous coal (Illinois No. 6, 11,100 Btu/lb) and a nominal furnace residence time of 3.5 seconds. Resulting flue gas flow rates will range from roughly 425 to 640 scfm with a nominal value of 530 scfm based on 20% excess air. Firing a subbituminous coal or lignite will increase the flue gas volume, decreasing residence time to roughly 3 seconds. However, the high volatility of the low-rank fuels will result in a high combustion efficiency (>99%). It is planned to orient the furnace vertically (downfired) and has based the burner design on a swirl burner currently used on two pilot-scale pulverized-coal (pc)-fired units that are fired at 600,000 Btu/hr. Slagging furnace dimensions will be 48-in. inside diameter (ID) by roughly 18 ft in length. Exhibit 2.2-8 illustrates the furnace, slag tap/pot, slag screen, dilution quench zone, CAH section, and cooling air preheaters.

The vertically oriented furnace shell has been designed to include four distinct furnace sections that, when bolted together, make up the pilot-scale slagging furnace. The top section of the furnace will support the primary burner connection. The RAH panels will be located in the upper middle furnace section. The lower middle furnace section will support the auxiliary gas burner; the bottom section of the furnace includes the furnace exit to the slag screen as well as the slag tap opening.

Construction materials for the furnace shell will be mostly carbon steel. The only exceptions will be the flanged pipe connections for the primary and auxiliary burners, since their refractory protection will be limited. The primary burner piping connection to the furnace will be 8-in. Schedule 40 stainless steel material. The auxiliary burner piping connection to the furnace will be 3.5-in. Schedule 40 stainless steel material.
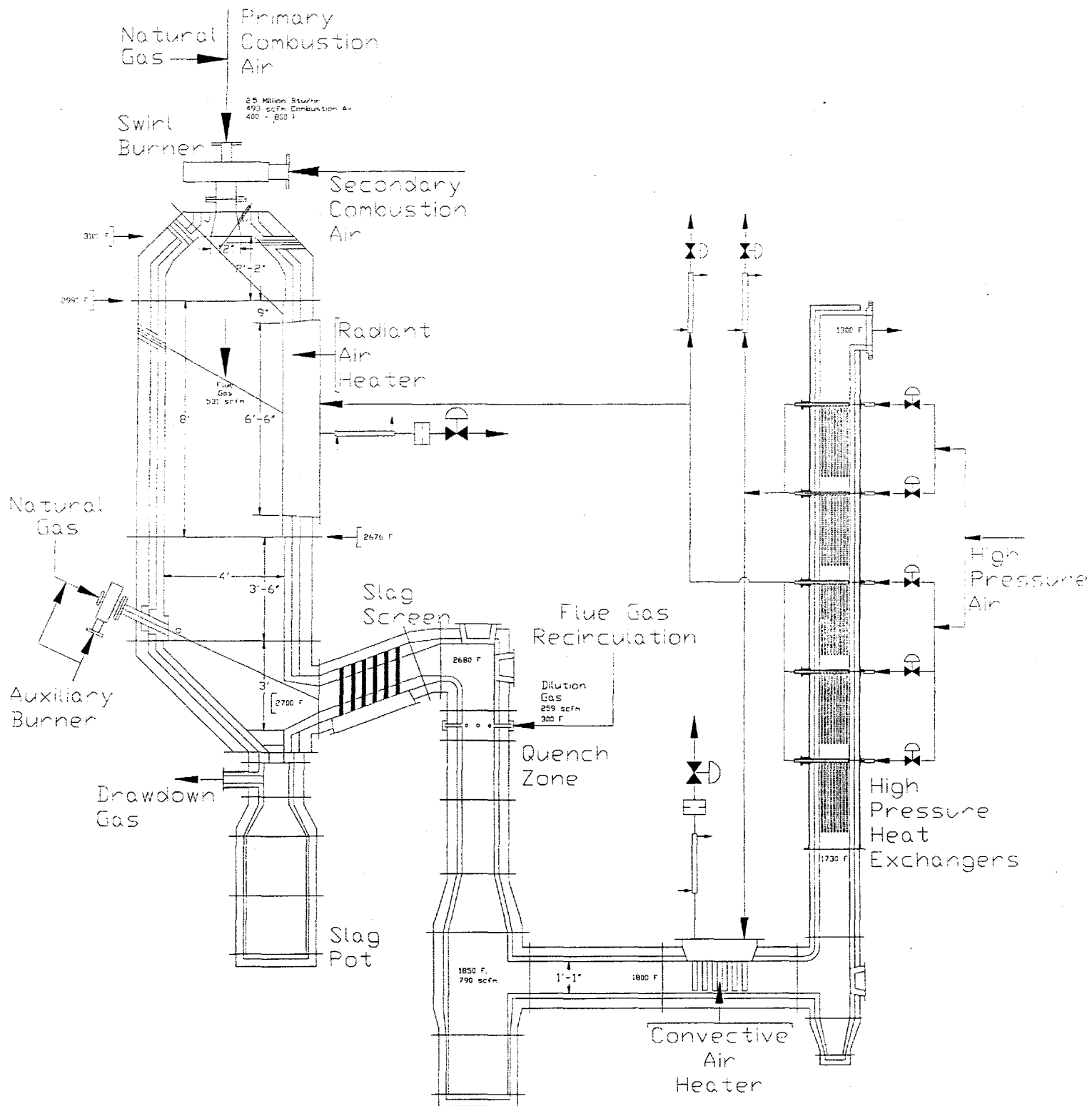
Combustion 2000 Slagging Furnace and Refractory Components
Exhibit 2.2-8

Temperature measurement in the furnace will be extremely important. Furnace exit temperature will be measured using a minimum of two methods. Methods to characterize the furnace during shakedown will include Type S thermocouples, an optical method, and a high-velocity thermocouple (HVT). A minimum of four additional thermocouple locations have been designated for the furnace interior in the final design. Temperature measurements at the interface between the hard-face and intermediate refractory layers are planned as well as between the intermediate and insulating refractory layers. Thermocouple data will be automatically logged into the data acquisition system. A pressure transmitter and gauges will be used to monitor static pressures in order to monitor furnace performance. These data will be automatically logged into the data acquisition system. As a backup, furnace data will be recorded manually on data sheets on a periodic basis.

Observation ports will be located in the furnace to permit visual observation of the primary burner flame, auxiliary burner flame, RAH panels, slag screen, and slag tap. With the exception of the furnace exit (inlet to the slag screen), there are no plans at this time to include additional sampling ports in the furnace walls. However, in order to adequately characterize the furnace during shakedown, and since RAH test panels will not necessarily be available for all furnace operating periods, the first set of doors built for the RAH panel locations will have ports to permit the insertion of temperature and heat flux measurement probes.

The slag tap is intended to be as simple and functional as possible. To that end, the current slag tap design is a simple refractory-lined hole in the bottom of the furnace. The diameter of the slag tap will be 6 in. initially, with the potential to reduce the diameter to 2 in. by simply repouring refractory. To minimize heat losses associated with the slag tap, slag will be collected in an uncooled, dry container with refractory walls. A design feature included at this time will involve drawing a small amount of flue gas through the slag tap to maintain temperature and promote slag flow. The exact flow rate of the drawdown gas required will be determined during system shakedown, but will be <10% of the total flue gas flow rate. The drawdown gas temperature will be reduced using indirect cooling and will reenter the system upstream of the baghouse. Alternative slag tap design options have also been considered. The most complicated option would involve the use of water-cooled hearth plates with a slag tap burner originally designed for use on a ton/hr slagging gasifier. However, it is believed that the combination of the auxiliary gas burner near the furnace exit and the drawdown gas option will result in effective slag tap operation.

The slag pot will consist of several refractory-lined modular components. The refractory in the slag pot will consist of two layers: 1 in. of high-density material and 3 in. of insulating refractory. The high-density refractory is intended to be sacrificial when slag samples are collected for analysis and maintenance performed after a test. The actual size of the slag pot will be 2 ft ID and allow for a variable length (3 to 9 ft) with the installation of as many as four spool piece sections. Depending on the frequency and duration of system operation, it may be necessary to have two complete slag pots. The use of a single slag pot for a week of operation is desirable.

Construction materials for the slag pot shell will be carbon steel. The only exception will be the flanged pipe connection for the drawdown gas because its refractory protection will be limited. The drawdown gas piping connection to the slag pot will be 6-in. Schedule 10 stainless steel material. An observation port in the slag pot is being considered. If it can be placed properly and kept relatively clean, it would permit visual evaluation of slag tap performance.

Temperature measurement in the slag pot near the slag tap may be useful as an indicator of slag tap performance. Therefore, a thermocouple will be located in the top section of the slag pot opposite the drawdown gas exit. Thermocouple data will be automatically logged into the data acquisition system. A pressure indicator will be used to monitor static pressure in the same location in order to monitor slag tap performance. These data will be recorded manually on data sheets on a periodic basis.

Combustion air preheat capabilities will range from 300E to 800EF. Two tube-and-shell heat exchangers operated in series to recover heat from the flue gas to preheat combustion air will be used. However, it may also be necessary to include an electric air preheater to achieve desired flexibility with respect to combustion air temperature control. The need for an electric air preheater will be based on performance data developed during system shakedown.

The refractory walls will consist of three castable refractory layers: 2.75 in. of high-density (7 Btu-in./ft^2-EF-hr), slag-resistant material; 2.75 in. of an intermediate refractory (4.4 Btu-in./ft^2-EF-hr); and 5.25 in. of a low-density insulating refractory (1.8 Btu-in./ft^2-EF-hr). Three refractory layers will be necessary to avoid overheating the low-density insulating refractory. Selection of the insulating and intermediate refractory has been made. However, selection of the slag-resistant material will be based on bench-scale test results. A final decision concerning refractory selection will be made in early August after the completion of bench-scale refractory tests evaluating temperature and slag effects on refractory performance.

Exhibit 2.2-9 summarizes the design parameters upon which the furnace design was based. This table has been recently updated from previous submissions to reflect minor changes resulting from design modifications and revised calculations. Detailed fabrication drawings for the furnace and slag pot shells have been completed. Material procurement and fabrication of the furnace and slag pot shells will begin once the design has been reviewed .

Primary and Auxiliary Burners

The primary burner will be natural gas- and coal-capable, with coal particle size assumed to be a standard utility grind, 70% –200 mesh. Some burner turndown is desirable and has been factored into the burner design. Flame stability will be assessed by observation of the flame and its relation to the burner quarl as a function of secondary air swirl and operating conditions at full load and under turndown conditions. The basic burner design is an International Flame Research Foundation (IFRF)-type adjustable secondary air swirl generator, illustrated in Exhibit 2.2-10 and 2.2-11. An IFRF-type adjustable secondary air swirl generator uses primary and secondary air at approximately 15% and 85% of the total air, respectively, to adjust swirl between 0 and a maximum of 1.9.

Exhibit 2.2-9

Flow and Heat-Transfer Calculations for Pilot-Scale Slagging Furnace and Refractory Ducts

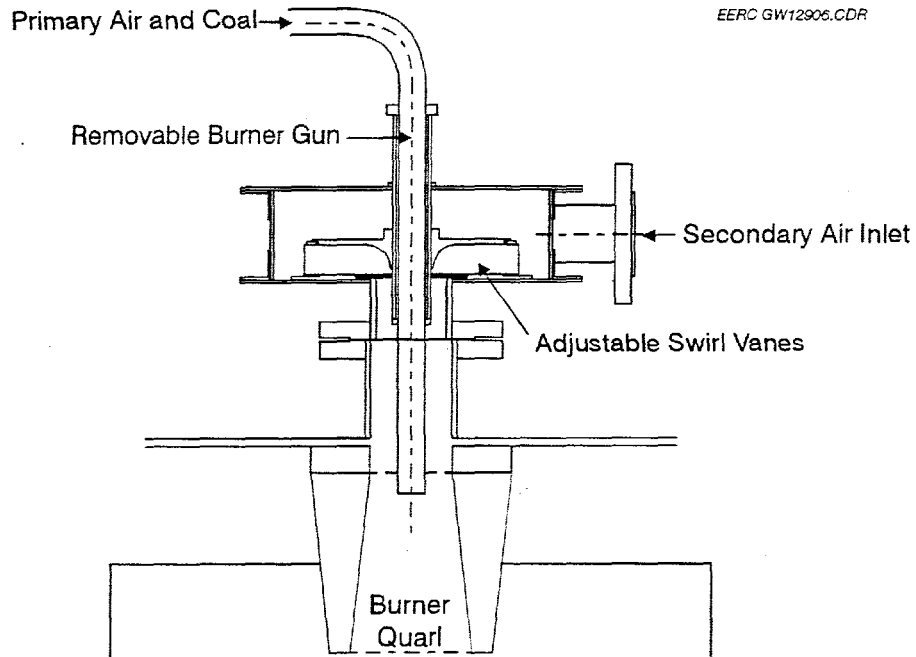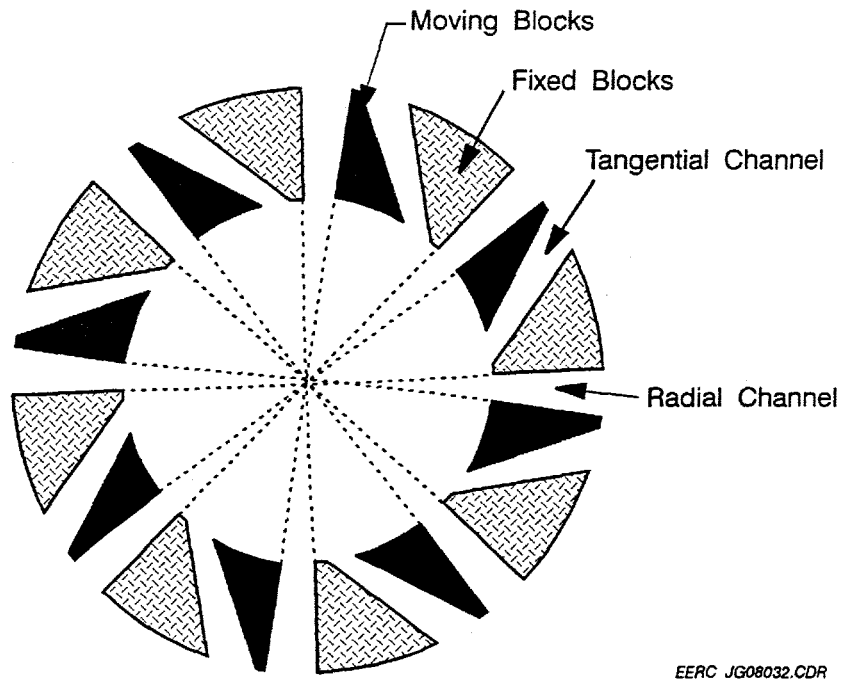| Illinois No. 6 Bituminous					
Furnace			Furnace		
Furnace ID, in.	48	48	Furnace ID, in.	48	48
Firing Rate, MMBtu/hr	2.5	3.0	Firing Rate, MMBtu/hr	2.5	3.0
Coal Feed Rate, lb/hr	225	270			
Air Flow Rate, scfm	493	592	Slag Screen Inlet		
Flue Gas Flow Rate, scfm	531	637	Gas Temp., EF	2700	2900
Flue Gas Flow Rate, acfm	3431	4240	Flue Gas Flow Rate, acfm	3227	4117
Furnace Gas Velocity, ft/s	4.6	5.6	Gas Velocity, ft/s	59.6	76.0
Exit Gas Velocity, ft/s	29.8	38.0			
Flue Gas Residence Time, s	3.5	2.8	Dilution Gas Requirements		
			Gas Velocity in, ft/s	57.5	73.4
Auxiliary Burner, MMBtu/hr	0.075	0.202	Exit Gas Temp., EF	1880	1880
Wall Losses, MMBtu/hr	0.177	0.184	Dilution Gas Temp., EF	300	300
Other Losses, MMBtu/hr	0.200	0.200	Calc. Dilution Gas, scfm	259	391
			Total Flue Gas Flow, scfm	790	1029
Furnace Section Length, ft	16	16	Flue Gas Flow Rate out, acfm	3556	4631
Refractory 1 Thickness, in.	2.75	2.75	Gas Velocity out, ft/s	64.3	83.7
Refractory 2 Thickness, in.	2.75	2.75			
Refractory 3 Thickness, in.	5.25	5.25	Dilution Gas Nozzles		
Furnace Weight, tons	13.6	13.6	Nozzle Diameter, in.	1.25	1.25
			No. of Nozzles	8	8
Inlet Gas Temperature, EF	3100	3100	Dilution Gas Flow, acfm	378	572
Avg. Gas Temperature, EF	2900	3000	Dilution Gas Velocity, ft/s	93	140
Exit Gas Temperature, EF	2700	2900			
Refractory 1 Surface Temp., EF	2786	2885	Convective Air Heater		
Refractory 2 Surface Temp., EF	2480	2568	Gas Temp., EF	1800	1800
Refractory 3 Surface Temp., EF	2042	2113	Flue Gas Flow Rate, acfm	3435	4472
Furnace Skin Temperature, EF	247	253	Gas Velocity, ft/s	48.8	63.5

Assumptions

Excess air is 20%.

Hard-face refractory has a thermal conductivity of 7 Btu-in./ft^2-EF-hr.

Intermediate layer of Harbison–Walker Lightweight Castable 30 refractory has a thermal conductivity of 4.4 Btu-in./ft^2-EF-hr

Insulating layer of Harbison–Walker Lightweight Castable 26 refractory has a thermal conductivity of 1.8 Btu-in./ft^2-EF-hr.

Primary Air and Coal→

Removable Burner Gun —→

Secondary Air Inlet ←—

Adjustable Swirl Vanes

Burner
Quarl

IRF Adjustable Swirl Burner
Exhibit 2.2-10

Moving Blocks

Fixed Blocks

Tangential Channel

Radial Channel

EERC JG08032.CDR

Cross Section of a Movable Block Assembly
Exhibit 2.2-11

"Swirl" is defined as the ratio of the radial (tangential) momentum to axial momentum imparted to the secondary air by movable blocks internal to the burner and is used to set up an internal recirculation zone (IRZ) within the flame that allows greater mixing of combustion air and coal. Swirl is imparted by moving blocks to set up alternate paths of radial flow and tangential flow, creating a spin on the secondary air stream that increases the turbulence in the near-burner zone. At the fully open position of the swirl block, the secondary air passes through the swirl burner unaffected, and the momentum of this stream has only an axial component (the air enters the combustion chamber as a jet). As the angle of the blocks changes, the air begins to spin, or swirl, and the radial component to the momentum is established, creating the IRZ in the near-burner region. It is the ratio of this radial component of the momentum to the axial component that establishes the quantity defined as swirl.

The adjustable swirl burners currently used consist of two annular plates and two series of interlocking wedge-shaped blocks, each attached to one of the plates. The two sets of blocks can form alternate radial and tangential flow channels, as shown in Exhibit 2.2-11, such that the air flow splits into an equal number of radial and tangential streams, which combine farther downstream into one swirling flow. By a simple rotation of the movable plate, radial channels are progressively closed and tangential channels opened, so that the resulting flux of angular momentum increases continuously between zero and a maximum value. This maximum swirl depends on the total air flow rate and the geometry of the swirl generator. Swirl can be calculated from the dimensions of the movable blocks (the ratio of the tangential and radial openings of the blocks) or from the measurement of the velocity of the air stream (obtaining both radial and axial components). The following description of that calculation is provided by Beér and Chigier (1972):

When rotating motion is imparted to a fluid upstream of an orifice, the fluid emerging from the orifice has a tangential velocity component in addition to the axial and radial components encountered in nonswirling jets. The presence of the swirl results in radial and axial pressure gradients which, in turn, influence the flow field. In the case of strong swirl, the adverse axial pressure gradient causes reverse flow along the axis, setting up the internal recirculation zone.

In swirling free jets or flames, both axial flux of the angular momentum ($G\varphi$) and the axial thrust (G_x) are conserved. These can be written as follows:

$$G\varphi = {_0\int^R} [(Wr) \rho U 2\pi r] \, dr = const$$

$$G_x = {_0\int^R} [U \rho U 2\pi r] \, dr + {_0\int^R} [p 2\pi r] \, dr = const$$

where U, W, and p are the axial and tangential components of the velocity and static pressure, respectively, in any cross section of the jet. Since both of these momentum fluxes can be considered to be characteristic of the aerodynamic behavior of the flame, a nondimensional criterion based on these quantities can describe the swirl intensity as:

$$S = G\varphi / G_x R \quad (R = exit \, radius \, of \, the \, burner \, nozzle)$$

where U, W, and p are the axial and tangential components of the velocity and static pressure, respectively, in any cross section of the jet. Since both of these momentum fluxes can be considered to be characteristic of the aerodynamic behavior of the flame, a nondimensional criterion based on these quantities can describe the swirl intensity as:

$$S = G\varphi/G_x R \quad (R = \text{exit radius of the burner nozzle})$$

Experiments have shown that the swirl number S indicates the flow similarity between swirling jets produced by geometrically similar swirl generators. Other similarity criteria which take account of nonisothermal conditions and of confinement of jet flow by walls can also be applied in conjunction with the swirl number. The calculation of swirl in other types of swirl generators, such as the air registers on a utility boiler, are also described by Beér and Chigier (1972), although not mentioned here.

Secondary air swirl is used to stabilize the flame. In the absence of swirl, loss of flame may result, increasing the risk of dust explosion. As swirl is applied to the combustion air, coal particles are entrained in the IRZ, increasing the heating rate of the particles, leading to increased release of volatiles and char combustion. The flame becomes more compact and intense as swirl is increased to an optimum level, which is characterized in existing EERC pilot-scale test facilities as the point at which the flame makes contact with the burner quarl. Increasing swirl beyond this level can pull the flame into the burner region, unnecessarily exposing metal burner components to the intense heat of the flame and possible combustion in the coal pipe.

Increasing swirl to provide flame stability and increased carbon conversion can also affect the formation of NO_x. The high flame temperatures and increased coal–air mixing associated with increased swirl create an ideal situation under which NO_x may form. In full-scale burners with adjustable vanes, swirl is often increased to reach the optimum condition and then decreased slightly to reduce the production of NO_x. Although NO_x emissions are of interest, their control is not a key objective for the pilot-scale slagging furnace. Therefore, burner operational settings will be based on achieving desired furnace exit temperatures and slag conditions in the furnace. Flame stability under turndown conditions will be characterized by firing the primary burner at reduced load (typically 66% to 85% of the full load rate), maintaining the same primary air flow, and adjusting the secondary air flow to meet excess air requirements.

The primary burner design is simply a scaled-up version of the two existing burners based on increased combustion air volumetric flow rates. Materials of construction for the primary burner are entirely stainless steel because of the combustion air (up to 800EF) temperature ranges to which it will be exposed. Combustion air flow rates through the primary burner will range from about 400 to 600 scfm depending on furnace firing rate and the fuel type (bituminous, subbituminous, or lignite) fired.

An auxiliary gas burner (500,000 Btu/hr) will be located in the area of the furnace exit in order to ensure desired slag flow from the furnace and the slag screen. This auxiliary burner will compensate for heat losses through the furnace walls, site ports, and RAH test panels. The use of the auxiliary gas burner will be beneficial during start-up to reduce heatup time and to prevent the freezing of slag on the slag screen when initially switching to coal firing. The auxiliary gas burner will be fired near stoichiometric conditions to avoid high excess air levels in the system. It is anticipated that the auxiliary gas burner will be fired at relatively low rates (<200,000 Btu/hr) once

the furnace reaches thermal equilibrium. Materials of construction for the auxiliary burner are also entirely stainless steel.
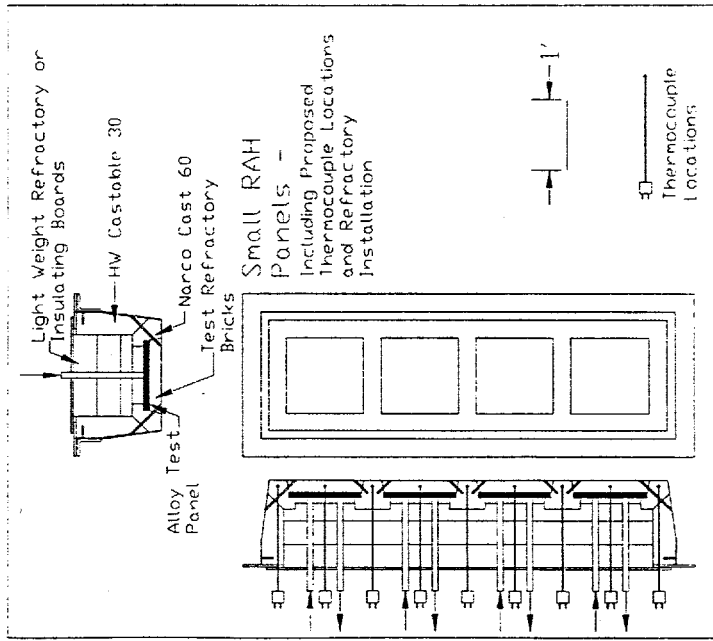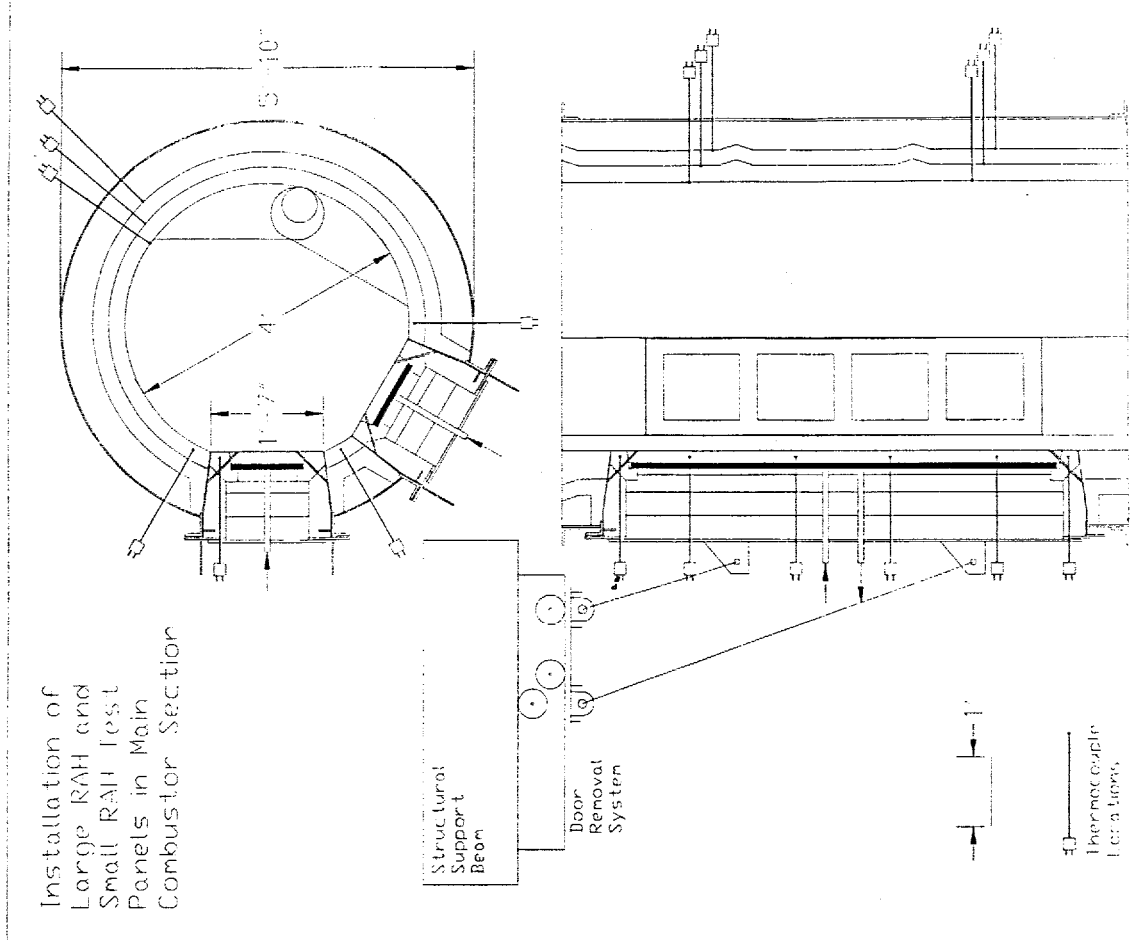
Inlet combustion air piping to the primary burner will include insulated 6-in. Schedule 5 stainless steel for the secondary air and 1-, 2-, and 4-in. Schedule 40 stainless steel for the primary air/coal feed line. The primary burner piping connection to the furnace will be 8-in. Schedule 40 material. For the auxiliary burner, inlet combustion air piping sizes will be 1- to 2-in. Schedule 5 and 40 material. The auxiliary burner piping connection to the furnace will be 3.5-in. Schedule 40 material.

Thermocouples will be installed in order to monitor inlet combustion air temperatures for each burner. Thermocouple data will be automatically logged into the data acquisition system. Pressure transmitters and gauges will be used to monitor static and differential pressures in order to monitor burner performance and measure combustion air flow rate. These data will be automatically logged into the data acquisition system, and flow control valves will be used to adjust and maintain desired combustion air flow rates. As a backup, burner data will be recorded manually on data sheets on a periodic basis. During system shakedown, burner performance at full load and reduced load conditions will be evaluated and documented.

Cleaning and maintenance of the burners are expected to be minimal. However, when necessary, burner maintenance will be accomplished by unbolting the flanged connections between the burner and the furnace and secondary and primary air lines. When we remove the top of the slagging furnace to inspect the interior, it will be necessary to first disconnect the combustion air and fuel feed lines and remove the primary burner.

Radiant Air Heater Panels

A key furnace design feature will be accessibility for installation and testing of one large RAH panel and four small panels. Plans at this time call for the furnace design to accept a large RAH panel with a maximum active size of 1 ft × 6 ft. This size was selected to minimize furnace heat losses and based on panel manufacturing constraints. Flame impingement on the RAH panels is not necessarily a problem. Cooling air for the large RAH panel will be provided by an existing air compressor system having a maximum delivery rate of 510 scfm and a maximum stable delivery pressure of 275 psig. Backup cooling air is available from a smaller compressor at a maximum delivery rate of 300 scfm and pressure of <100 psig. It will be necessary to heat the cooling air to achieve the 1300EF radiant panel cooling air inlet temperature desired. Outlet cooling air temperatures from the large RAH panel will range from 1375E to 1800EF by adjusting cooling air flow rate. Cooling air pressure for the large radiant panel will be roughly 150 psig. Based on some limited heat-transfer calculations, the cooling air flow rate will be <200 scfm. Flue gas heat exchange and electrical heating will be used to meet heated cooling air temperature requirements for the large RAH. The advantage of a combination of heat sources for the cooling air stream at this scale is greater flexibility and range of control. Exhibit 2.2-12 and 2.2-13 illustrate the RAH panels, including the approach to insulation and proposed location of thermocouples. Proper insulation and thermocouple location will be required to minimize and document edge effects, respectively, as well as adequately define surface temperature distributions, total heat absorption, and local heat flux.

Installation of
Large RAH and
Small RAH Test
Panels in Main
Combustor Section

Structural
Support
Beam

Door
Removal
System

Thermocouple
Locations

Light Weight Refractory or
Insulating Boards

HW Castable 30

Narco Cast 60
Test Refractory

Test Refractory
Bricks

Alloy Test
Panel

Small RAH
Panels –
Including Proposed
Thermocouple Locations
and Refractory
Installation

Thermocouple
Locations

RAH Test Panels and Installation
Exhibit 2.2-12
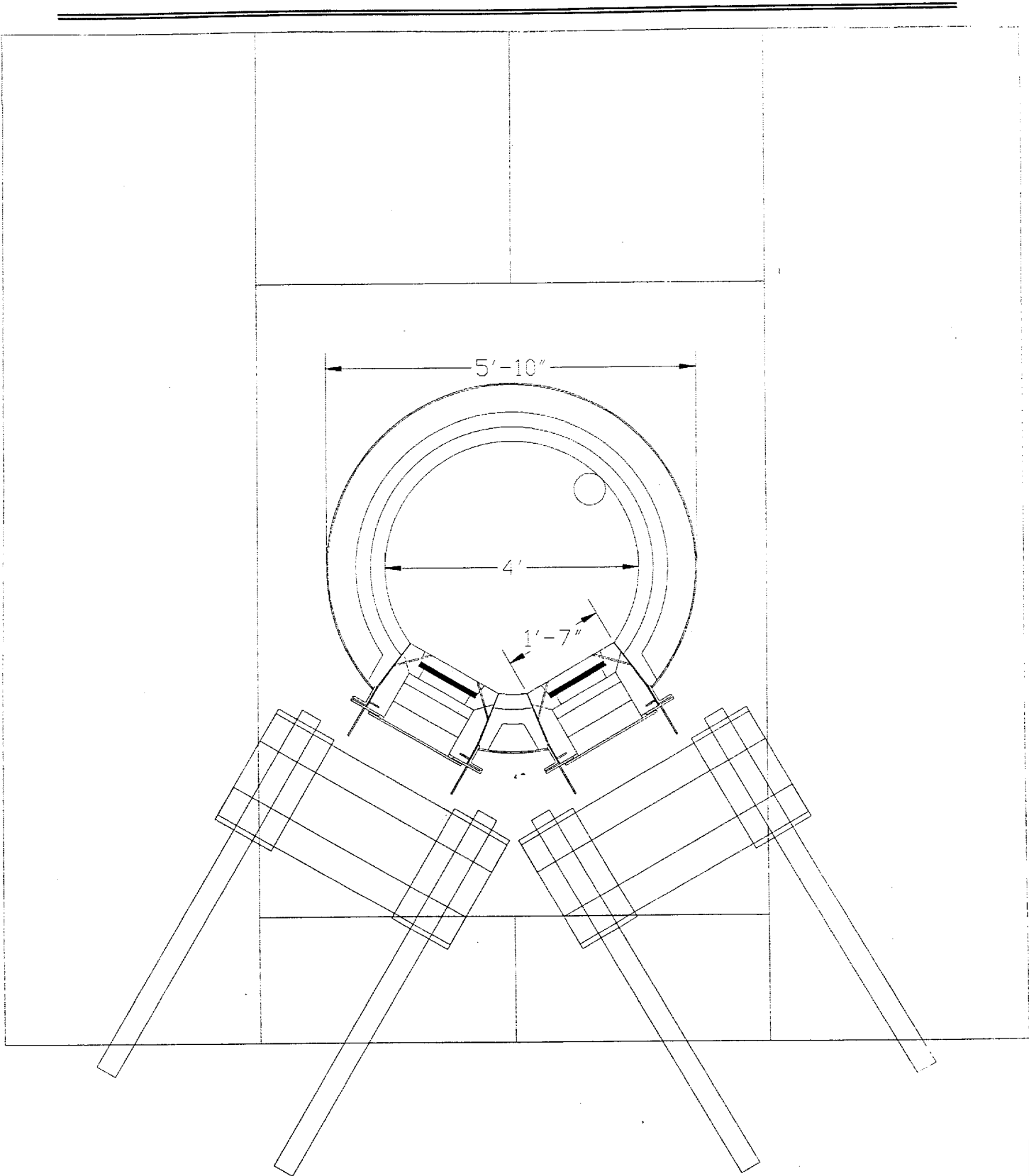
Door Removal System and Centerline Locations of Support Beams
Exhibit 2.2-13

Furnace design will also permit the installation of four 1-ft × 1-ft RAH panels. The actual size of the test brick for each of the small panels is 10 in. × 10 in., with an increased size to 12 in. × 12 in. on the front face of the alloy test panel. Cooling air for the small RAH panels will be provided by an existing air compressor system having a maximum delivery rate of 510 scfm and a maximum stable delivery pressure of 275 psig. Backup cooling air is available from a smaller compressor at a maximum delivery rate of 300 scfm and pressure of <100 psig. Cooling air temperature at the inlet of the small RAH panels will be low, facility-ambient temperature. At this time, the operating pressure of the cooling air system for the small RAH panels is assumed to be 150 psig, with a flow rate of <100 scfm. The outlet cooling air temperature for the small RAH panels has not been specified; however, it is assumed to be less than 1800EF. Again, actual outlet cooling air temperatures will be controlled as a function of cooling air flow rate. Exhibit 2.2-12 illustrates the small RAH panels, including the proposed location of thermocouples. Proper insulation and thermocouple location will be required to minimize and document edge effects, respectively.

Slag Screen

The slag screen design has been developed by PSI. Recent discussions have resulted in a nominal flue gas approach velocity of 56 ft/s and an inlet flue gas temperature of 2700EF. The flue gas outlet temperature from the slag screen must be >2450EF to minimize the potential for slag freezing in the slag screen. The slag screen will consist of six rows of three 1.5-in.-diameter vertical tubes mounted in a sloped duct to facilitate slag flow from the slag screen into the furnace slag tap. The centerline-to-centerline tube spacing in each row is 3.75 in. Centerline-to-centerline spacing between individual rows is 4.5 in. Duct dimensions for the slag screen are proposed to be 10 in. × 13 in. × 3.5 ft. The resulting flue gas velocity through the slag screen will be roughly 85 ft/s. Uncooled mullite tubes have been proposed for use in the slag screen to minimize heat loss and avoid slag freezing in the last few rows of tubes. Routine on-line cleaning of the slag screen is not anticipated to be a requirement. However, the availability of one or more ports permitting the use of an air lance for periodic cleaning will be factored into the final design. The availability of ports for collecting gas and solid samples at the inlet and outlet of the slag screen will also be included in the final design, along with pressure taps for measuring slag screen differential pressure.

Furnace exit design will involve the use of a refractory-lined spool piece that can be interchanged with the slag screen. This will permit furnace operation with and without the slag screen.

Dilution/Quench Zone

Based on the modeling of the dilution/quench zone, a modified process illustration (Exhibit 2.2-7) of the overall slagging furnace system was prepared. The modified layout orients the circular dilution/quench zone vertically, maintains a 1-ft diameter in the area of the flue gas recirculation nozzles, and then expands the duct diameter to 2 ft to provide adequate residence time within duct length constraints. The duct section containing the flue gas recirculation nozzles will be a spool piece in order to accommodate potential changes to the size, number, and orientation of the flue gas recirculation nozzles. The vertically oriented dilution/quench zone will be refractory-lined (hard face and insulating refractory) and located immediately downstream of the slag screen. Flue gas recirculation will be used to cool the flue gas in the dilution/quench zone and freeze

remaining slag particles. A centrifugal flue gas recirculation fan will remove flue gas from the system immediately downstream of the induced-draft (ID) fan. The 4-in. stainless steel piping transporting the dilution gas will be insulated to avoid condensation problems. Dilution gas will be injected into the quench zone through eight 1-in. nozzles at a total flow rate of 274 to 329 scfm, depending on furnace firing rate. The design assumes a dilution gas temperature of 300EF and a flue gas exit temperature of 1850EF from the quench zone. A flow control valve will be used to control the flue gas recirculation rate to achieve the desired flue gas exit temperature from the dilution/quench zone.

The evaluation of selective noncatalytic reduction (SNCR) is not a priority at this scale. Therefore, no consideration will be given to SNCR evaluation when the design of the dilution/quench zone is finalized. However, ports will be located in the dilution/quench zone to permit the addition of NH_3 or other additives if desired. Flue gas-sampling ports will be located in and downstream of the dilution/quench zone. These options were requested by PSI to permit evaluation of new measurement techniques for NO_x, NH_3, and other species in the dilution/quench zone.

Convective Air Heater

The flue gas flow rate to the CAH section will be 790 to 1030 scfm (3430 to 4470 acfm at 1800EF). A square duct dimension of 1.17 ft^2 should result in a flue gas approach velocity of 50 to 65 ft/s to the CAH. Based on past discussions, the CAH will consist of three or four rows of 2-in.-diameter tubes. Tube spacing will be a minimum of 4 in. on center, with an overall CAH section dimension of 13 in. × 13 in. × 20 in. Cooling air for the CAH will be provided by an existing EERC air compressor system having a maximum delivery rate of 510 scfm and a maximum stable delivery pressure of 275 psig. Backup cooling air is available from a smaller compressor at a maximum delivery rate of 300 scfm and pressure of <100 psig. Cooling air heating and flow rate control will be necessary to achieve the 700EF minimum (1000EF maximum) inlet cooling air temperature desired, effectively controlling surface temperatures, and provide for an inside heat-transfer coefficient similar to the commercial design. At this time, the operating pressure of the cooling air system is assumed to be 150 psig. It is anticipated using flue gas heat exchange and some limited electrical heating to meet heated cooling air temperature requirements for the CAH. The advantage of a combination of heat sources for the cooling air stream at this scale is greater flexibility and range of control. The cooling air exit temperature from the CAH should not exceed 1300EF. Cooling air flow rate will be used to control cooling air exit temperature using a flow control valve.

Observation ports are planned for the CAH section. The number and location of the observation ports will depend on the CAH design. In addition, ports for inserting air lances for intermittent manual cleaning of the CAH will be included. Again, the number and location of these ports will depend on the CAH design. Critical measurements relative to the CAH will include accurate surface temperatures, cooling air temperatures, cooling air flow rates, and pressure. CAH testing to evaluate heat-transfer performance is a high priority, requiring extensive instrumentation to monitor performance adequately. An important secondary priority is length of material life in relation to operating conditions and ash deposition.

Emission Control

A pulse-jet baghouse will be used for final particulate control on the pilot-scale slagging furnace system. The intent is that the baghouse design will permit operation at both cold-side (250E to 400EF) and hot-side (600E to 700EF) temperatures. The primary baghouse chamber and ash hopper walls will be electrically heated and insulated to provide adequate temperature control to minimize heat loss and avoid condensation problems on start-up and shutdown. Inlet and outlet piping (8-in. Schedule 5 304L) and the clean-air plenum will be insulated. Because of the planned operating conditions, materials of construction will be primarily 304L stainless steel (12-gauge sheet metal, 1.5×1.5-, 2.5×2.5-, 3.5×3.5-, 3×6-in. angle iron, and 3/16-in. plate material). The main baghouse chamber was designed with internal angle iron supports to handle a negative static pressure of 15 in. W.C.

Flue gas flow rates to the baghouse are expected to range from a low of 630 scfm (980 acfm at 350EF, based on a furnace firing rate of 2 MMBtu/hr) to a maximum of 1030 scfm (2300 acfm at 700EF, based on a furnace firing rate of 3 MMBtu/hr). Therefore, the baghouse design is based on an average flue gas flow rate of 850 scfm (1325 acfm at 350EF or 1900 acfm at 700EF, based on a nominal furnace firing rate of 2.5 MMBtu/hr). The baghouse is sized to accommodate a maximum of 36 bags mounted on wire cages with 2-in. bag spacing. Bag dimensions will be nominally 6 in. in diameter by 10 ft in length, providing a total filtration area of 565 ft^2. Arranging the bags in six rows of six bags each allows the number of bags on-line to be changed by installing different tube sheets. For example, when the baghouse is operated at 350EF and 850 scfm (1325 acfm), only 24 bags will be required to achieve a filter face velocity of 3.5 ft/min. If all 36 bags are installed, the filter face velocity would be roughly 2.3 ft/min. In the event that the baghouse is operated at a hot-side condition (1900 acfm at 700EF), 30 bags would result in a filter face velocity of 4 ft/min, and 36 bags would decrease the face velocity to 3.4 ft/min. At a maximum potential flow rate of 2300 acfm (1030 scfm at 700EF), 36 bags would result in a filter face velocity of 4.1 ft/min.

Initially, only one tube sheet will be constructed, permitting the installation of 36 bags (565 ft^2 of filtration area) arranged in a six-by-six array. Installing the maximum number of bags will permit the overall system to be evaluated over the broadest potential range of operating conditions during shakedown while minimizing the potential impact of the baghouse on overall system performance. Each filter bag will be secured to the tube sheet using a snap band sewn into the top cuff. Stainless steel wire cages with 20 vertical wires and 6-in. ring spacing will provide bag support. The pulse-jet baghouse will be a single compartment capable of either on- or off-line cleaning. Flue gas will enter the baghouse in an area just below the bottom of the cage-supported bags and above the ash hopper. Access to the filter bags and stainless steel wire cages will be gained by removing the cover to the clean air plenum at the top of the baghouse. The baghouse ash hopper will be supported at the fourth level (roughly 30-ft elevation) providing access to the clean air plenum on the fifth level to facilitate installation, inspection, maintenance, and removal of filter bags and cages.

Low-watt-density heat cable made for conductive surfaces will be used to preheat the surface of the baghouse chamber to prevent moisture condensation during start-up and to minimize baghouse heat losses over the operating range of interest (350E–700EF); heat cable will be run vertically on each of the four baghouse walls spaced on 4- to 6-in. centers. The individual elements will be wired in parallel to minimize the impact of single-element failures. The baghouse ash hopper will

be heated in a similar manner. Five temperature controllers will be used to control electrical resistance heating on the pulse-jet baghouse.

Pulse-jet cleaning will be triggered as a function of baghouse differential pressure or as a function of time. The baghouse pulse-jet-cleaning system will be operated by a controller that permits adjustment of cleaning frequency and pulse duration. Timers will be used to set pulse duration and off time, while counters total baghouse operating time and test time in hours and total and test cleaning cycles. Filter bag cleaning will occur when the controller opens the solenoid-operated valves between the pulse-air reservoir and the six pulse-air manifold lines. Each manifold line will provide pulse air to six filter bags. Six filter bags will be cleaned simultaneously, with a short delay between each set of filter bags to allow air pressure to recover in the pulse-air reservoir.

Air for bag cleaning will be provided by an existing air compressor system having a maximum delivery rate of 510 scfm and a maximum stable delivery pressure of 275 psig. Backup air is available from a smaller compressor at a maximum delivery rate of 300 scfm and pressure of <100 psig. High-pressure/low-volume and low-pressure/high-volume cleaning options are included in the design of the pulse-air system. In order to operate at a low-pressure/high-volume condition in the pulse-jet baghouse, a pulse volume of 0.03 ft^3/ft^2 of fabric surface, or roughly 0.5 ft^3/bag, will be necessary at a pulse-air reservoir pressure of <40 psig. The pulse volume for each set of six bags will be 3 ft^3. For a high-pressure/low-volume case, 0.01 to 0.02 ft^3/ft^2 of fabric surface is common, and the pulse-air reservoir pressure will be 40 to 100 psig. Therefore, a maximum pulse volume of 1.9 ft^3 will be required to clean one set of six bags. The required pulse duration to achieve a desired pulse-air volume as a function of pulse pressure will be determined during system shakedown.

Flue gas sample ports will be installed in the inlet and outlet piping of the baghouse to permit flue gas flow rate measurements and sampling for gaseous/vapor-phase constituents as well as fly ash. Specific routine measurements to be made will include flue gas oxygen, sulfur dioxide, and nitrogen oxide concentrations using on-line instruments. Fly ash particle-size distribution and mass loading will be determined periodically using standard Environmental Protection Agency (EPA) methods. Hazardous air pollutants (HAPs) will be measured on a limited basis using EPA Method 29. Sight ports (4 in. OD) are located at two elevations in the baghouse to permit inspection of bag surfaces on the dirty side and two locations in the clean-air plenum to permit visual inspection of the tube sheet surface and the exit of several bags.

Thermocouples will be installed in the inlet and outlet piping, as well as at four locations along the length of the baghouse chamber. Differential pressure across the chamber and static pressure at the outlet of the chamber will be monitored continuously with pressure transducers. Gauges will also be used to visually monitor baghouse differential and static pressure at the main combustor control panel. Baghouse thermocouple and pressure transducer data will be automatically logged into the data acquisition system. As a backup, baghouse data will be recorded manually on data sheets on a periodic basis.

Baghouse ash removal will be accomplished by opening a 6-in. knife valve at the bottom of the hopper, allowing ash material to drain through a 6-in. stainless steel pipe into a 55-gallon drum on the main floor level. Ash containers of this size facilitate handling and are adequate for ash accumulation during 100-hr and longer test periods, with only periodic replacement required. Construction of the baghouse has been completed. Exhibit 2.2-14 is a photograph of the main

chamber, clean air plenum, and ash hopper. Installation and insulation of the baghouse are anticipated in July.
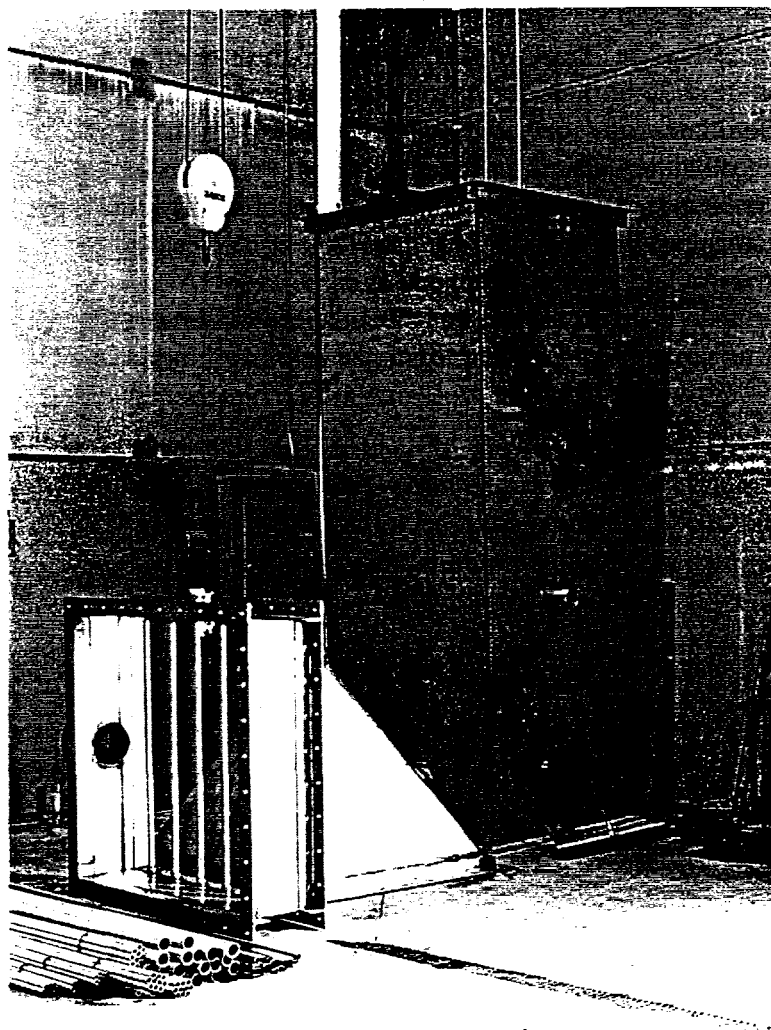
**Photograph Illustrating the Pulse-Jet Baghouse Components Fabricated
Exhibit 2.2-14**

The EERC is not planning to install a sulfur dioxide control system. Initial dispersion modeling data developed by the North Dakota State Department of Health indicate that sulfur dioxide emissions would have to be limited to 16 lb/hr to avoid exceeding the ambient standard. Based on a 2.5-MMBtu/hr coal-firing rate, the EERC is not concerned about the potential 16-lb/hr sulfur dioxide limit or the need for a sulfur dioxide control system. If the coal-firing rate were actually 3 MMBtu/hr, a small reduction (10%) in sulfur dioxide emissions might be required.

Instrumentation and Data Acquisition

The instrumentation and data acquisition components for the pilot-scale slagging furnace system will address combustion air, flue gas, cooling air, cooling water, and other appropriate measurements (temperatures, static and differential pressures, and flow rates). Flue gas will be monitored for oxygen, sulfur dioxide, carbon monoxide, carbon dioxide, and total nitrogen species (nitric oxide and nitrogen dioxide) on a continuous basis at the furnace exit. A set of existing gas analyzers for oxygen, sulfur dioxide, and nitrogen species will be available to monitor a second system location simultaneously. Surface temperature measurements are anticipated for the RAH panels and CAH section. In addition, heat flux measurements for the furnace, RAH panels, and CAH section have been recommended. Orifice plates or other on-line devices (monitored with pressure transducers and gauges on the main combustor control panel) will be installed at various points in the system to measure combustion air flow rate, flue gas flow rate, flue gas recirculation rate, and cooling air flow rates.

The data acquisition system will be based on a Genesis software package and a personal computer. This type of data acquisition system is currently used at the EERC on a number of pilot-scale units. All process data points will be logged into the data acquisition system. It is uncertain at this time of how much integrated system control will be required or desired. Decisions concerning the level of integrated control implemented will be made based on relative cost.

Reference

Beér, J.M.; Chigier, N.A. *Combustion Aerodynamics;* John Wiley & Sons: New York, 1972; pp 100–146.

Laboratory-/Bench-Scale Activities

Laboratory Activities

Experimental

A total of ten commercial and five experimental monolithic castable refractories have been evaluated for possible use in the pilot-scale slagging combustor through static corrosion tests. Two applications are being evaluated. The first is for a corrosion-resistant coating for the radiant-zone alloy heat exchanger. SiC-based refractories have been mainly tested for this use. The second application is for the insulating lining of the furnace in the radiant zone, and alumina-based refractories are being tested for this use. Several commercial refractories were donated by the following manufacturers:

- **Norton Co.** (GC950 SiC-based castable)
- **Plibrico** (L-2825, L-2803 or Plicast Cement Free 96, Plicast 40 Al_2O_3-based castables)
- **Carborundum** (Carbofrax 11LI SiC-based castable)
- **Harbison–Walker** (Castolast G and Descon A98, Al_2O_3-based castables)
- **Green** (Greencast 94 Al_2O_3-based castable)
- **BMI** (Hydrecon Tabcast CR-10 LCV Al_2O_3 + 9.5% Cr_2O_3 castable)
- **NARCO** (Narcocast 60 Al_2O_3-based castable)

The chemical and physical properties for the refractories are given in Exhibit 2.2-15 and -16.

Four experimental SiC castable formulations were designed at the EERC. Two are composed of SiC:Al_2O_3 weight percentages of 90:10 and 70:30. The other two castables are composed of SiC:Al_2O_3:SiO_2 in two formulations, 95:3.5:1.5 (respective weight percents) and 90:7:3. Another experimental SiC castable, L-2824, was provided by Plibrico.

Static corrosion tests were performed at 1430E and 1700EC for 100 hours using either Rochelle slag from the Northern States Power Company Riverside Plant or Illinois No. 6 slag from Illinois Power Company's Baldwin Plant. Not all of the refractories were tested at each temperature nor with each slag. Exhibit 2.2-17 shows the compositions of the slags.

Refractories tested at 1430EC included the five experimental SiC-based refractories 90:10, 70:30, 95:3.5:1.5, 90:7:3, and L-2824), the two commercial SiC-based castables (GC950 and Carbofrax 11LI), and two alumina-based castables (L-2825 and L-2803).

Those tested using the Illinois No. 6 slag included all of the commercially available refractories and three of the experimental ones; therefore, all of the refractories were tested except for two of the experimental SiCs (95:3.5:1.5 and 90:7:3). After the exposure, the blocks were cut in half vertically, and the refractory surface recession was measured at three places on each half of the blocks, for a total of twelve measurements per refractory.

Results

Maximum slag penetration was determined by scanning electron microscopy (SEM) analysis. Several photos over a large area of each sample were consolidated to form a composite photo for each sample. The first photo was taken at the bottom corner of the slag well, then consecutive

photos were taken below each previous photo, until the bottom edge of the refractory block was visible. The slag penetration was determined at the deepest point of visible penetration. Exhibit 2.2-18 and -19 show the slag penetrations and surface recessions for the Illinois No. 6 slag tests. The 70:30 mixture was not included in Exhibit 2.2-18 because it was impossible to obtain an accurate measurement because of chipping of the refractory during machining. The alumina-based refractories are not shown because the slag completely penetrated into the refractories.

Exhibit 2.2-15
Properties of Candidate Monolithic Refractories

Material Name:	Narcocast 60	Carbofrax 11LI	GC950	Descon A98	Castolast G
Manufacturer:	NARCO	Carborundum	Norton	Harbison–Walker	Harbison–Walker
Max. Temperature					
EC	1732	1482		1816	1816
EF	3100	2700		3300	3300
Composition, wt%					
SiC	0	83	82	0	0
Al_2O_3	62	13	12	98	94
SiO_2	28	1	2	<1	<1
Fe_2O_3	1	<1	0	<1	<1
TiO_2	2		0	<1	0
CaO		3	3	2	6
MgO	<1	<1	0	<1	<1
Cr_2O_3	0	0	0	0	0
P_2O_5	0	0	0	0	0
Alkaliesy	<1	<1	0	<1	<1
Other	0	0	1	0	0
Thermal Conductivity, Btu in./ft^2-EF-hr					
500EF	5.0			NA	NA
1000EF	5.6				
1500EF	6.0				
2000EF	6.5		53		
2200EF		40–60			
Bulk Density					
g/cm^3		2.3	2.6	3.1	2.7
lb/ft^3		145	160	192	168
Permanent Linear Change, %					
2500EF (1370EC)	+0.7				
2910EF (1600EC)				−0.4	Negligible
3100EF (1704EC)	+1.6				
3140EF (1727EC)					
Price per Pound, $	0.29			1.16	1.25

Exhibit 2.2-16
Properties of Candidate Insulating Refractories

Material Name:	Hydrecon Tabcast	Greencast 94	Plicast Cement Free 96 (L-2803)	Plicast 40	L-2825
Manufacturer:	CR-10 LCV BMI	A.P. Green	Plibrico	Plibrico	Plibrico
Max. Temperature					
EC	1760	1870	760	1816	
EF	3200	3400	200	3300	
Composition, wt%					
Al_2O_3	89	95	95	96	99
SiO_2	<1	<1	4	<1	<1
Fe_2O_3	<1	<1	<1	<1	0
TiO_2	<1	0	0	0	0
CaO	1	5	<1	4	0
MgO	0	<1	0	<1	0
Cr_2O_3	10	0	0	0	0
P_2O_5	0	0	0	0	0
Alkalies	<1	<1	<1	<1	0
Thermal Conductivity, Btu in./ft²-EF-hr			18.5	12.0	
500Ef			15.0	11.0	
1000EF			14.2	10.5	
1500EF		9.7	14.0	11.0	
2000EF					
Permanent Linear Change, %					
2000EF (1093EC)	−0.1		−0.3	−0.2	
2500EF (1370EC)		−0.3 to −0.7			
3000EF (1646EC)			−0.1	−0.3	
3200EF (1760EC)				−0.8	
3400EF (1870EC)		−0.5 to −1.5			
Price per pound, $	0.83	1.34	1.19	1.55	

Exhibit 2.2-17
Bulk Composition of Coal Slags Used in Static Corrosion Experiments

Oxide, wt%	Illinois No. 6 (Baldwin Plant)	NSP Rochelle (Riverside Plant)
Na_2O	0	1
MgO	1	6
Al_2O_3	19	19
SiO_2	53	47
P_2O_5	0	<1
SO_3	0	<1
K_2O	2	<1
CaO	7	20
TiO_2	1	1
Fe_2O_3	18	5
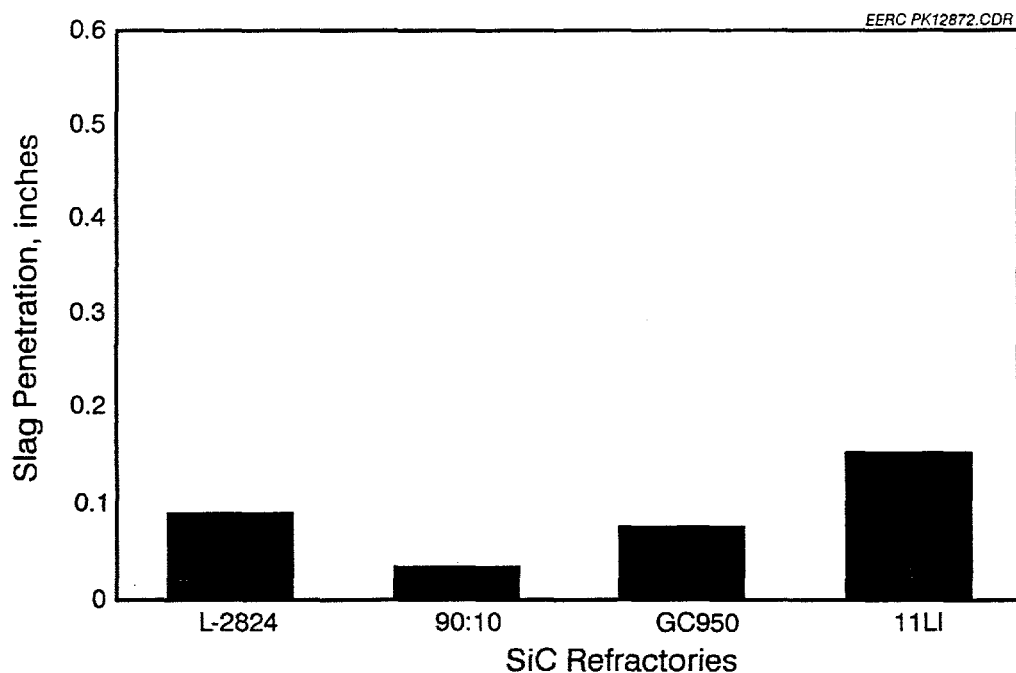
EERC PK12872.CDR

Slag Penetration after the 100-hr Test @ 1430°C with the Illinois No. 6 Baldwin Slag
Exhibit 2.2-18
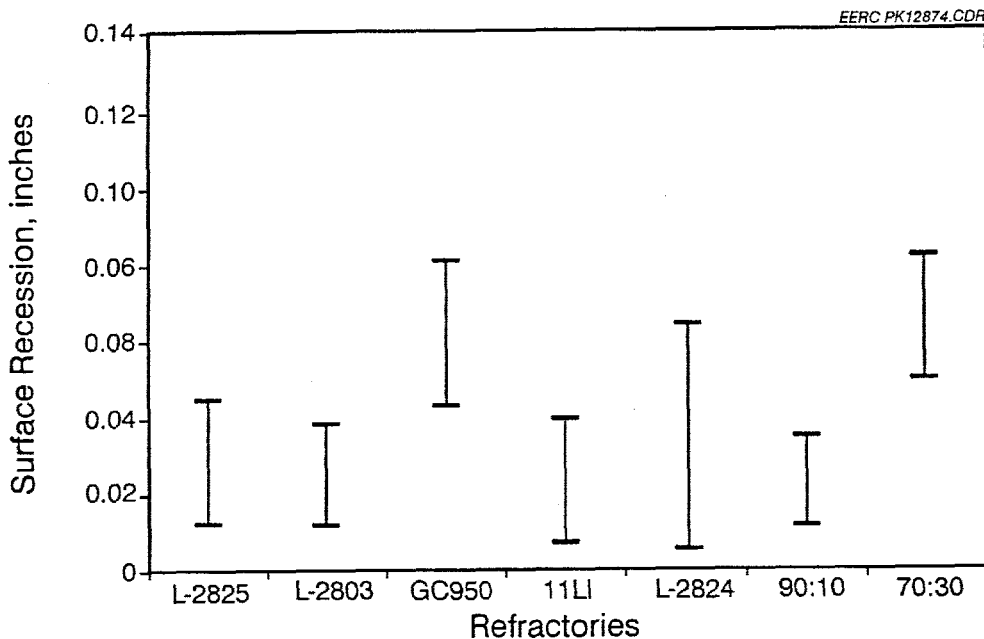
Surface Recession, inches

0.14 —
0.12 —
0.10 —
0.06 —
0.08 —
0.04 —
0.02 —
0 —

L-2825 L-2803 GC950 11LI L-2824 90:10 70:30

Refractories

**Surface Recession after the 100-hr test @ 1430°C with the
Illinois No. 6 Baldwin Slag
Exhibit 2.2-19**

All seven of the SiC-based refractories, plus the two alumina-based refractories, were tested at 1430EC using the Rochelle slag. Exhibit 2.2-20 shows the slag penetration as determined by SEM analysis, and Exhibit 2.2-21 shows the surface recession. With both slags, the experimental SiC:Al_2O_3 - based (90:10) refractory performed the best.

In general, under static conditions at 1430EC, the slag penetration into the experimental 90:10 is less by a factor of two than into the commercially available SiC-based refractories. The slag penetrations into the other experimental refractories are generally similar to the commercial refractories. Surface recession is generally comparable for all the refractories, although the experimental 95:3.5:1.5 has the greatest standard deviation.

Because of the high temperatures expected in the pilot-scale slagging combustor, efforts were focused on finding refractories with higher maximum-use temperatures. These refractories would be used as the insulating lining of the radiant zone of the furnace. Several refractories were identified for this use: Castolast G, Greencast 94, Plicast 40, L-2803 or Plicast Cement Free 96, Descon A98, Hydrecon Tabcast, and Narcocast 60. All of these refractories are alumina-based castables designed for temperatures of at least 1700EC (Tables 3-1 and 3-2). Hydrecon Tabcast also has the addition of 9.5 wt% Cr_2O_3 for better corrosion resistance.
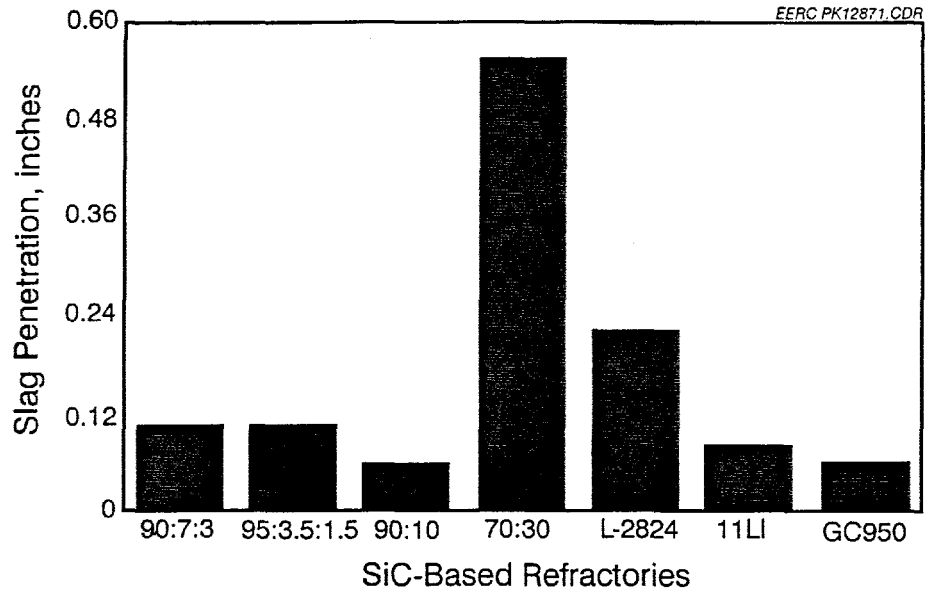
Slag Penetration after the 100-hr test @ 1430°C with the NSP Rochelle Slag
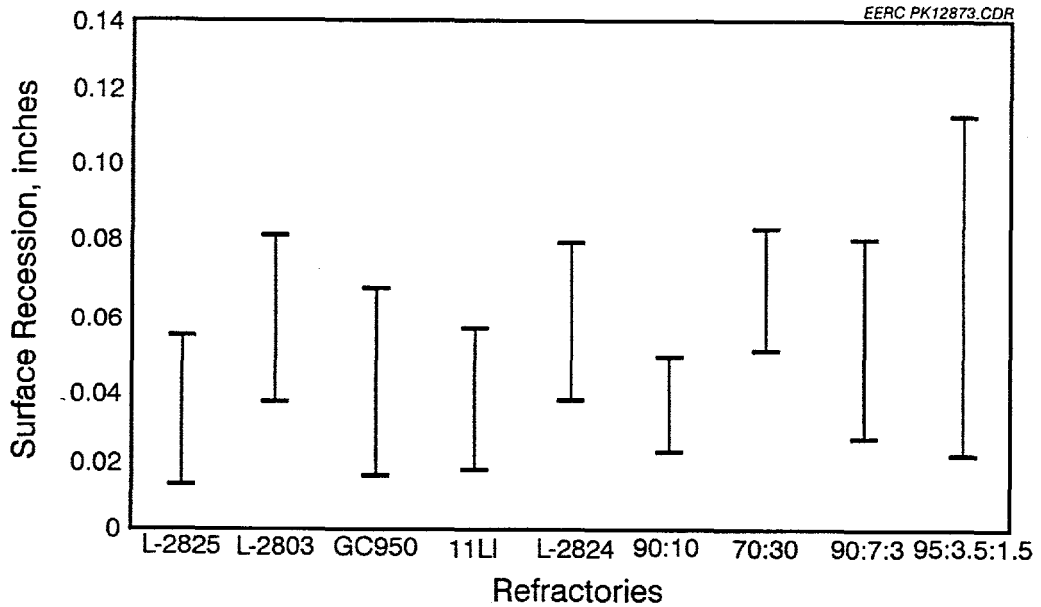
Exhibit 2.2-20

Surface Recession after the 100-hr test @ 1430°C with the NSP Rochelle Slag

Exhibit 2.2-21

A temperature of 1700EC, the expected maximum hot-face temperatures of the pilot-scale slagging combustor, was selected for static corrosion tests based on data from UND EERC engineers. A total of six refractories were tested under static conditions using the Illinois No. 6 slag. Exhibit 2.2-22 and -23 show calculated slag penetrations and shrinkage after the static test.

After firing, the Narcocast 60 refractory showed significant localized microcracks, mainly in the matrix around the large alumina granules. The cracks enlarged with increasing temperatures, from 1550E to 1700EC. In the presence of flowing slag, the cracks would enhance corrosion rates; therefore, this refractory was eliminated for further testing.

Exhibit 2.2-22
Results from 100-hour Static Slag Exposure Test

Material Name:	Descon A98	Castolast G	Greencast 94	Hydrecon Tabcast
Manufacturer:	Harbison–Walker	Harbison–Walker	A.P. Green	BMI
Test Temperature:				
EC	1700	1700	1700	1700
EF	3090	3090	3090	3090
Length of test, hr	100	100	100	100
Visible Slag Penetration:				
Darkest Area	8.12 mm	6.79 mm	6.71 mm	9.08 mm
Lighter Area	9.27 mm	17.85 mm	16.13 mm	7.46 mm
Percent Linear Change, %				
Average (@ 1700EC)	0.51 (shrinkage)	0.43 (shrinkage)	0.2 (expansion)	0.27 (shrinkage)

Exhibit 2.2-23
Results from 100-hour Static Slag Exposure Test

Material Name:	Plicast Cement Free 96	Plicast 40
Manufacturer:	Plibrico	Plibrico
Test Temperature:		
EC	1700	1700
EF	3090	3090
Length of test, hr	100	100
Visible Slag Penetration		
Darkest Area		
Lighter Area	4.58 mm	11.90 mm
	14.78 mm	17.84 mm
Percent Linear Change, %		
Average (@ 1700EC)	1.33 (shrinkage)	0.56 (shrinkage)

SEM analysis was performed on each refractory after the 100-hour static test at 1700EC.

Chemical point analysis was attempted on different areas of the blocks, to compare composition of the refractory before and after slag penetration. The results were highly variable because of instrument fluctuation and other technical difficulties; therefore, the results are not included in this report. However, slag infiltration was determined from SEM photos.

Exhibit 2.2-24 shows photos of Greencast 94, Castolast G, and Plicast 40 after the static slag exposure test. The photo shows distinct layers of discoloration which are darkest next to the slag well and become progressively lighter away from the slag wells. This coloration is caused by the outward diffusion of the slag into the refractory. Air bubbles entrapped in the blocks during preparation are visible as circular void spaces. These may be reduced, or possibly eliminated, by vibrating the material for a longer time.

No surface corrosion is visible on any of these blocks. The erosion of the binder around the larger alumina granules is greatest in the Plicast 40 blocks. This is even more evident in Exhibit 2.2-25, which is an SEM composite micrograph of Plicast 40 after the slag exposure. Well-developed microcracks are visible in the hand specimen and appear worse where slag penetrated the refractory. The cracking indicates a difference in the thermal expansion of the slag and the refractory, which means the refractory may be prone to erosion in the presence of flowing slag. Therefore, Plicast 40 will not be used in the dynamic test.

Visible slag penetration into the Castolast G and Greencast 94 was similar. Microcracks are absent in both, but the Castolast G formed a crack at the interface where slag penetrated the refractory and the underlying unaffected refractory. This may be due to the differences in thermal expansions of the two regions. The cracking appeared to be the only disadvantage with the Castolast G. Greencast 94 also performed well, so both of these refractories will be used in the dynamic test.

Exhibit 2.2-26 shows photos of Plicast Cement Free, Descon A98, and Hydrecon Tabcast after the static test. Plicast Cement Free changed color from grayish-white before firing to reddish-brown after firing. The color change is due to the oxidation of the iron in the refractory mix. The large void spaces are caused by air entrapped during sample preparation. Slag penetration was similar in the Descon A98 and Plicast Cement Free, but the Hydrecon showed almost no slag penetration. Visible surface corrosion is greatest in Plicast Cement Free, and Descon A98 also showed some corrosion. The maximum corrosion is located at the base of the slag well in the corner, where the walls and floor of the well intersect. This may be due to preferential cracking of the refractory in these high-stress regions. Microcracks are not present in either the Plicast Cement Free or Hydrecon Tabcast blocks. Both the Descon A98 and Plicast Cement Free will be used in the dynamic testing.

Hydrecon Tabcast CR-10 LCV (chrome-containing) performed the best of all the refractories tested. However, because of environmental issues related to the disposal of chrome-containing refractories, this refractory will not be included in the initial dynamic corrosion tests. These blocks changed color from bright green before firing to reddish-purple after firing. This color change occurred from the oxidation of the chromium. A dramatic difference in the amount of slag penetration of the Hydrecon Tabcast and the Plicast 40 is evident in Exhibit 2.2-25. Dynamic testing of Castolast G, Descon A98, Plicast Cement Free, and Greencast 94 will begin in the next quarter.
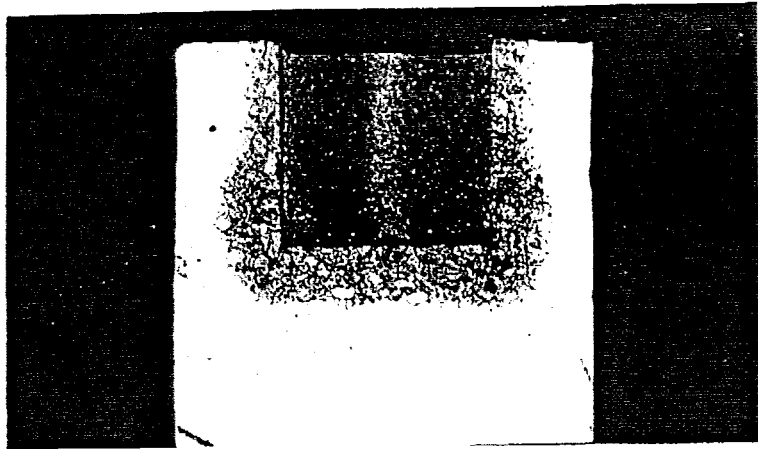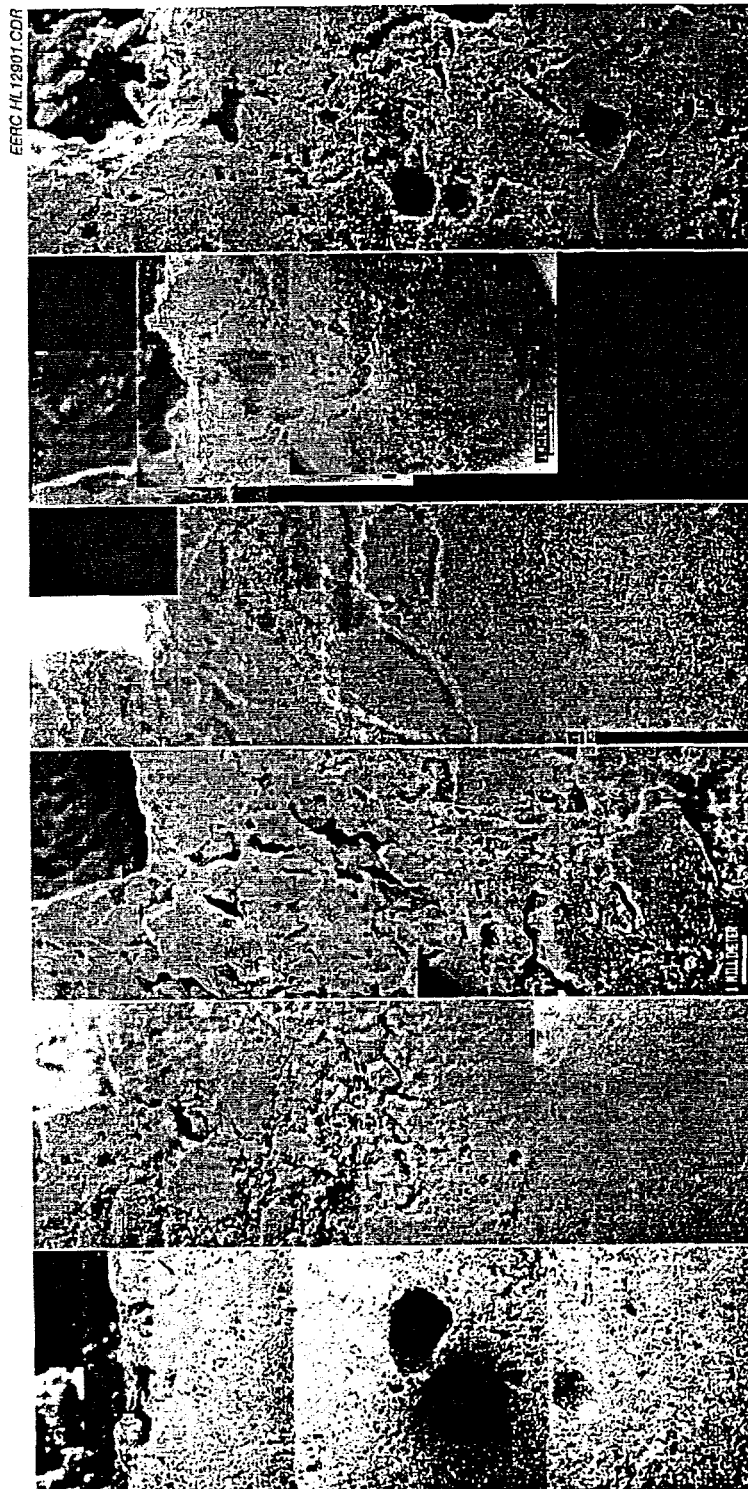
Greencast 94
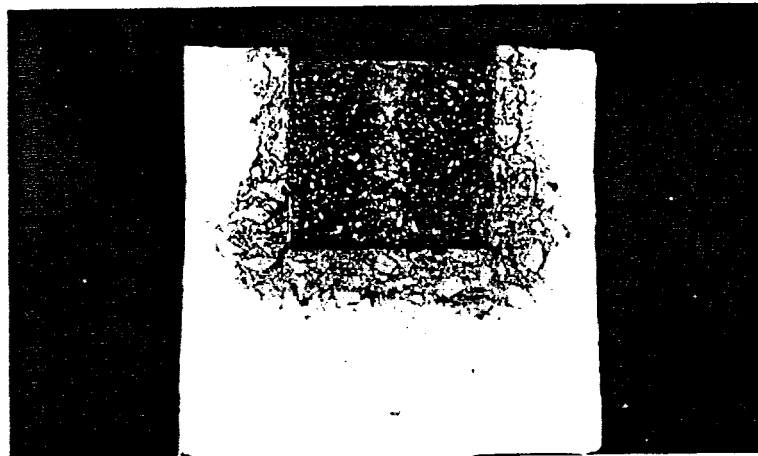
Castolast G
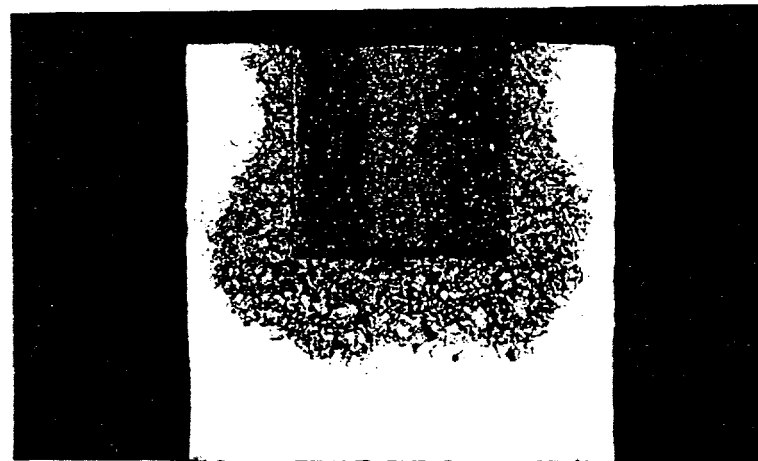
Alumina-Based Castables after 100-hr Exposure at 1700°C using Illinois No. 6 Slag
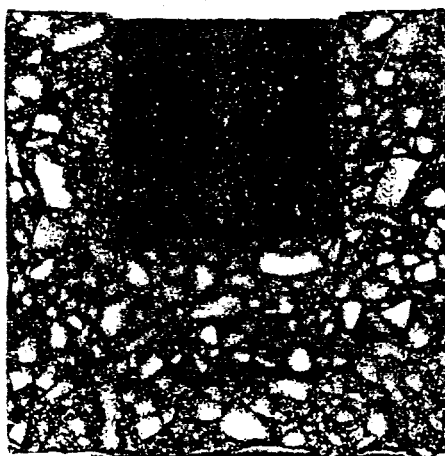Exhibit 2.2-24

Composite SEM Photos of Alumina-Based Refractories after the 100-hr Static Slag Exposure to Illinois No. 6 Slag
Exhibit 2.2-25

Plicast Cement Free
Al$_2$O$_3$ based Castable

Descon A98

Hydrecon Tabcast CR-10 LCV
Alumina-Based Castables and one with 9.5% Cr2O3 (Hydrecon Tabcast)
after 100-hr Exposure at 1700°C
using Illinois No. 6 Slag
Exhibit 2.2-26

Furnace Design

The dynamic slag application furnace (DSAF) was designed and built to simulate conditions of dynamic corrosion on the vertical wall of a refractory-lined slagging combustor. The DSAF is a 23-in. × 23-in., double chamber furnace, with each chamber, 23 in. × 11 in., gliding on rollers away from each other in the open mode (Exhibit 2.2-27 and -28). It has the capability of testing refractory test samples up to a maximum of 1700EC and is designed to handle up to four test samples simultaneously. It uses 14 molybdenum disilicide ($MoSi_2$) heating elements, with a 4-in.-thick insulation wall on the vertical walls and 5-in.-thick insulation wall on the horizontal walls.

Four slag injector feed ports and two view ports are located on the top of the furnace. Each view port is a 6-in.-long 99.8% dense recrystallized alumina ceramic tube with a Vycor™ window at the cold junction and a sapphire window at the high-temperature junction. The injector feed tubes are designed in two stages: a water-cooled stainless steel tubing which goes 2 in. into the furnace insulation and a 4-in. alumina tube which hangs 2 in. into the furnace chamber (Exhibit 2.2-29 and -30).

Two exit ports for the spent slag are located at the bottom of the furnace. These are made of the same material as the view port. The spent slag exits through ceramic tubes into a 24-in. × 27-in. water quench vessel. The quench vessel is equipped with a 6-in. × 10-in. view port. The water level is kept at a constant 1 in. depth with fresh water introduced continuously.

Four thermocouple junctions are located on both sides of the vertical surface wall of the furnace. These thermocouples read the temperature on the vertical wall surface of the refractory test sample. Two additional thermocouples are located 1 in. from the bottom of the furnace that read the temperature of the exit ports. Data from all 12 thermocouples are collected through a data acquisition software at a rate of one data point in every 60 seconds for each thermocouple.

The Ktron™ feeder is a precise low-rate volumetric feeder with a full hopper agitation made of 316 stainless steel material. The Ktron feeder can be controlled by either manual or remote methods. The transfer of the slag granules from the feeder is controlled by a double intermeshing set of augers. At the end of the transfer tube is a custom-designed feeder splitter to perform a 1- to 2- to 4-way split of the slag granules into the four feed injector entry ports, which are connected by high-temperature Tygon™ tubing to the water-cooled stainless steel feed injectors.

For this experimental setup, the feeder was calibrated to deliver a slag area flow rate per unit refractory equal to that projected for the pilot-scale slagging combustor. The calculated value was 51 g of slag through each feed injector entry port during a 1-hour time period, hence a total of 204 g of slag for all four entry ports. The feeder hopper can hold about 50 pounds of slag material or enough for 100 hours of operation.

An air entry port is located on the top of the splitter which is connected to the slag feeder. An air flow rate of 125 cm³/min will be used for each entry port for DSAF experiments. The primary function of the air is to keep the hot air from rising up through these feed entry ports and, secondly, to cause a positive air pressure for both the slag granules and melt to flow down through the exit ports.
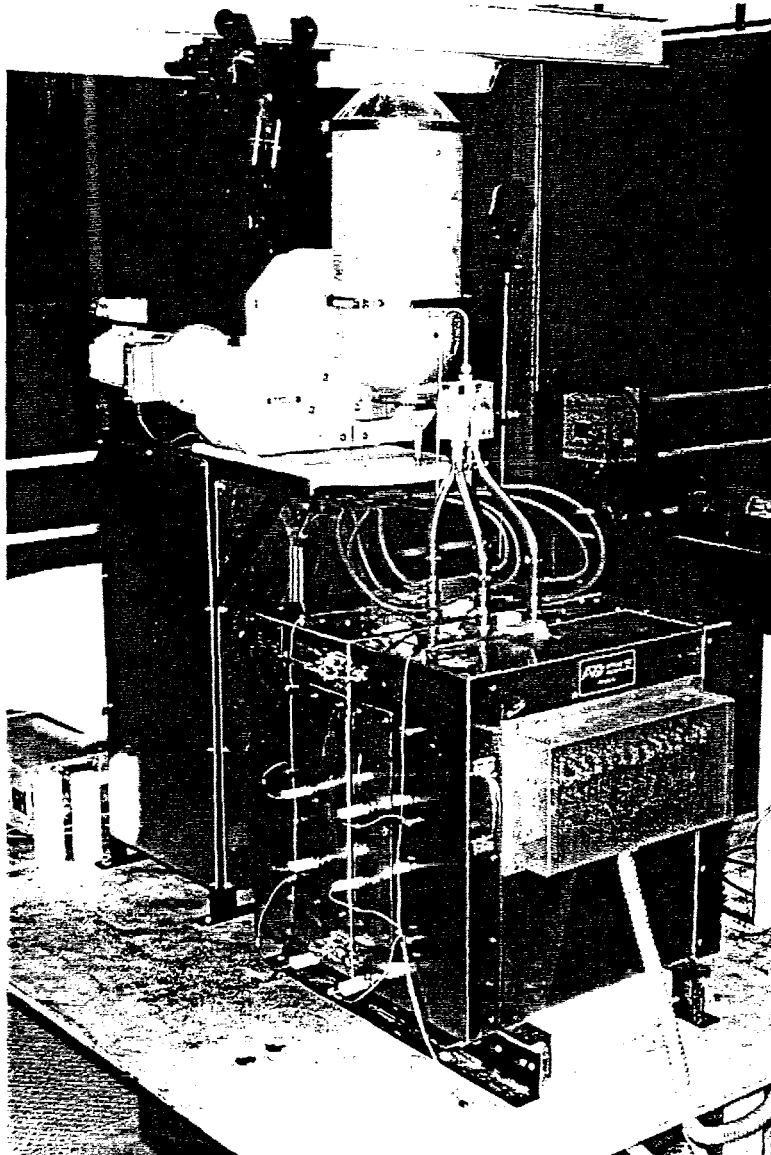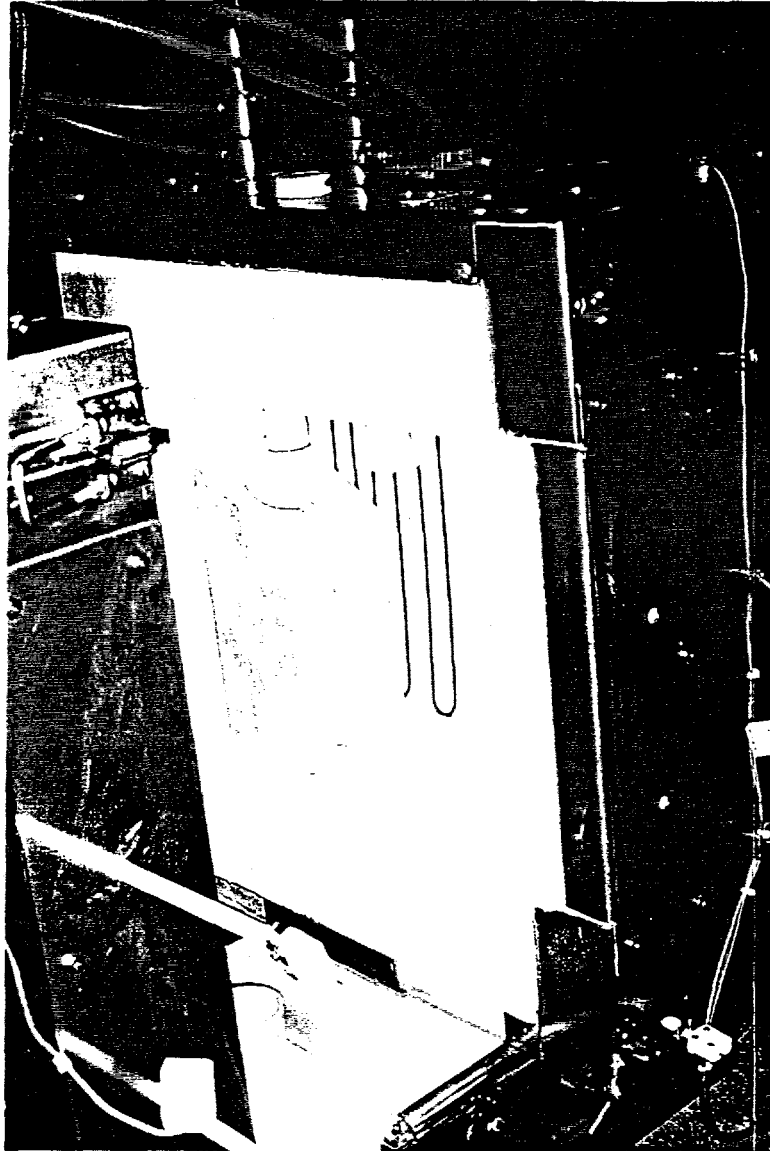
The DSAF Assembly Showing the Furnace and the Slag Feeder
Exhibit 2.2-27
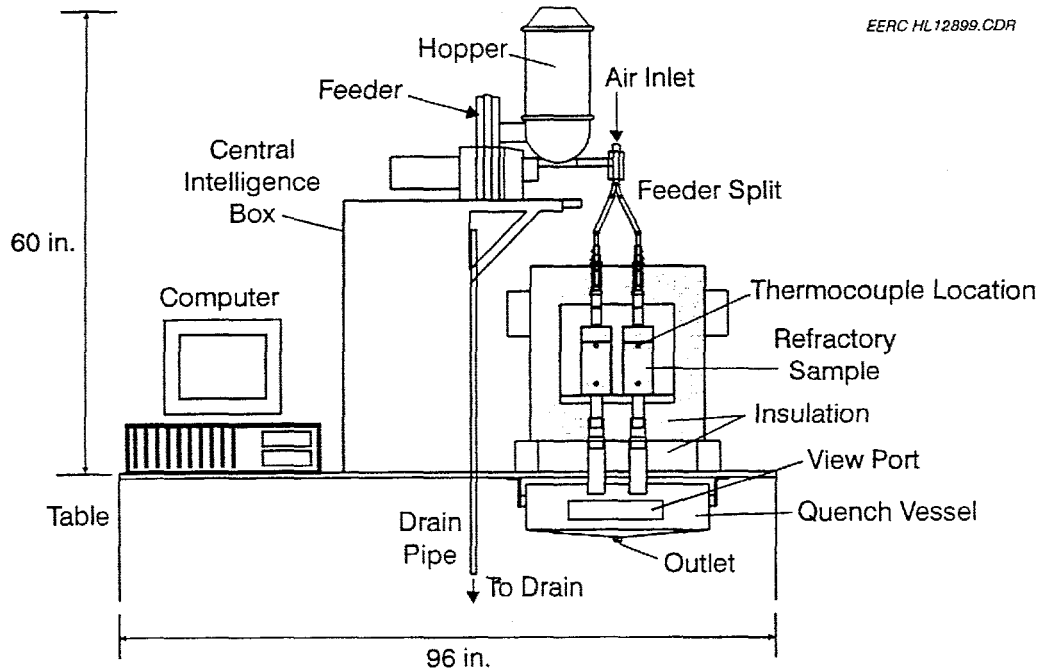
Schematic of DSAF
Exhibit 2.2-28

Legend

A = Thermocouple Location
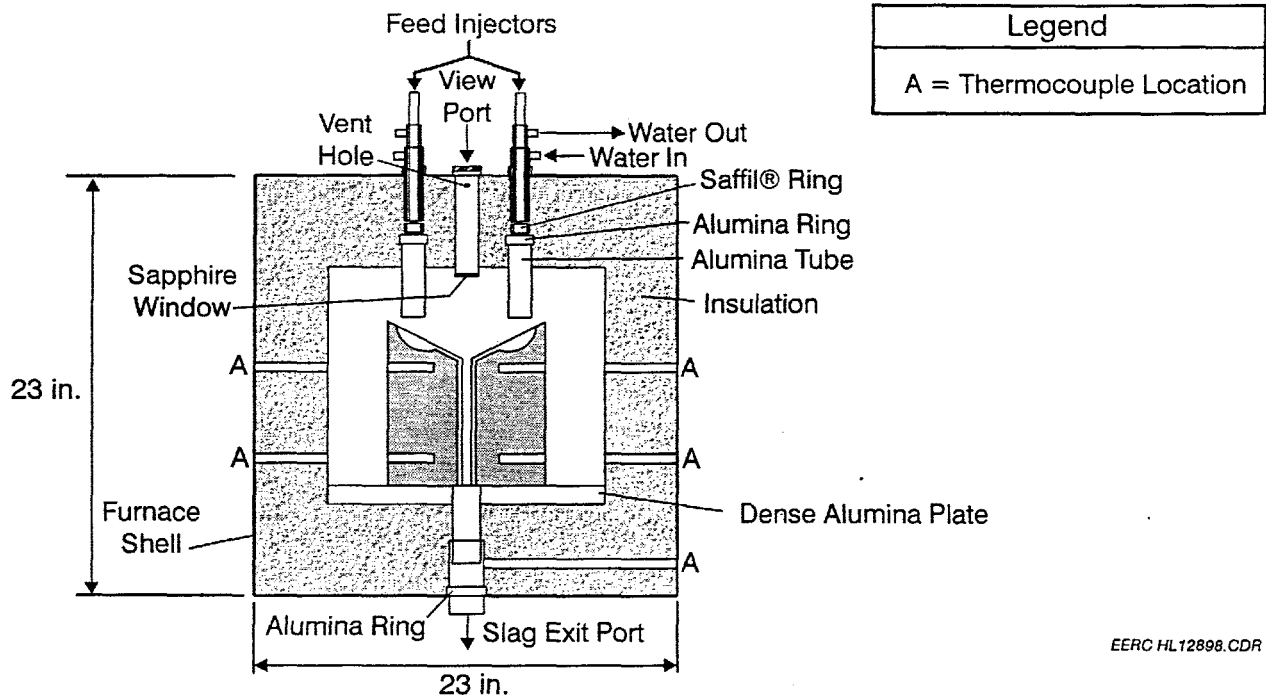
Schematic of the Inside of the DASF with a Sample in Place
Exhibit 2.2-29

Photo Showing a Refractory Sample Inside the DSAF with the Slag Port Above the Sample
Exhibit 2.2-30

Experimental

The refractory test samples are 4 in. × 4 in. × 9 in. tall with a 30 degree incline on the top surface. On this incline surface is a well, 1 in. × 1/8 in. deep, which is drained by a open vertical channel (Exhibit 2.2-30). These refractory samples are placed on a dense alumina plate in the furnace. All the refractory sample was cast in a rubber mold. The rubber mold replicate was made from a wooden mold. Test samples of Castolast G and Descon A98, (Harbison–Walker), Greencast 94, (A.P. Green), Plicast Cement Free 96, (Plibrico) and Hydrecon Tabcast, (BMI) have been made and fired to 1600EC. The preparation of these castable refractory test samples will

always be a challenge, because there is always the possibility of the result of poor packing densities in the final product. The corrosion kinetics will be very difficult to interpret since there will be no easy approach for direct comparison of the data since their physical characteristics will always be different.

A shipment of eight 55-gallon drums of slag from the Illinois Baldwin Plant was crushed and classified this quarter. The slag has been classified to +16 to −20-mesh size. An x-ray fluorescence analysis of the slag has been completed, and the results show that the new slag has a composition identical to the Illinois No. 6 slag used in the static corrosion tests (Exhibit 2.2-17).

Results

An initial 5-hour exposure test of the DSAF was completed at 1600EC on four of the castable refractory samples. The refractories tested include Plicast Cement Free, Descon A98, Greencast 94, and Castolast G. The furnace was heated to 1600EC over 18 hours. The furnace was held at 1600EC for 2 hours before the slag feeder was started. The slag feed rate was 50 g/hour for a total of 250 g/slag per sample for the 5-hour period. The DSAF performed well under these conditions. Slag was observed flowing out of one exit port; however, the other exit ports showed only minor amounts of slag exiting the furnace. The slag feed was stopped, and the furnace was held at 1600EC for 1 hour to allow any residual slag to flow out of the furnace.

After the furnace was cooled to ambient temperature, the DSAF was opened and the refractories examined. Initial observations of the refractories show dramatic differences in the corrosion resistances when compared to the results from the static slag cup test (Exhibit 2.2-31). After testing in the DSAF, the slag dissolved deep holes into the middle of the Descon A98, Greencast 94, and Castolast G refractories. The corrosion and erosion mechanisms which occurred in these samples started from the dissolution of the binder or cement phase of the refractory. Most of the slag penetrated the center of the samples rather than pooling and running down the vertical channel. The Plicast Cement Free showed some dissolution of the binder in the slag well and the vertical channel; however, the slag infiltration was much less than the other samples. Although the refractories did not perform well under the test conditions, the DSAF operated successfully.

During the next quarter, testing in the DSAF will focus on lower, more realistic temperatures (1500EC) for the slagging combustor. Plicast Cement Free, Descon A98, and Greencast 94 samples will be evaluated at this temperature for several hours to determine if the lower temperature will increase the chance for refractory survivability. An additional material, Hydrecon Tabcast (9.5 wt% Cr_2O_3) from BMI, will also be tested. There are some concerns that chrome-containing refractories may pose an environmental disposal problem. The disposal of chrome-containing refractories and the environmental implications will be investigated next quarter.
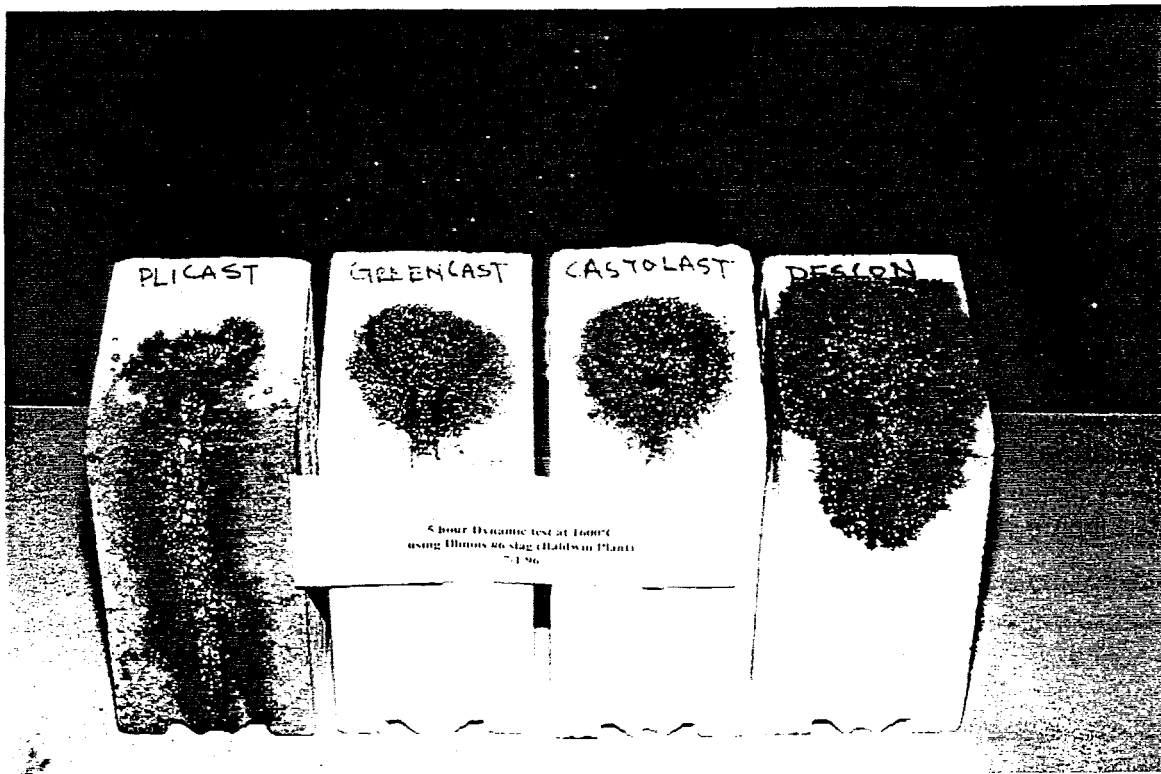
**Photo of the Refractories Tested inthe DSAF for 5 hours at 1600°C**
Exhibit 2.2-31

Metals Selection

Prior alloys under consideration were the nickel-based superalloys, but they did not have sufficient strength and creep resistance at the desired application temperature. The metallic effort is now focused on the family of oxide-dispersion strengthened alloys produced by mechanically alloying. Mechanically alloying is a dry, high energy milling operation that produces composite metal powders with controlled, extremely fine microstructures. During the processing of the powders, various metal powder particles are trapped between the rapidly colliding grinding balls and, under the controlled conditions of mechanically alloying, the powders are cold-welded together.

Mechanically alloyed powders are consolidated by placing them into sealed cans for extrusion or hot pressing, followed by conventional hot and cold working processes. Exhibit 2.2-32 shows a MA- 758 tube, approximately 2.5 inches in diameter. The wall thickness is approximately one quarter of an inch. The tubes are seamless and can be produced in forty foot lengths.

The composition of the candidate MA alloys being considered for the RAH are listed in Exhibit 2.2-33. The principal alloying element is chromium which imparts oxidation and corrosion resistance. The oxide dispersion imparts strength.
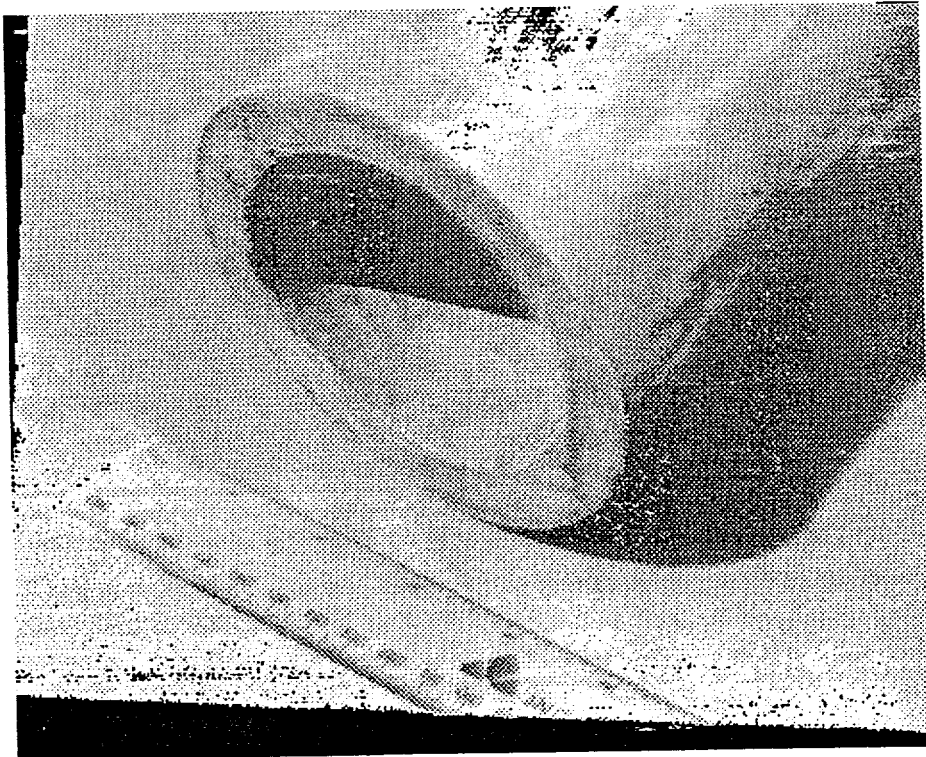

MA-758 Extruded Tubing
Exhibit 2.2-32

Exhibit 2.2-33
Chemical Composition of Candidate Alloys (Vendor Data)

	Concentration Wt. %						
Alloy	Nickel	Chromium	Carbon	Aluminum	Titanium	Yttria	Iron
MA-754	Bal	20	0.05	0.3	0.5	0.6	1
MA-758	Bal	30	0.05	0.3	0.5	0.6	1

The initial alloys chosen for the RAH were based on the family of cast nickel base alloys. These alloys were developed for the gas turbine engines that are employed in flight as well as in the industrial and marine applications. Although the alloys are extremely strong over a wide temperature range, the MA alloys exhibit superior strengths at the highest temperatures. Equally important, the processing of the MA alloys is not only easier but is more cost effective. A comparison of the stress rupture properties of the MA alloys versus the nickel base superalloys is shown in Exhibit 2.2-34.
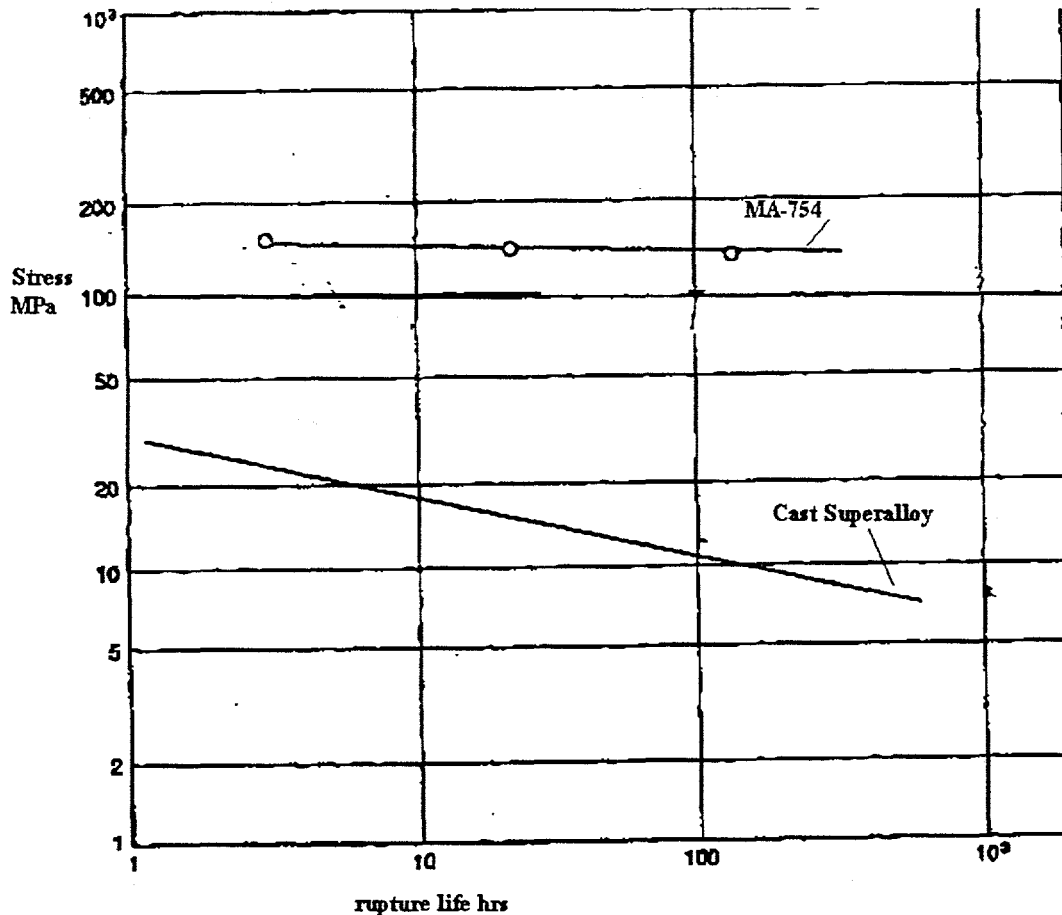
Stress Rupture Comparisons At 1100°C (Literature Data)
Exhibit 2.2-34

The bulk of the effort during this reporting period was directed at defining the long term oxidation properties of the MA alloys. Coupons of MA-754 and MA-758 were exposed for durations up to 900 hours at 1000, 1100, 1200 and 1300°C. The specimens were periodically

removed from the furnaces in order to accumulate the weight change data which are reproduced in Exhibit 2.2-35 and -36. Initially the alloys exhibited positive weight gains, but characteristic of all high temperature structural alloys, the oxide scales spall. The annual regression rate according to the National Association of Corrosion Engineers (NACE) should not exceed 0.5 mm (0.020 in.) per year. The time, in hours for each of the alloys to exhibit a regression rate of 0.5 mm /yr. is shown in Exhibit 2.2-37. It is apparent that both alloys meet the current requirements.
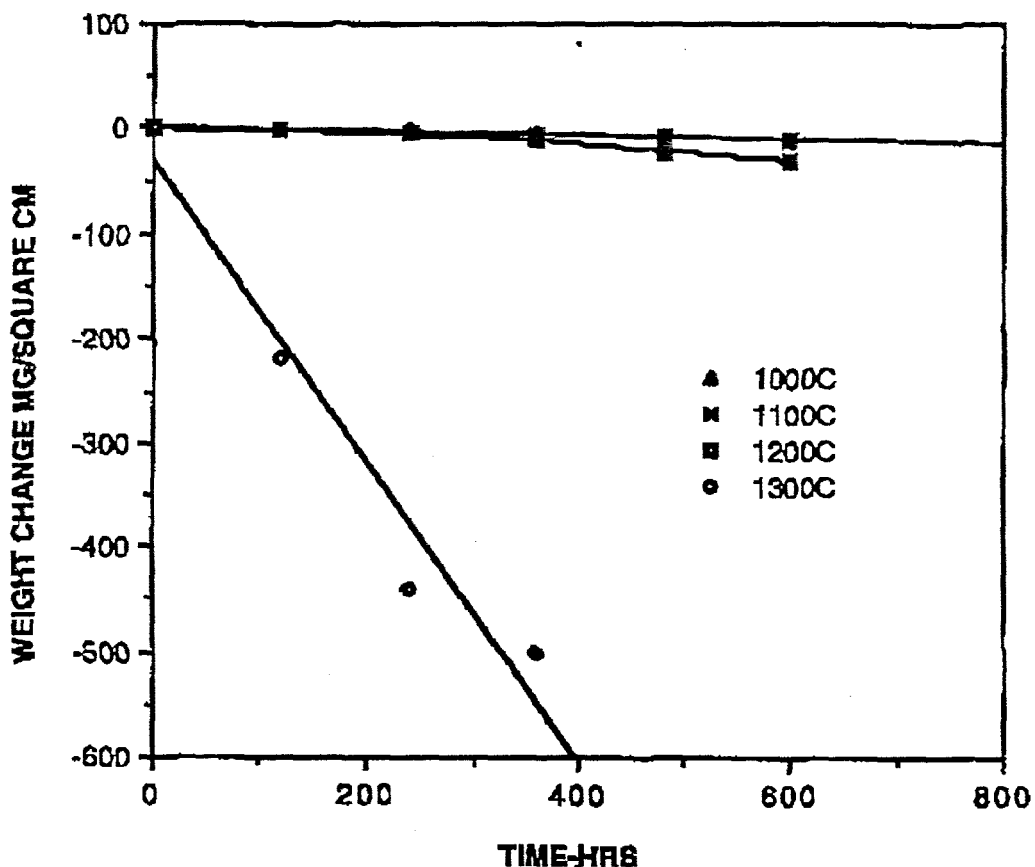
Oxidation of MA-754 (UTRC Data)
Exhibit 2.2-35

Exhibit 2.2-37
Calculated Time, Hours for 0.5 mm Loss at C

	Time, hours for loss of 0.5 mm			
Alloy	1000°C	1100°C	1200°C	1300°C
MA-754	24,900 hr.	22,700 hr.	8,000 hr.	300 hr.
MA-758	53,800 hr.	31,400 hr.	10,800 hr.	1,500 hr.

WEIGHT CHANGE MG/SQUARE CM

100

0

-100

-200

-300

0   200   400   600   800   1000

TIME HOURS

□ 1000C
● 1100C
■ 1200C
◇ 1300C
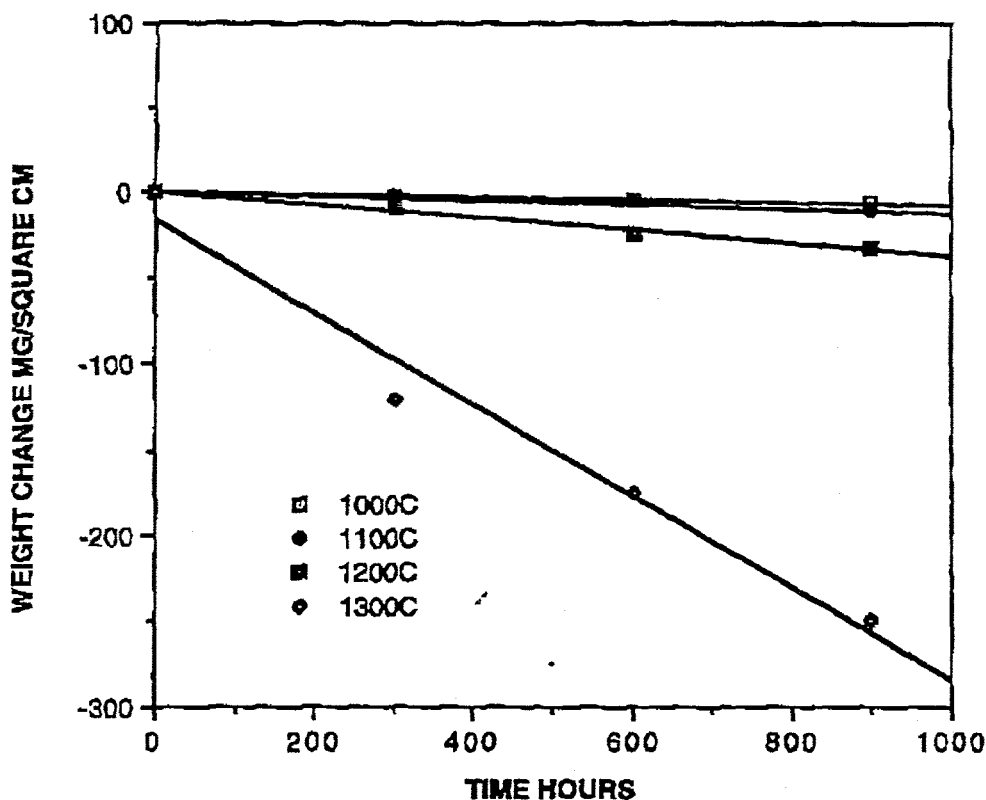
Oxidation of MA-758 (UTRC Data)
Exhibit 2.2-36

Ceramics for the RAH Lining

Initial Refractory Ceramic Candidate Selection

As discussed in the previous quarterly report, an initial selection of refractory candidates was made which was based primarily on the results of a 100 hour coal combustor/heat exchanger rig test conducted during the Phase I portion of the HIPPS program. This test identified several material families which showed promise for the RAH application, while also indicating which families of materials were not worth further consideration.

The materials which performed poorly in the 100 hour test included bonded fused grain alumina, bonded fused grain alumina-zirconia-silica (AZS), and the two castables: mullite bonded silicon carbide, and alumina bonded silicon carbide. Excessive infiltration, corrosion and erosion by the molten coal slags were evident. The interested reader is referred to the topical report written on this test. These families of materials just described were not considered for Phase II.

From the corrosion test results, all three of the fusion cast refractories performed well, including fusion cast α/β alumina, AZS, and 30% chromia-alumina. Bonded fused grain 30% chromia-alumina also held up to corrosion well. Both chrome oxide containing materials formed complex iron oxide/chrome oxide/aluminum oxide reaction layers which appeared to inhibit further corrosion. Based on these results, a broad list of potential refractory lining materials was compiled, which included the entire family of bonded fused grain chromia-alumina materials (from Harbison Walker), as well as fusion cast aluminas (Carborundum A2, Corhart SR504C), α/β

aluminas (Carborundum Monofrax M, Corhart Jargal M), fusion cast chrome oxide containing refractories (Carborundum Monofrax E and K3, and Corhart ER2161), and several fusion cast AZS materials (Carborundum Monofrax S-3, S-4, S-5, and Corhart Unicore I and Unicore 501). This initial list of 14 candidate materials was made as broad as possible in order to select those few materials which would best meet the following requirements:

1. High thermal conductivity,
2. High resistance to coal ash corrosion,
3. High emissivity (or ability to be coated for high emissivity),
4. Good thermal shock resistance,
5. Ability to be shaped and mechanically attached,
6. Service temperature,
7. Mechanical and structural integrity at use temperature,
8. Manufacturing cost.

By reviewing and evaluating the above mentioned requirements for each of the 14 candidate materials using the available information from the vendors and the technical literature, the total number of candidates was further reduced to 6 of the most promising compositions, which are:

1. Jargal M and Monofrax M (α/β Al_2O_3),
2. Monofrax E (78Cr/Al oxide),
3. Monofrax K-3 (27Cr/Al oxide),
4. Monofrax S-4 (alumina/zirconia/silicate),
5. Monofrax A-2 (α-Al_2O_3),
6. SR-504C (Ca-modified Al_2O_3).

These six candidates were further evaluated during this reporting period by reviewing or gathering additional, and more detailed property or performance data, in order to select the best single candidate for the lining. This evaluation process is on going and is discussed next.

Two of the candidate materials, SR-504C from Corhart, and Monofrax A-2, from Carborundum, are no longer in production, but their compositions, high thermal conductivities and past performance as high-temperature, corrosion-resistant materials, makes them attractive candidates; and more data and samples have been requested from the vendors. If there is sufficient demand for these compositions, they probably could be manufactured again. However, their corrosion resistances are not as good as the other candidate materials.

Evaluation of Downselected Materials Candidates

In order to further evaluate the downselected materials, it was necessary to gather or generate additional data, since much of the information on properties such as flexural strength, thermal conductivity, and emissivity were not available, or the accuracy of some of the data was questionable. In addition, data on the long term corrosion resistance of these materials in slag contact under conditions that simulate the RAH operating conditions is critical information that is not yet available. The progress in the gathering of the relevant data is summarized next.

Four-Point Flexural Testing

Specimens 3" x 0.65" x 0.30" (76 x 16.6 x 7.6 mm) were machined from samples supplied by the vendors. The materials included Jargal M, Monofrax E, Monofrax K-3, and a composition similar to Monofrax S-4. The tests were conducted over a range of temperatures from ambient to 2500°F (1370°C). Exhibit 2.2-38 compares the flexure strength of the 4 materials from room temperature to 2500°F. While the AZS samples were the strongest at room temperature, they were also the weakest at temperatures above 2400°F. This was due to a large amount of glassy phase in the composition, which softens at the service temperature in order to accommodate the erratic thermal expansion behavior of the zirconia phase, and which enhances the deformation of the material under load, as shown in Figure 6. The Jargal M, which contains 95% Al_2O_3 is essentially free of glass, and while it was the lowest in strength at room temperature, it retained its strength up to 2500°F and was one of the strongest of the 4 materials tested at temperatures above 2400°F, as shown in Exhibit 2.2-38 and -39. The strength of the chrome/alumina samples, which contain complex magnesia-chrome-alumina spinel and other phases (Monofrax E and K-3), were intermediate at room temperature. With increasing temperature, the strength of the Monofrax E samples decreased slightly in strength up to 2400°F, while the strength of the high (78%) chrome sample (Monofrax K-3) was greatly reduced at this temperature (Exhibit 2.2-38). Both of these materials contain a glassy phase; the Monofrax K-3 contains the largest amount of glass (about 5% glass). The load/deflection (calculated stress-strain) curves of the four materials are compared in Exhibit 2.2-39.

The values of elastic modulus as in function temperature were critical for design considerations, and E vs. T are compared in Exhibit 2.2-40. The elastic modulus of both the Monofrax E and the Jargal M samples changed (increased) slightly with increasing temperatures up to 2400°F, where as the moduli of the Monofrax E and the AZS samples decreased significantly at temperatures above 1800 - 2000°F.
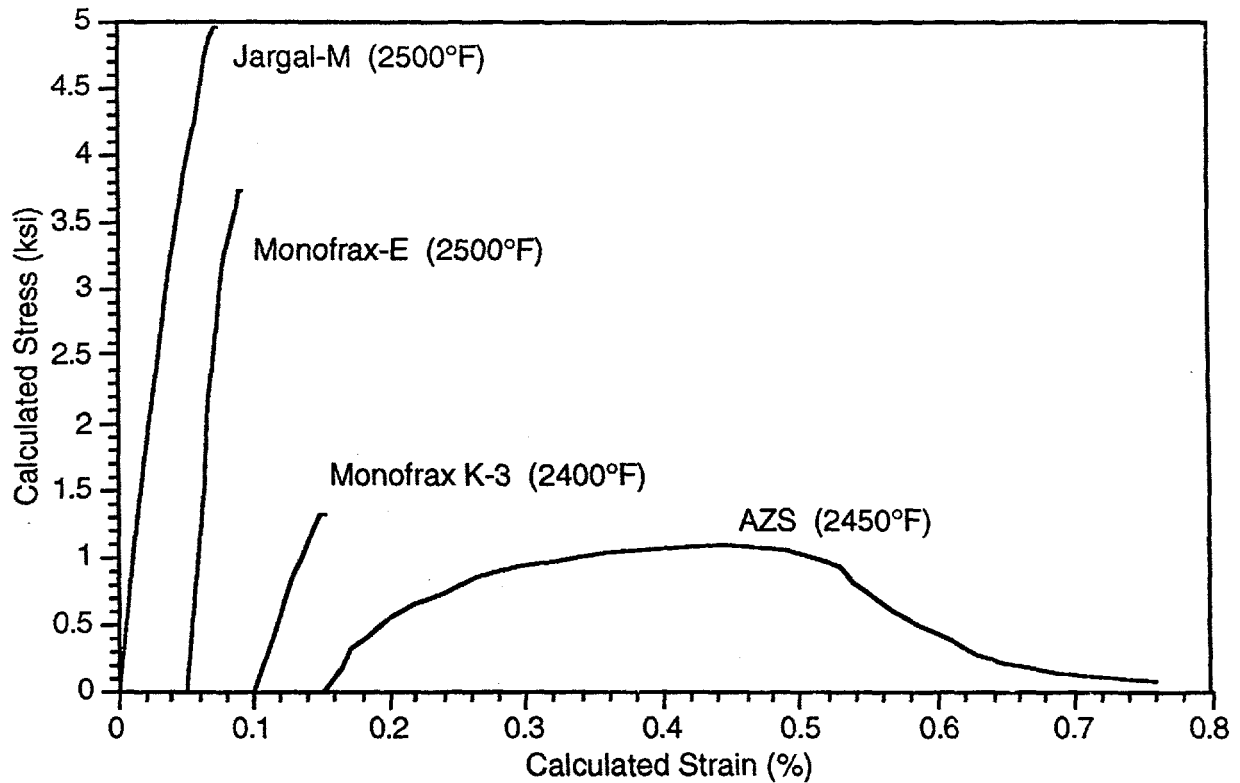
Thermal Conductivity Measurements

Since the effectiveness of the design of the refractory lining for the RAH is dependent on accurate values of thermal conductivity, a brief review was conducted on the available thermal conductivity data for the candidate materials and on the measurement techniques used to generate the data. Of the five common methods to measure thermal conductivity, which include: 1) dynamic radial heat flow, 2) laser flash, 3) hot wire, 4) guarded hot plate, and 5) calorimeter; method 5 was considered to be the most reliable. Each of the measurement techniques has certain advantages over the others [1], but the method for obtaining the most reliable data for thick [> 2" (51 mm)] refractory samples with heterogeneous phases and relatively large pores and grain sizes is based on the calorimetric method commonly used for refractory brick (ASTM C201)[2]. The available thermal conductivity data for Jargal M, and Monofrax E, K-3, and S-4 were measured by the laser flash method [3]. Therefore it was decided to obtain additional samples of these materials and have the thermal conductivity measured by the calorimeter technique. Several organizations were contacted which provide thermal conductivity measurements. A summary of the contacts and results are presented in Exhibit 2.2-41. Of the organizations listed in this table, only Harbison Walker and the ORTON Foundation have the capability to provide the calorimetric thermal conductivity test. Plans are underway to have test performed starting in the next Quarter.
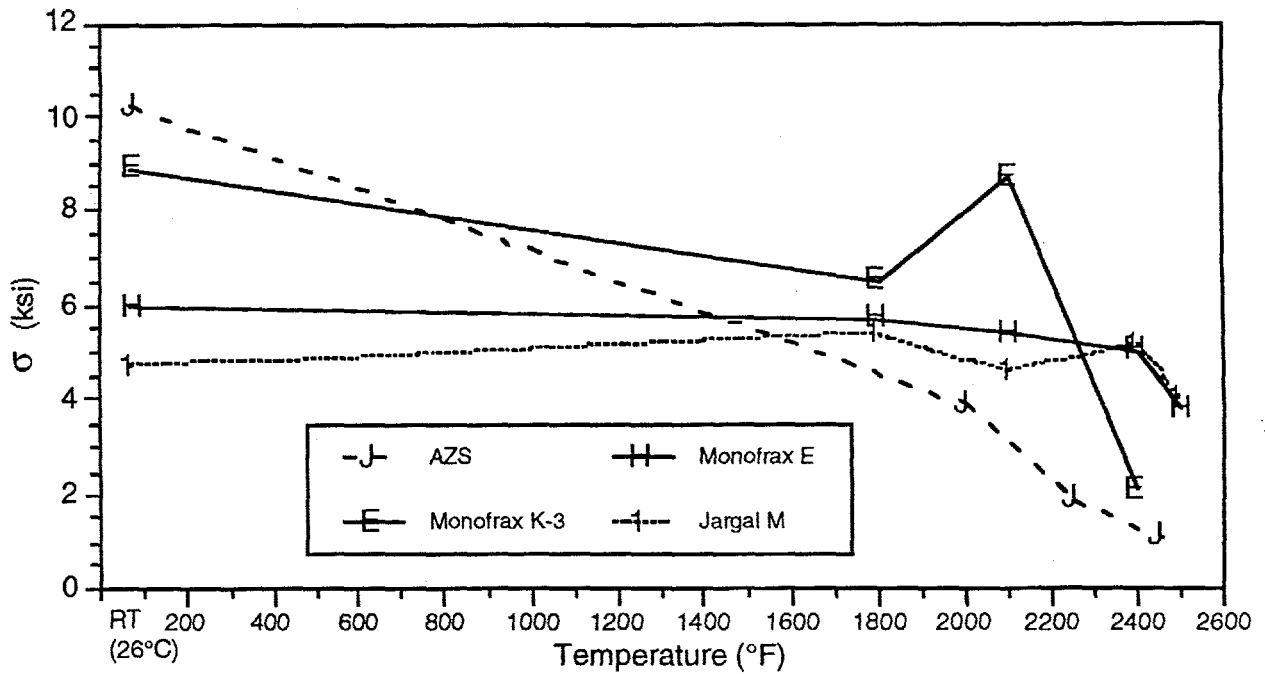
Comparison Of 4-Point Flexure Strength Of Refractory Materials At Temperatures Up To 2500°F
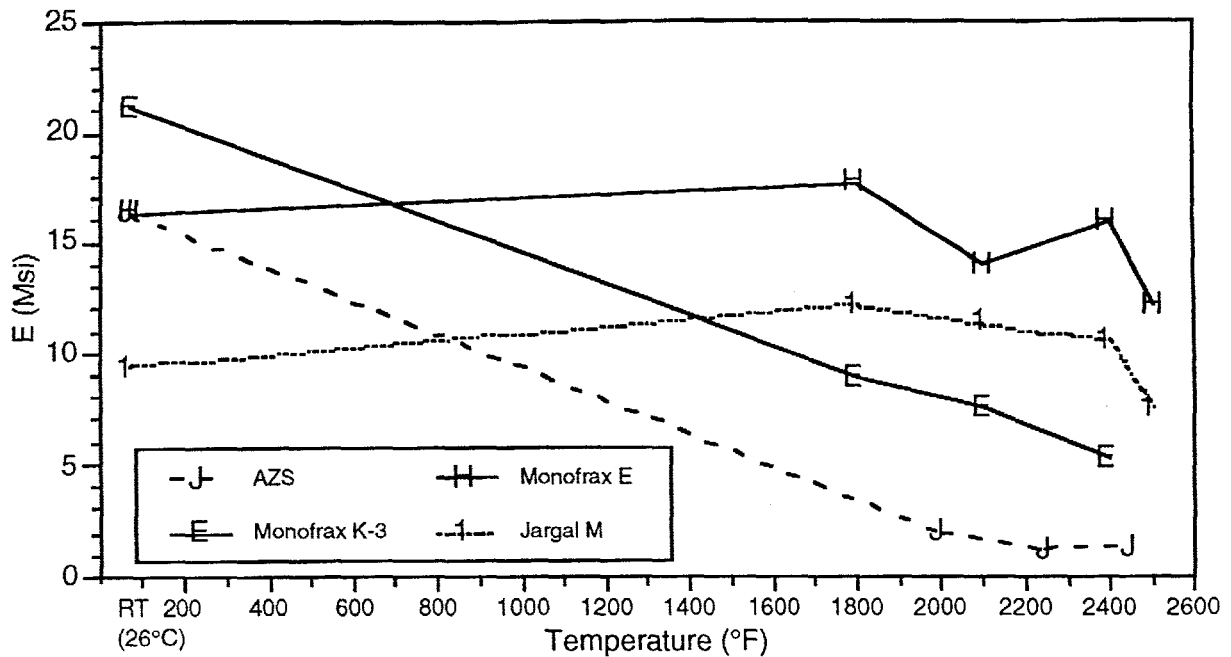
Exhibit 2.2-38

Comparison Of Calculated Stress-Strain Curves From 4-Point Flexure Tests For Several Refractory Materials

Exhibit 2.2-39

Exhibit 2.2-41
Sources for Thermal Conductivity Measurements on Refractories

Source	Type Test	Contact
ORNL - High Temp. Materials Lab	1) <u>Laser Flash</u> - (new $250 K unit); -100 to 2500°C; meas. in air, vacuum, inert gas; unit holds 6 samples in turret 2) <u>Xeon Flash</u> - near room temp. measurements 3) <u>3-Omega</u> - Deposit electrodes on sample (for smooth surface & thin films, to 500°C) 4) <u>Scanning Microscope Thermal Conductivity Probe</u> - based on ORNL design of modified atomic force microscope; tip is thermocouple head; bring different phases to constant temperature. Excellent for fiber composites & multiphase mat'ls 5) <u>Amber IR Camera</u> - detect DT to 0.015°C. Very rapid scan; sample size 1 ft. x 1 ft. down to 1 mm x 1 mm (special focusing lenses)	Dr. Arvid Posto, Director (423) 574-5123 Dr. Ralph Dinwadde (Thermal Cond. Expert) (423) 574-7599
Penn. State	1) <u>Laser Flash</u> - (purchased for large NASA contract on composites) 2) <u>Simple Thermal Conductivity Unit</u> - (for students; used for scanning materials)	Dr. Carlo Pantano (814) 863-2071 (responsible for mat'ls characterization)
Harbison Walker	1) <u>Calorimetric Thermal Conductivity</u> - (meas. full brick size 9" x 4™" x 1 - 2", max. face temp. 2600 - 2800°F). Best method for determining k for refractory brick and other linings. H/W has been measuring thermal conductivity for over 30 years, using ASTM C-201, and has excellent reputation in this area. Test takes 7 - 9 days/sample 2) <u>Hot Wire Method</u> - used in refractory development programs (comparative data) 3) <u>Slag Drip Tests</u> - 4 furnaces for this service (hot slag dripped on heated refractories)	Dave Stiles (Refractory Materials & Furnace Design) (412) 562-6595 Tom Kleeb (H/W Contract Services) (412) 469-6103 (member of ASTM Committee C-201) Leigh Brooks (Thermal Conductivity Expert; Physics Group) (412) 469-6136
ORTON Foundation (Westerville, Ohio)	1) <u>Calorimetric Thermal Conductivity Testing</u> - (ASTM C-201) Hot face temperatures 2600 - 2800°F, sample size: std. 9 x 4™ x 2™" brick or fusion cast slab 18" x 13™" x 1 - 2" 2) <u>Hot Wire Method</u> - (ASTM C11-13) to 1200°C (2192°F) 3) <u>Radial Heat Flow</u> - to 1200°C (2192°F) sample - 2•" dia. x 5" long cylinder	Dr. Joe Homeny (614) 895-2663 x23

Comparison of elastic modulus (4-point flex) of refractory materials at temperatures up to 2500°F.
Exhibit 2.2-40

Corrosion Testing

A critical factor in the selection of the best refractory lining material is the development of a data base on the corrosion resistance of the lining in order to assure a long term (up to 20,000 hours, eventually) service life. A testing protocol has been developed, which follows a progression for testing refractory materials from short term laboratory tests to increasing longer terms and more severe conditions that approach the RAH service conditions. Five corrosion testing rigs are included in the plan, and the features and characteristics of each test is described in Exhibit 2.2-42. During this Quarter, an ash dipping corrosion tester was designed and assembled. This unit will be capable of immersing 4 refractory samples into a crucible containing the molten slag, and then raising the samples and allowing the slag to drip off. This cycle can be repeated automatically for several hundreds of hours. A second corrosion test was set up using a modified Dills burner rig, whereby dry ash is injected into a flame, melted and allowed to impinge and flow over the surface of the sample, where the front face is heated to 2600°F and above, and at the same time where the back surface can be cooled so that a thermal gradient that simulates RAH conditions can be achieved. Progress on the testing and results will be reported in the next Quarter.

Exhibit 2.2-42
Planned Corrosion Rig Tests for C2000 RAH Lining Materials and RAH Materials

| Test Particulars	UNDEERC Ash Exposure Furnace (H Larmie)	UTRC Ash Dipping System (J. Holowczak/ N. Bornstein)	UTRC Modified Dills Burner Rig (H. Eaton)	UNDEERC 2 MM Btu/Hr HITAF Demonstrator (TBD)	ABB 50 MM Btu/Hr Upfired Combustor (TBD)
Facility Description 1. General 2. Size 3. BTU/Hr 4. Max. Temp. 5. Sample Size 6. Technician Req.	1. Electrically heated air furn-ace w/4 top ash feeder(s) and 2 exit ports 2. 3.6 cu. ft. (0.1 cu. meter) 3. N/A 4. 1700°C(3100°C) 5. Four 4" x 4" x 9" 6. Check briefly every 2 days	1. Electrically heated air furnace w/ molten ash in crucible 2. 2 cu. ft. (0.06 cu. meter) 3. N/A 4. 1600°C 5. Four 0.5"x0.5" x 2" 6. Check every 2 days	1. Dills burner rig run on liquid fuel with dry ash feed into flame 2. 8 cu ft (0.2 cu meter) 3. 500 kBTU/hr 4. 1800°C 5. Six 6" x 3" x 1.5 " 6. Technician present at all times	1. Down PC-fired combustion system for RAH & CAH testing 2. 4 ft diameter 3. 3 MM Btu/hr 4. 1600°C 5. RAH: One 1' x 6' panel, four 1'x 1' panels, CAH: nine 2" tubes 6. Two technicians at all times	1. Upfired PC combustion system w/RAH test panels installed 2. 3. 50 MM Btu/hr 4. 5. RAH: Two 30" x 20 ' subscale RAH panels 6. Technician intensive
Ash Application Method 1. Feed 2. Inlet Temp. 3. Flow Rate	1. Overhead screw feeder(s) 2. Room temp. 3. Adjustable, continuous	1. Liquid ash in crucible (260 cu. cm) 2. 1450°C 3. Drips off via gravity	1. Dry ash fed into flame, prior to impact on samples 2. 1450°C 3. Adjustable	1. Generated via coal combustion 2. Furnace temp. 3. Continuous	1. Generated via coal combustion 2. Furnace temp. 3. Continuous
Ability to Simulate RAH Conditions (see also Ash Application above) 1. Refractory surface temp. 2. Delta T through Refractory 3. Gas Environment 4. Test Longevity	1. 1450°C (adjustable) 2. None 3. Only those species adsorbed during initial ash generation 4. Up to 5% of expected RAH life	1. 1450°C (adjustable) 2. None 3. Potential to add controlled atmosphere 4. Up to 5% of expected RAH life	1. 1500°C+ 2. Backside of samples cooled to 1100°C 3. Can dope with sulfur, alkali, etc. 4. Brief (< 5 hr)	1. 1425°C 2. 220°C (400°F) 3. Flue gas, very similar to full scale RAH 4. Several 100 hr tests	1. 1425°C ? 2. 220°C (400°F) 3. Flue gas, very similar to full scale RAH 4. Several 100 hr tests

Test Particulars	UNDEERC Ash Exposure Furnace (H Larmie)	UTRC Ash Dipping System (J. Holowczak/ N. Bornstein)	UTRC Modified Dills Burner Rig (H. Eaton)	UNDEERC 2 MM Btu/Hr HITAF Demonstrator (TBD)	ABB 50 MM Btu/Hr Upfired Combustor (TBD)
Advantages	- Operates with minimal monitoring - Low cost - Flowing slag cont. refreshed - Test periods up to 5% RAH lifetime	- Operates with minimal monitoring - Low cost - Ash shear rate at surface similar to RAH - Test periods up to 5% RAH lifetime - Possibly modified for controlled atmosphere	- Provides kinetic data by testing ABOVE expected RAH temps - Has provision for imposing thermal gradient on samples - Can dope fuel w/gas species	- Accurately simulates full scale RAH - Lower running costs than larger scale test systems - Flexible operating conditions	- Accurately simulates full scale RAH - Flexible operating conditions - Reduced scale up uncertainties
Disadvantages	- Poor temp. uniformity? - Cool ash feed - No temp gradient - Min. gas species present	- Ash not refreshed - No temp. gradient - Min. gas species present - Possible chromia & alumina pick-up from crucible	- Expensive to run - Short run time - High gas velocity - Potential thermal shock of samples	- Expensive to run (compared to lab scale tests) - High cost limits total run time - Scale up uncertainties	- Expensive to run (compared to lab scale tests) - High cost limits total run time - Scale up uncertainties

Emissivity

There are no available data on the emissivity of the refractory candidates listed in Exhibit 2.2-43 or on the metallic heat exchanger tubes. Therefore, arrangements have been made to have the measurements taken at a nearby P&W laboratory. The emittance measurements of various surfaces at high temperatures will be made using a Thermogage emissometer shown schematically in Exhibit 2.2-44. The test specimen is mounted on a graphite rod connected to a hydraulic actuator. This allows the specimen to be translated rapidly from the center of the black body furnace where it is surrounded by hot walls, to the end of the furnace where the sample surroundings are cool. A radiometer is positioned so that it can view the test specimen at both locations. A broad spectrum radiometer is used to obtain "total normal" emittance, while a narrow spectral band radiometer is used to obtain data in a particular spectral band. The output from the radiometer is connected to a digital oscilloscope to record data taken during emittance testing.

The test procedure is as follows. The sample is brought up to the test temperature and allowed to equilibrate within the black body. The radiometer is positioned to obtain data and a trace on the oscilloscope is triggered. The radiometer is then shuttered (to obtain a zero energy base line). It is then unshuttered, the black body energy measured, and then the specimen is propelled out to the end fast enough that the change in specimen temperature is negligible. The emissivity of the specimen is calculated from the ratio of the energy emitted by the specimen at the end of the tube to

the energy emitted by the specimen inside the black body. The refractory ceramics are to be tested in both "as cast" and machined surface conditions.
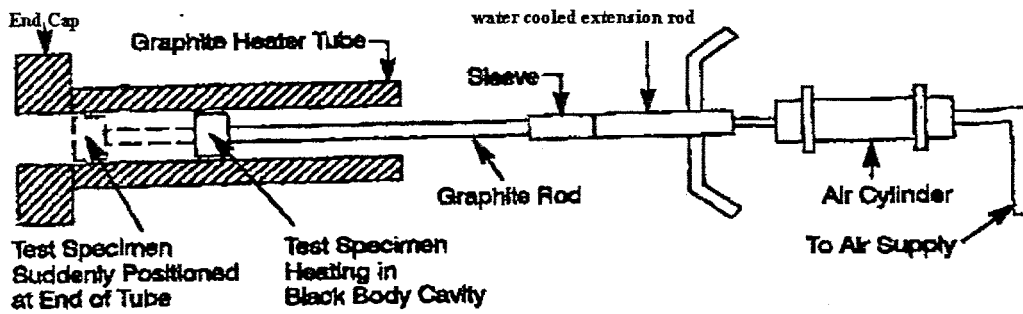
Schematic of Emissivity Test Apparatus
Exhibit 2.2-44

Refractory Materials Data Base

The data base that has been developed thus far for Jargal M, and Monofrax E, K-3, S-4, and A are summarized in Exhibit 2.2-43. The 4-point flexure strength and modulus shown in the table for the first four materials were measured at UTRC during this Quarter and were just discussed. The thermal conductivity data and expansion data are based on vendors values. The thermal conductivity measurements by the calorimetric method, the emissivity tests, and the corrosion tests at UTRC will begin or continue in the next quarter.

Exhibit 2.2-43
Refractory Candidates for RAH

Properties & Characteristics	Jargal M	Monofrax E	Single Lining Monofrax K-3	Monofrax S-4	Monofrax A
Refractory Type					
• Tradename	Jargal M	Monofrax E	Monofrax K-3	Monofrax S-4	Monofrax A
• Supplier	Corhart	Carborundum	Carborundum	Carborundum	Carborundum
• Composition	$\alpha/\beta\ Al_2O_3$	Cr/Al-oxide	Cr/Al-oxide	AZS [ER1681]*	$\alpha\ Al_2O_3$
Al_2O_3	95.0	6.5	58.6	49.7 50.9	98.2
Cr_2O_3	--	77.7	27.1	-- --	--
ZrO_2	--	--	--	33.0 32.5	--
SiO_2	0.5	--	1.6	14.0 15.0	0.7
MgO	--	8.0	6.1	-- --	--
CaO	--	--	--	-- --	--
Alkali (Na_2O, K_2O)	4.0	1.7	0.7	1.8 1.3	1.1
Fe_2O_3	--	6.1	5.9	-- --	--
Fe_2O_3, TiO_2, CaO	0.5	--	--	1.5 0.3	--
• Max. Service Temp. °F (°C)	3270 (1800)	> 3000 (1650)	> 3000 (1650)	2950 (1620)	3400 (1870)
• Density pcf (g/cc)	198 (3.17)	260 (4.17)	239 (3.83)	236 (3.78)	235 (3.76)
• Apparent Porosity (%)	15.5	5.0	4.0	1.0	2.0

4-Pt. Flex

Temperature °F (°C)	Jargal M ksi (MPa)	Monofrax E ksi (MPa)	Monofrax K-3 ksi (MPa)	Monofrax S-4 ksi (MPa)	Monofrax A ksi (MPa)
RT	4.7 (32.4)	6.0 (41.3)	8.9 (61.4)	10.1 (69.6)	-- --
1800 (983)	5.4 (37.2)	5.7 (39.3)	6.5 (44.8)	-- --	-- --
2000 (1093)	-- --	-- --	-- --	3.9 (26.9)	-- --
2100 (1149)	4.6 (31.7)	5.4 (37.2)	8.7 (60.0)	1.9 (13.1) 2250°F	-- --
2400 (1316)	5.2 (35.9)	5.0 (34.5)	2.1 (14.5)	1.1 (7.6) 2450°F	-- --
2500 (1371)	4.0 (27.5)	3.8 (26.2)	-- --	-- --	-- --

Elastic Modulus

Temperature °F (°C)	Jargal M Msi (GPa)	Monofrax E Msi (GPa)	Monofrax K-3 Msi (GPa)	Monofrax S-4 Msi (GPa)	Monofrax A Msi (GPa)
RT	9.4 (64.8)	16.3 (112.4)	21.1 (145.6)	16.3 (112.4)	-- --
1800 (983)	12.1 (83.4)	17.6 (121.3)	8.9 (61.4)	-- --	-- --
2000 (1093)	-- --	-- --	-- --	2.0 (13.8)	-- --
2100 (1149)	11.3 (77.9)	14.0 (96.6)	7.6 (52.4)	1.2 (8.3) 2250°F	-- --
2400 (1316)	10.6 (73.1)	15.9 (104.7)	5.3 (36.6)	1.3 (9.0) 2450°F	-- --
2500 (1371)	7.6 (52.4)	12.1 (109.1)	-- --	-- --	-- --

*Corhart (SEPR)

Exhibit 2.2-43

Refractory Candidates for RAH (cont.)

Properties & Characteristics		Single Lining				
Refractory Type						
• Tradename		Jargal M	Monofrax E	Monofrax K-3	Monofrax S-4	Monofrax A
• Supplier		Corhart	Carborundum	Carborundum	Carborundum	Carborundum
• Composition		α/β Al$_2$O$_3$	Cr/Al-oxide	Cr/Al-oxide	AZS [ER1681]*	α Al$_2$O$_3$
• Thermal Conductivity ** W/M-°K						
RT - °F	°C					
RT		6.50	- - -	5.29	6.20	: --
932	(500)	3.75	4.61	4.45	3.25	: --
1832	(1000)	3.57	3.68	3.30	2.76	6.9 ‡
2282	(1250)	3.76	3.38	3.09	2.60	7.2 ‡ (1200°C)
2732	(1500)	4.08	3.26	2.80	2.26	: --
2912	(1600)	4.30	3.20	2.61	2.21	: --
• Coeff. of Thermal Expansion Temperature						
°F	°C	ppm/°F ppm/°C	ppm/°F ppm/°C	ppm/°F ppm/°C	ppm/°F ppm/°C	ppm/°F ppm/°C
2000	(1100)	12.4 (6.9)	12.1 (6.7)	16.7 (9.3) 1200°C	16.2 (9.0) 1000°C	16.4 (9.1)1000°C
2400	(1315)	12.4 (6.9)	12.1 (6.7)	- - - - - -	- - - - - -	- - - - - -
2600	(1427)	12.4 (6.9)	12.1 (6.7)	- - - - - -	- - - - - -	- - - - - -
• Corrosion - 100 hr. test IL.-slag		+ +	+ (est)	+ +	+ (est)	- - -
• Emissivity †		TBD	TBD	TBD	TBD	TBD
• Thermal Shock Resistance ‡		Fair - good	Fair	Fair - good	Fair - good	Fair - good
• Cost - relative index (100) ‡		100 - 130	250	200	130 - 150	130 - 160

*Corhart (SEPR)

** Thermal conductivity by laser flash technique

† To be determined

‡ F.V. Toolay, *Handbook of Glass Manufacturing*, Vol. I, 3rd Edition, Ashlea Pub. Co., 1984

Summary

During this Quarter, progress was made in identifying and downselecting the metals and refractory materials candidates, which have the best combination of properties for the RAH. For the metallic heat exchanger tubes, a family of oxide-dispersion (ODS) alloys was identified, and two such alloys were described in the report. These alloys were selected because they exhibit superior elevated strength, low creep, and oxidation resistance over other superalloys that were discussed in previous reports.

Based on a review of the available property data and discussions with refractory vendors, a list of candidate refractories was narrowed down to 6 materials during this reporting period. Also, in order to further evaluate the current refractory materials and alloys of interest, tests have been initiated or are in the process of being set up to generate critical data that are missing, including thermal conductivity, resistance to slag erosion, and emissivity. Testing will continue in the next quarter. In addition, plans have been made to visit vendors [Huntington Alloys for ODS alloys, and GRP Inc. (formerly Carborundum-Monofrax Div.) for fused cast refractories] in the next quarter. The purpose will be to discuss the properties, performance in service, and manufacturing issues for these materials.

References

1. G.S. Sheffield & J. R. Schorr, "Comparison of Thermal Diffusivity and Thermal Conductivity Methods", Bull. Amer. Cer. Soc., 70 (1), 102-106 (1991).

2. Pvt. communication, D. Stiles (Harbison Walker) and J. Homeny (ORTON Foundation).

3. Pvt. communication, S. Winder (Carborundum Co.).

Task 2.3 Ash Modeling

Slag Viscosity Modeling Under HITAF Conditions

To verify that the correlations for viscosity and T_{cv} are accurate, the ash viscosities measured by EERC that were reported in the Quarterly Report for October-December, 1995 were reviewed. Upon evaluation of the data, it was concluded that the Illinois 6 slags as measured in air or air+water were not oxidized (i.e., all the iron was in the +2 oxidation state) and thus will not be applicable to the HITAF.

The four slags measured in the Quarterly Report were: 1) Rochelle ash; 2) Rochelle ash collected from NSP's Riverside station; 3) Illinois 6 slag from a cyclone boiler (Coffeen) with added CaO; and 4) Illinois 6 slag from a cyclone boiler (Baldwin). The atmosphere of the gas in contact with the slag during the viscosity measurement was controlled to be either air, air plus 10% H_2O, or a reducing gas mixture (as described in the Quarterly Report).

Since the Rochelle ash does not have much iron (Exhibit 2.3-1), the composition of the atmosphere should not have a big effect on viscosity. This can be seen in Exhibits 2.3-2 and 2.3-3). The Kalmanovitch-Urbain model[1] predicts viscosity well up to about 150 to 250 poise. Above this range, the viscosity is much higher than that predicted by the model due to crystallization. This critical viscosity temperature, T_{cv}, is evident from the figure.

Exhibit 2.3-1
Composition of Slags from Quarterly Report
(October-December 1995), in wt%

Oxide	Rochelle Ash	Rochelle - NSP	Illinois 6 + CaO Slag (Coffeen)	Illinois 6 Slag (Baldwin)
SiO_2	38.8	47.1	52.5	53.4
Al_2O_3	20.8	18.6	16.3	18.6
Fe_2O_3	6.1	5.3	13.6	17.6
TiO_2	1.5	1.4	0.7	0.7
P_2O_5	1.1	0.6	0.2	0.0
CaO	23.2	19.8	13.1	7.1
MgO	6.5	5.7	1.2	0.9
Na_2O	1.4	0.9	0.8	0.0
K_2O	0.3	0.4	1.6	1.7
SO_3		0.3	0.1	
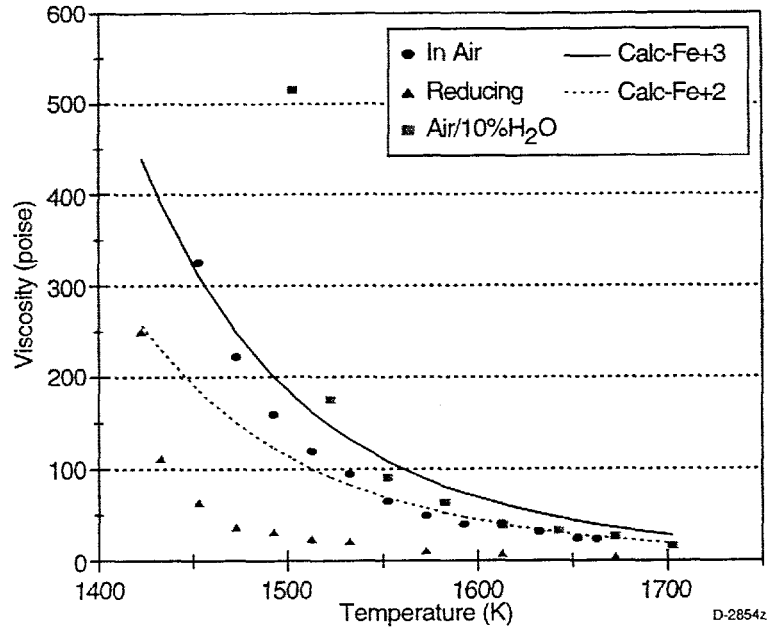
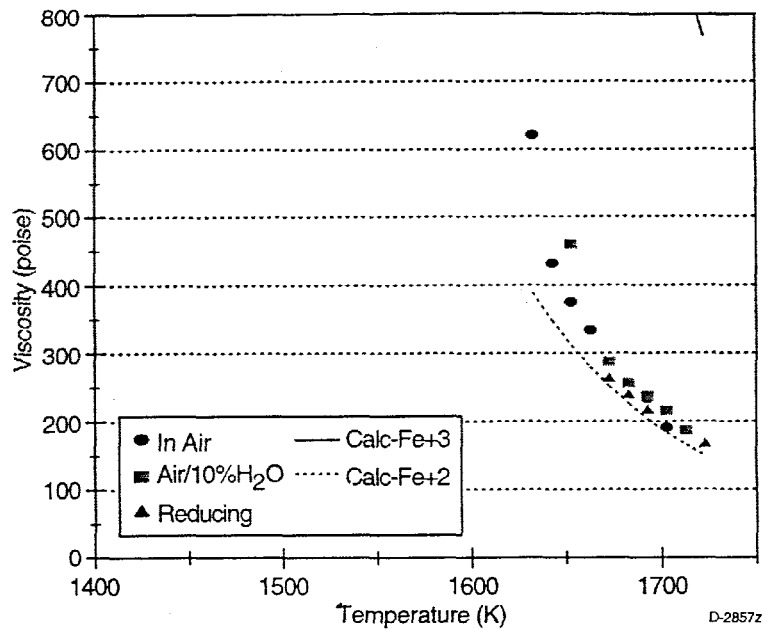**Viscosity-Temperature Curve: Rochelle Ash**
Exhibit 2.3-2
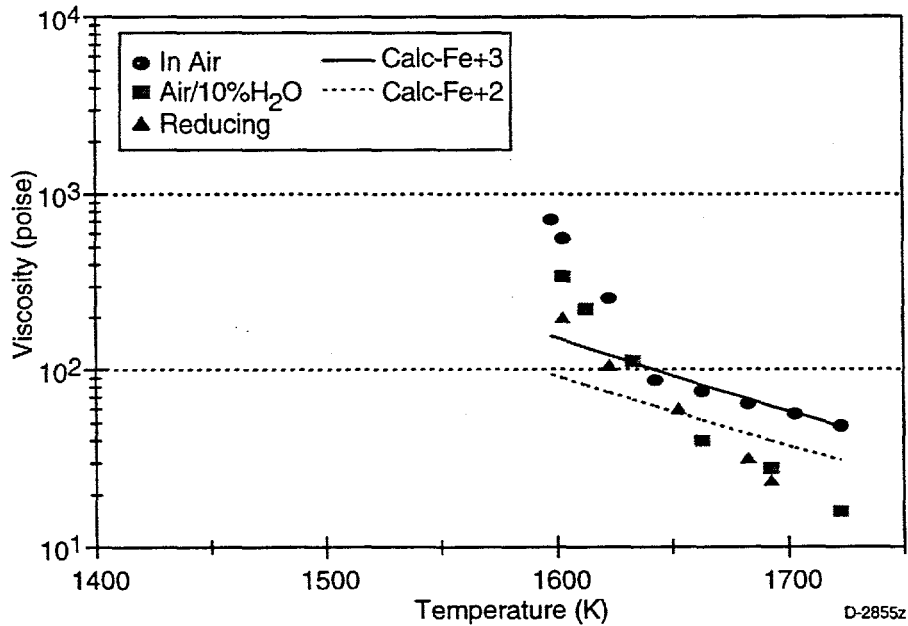
Viscosity-Temperature Curve: Rochelle Slag (NSP)
Exhibit 2.3-3

The Illinois 6 slags, in contrast to the Rochelle ash, contain a lot of iron. Since the slags were produced in a very reducing environment, we would expect that all the iron in these slags to exist as Fe(II). Even though EERC tried to ensure that the slags would oxidize for the viscosity measurements in air, it is evident from Exhibits 2.3-4 and 2.3-5 that the Illinois 6 slags were not oxidized when viscosity was measured. The model prediction for "oxidized" slag (i.e., all iron as Fe(III)) is much higher than the measured viscosity in air. Furthermore, there is almost no differencebetween the viscosities measured in air and the viscosity measured under reducing conditions. For a high iron coal such as Illinois 6, one expects to see such a difference.
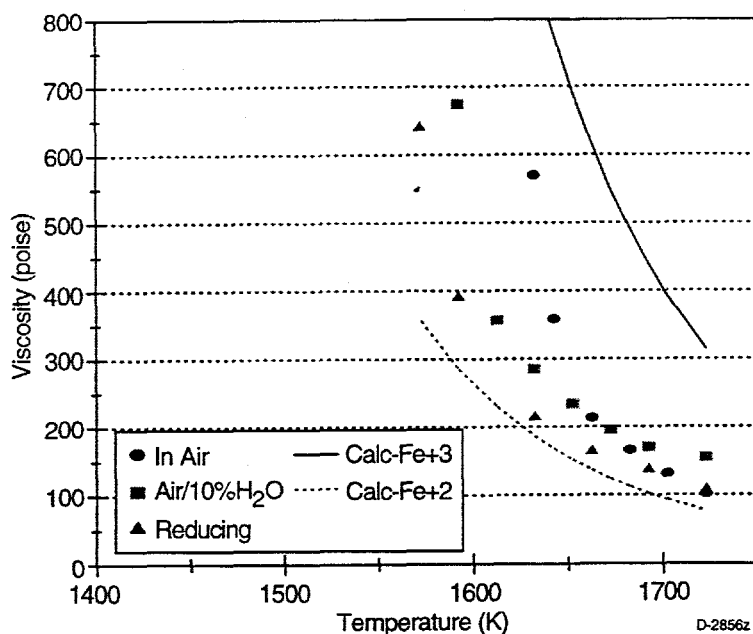
Viscosity-Temperature Curve: Coffeen Slag (Illinois 6 Plus Lime)
Exhibit 2.3-4

Viscosity-Temperature Curve: Baldwin Slag (Illinois 6)
Exhibit 2.3-5

To verify that Illinois 6 should show an effect of atmosphere on viscosity, the data published by Jan Nowok[2] was modeld. He measured the viscosity of Rochelle and Illinois 6 ash (not slags) in air and a reducing (CO/CO_2) mixture. The composition of these ashes (Exhibit 2.3-6) are similar to the ones measured in this program. Nowok also used Mössbauer spectroscopy to verify the $Fe^{+3}/\Sigma Fe$ ratio. The Illinois 6 ash measured in reducing atmosphere had a ratio of 0.16. That is, under reducing conditions 84% of the iron in Illinois 6 was Fe^{+2}.

Exhibit 2.3-6
Composition of Ashes Studied by Nowok (1995)

Oxide	Rochelle	Illinois 6
SiO_2	37.5	46.6
$Al2O_3$	20.1	23.1
Fe_2O_3	5.8	18.3
TiO_2	1.5	1.2
P_2O_5		
CaO	26.9	5.6
MgO	6.1	1.6
Na_2O	1.8	0.5
K_2O	0.3	3.1
SO_3		

Exhibits 2.3-7 and 2.3-8 show the viscosity-temperature curves for these two ashes. Once again, there is little difference with atmosphere on the viscosity of Rochelle ash, but a significant difference of that of Illinois 6. The viscosity model also does a good job of predicting both oxidizing and reducing conditions for Illinois 6.
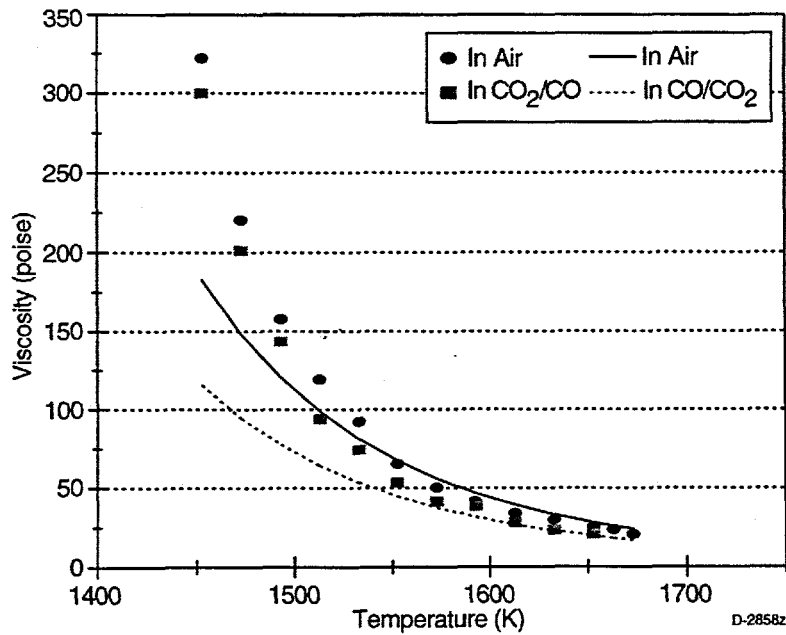
Viscosity-Temperature Curve for Rochelle Ash (Ref. 3)
Exhibit 2.3-7
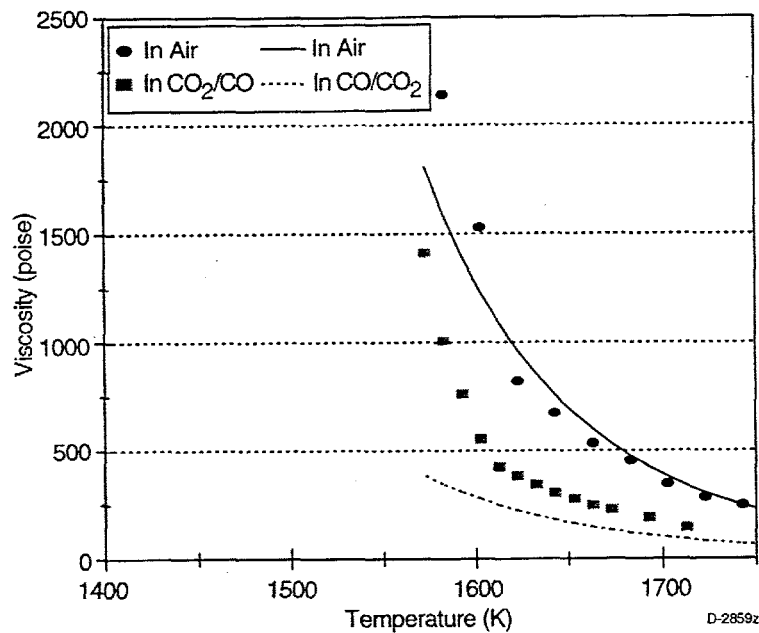
Viscosity-Temperature Curve for Illinois 6 Ash (Ref. 3)
Exhibit 2.3-8

In previous work, it was noted that synthetic slags containing initially all iron as Fe^{+2} are difficult to oxidize.[3] We heated 30 micron glass particles at 1350 C in a drop tube furnace. After heating in pure oxygen and a residence time of about 3 seconds, only 9 to 28% of the iron was converted to Fe^{+3}. A model was developed which suggested that melt diffusion was the limiting mechanism for iron oxidation under these conditions.

Finally, the correlation of Hoy et al. for T_{cv} was examined. The temperature of critical viscosity is an important parameter in our model of flowing slag in the HITAF radiant air heater and slag screen. As Exhibit 2.3-9 shows, this correlation did not do a very good job of predicting T_{cv}. For Rochelle coal, the predicted value was consistently low by about 75 K. For Illinois 6, the predicted value was not well-correlated with the observed value.

In the design of the commercial slag screen, a critical viscosity temperature of 1673 K for Illinois 6 and 1400 K was used for the PRB coal. Examination of the data indicates that the value of T_{cv} for the Illinois 6 is appropriate, but that the value chosen for the PRB coal is too low by about 100 K. Thus it is necessary to measure the critical viscosity temperature of the design coals because there is not a good correlation for this quantity. Existing viscosity models, however, do a good job of predicting slag viscosity.

Exhibit 2.3-9
Calculated and Observed Values of T_{CV}

Sample	Calculated T_{cv}, K	Observed T_{cv}, K	Delta
Rochelle (Quart)	1433	1500	(67)
Rochelle NSP (Quart)	1533	1625	(92)
Illinois 6 + CaO (Quart)	1728	1615	349
Illinois 6 (Quart)	1728	1625	103
Rochelle (Nowok)	1425	1495	(70)
Illinois 6 (Nowok)	1476	1625	(149)

Slag Screen Design

As discussed in the Quarterly January-March, 1996 report, the engineering model of the slag screen was modified. The model now predicts capture by the tubes, slag flow along the bottom of the duct, heat transfer through the duct, slag flow and heat transfer along the tubes, and the pressure drop across the slag screen. The model was used to perform a parametric evaluation of the potential slag screen designs.

Based on the parametric evaluation, a refined commercial slag screen design was proposed. This design uses 2.5 in. studded Schedule 40 tubes (actual OD 2.875 in.) and an inlet velocity of 164 ft/sec (50 m/sec). The tubes are covered with approximately 1/2 in. (11 mm) of refractory. The design consists of two banks of three rows of tubes with the same normalized spacing as previous designs. The model was then used to predict the performance of the slag screen for the three coals of interest; Illinois No. 6 (I6), Wyodak-Rochelle (WR), and Wyodak-Anderson (WA). The important inputs and results of these conclusions can be seen in Exhibit 2.3-10.

Exhibit 2.3-10
Important Model Inputs and Results

Parameter	Illinois No. 6	Wyodak Rochelle	Wyodak Anderson
T_{cv} [K]	1673	1500	1500
Gas temp. drop [K]	108	146	141
Mass removal [%]	33.3	19.5	30.2
Max slag thickness on tubes [mm]	62.3	12.3	15.7
Max slag thickness on floor [mm]	56.9	1.1	1.5

The predicted cumulative capture efficiency, Exhibit 2.3-10, is relatively low for these three coals, but it is still acceptable, especially if it is taken as a lower bound (Quarterly report, Jan-Mar 1996). It is important to note that ~40% collection efficiency is typical for commercial down-fired slagging combustors currently in operation. The slag thicknesses on the second tube bank are fairly high, which could potentially reduce the efficiency of these tube rows. The thickness of the frozen layers were found to dominate the overall slag layer thickness. The frozen layer on the tubes in the second tube bank, and on the duct floor in this region, are much higher than those at the inlet due to the lower gas temperatures in this region. However, due to the spacing of the tubes the slag screen cannot plug, so this design will be acceptable. Further, the reduction in the flow area of the duct related to the frozen slag layer on the floor is minimal (less than 3%). Finally, the pressure drop, 3.9 in. of water (0.14 psi) is probably acceptable, although just barely.

The effect of the slag screen on the ash loading can be seen in Exhibit 2.3-11. Not surprisingly, the Illinois No. 6 coal had the highest predicted ash loading after the slag screen. The data presented in Exhibit 2.3-12 suggests that the ash psd entering the CAH will be similar for the Illinois No. 6 and Wyodak-Anderson coals. The initial ash psd for these two coals was also similar. The ash from the Wyodak Rochelle entering the CAH is likely to contain a significantly higher fraction of fine particles and therefore may present more of a sintering problem. These results can then be used to estimate the particle losses that can be expected in the quench zone, and to design a pilot scale slag screen with a similar outlet ash psd.

Exhibit 2.3-11
Effect of Slag Screen on Ash Feedrate into CAH

	Wyodak-Rochelle	Wyodak-Anderson	Illinois No. 6
D_p [μm]	Ash mass into slag screen [kg/h]		
1.25	288	152	242
3.75	479	322	412
7.5	400	338	673
15	274	525	901
60	194	305	512
60	72	68	230
TOTAL	1707	1710	2970
D_p [μm]	Ash mass into CAH [kg/h]		
1.25	288	152	242
3.75	479	322	412
7.5	400	338	673
15	166	318	545
30	38	60	101
60	3	2	8
TOTAL	1374	1192	1981

D-2844
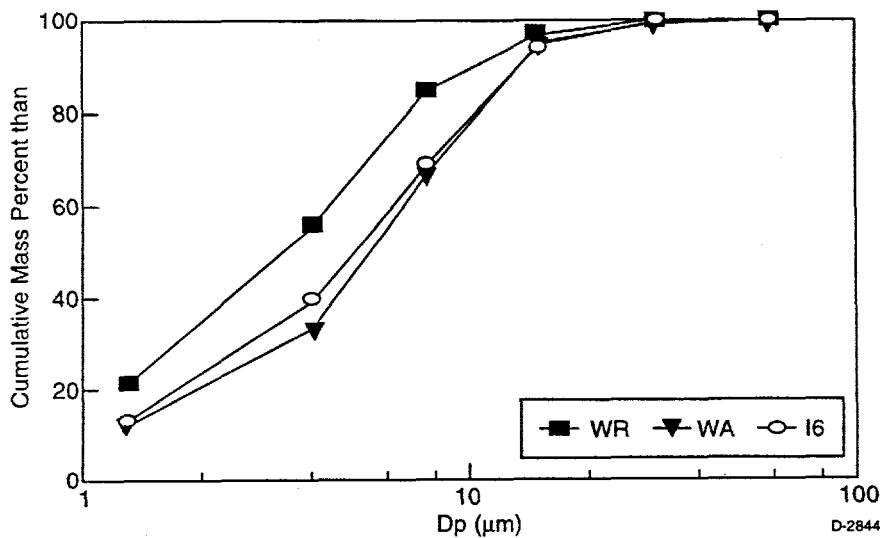
Inlet Ash PSD to CAH
Exhibit 2.3-12

Pilot Scale Slag Screen Design

Once the design on the commercial slag screen was completed, the design of the slag screen for the EERC pilot scale facility was begun. Originally the slag screen for the pilot scale facility was going to be a scaled-down version of the commercial slag screen. The plan at that point was to utilize measurements from the pilot scale experiments to validate the models that will be used to finalize the commercial design. However, the data required to fully validate the models was evaluated, it wasquickly realized that it wouldn't be cost-effective (or technically feasible in some cases) to collect the required data on the pilot scale slag screen. The small size of the slag screen, causing significant wall effects, will also prevent us from using the data to finalize the commercial slag screen design. Therefore, it was decided that the primary goal of the pilot scale slag screen will be to provide an ash psd entering the CAH that is comparable to that expected in the commercial plant -- providing a more realistic test for the convective air heater.

The pilot scale slag screen was designed to meet the following criteria:

1. the slag screen must not plug in the event of large deposit buildup on the tube surface,

2. flow in the slag screen must not be restricted by slag buildup on the floor,

3. the pressure drop in the slag screen must not exceed 2 in. of water,

4. the materials in the slag screen must be inexpensive and robust -- this criteria will allow us to modify the design quickly if required,

5. the Reynolds number (based on the tube diameter) must not go below 2100 to ensure turbulent flow models apply.

Based on these criteria the slag screen simulation model (SSSiM) was used to design a suitable pilot-scale slag screen. A simplified spreadsheet, based on the scaling equations, was used estimate the acceptable tube size, tube spacing, and operating velocity. The resulting design was similar to the commercial scale design, but had a few minor variations. First, much smaller tubes and a slightly closer tube spacing were used in order to maximize the number of tubes in a row while still maintaining turbulent flow. Another change from the commercial scale design is the absence of a large space between the third and fourth rows of tubes. Since on-line cleaning of the tubes on the pilot scale will not be performed, and since simulation of commercial scale is no longer desired, the path between rows 3 and 4 was removed to conserve space.

Once the spreadsheet was used to define the optimum tube parameters and operating conditions, the full SSSiM was used to determine the temperature drop across the slag screen. It was assumed that the gas within each mullite tube was kept at some fraction of the gas temperature. This assumption was based on the fact that the tubes are sealed on both ends (no convective cooling) and that the heat loss due to conduction from the tube material to the wall is fairly low.

One effect of the smaller size that was immediately obvious was the higher heat loss in the smaller unit, due to a higher surface to volume ratio. In order to estimate the safe range of operation, the gas temperature inside the tube was varied from 90 to 99% of the gas temperature outside the tube. At temperatures below 93% of the gas temperature (2500°F) the slag on the floor of the duct built up enough to severely constrict the flow. At temperatures above 95% of the gas temperature (2570°F) the flow was not constricted at all. As the tube is effectively isolated in the gas stream, and the flue gases can enter the tubes as discussed below, it is likely that the gas temperature inside the tubes (and the tube temperature) will equilibrate to a temperature very close

to the bulk gas temperature. However, it is important to monitor this temperature inside the tubes to ensure that the tube walls are above the critical temperature at all times. To accomplish this it is recommended that thermocouples be placed into a tube in the first and last row.
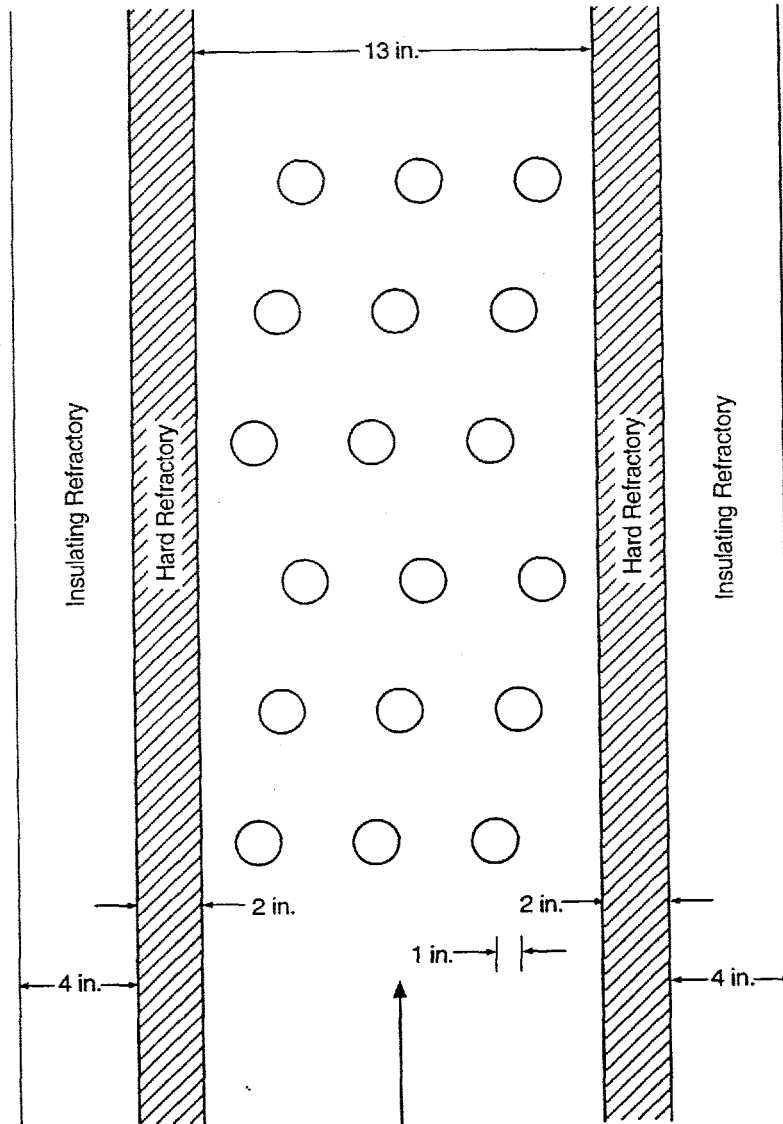
The pilot-scale slag screen is shown to scale in Exhibits 2.3-13 and 2.3-14. The slag screen design information is outlined below.

- The tubes will consist of 1.5 inch (OD) uncooled mullite tubes.

- There will be 6 rows of tubes, 3 tubes per row.

- The centerline spacing of tubes in each row will be 3 3/4 in.

- The centerline spacing between rows will be 4_ in.

- There will be a 4 in. layer of insulating refractory on all walls.

- There will be a 2 in. layer of hard refractory on the side walls.

- There will be a 6 in. layer of hard refractory on the roof and floor.

- The height of the duct will be 8 3/4 in. (without refractory).

- The width of the duct will be 13 in. (without refractory).

- The gas velocity entering the slag screen will be approximately 60 ft/sec.

Each of the mullite tubes will have several 'breather' holes drilled or cut into the sides. These holes will allow the pressure inside the tubes to balance with that in the slag screen during heat up -- to prevent the air trapped in the tubes during casting from cracking the tubes due to the increased pressure as the tubes are heated up. These holes will also allow the temperature inside the tubes to equilibrate with the gas temperature outside the tubes. By placing the holes on the side of the tubes (in between the tubes in a row) plugging of the holes by flowing slag can be avoided. The use of uncooled tubes will also prevent a large buildup of frozen ash on the tube surfaces.

Although the current design calls for mullite tubes, another material can be substituted based on the EERC slag corrosion data to prevent the slag from 'eating through' the tubes during the experiment. The current plan is to supply the tubes to EERC who will then cast and install the slag screen. The final dimensions of the slag screen will depend on the final casting, but will be approximately 25 in. wide, 28 3/4 in. tall, and 50 to 60 in. long. The length includes room for approximately 6 tube diameters at the entrance to allow the flow to settle down before entering the slag screen. EERC will finalize the length based on the length of the duct between the furnace and the dilution zone. The slope of 20° included in the current EERC design will be sufficient to ensure that the slag flows from the slag screen into the slag tap.

The lower gas velocity (as compared to the commercial design) is expected to yield a pressure drop of less than 1 in. of water -- well within the design criteria. Another important feature of the slag screen design is the placement of the rows. As with the commercial slag screen, the rows in the smaller scale slag screen are offset so that even if the deposits on the leading edge and trailing edge of the tubes connect there will still be an open path through the slag screen. Therefore, although the efficiency of the slag screen will decrease if the tube deposits grow much larger than predicted -- the design should prevent catastrophic plugging.

Top View of Pilot Scale Slag Screen
Exhibit 2.3-13
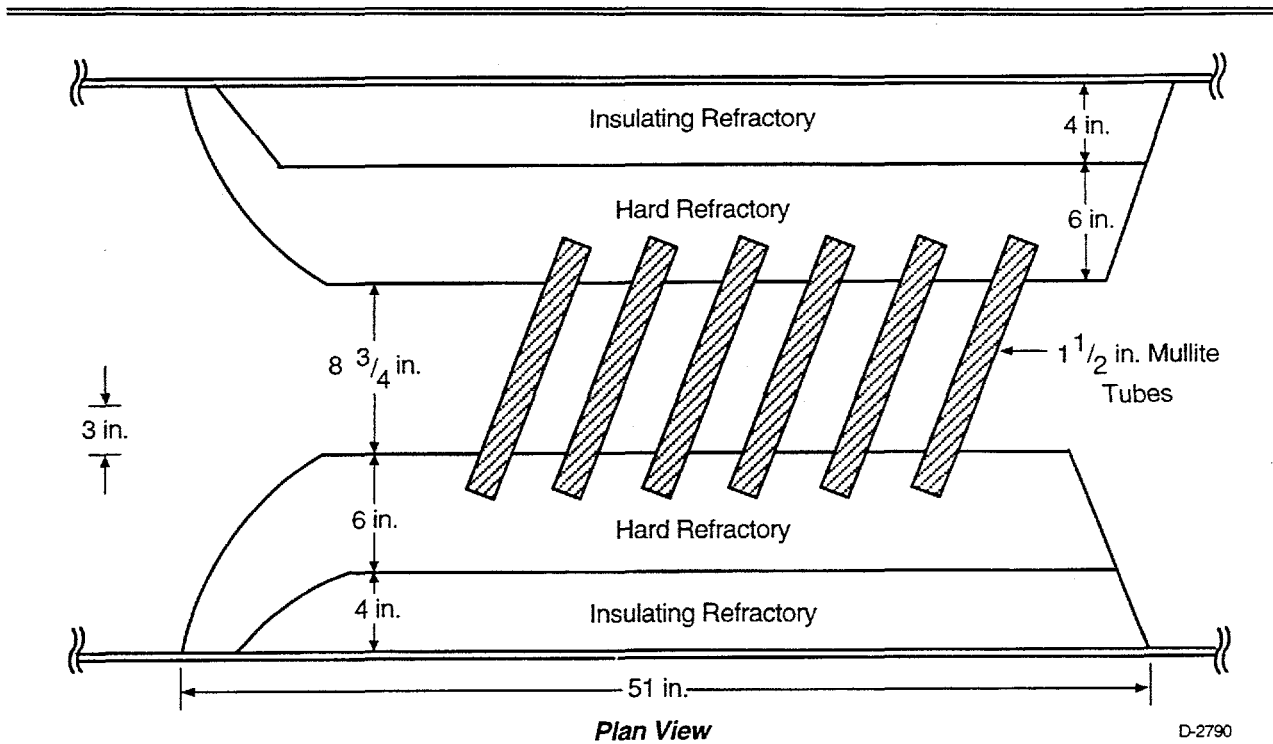
Plan View of Pilot Scale Slag Screen
Exhibit 2.3-14

As mentioned above, the primary goal of the pilot scale slag screen is to generate an ash psd entering the CAH that is comparable to that expected in the full scale. A comparison of the collection efficiencies for both designs (assuming particle dispersion between rows) can be seen in Exhibit 2.3-15. As can be seen from this figure, the collection efficiencies are very similar, therefore we should get similar ash particle size distributions and loadings into the dilution zone.
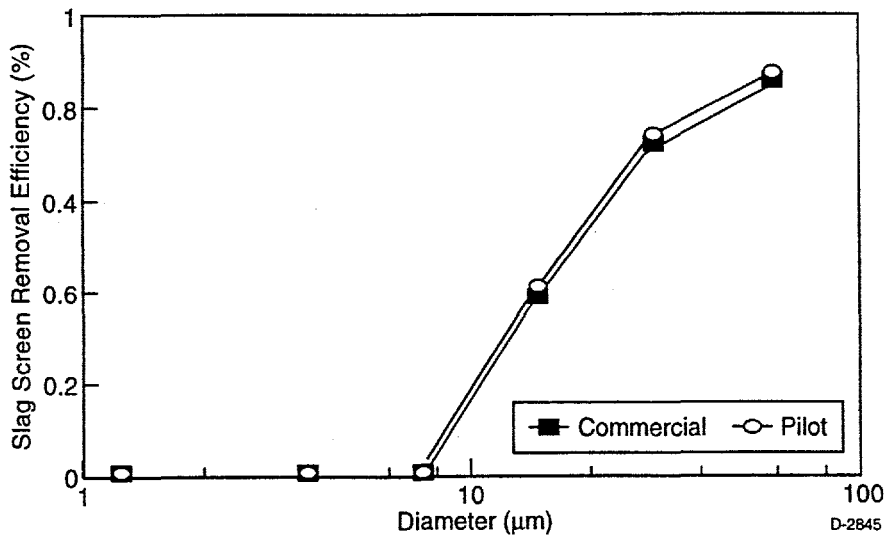
Viscosity-Temperature Curve for Rochelle Ash (Ref. 3)
Exhibit 2.3-15

Sintering of Convective Air Heater Deposits

In the Phase I program, a criterion of deposit removability in the convective air heater was developed (described in the Phase I Final Report). This quarter, these calculations were reviewed to determine how to improve them as required in Phase II. The results are briefly summarized below. The question that was addressed is as follows: what is the maximum flue gas temperature such that ash deposits on heat transfer surfaces can be removed easily?

Answering this question involves a three step process. First, it is necessary to establish a criterion for deposit removability by sootblowers. Based on earlier measurements of deposit strength, a minimum deposit porosity of 25% was established. The second step will be to calculate sintering rates in the deposit to make sure that the deposit does not reach the "critical" porosity too quickly for easy removal. The result will be a maximum allowable deposit surface temperature. Finally, using the maximum allowable deposit surface temperature, a heat transfer calculation will be performed to arrive at the maximum allowable flue gas temperature as a function of deposit thickness. The results depend on the composition of the coal ash.

Models for the sintering of coal ash deposits are based on viscous flow of the ash. The earliest work by Frenkel[4] concerned the rate of coalescence of two spheres such that the energy dissipated in viscous flow equals the energy gained by a decrease in surface area. Frenkel's model is applicable to the early stages of deposit sintering and can provide a qualitative indication of the degree of sintering.[5] Mackenzie and Shuttleworth[6] developed a model for the shrinkage of closed pores which occurs in the later stages of densification. Scherer[7] developed a more general model for sintering of open pores using an array of intersecting cylinders. He showed that his model reproduced the behavior of the Mackenzie and Shuttleworth model for values of porosity less than about 0.7.

For the purposes of modeling sintering of coal ash deposits from approximately 50% to 0% porosity, the model of Mackenzie and Shuttleworth will be used. This model describes the change in porosity as a function of time as follows:

$$\frac{\varepsilon}{\varepsilon} = e^{-\frac{3t\sigma}{2r_0\mu}}$$

In this analysis, viscosity will be calculated based on the bulk composition of the ash. As discussed below, using bulk viscosity provides only an approximate answer since the composition of individual ash particles in the deposit can differ greatly from the bulk composition. A constant surface tension will be assumed. For the sintering calculation, the ratio of surface tension to viscosity is the quantity of interest. Both surface tension and viscosity are functions of temperature. Surface tension depends approximately on the square root of temperature, while viscosity shows an exponential dependence on temperature.[8] Given that the viscosity changes by several orders of magnitude over the temperature range of interest, it is reasonable to neglect the variation of surface tension with temperature.

According to Raask,[8] viscosities in the range of 10^7 to 10^{11} poise are relevant to the formation of sintered deposits in coal-fired boilers. Senior and Srinivasachar[9] developed a model for viscosity of silicates in the range of 10^5 to 10^9 poise. Other models of slag viscosity work well

for flowing slag (i.e., viscosity less than about 10^3 poise), but cannot be applied to the much higher viscosities found in deposits. Using the ASTM ash composition for Illinois 6 and Wyodak coals (as reported in the Phase I Final Report), the viscosity was calculated as a function of temperature from 1000 K to 1400 K. Exhibit 2.3-16 displays the viscosity-temperature curves for oxidizing (all iron as $Fe+^3$) conditions calculated as described in Ref. 9.


D-2304
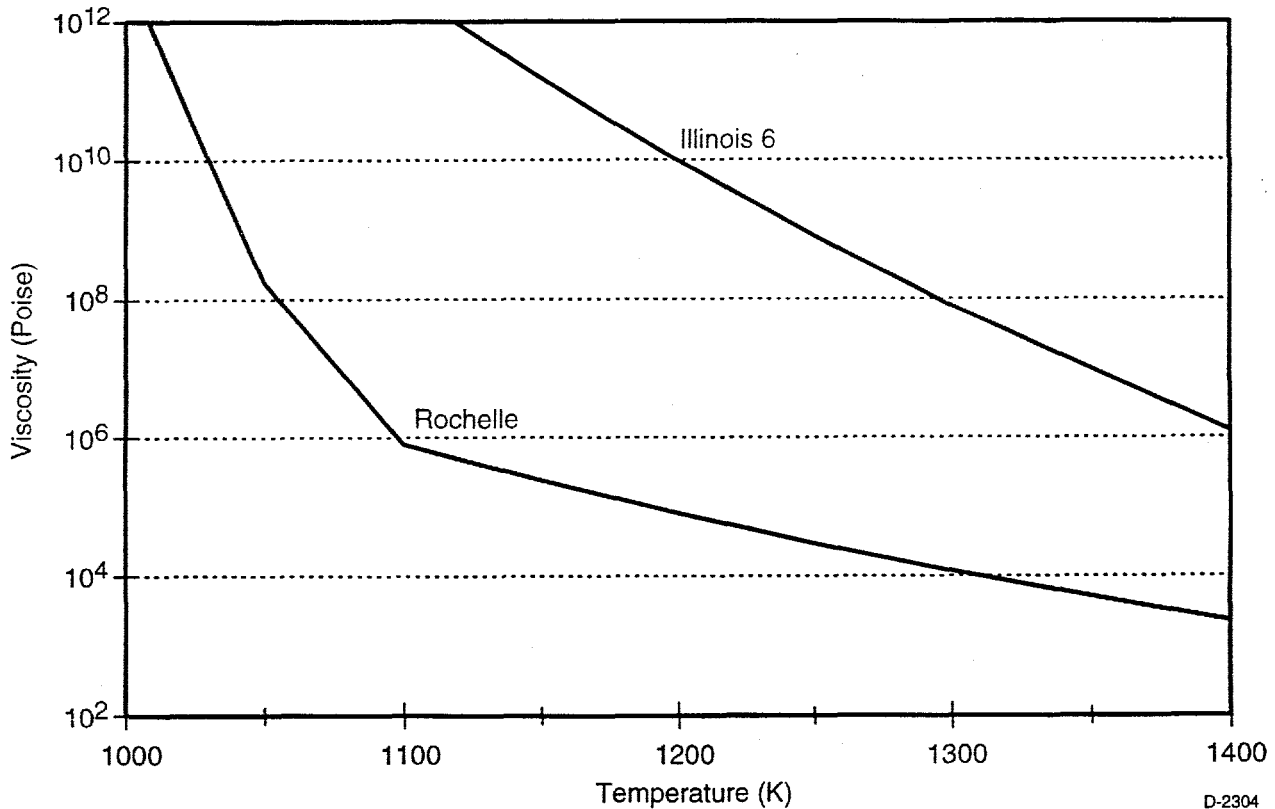
Viscosity-Temperature Curves for Oxidizing Conditions
Exhibit 2.3-16

Densification calculations were performed using the method of MacKenzie and Shuttleworth.[6] The bulk ash composition was used to calculate the viscosity and a surface tension of 400 dyne/cm was assumed based on measurements of surface tension in a number of coal ash samples.[10] The initial deposit porosity was assumed to be 50% since deposits are observed to have low strength (implying little sintering) at this value of porosity. Based on Scherer's structural model for densification of a cubic lattice,[7] the pore radius was set equal to half the average particle diameter (Exhibit 2.3-17).

Exhibit 2.3-17
Ash Particle Size Distributions (in wt%)

Diameter, microns	Illinois 6	Wyodak-Rochelle
1-2.5	1.5	16.8
2.5-5	9.0	34.8
5-10	19.9	25.6
10-20	34.8	19.2
20-40	29.5	3.2
40-60	5.3	0.6
Weighted average diameter	10.2	4.2

Exhibits 2.3-18 and 2.3-19 show densification as a function of time for Illinois 6 and Wyodak-Rochelle ash, respectively. The temperature at which porosity reaches the critical value of 25% in approximately 8 hours is 1170 K for Illinois 6 and 1015 K for Wyodak-Rochelle. These points correspond to a viscosity of approximately 3×10^{10} poise which is consistent with Raask's assessment of the range of viscosity for deposit sintering.

D-2305
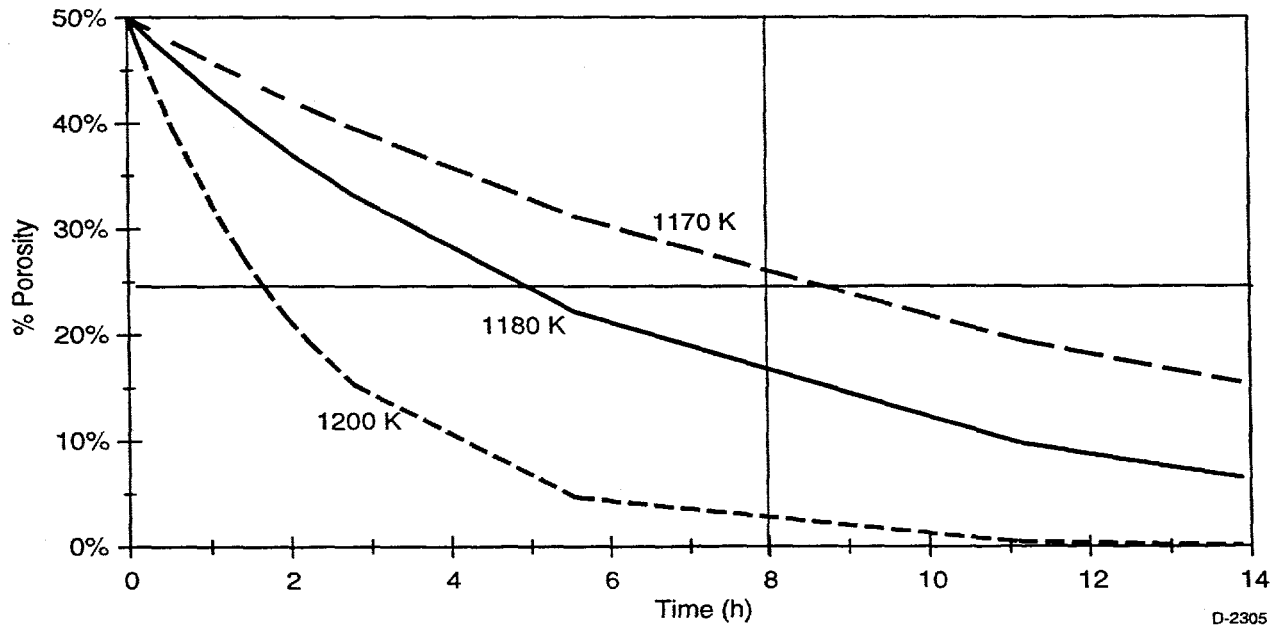
Densification of Illinois 6 Deposit
Exhibit 2.3-18
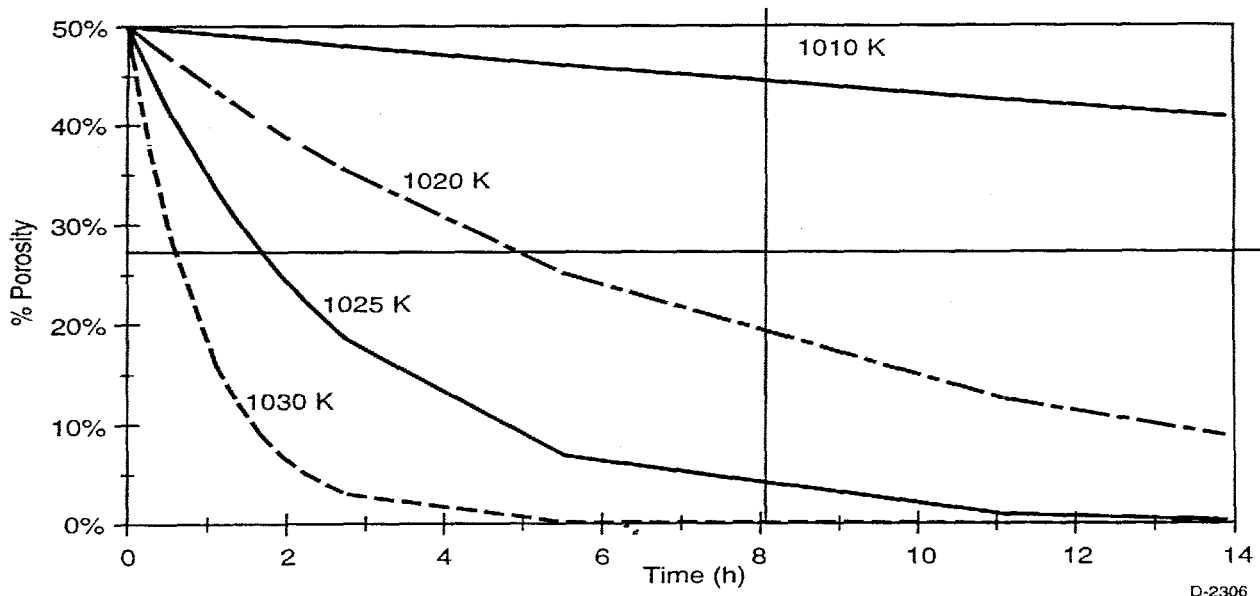
**Densification of Wyodak-Rochelle Deposit
Exhibit 2.3-19**

Having defined a maximum deposit surface temperature, T_s, such that the deposit can be easily removed, we can now compute the maximum flue gas temperature in the convective heat exchanger. In order to verify the approach, however, an example from a conventional coal-fired power plant will be presented first and then the results for the convective air heater conditions will be shown. Because we wish to find a maximum gas temperature, we will perform a steady state heat balance on the heat exchanger inlet using the maximum temperature for the working fluid.

The gas temperature can be calculated by solving the steady state heat transfer problem given the air and deposit surface temperatures. This involves solving three equations for three unknowns:

$$h_{fluid}\left(T_{w_1} - T_{fluid}\right) = \left(k_{tube} / x_1\right)\left(T_{w_2} - T_{w_1}\right) = \left(k_{ash} / x_2\right)\left(T_s - T_{w_2}\right) = h_g\left(T_g - T_s\right)$$

Variables are defined in Exhibit 2.3-20. The equations are solved for gas temperature, T_g, as a function of ash thickness, x_2.

Exhibit 2.3-20
Values Used to Calculate Steady State Heat Transfer

Parameter	Symbol [units]	Steam Reheater	HIPPS Air Heater
Working Fluid		Steam	Air
Working Fluid Temperature	T_{fluid} [K]	617	978
Tube Material		Carbon Steel	Inconel
Tube Thermal Conductivity	k_{tube} [W/m-K]	43.3	16
Tube thickness	x_1 [m]	0.0042	0.0032
Ash Thermal Conductivity	k_{ash} [W/m-K]	0.65	0.65
Gas heat transfer coefficient	h_g [W/m^2-K]	58.5	170
Working Fluid Heat transfer coefficient	h_{fluid} [W/m^2-K]	1226	545

As a check on the calculational approach, the maximum allowable flue gas inlet temperature was estimated for a conventional steam convective air heater. Since the first bank of tubes in a power plant, the secondary superheater, sees a lot of radiation, the second bank, the reheater was modeled. The gas temperature entering the reheater is typically 1380 K (2020 F) burning an Illinois 6 coal.[11] Ash deposits of 0.5 in. in 8 hours are typical and can be removed easily.

Exhibit 2.3-20 gives the parameters used for the steady state heat transfer calculation applied to a conventional steam reheater. The coal was assumed to be Illinois 6 coal having a maximum deposit surface temperature of 1170 K. The shaded region in Exhibit 2.3-21 shows that at a maximum gas temperature of 1380 K, deposits less than 3 cm (1.25 in.) should be removable. This agrees with the experience in coal-fired power plants.
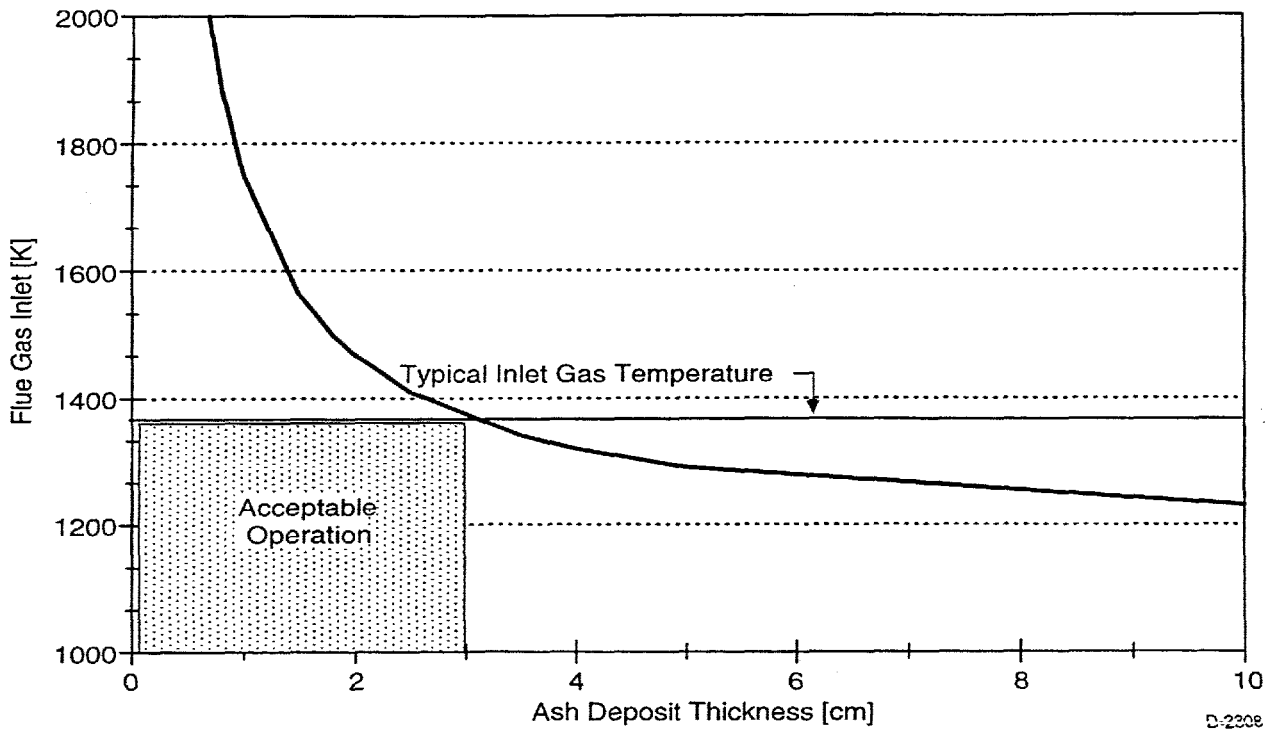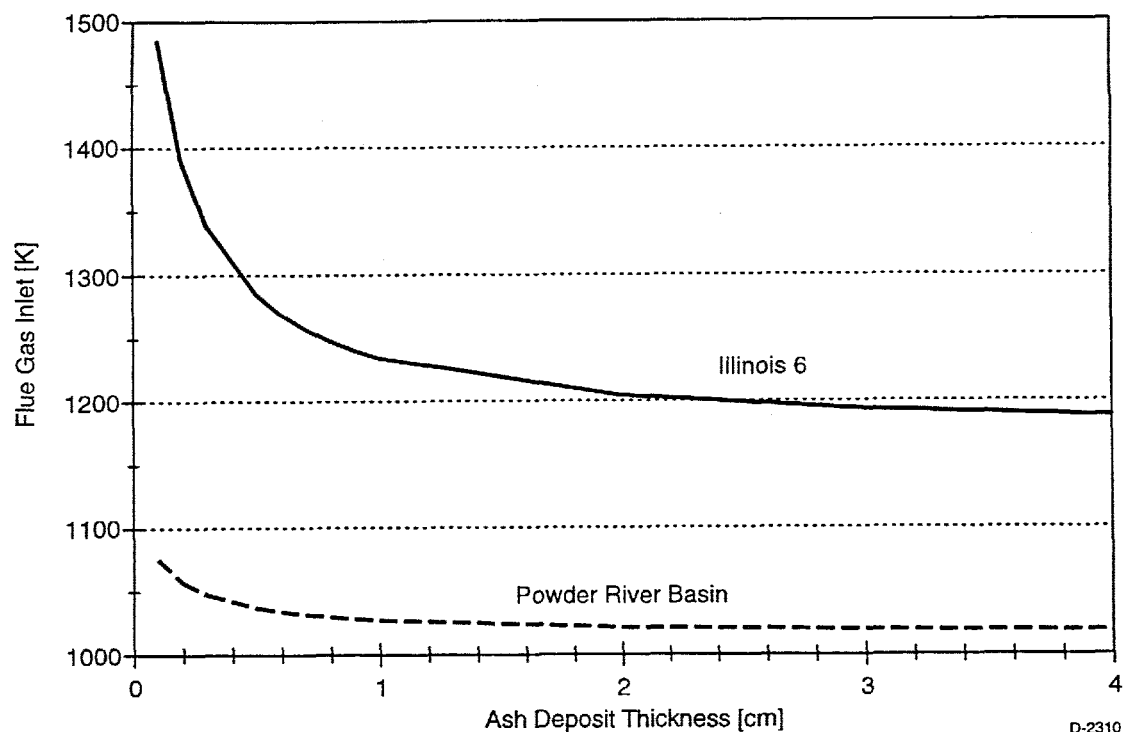
**Maximum Allowable Flue Gas Inlet Temperature for a
Steam Reheater (Illinois No. 6)
Exhibit 2.3-21**

Exhibit 2.3-22 illustrates the effect of switching to a PRB coal on the maximum gas inlet temperature. For the same deposit thickness, the flue gas temperature must be decreased by about 200 K. Coal-fired boilers designed to burn high-fouling coals such as Wyodak-Rochelle employ furnace exit gas temperatures which can be 200 to 350 K lower than those from units designed to burn bituminous coal.[12] Thus, the method provides a means to estimate conditions for deposit removability. Next, it will be applied to the design of the convective air heater in the HIPPS furnace.
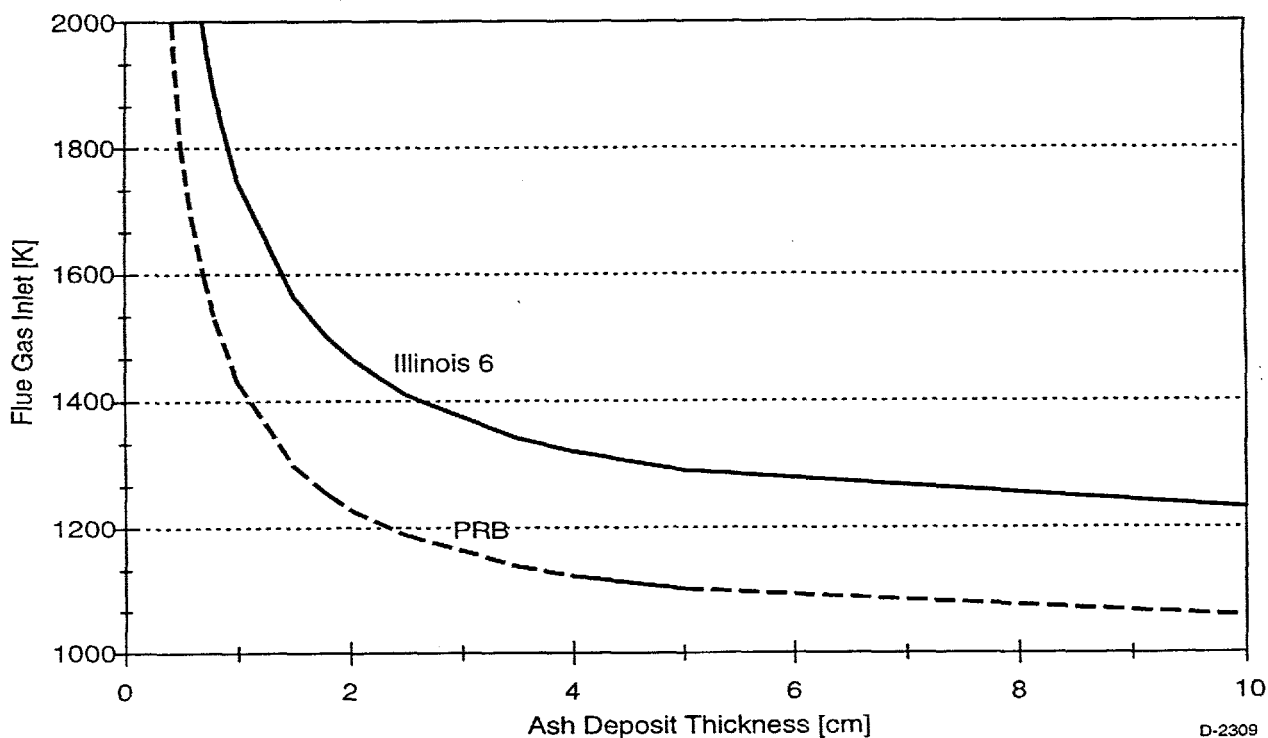
Maximum Allowable Flue Gas Inlet Temperature for a Steam Reheater, Comparison of Illinois No. 6 Coal and PRB (Wyodak-Rochelle)
Exhibit 2.3-22

Results for the HIPPS convective air heater calculation are shown in Exhibit 2.3-23 for Illinois 6 and Wyodak-Rochelle. For Illinois 6 the maximum allowable flue gas inlet temperature is very sensitive to deposit thickness if the deposit thickness is less than 1 cm. If the convective air heater surface is "clean", the inlet gas temperature can be high, 1500 to 1750 K (2200 to 2700 F), for the bituminous coal. However, a clean surface cannot be expected during normal operation, especially at the inlet to the convective air heater where ash deposition is expected to be the highest.

Modeling of deposition of the convective air heater[13] predicted a deposition rate about 0.06 cm/hr (0.025 in/hr). Deposits of less than 1 cm are expected over an 8-hour period. Therefore, an inlet temperature of 1255 K (1800°F) was chosen for the preliminary design for bituminous coals. Because the PRB coal, Wyodak-Rochelle, has a sintering temperature that is close to the working fluid temperature, the maximum allowable flue gas temperature is less than 1100 K (1520 F).

**Maximum Allowable Flue Gas Inlet Temperature
for HIPPS Convective Heater
Exhibit 2.3-23**

Using the critical porosity and the bulk ash properties for bituminous and sub-bituminous coals, the maximum allowable deposit surface temperature and the maximum allowable flue gas temperature in a convective heat exchanger were calculated. The calculation was carried out for conditions that represent the steam reheater section of a conventional pulverized coal-fired power plant and the result is consistent with observations from existing plants. As a result of this analysis, an inlet temperature of 1255 K (1800°F) was chosen for the preliminary convective air heater design.

The accuracy of this method could be improved by adding more detail to the model for calculation of sintering rate in ash deposits. A single pore size and ash composition are not realistic assumptions. Pore size is probably not as big an issue as the composition, given the strong dependence of viscosity on composition.[9] The composition of individual ash particles produced by a coal can vary widely as shown in Exhibit 2.3-24. For an eastern bituminous coal, the figure shows the frequency distribution of base/acid ratio based on the compositions of ash particles as compared with base/acid ratio determined from the bulk ash composition. A distribution of compositions implies that some ash particles will be relatively fluid at low temperatures while more refractory ones will not flow. Extending the sintering model to include a range of compositions will make the results more accurate.
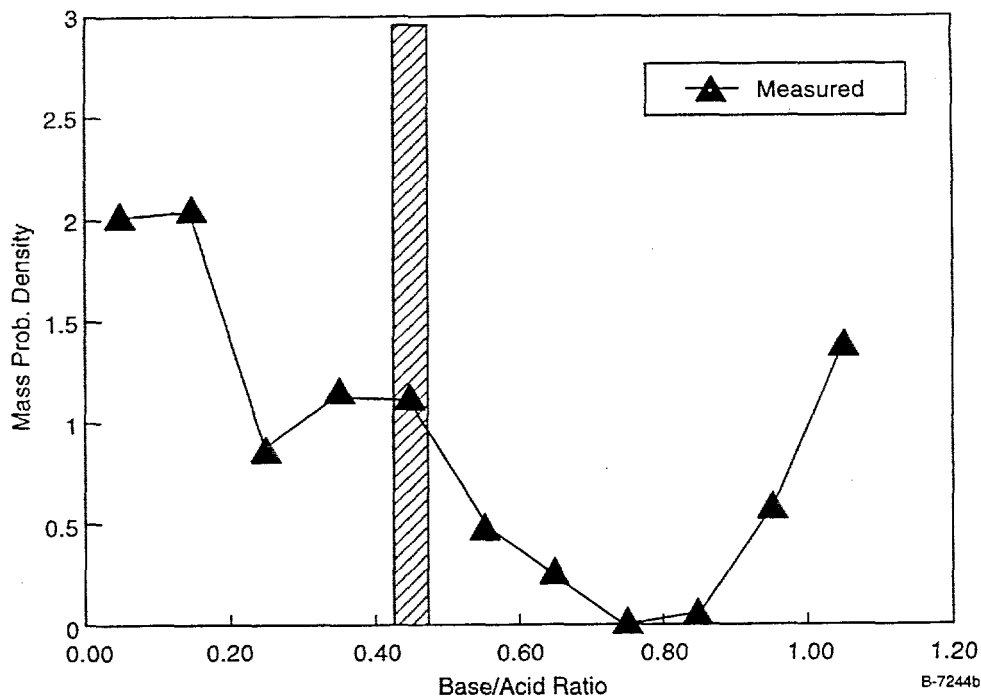
Distribution of Base/Acid Ratio of Illinois 6 Ash
Exhibit 2.3-24

The range of viscosity valves that is important for sintering of convective section deposits is high, 10^8 to 10^{10} poise. No data on coal ash are available in this range, although there exist many measurements on simpler oxide systems at low temperatures (many of these references are cited in Ref. 9). Well-controlled measurements of sintering rate in the laboratory can provide an indication of the viscosity[14] and this may be a way to generate a better approximation. Furthermore, we have not accounted for the formation of crystals in the deposit. It is well known that heat treatment of ash causes crystallization and that this occurs in the boiler. Amorphous deposits have higher strength than crystalline ones. Nowok et al[15] showed that heat treatment of a low rank coal ash reduced the strength. A more accurate method for calculating viscosity at low temperatures will also improve the accuracy and usefulness of the estimate.

Slag Screen Inlet Flow Field Analysis

Computational fluid dynamics has been used to estimate the distortion of the velocity field due to the inlet turn near the entrance of the slag screen for the full-scale configuration. Two calculations were run. In the first case, the inlet from the radiant air heater flow section to the slag screen consisted of a rectangular duct without a transition section to minimize flow distortion - see Exhibit 2.3-25. In the second case, a bellmouth-shaped transition section was used - see Exhibit 2.3-26. Both exhibits depict the section containing the radiant air heater (which was not simulated), the slag pot, and the slag screen section (without modeling the screen *per se*). Uniform flow was assumed at the inlet to the radiant air heater section (that is, at the top of each figure). The commercially-developed code, FLUENT, was used to perform these simulations.

In Exhibit 2.3-25, the case without transition, the flow is seen to separate along the inner radius of the turn into the slag screen. In contrast, Exhibit 2.3-26 indicates that the separated flow region is essentially eliminated by using a bellmouth with a radius of curvature of about 13 ft. In Exhibit 2.3-27 and -28, velocity contours are shown at a location corresponding to the estimated location for the beginning of the slag screen. It can be seen that the bellmouth is effective in reducing the sharp velocity gradients in the flow.

Due to the significant amount of turning of the flow in either case, consideration was given as to the effectiveness of the turn in removing ash particles prior to the screen; ascertain whether the the slag screen is necessary. Sample trajectories for two particle sizes in the two configurations are shown in Exhibits 2.3-29, -30, -31, and -32. Estimate of ash particle size range from about 1.25 microns to about 100 microns; the trajectories shown are considered to be representative. In every case, it is seen that the particles are able to accommodate to the flow field and enter the slag screen section.

Some additional numerical experiments were performed with much larger particle sizes to determine if any particles will fail to make the turn and be trapped in the slag pot. In Exhibit 2.3-33, it is seen that particles with diameters over 1000 microns can be trapped in the slag pot for the case without the bellmouth. Such particle sizes are much larger than the maximum anticipated.

The general conclusions of this study are as follows:

- The results show that the bellmouth eliminates the separated flow region and minimizes flow nonuniformity.

- A slag screen is required since the largest particles anticipated do not separate from the turning flow.

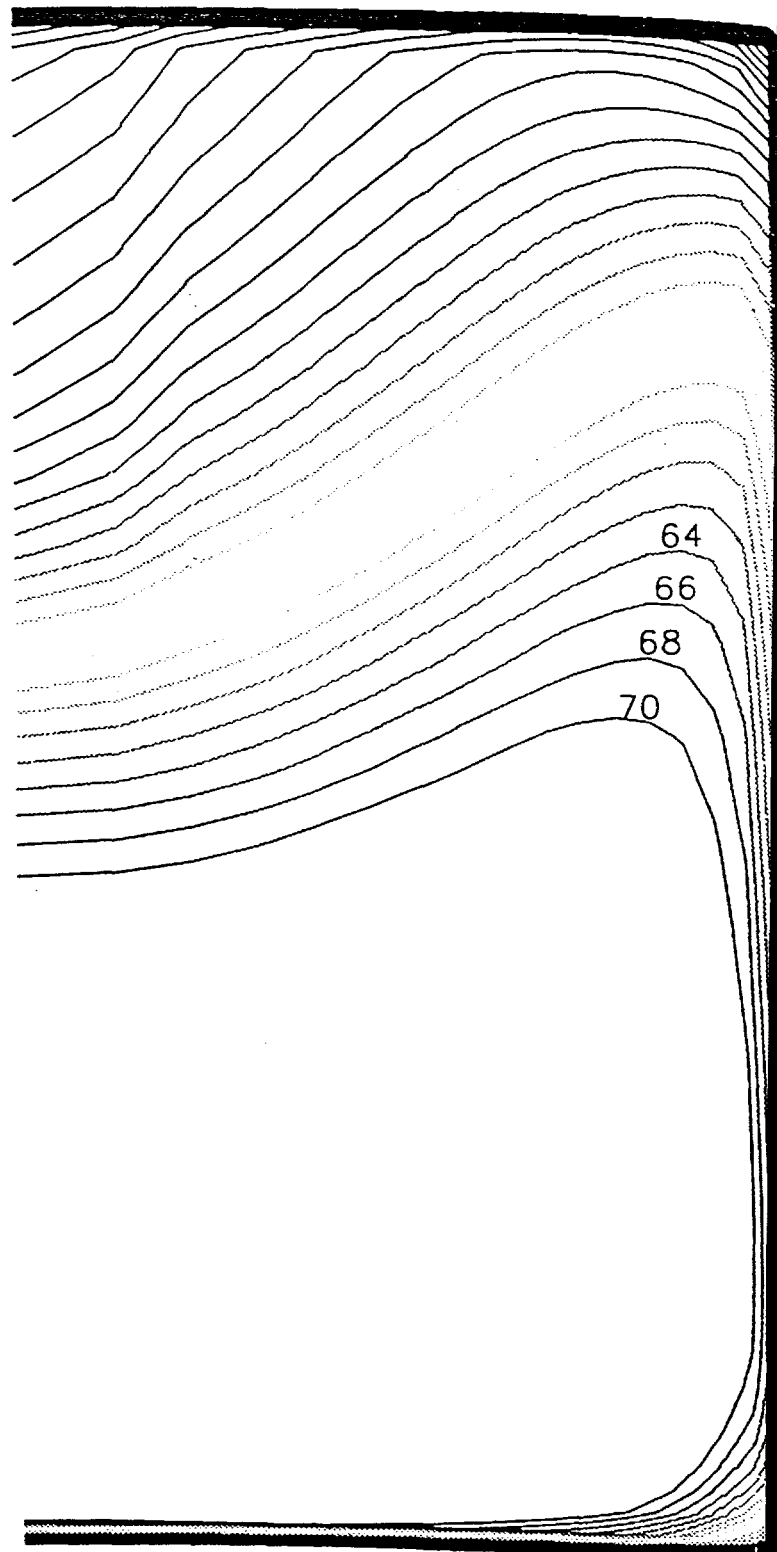- Particles accommodate to the low-speed flow independently of size.
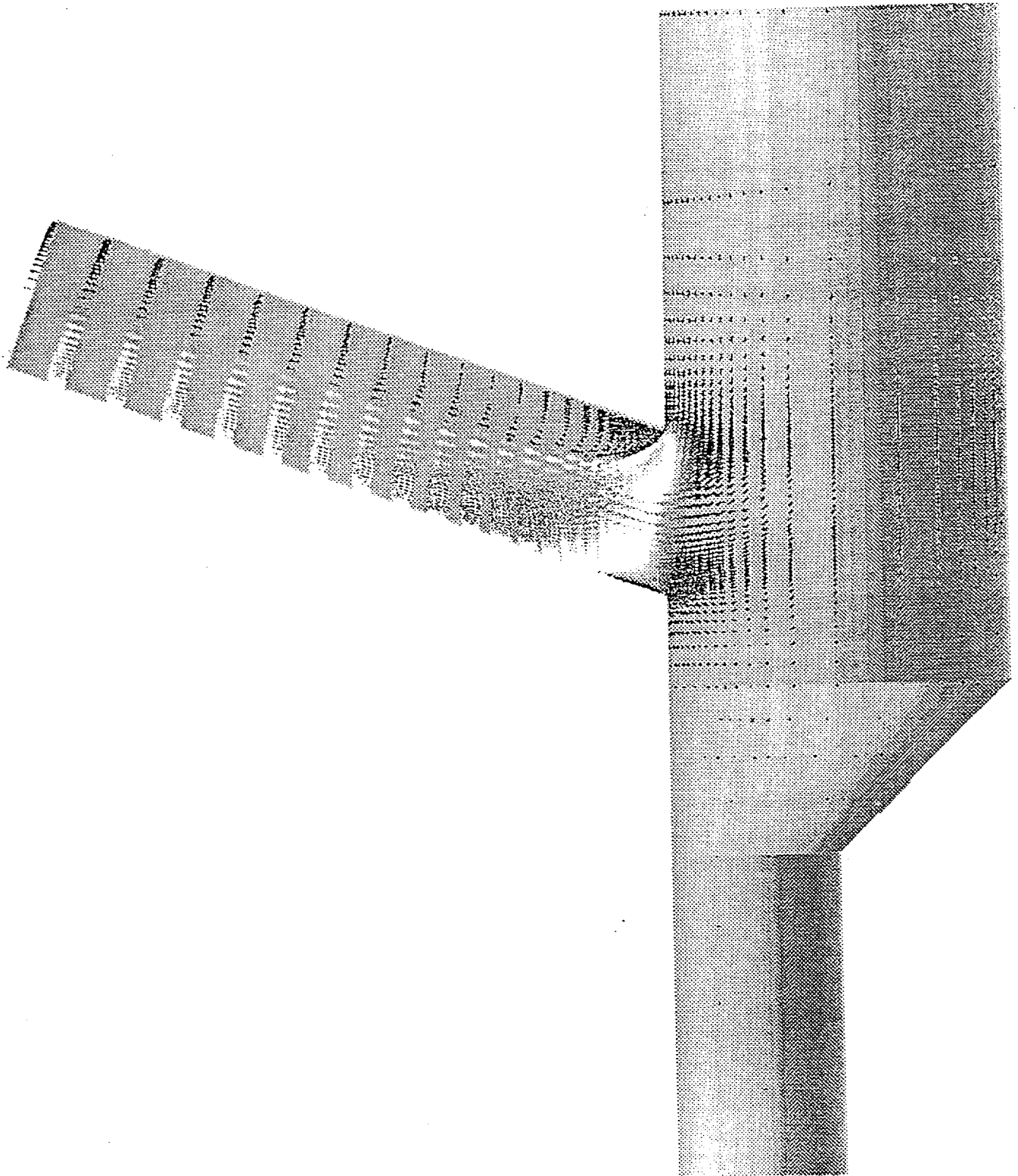
Velocity Vectors in Full-Scale Turn Without Transition Section
Exhibit 2.3-25
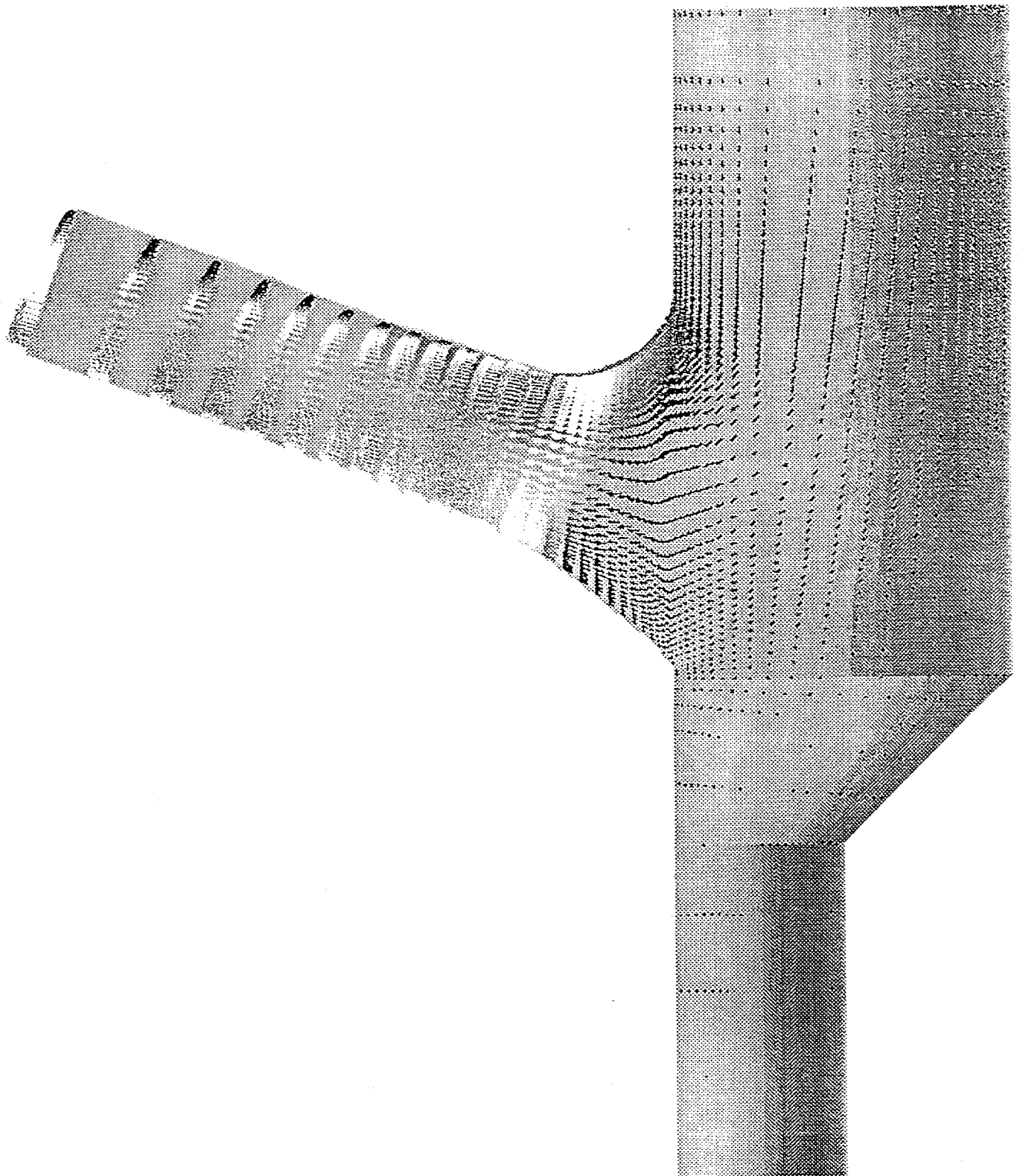
**Velocity Vectors in Full-Scale Turn With Vellmouth Transition Section
Exhibit 2.3-26**

Full Scale Turn with
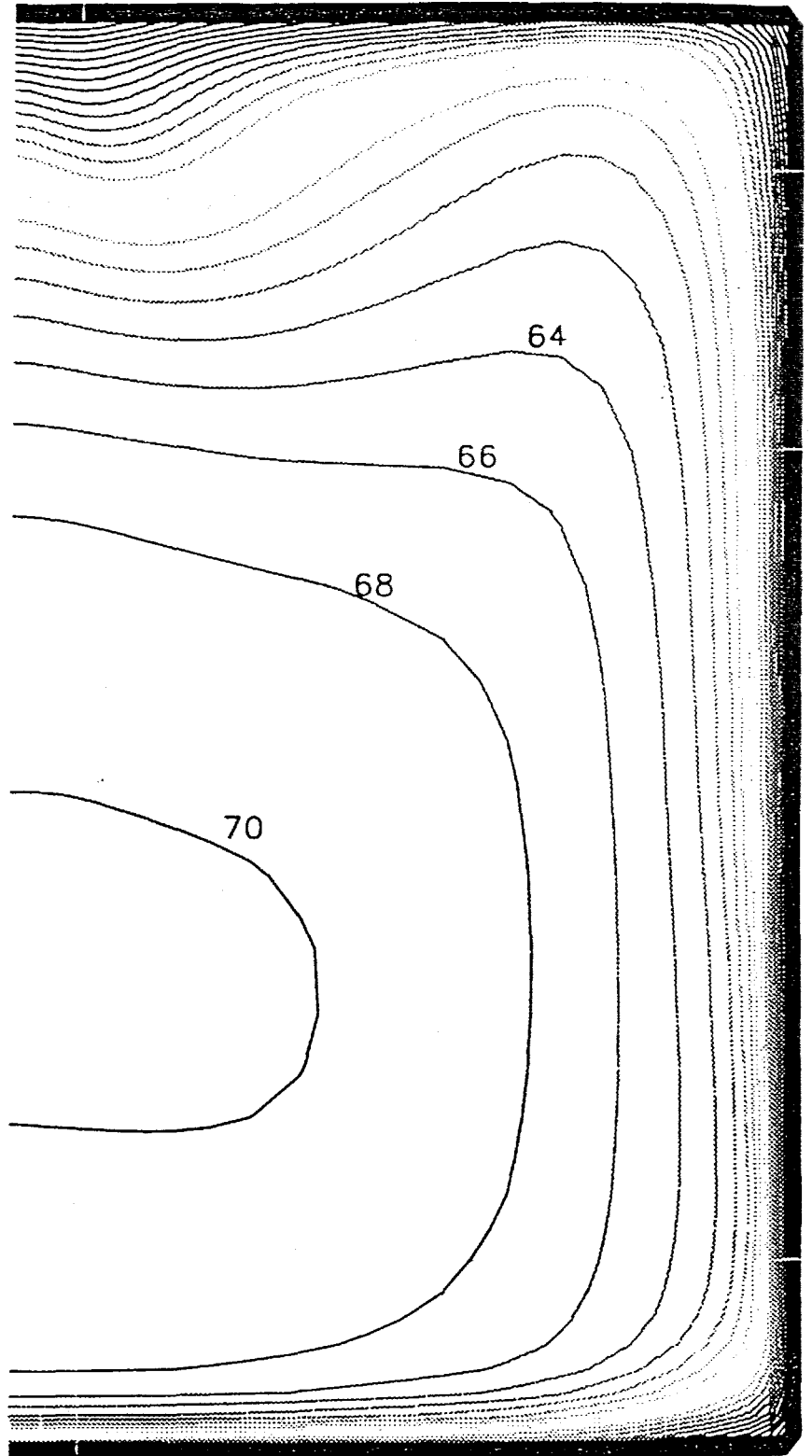No Transition

contours 20 ft upstream of exit

64

66

68

70

Uvel (fps)

70

0

Velocity Contours at Inlet to Slag Screen Without Transition Section
Exhibit 2.3-27

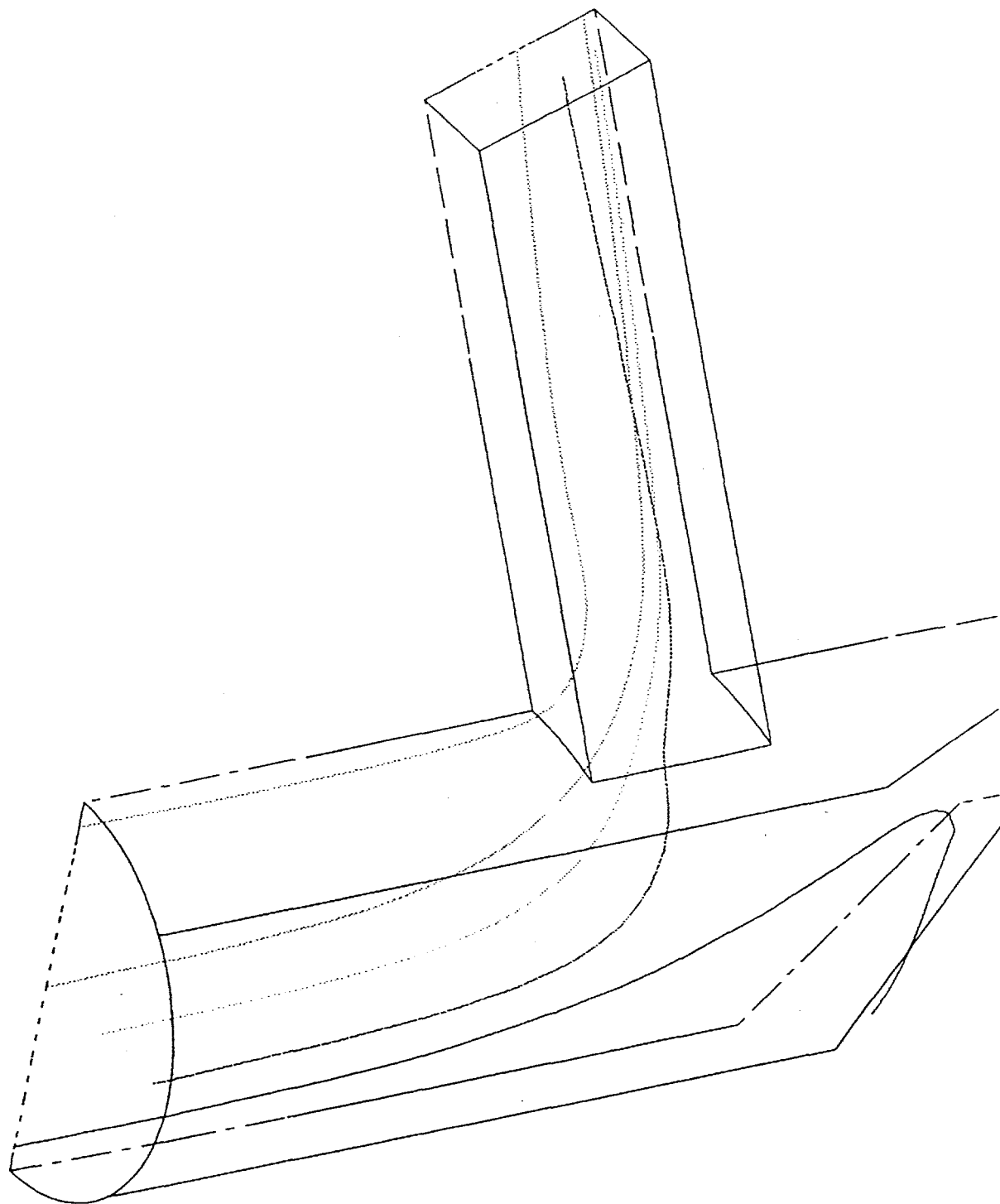Full Scale Turn with
Bellmouth Transition
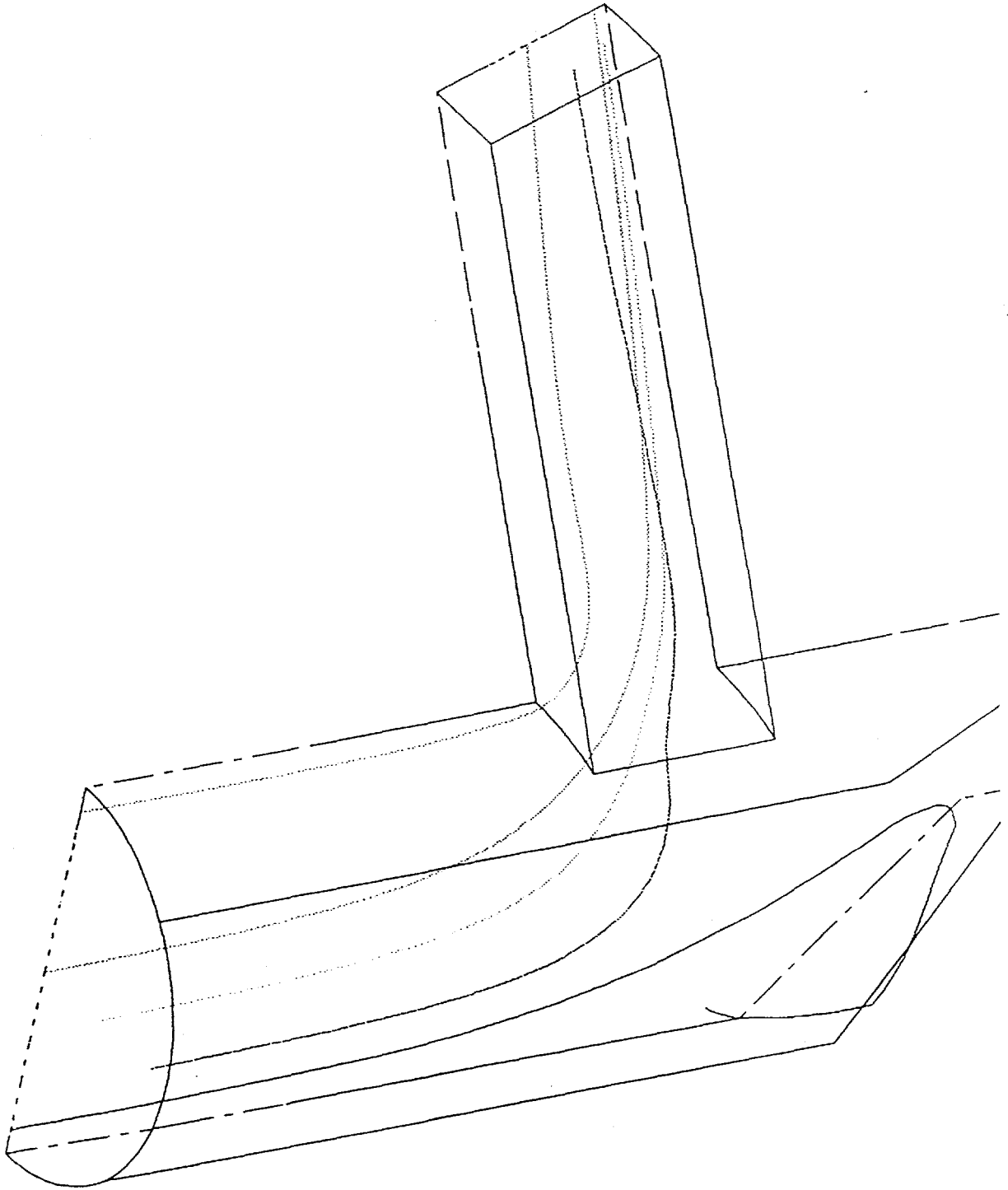
contours 20 ft upstream of exit

64

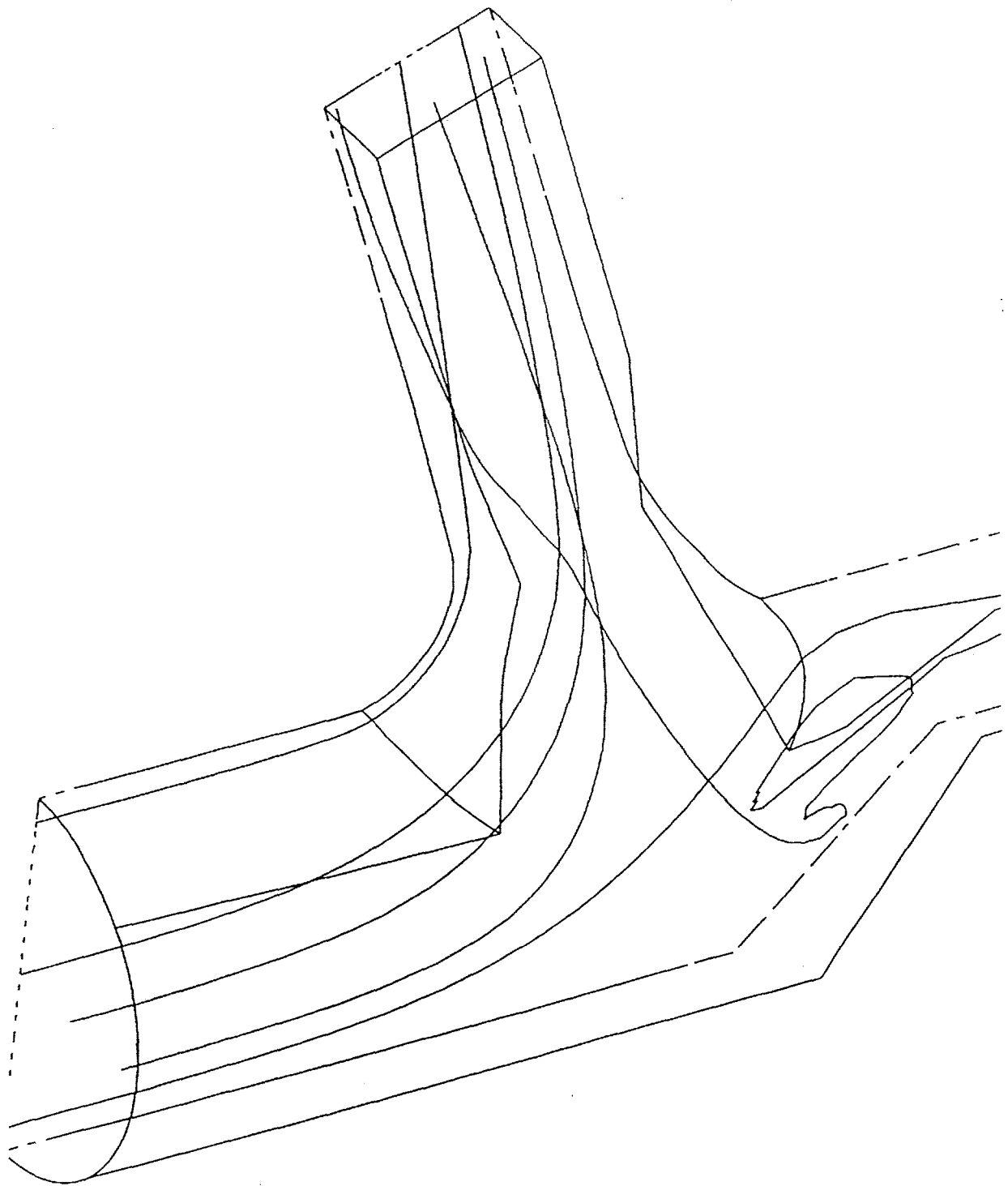66

68

70

Uvel (fps)

70

0

**Velocity Contours at Inlet to Slag Screen with
Bellmouth Transition Section
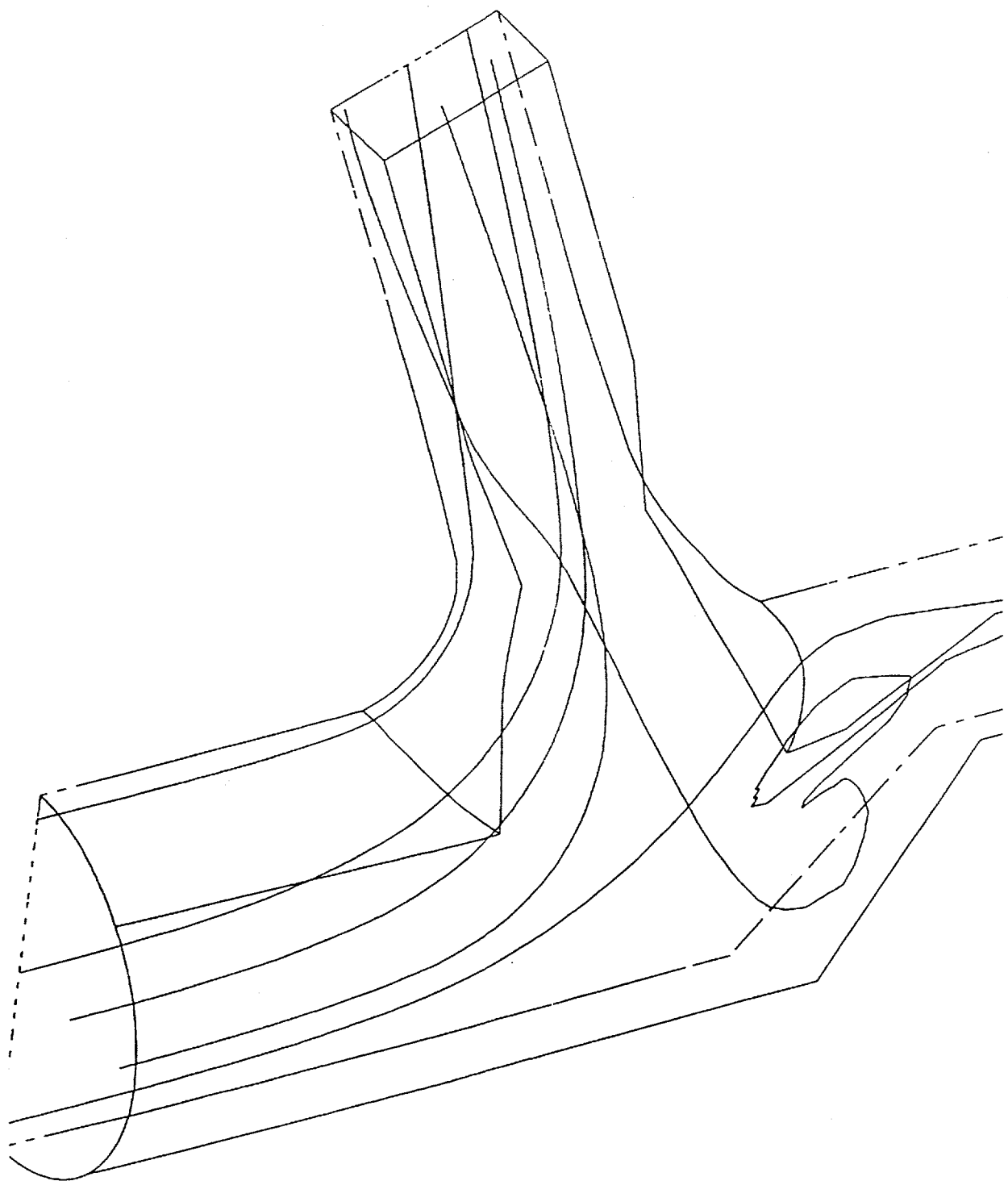Exhibit 2.3-28**

Trajectories for 50-Micron Diameter Ash Particles - No Transition Section
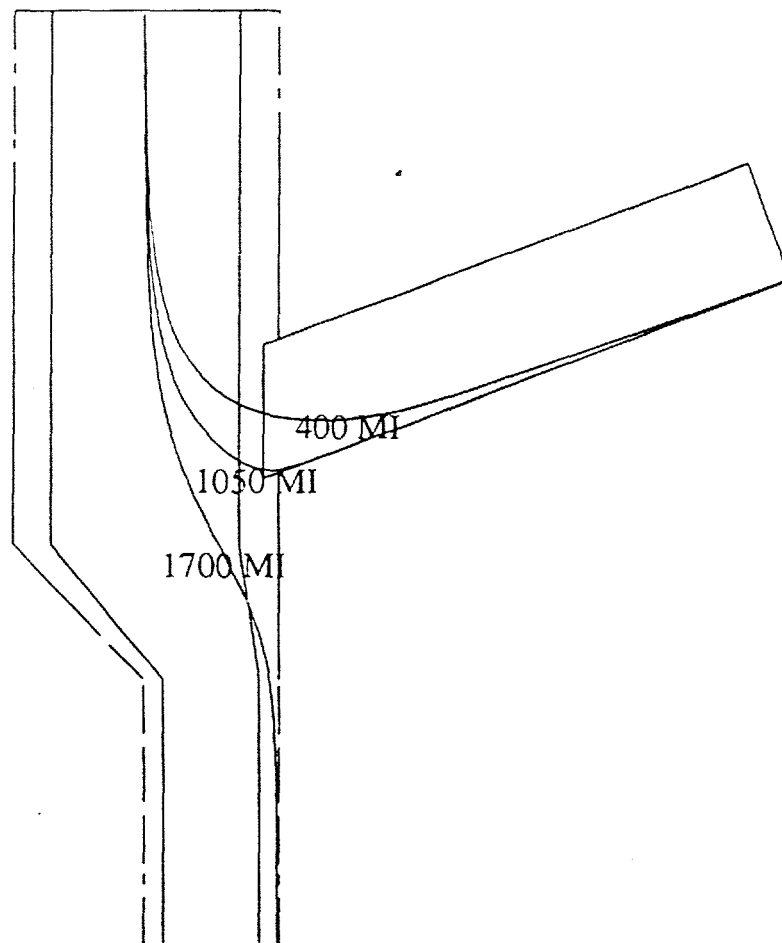**Exhibit 2.3-29**

**Trajectories for 1.25-Micron Diameter
Ash Particles - No Transition Section
Exhibit 2.3-30**

**Trajectories for 50-Micron Diameter
Ash Particles - Bellmouth Transition Section
Exhibit 2.3-31**

Trajectories for 1.25-Micron Diameter Ash Particles - Bellmouth Transition Section
Exhibit 2.3-32

Trajectories of Some Very Large Particles
Exhibit 2.3-33

400 MI

1050 MI

1700 MI

CFD Calculations for Pilot-Scale Quench Section

Results were obtained using computational fluid dynamics (CFD) for the pilot-scale quench section with either circular or rectangular cross-section. Calculations were performed to determine the rate of mixing of the main flow of flue gas with dilution air. In additional, temperature-time histories were computed for ash particles with various diameters to estimate whether the ash will be in the molten or solid state as it exits from the quench section or is trapped on the surface.

The results show that the flue and dilution flows become well mixed is a few duct diameters or heights.

The results also show that the particle temperatures remain much higher than the mixed flow temperature; therefore, adhesion efficiencies will also be high. Some improvements can be obtained using either overpenetration of the dilution jets or rectangular geometries

Quench Section Calculations - Baseline Results For Circular Geometry

For the purpose of these calculation, the quench section was assumed to be circular and to have a diameter (D) of one foot. The length of the section was to be determined as part of the calculations. However, using correlations for jet penetration and mixing, it was determined that, using eight 1-in. diameter dilution jets spaced circumferentially uniformly, mixing of the flue and dilution flows occurs in approximately two duct diameters. In the simulation, the duct extended six diameters in the downstream direction from the location of injection. A pipe of circular cross-section with length D/2 was placed upstream of the dilution jets. Flow conditions used in the simulation, together with the ideal mixed mean temperature, are presented in Exhibit 2.3-34.

Exhibit 2.3-34
## Flow Conditions for CFD Simulation of Quench Zone

	Flow rate, pps	Temp., F	Velocity, fps
Flue	0.8	2700	80.8
Dilution	0.4	300	218
Mass-averaged	-	1900	-

Note that the mixed mean temperature is based on a constant value of heat capacity. These flow conditions correspond to a dilution jet-to-flue gas momentum flux ratio (J) of about 30.

CFD results were obtained using the commercially available code, FLUENT. The computational domain extended in the circumferential direction from a plane of symmetry through a dilution jet to a plane of symmetry midway between jets - Exhibit 2.3-35. The number of grid cells was 79200. The calculation was continued until the flow field no longer changed significantly. To determine the extent to which mixing was completed, the mass-weighted average *deviation* of the temperature from the mean value was computed at each axial station. Note that the mean temperature is obviously constant after the dilution flow is injected. The mass-weighted average deviation of temperature was defined as follows:

$$\Delta T = \frac{\sum \dot{m} |T - \overline{T}|}{\sum \dot{m}}$$

Note also the use of absolute values in the above expression.
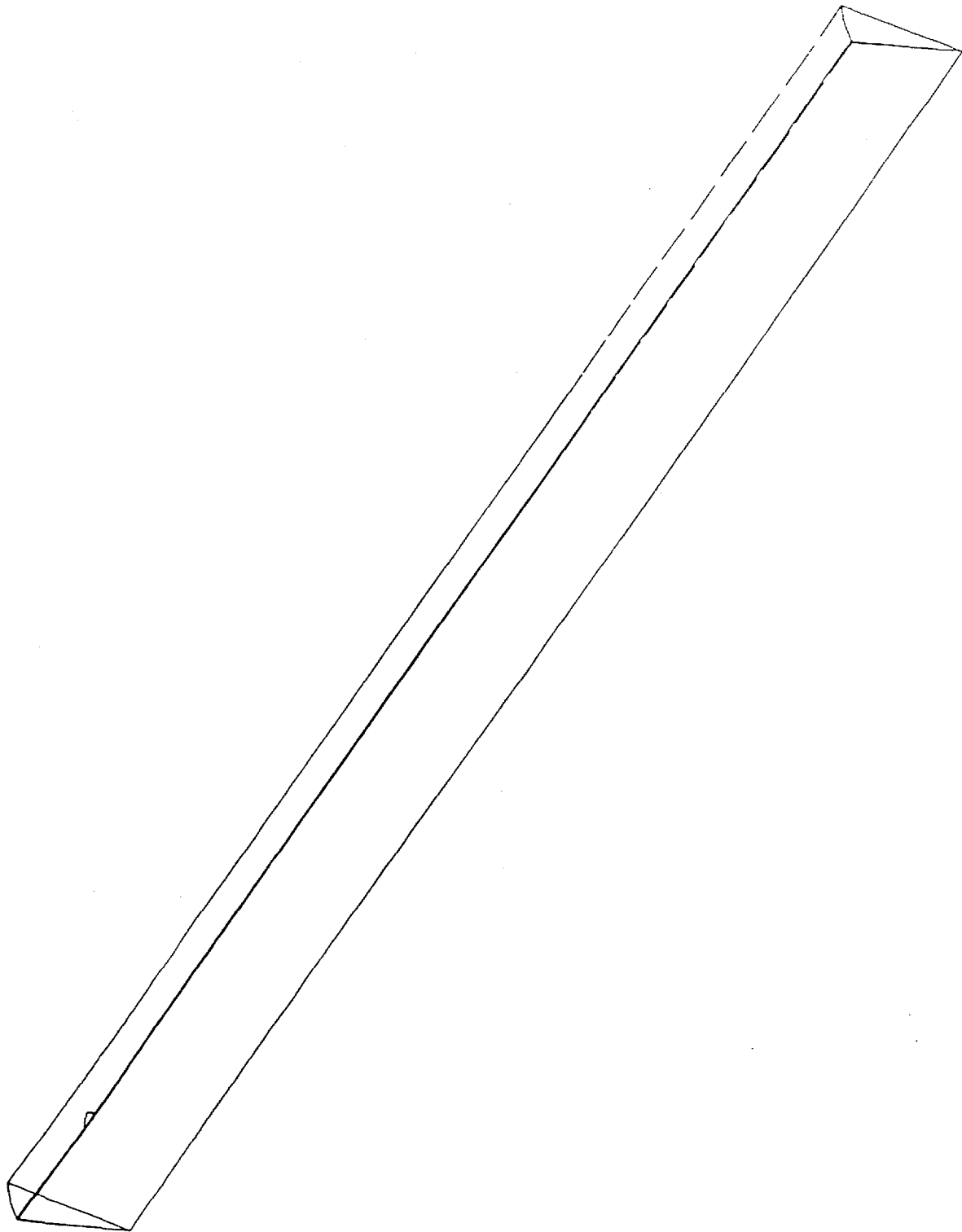
Quench Section with Cylindrical Geometry
Exhibit 2.3-35

Using this measure of mixedness, it was found that the mass-weighted temperature deviation was about three degrees F within two duct diameters and suggests that the flows are well mixed, a result in agreement with the available correlations. The variation of ΔT with distance is shown in Exhibit 2.3-36.

Optimum mixing occurs when the penetration of the dilution jet is approximately D/4 and the flow conditions used here were designed to obtain this value. Using the CFD results and defining penetration as the distance from the duct wall at which the minimum temperature occurs at each axial location, the penetration was computed and is shown in Exhibit 2.3-37. The CFD results show a somewhat larger penetration for this flow field.

Particle Temperature Histories

A series of particle trajectory calculations was made. In each case, particles of a uniform diameter were injected at an axial position of approximately D/2 upstream of the dilution jet. The variation of particle temperature with axial position was then recorded. The particles were assumed to have a density of 167 lbm/cuft (specific gravity of 2.7) and a heat capacity of 0.3 Btu/lbm-R. The particles were injected with an initial velocity and temperature equal to those of the flue gas. Mean trajectories were computed for particles located initially at 11 radial and 11 angular positions in the inlet plane; that is, 121 particles were injected at this location. Based on information provided by Physical Sciences, Inc. regarding the size distributions for the coals of interest, trajectories were computed for particles with diameters of 2.5, 5, 7.5, 15, 30, 50, 75 and 100 microns.

FLUENT terminated the trajectory calculation for each particle in the following manner. Some particles obviously exited the domain and were marked as "ESCAPED". Other particle trajectories intersected the wall of the section and were assumed to be TRAPPED there; whether the particles adhere to the surface is determined by the state of the particle (that is, by its temperature) when it strikes the surface. An objective of these calculations was to provide information on the temperature of these particles. In some cases, particle trajectory calculations were terminated for other reasons. For example, the program detects if a particle appears to be moving exceedingly slowly near a surface or computational boundary and then stops the calculation. Depending on the position of such particles, they were assigned to the TRAPPED class or to the ESCAPED class.

Based on the flow mixing results, the mean temperature and its standard deviation for each particle class are presented at two axial locations of 2D and 4D in the following tables. Note that mixing of the flue and dilution jet is essentially completed within two duct diameters. The results for the longer duct are provided to show that the particle temperature changes slowly in the downstream section. This slow rate of change is due to the fact that the particles move essentially with the gas velocity and, therefore, forced convection between the gas and particle is small.
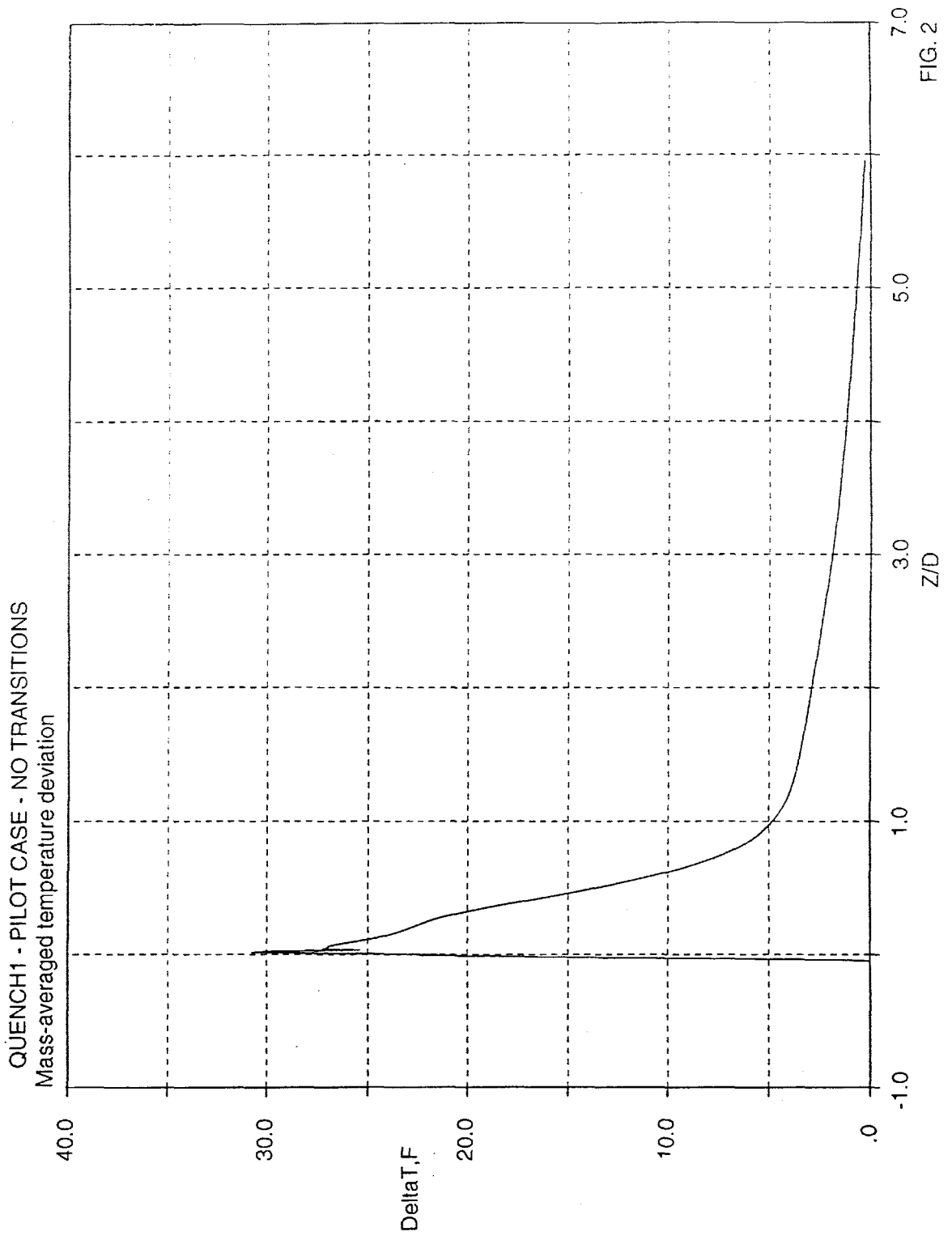
QUENCH1 - PILOT CASE - NO TRANSITIONS
Mass-averaged temperature deviation

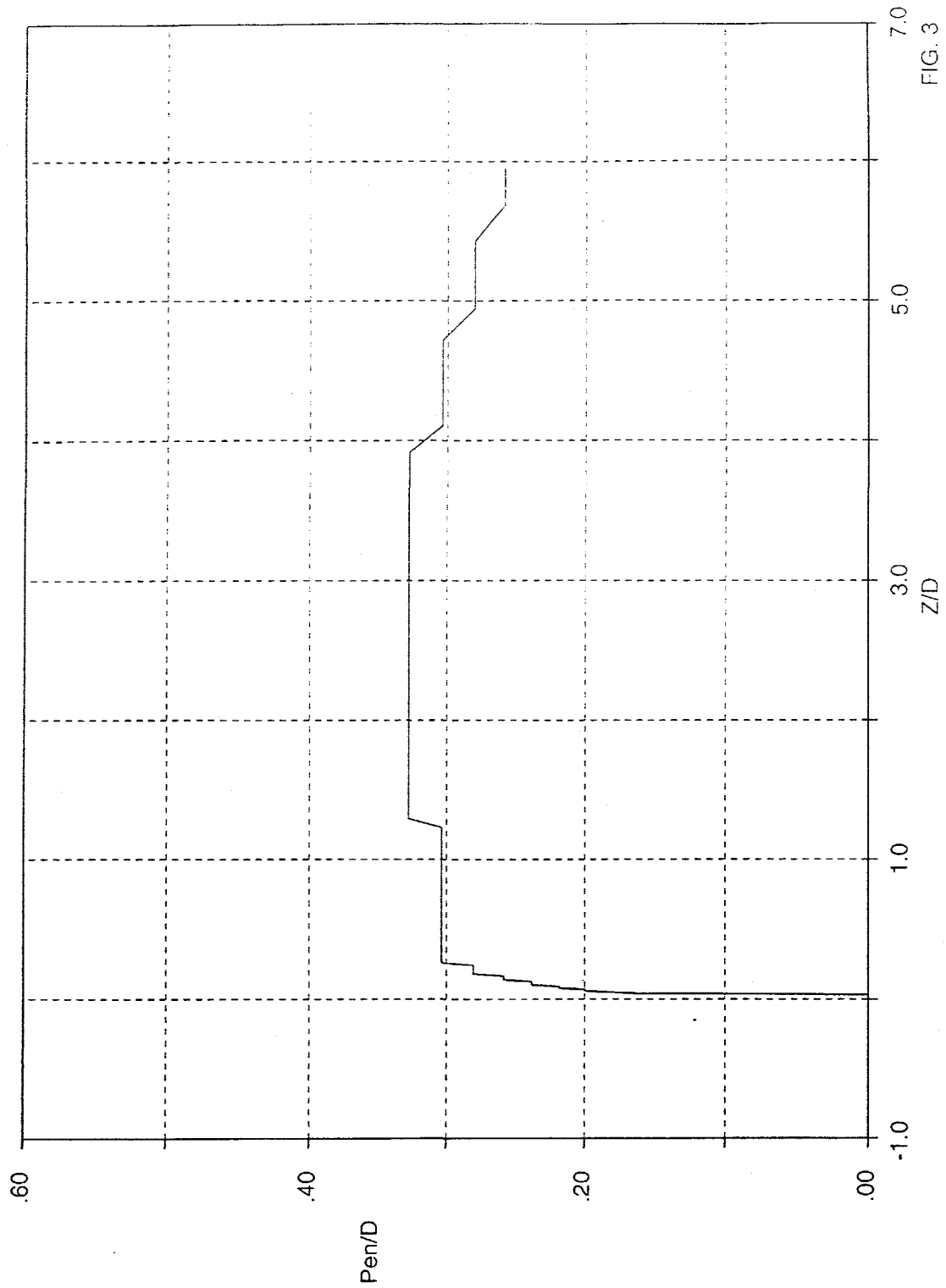FIG. 2

Quench 1 Pilot Case - No Transitions
Exhibit 2.3-36

Quench 1 Pilot Case - No Transitions
Exhibit 2.3-37

Statistical information for particles that remain in the gas flow at two axial stations is presented in Exhibit 2.3-38. The number of particles for a given class that is included in each statistic may vary from station to station since some particles may become trapped as they move downstream. Note the very large standard deviations of the smaller particles due to the fact that the small particles respond rapidly to the gas temperature, which varies significantly near the dilution jet. Note also that the temperature of each particle class remains significantly higher than the fully-mixed gas temperature (1900 F). This result is contrary to the estimates provided by PSI, as discussed below. It should also be noted that some entries of Exhibit 2.3-38 and -39 indicate that only a few particles are included in the sample. No attempt is made to assign statistical significance to such samples other than to note that the values recorded are probably representative of these classes of particles.

Exhibit 2.3-38
Quench 1Temperature Properties of Particles in Flow

Diam, μm	Z/D	Number	Tave, F	Std. Dev., F	TminF	Tmax F
2.5	2,4	115	2273	463	770	2691
5	2,4	114	2314	404	1143	2692
7.5	2,4	110	2325	403	1123	2694
15	2,4	99	2228	481	903	2693
30	2,4	83	2166	325	1490	2671
50	2,4	86	2288	227	1932	2557
75	2	89	2392	108	2191	2618
	4	88	2391	109	2191	2618
100	2	94	2447	75	2322	2623
	4	88	2447	77	2322	2623

For particles that are trapped in the vicinity of the surface of the quench section, the temperature statistics are shown in Exhibit 2.3-39. Here, the typical temperature, at least for smaller particles, is much higher than that shown in Exhibit 2.3-38 because the particles that have been trapped have not had sufficient time to cool to as great as an extent.

Exhibit 2.3-39
Quench 1 Temperature Properties of Trapped Particles

Diam, μm	Z/D	Number	Tave, F	Std. Dev., F	Tmin F	Tmax F
2.5	2,4	3	2483	176	2322	2671
5	2,4	3	2447	203	2278	2673
7.5	2,4	7	2313	256	1984	2676
15	2,4	19	2399	230	2013	2678
30	2,4	35	2447	242	1959	2684
50	2,4	32	2437	227	1979	2684
75	2	29	2452	191	2091	2682
	4	31	2424	214	2011	2682
100	2	24	2517	115	2250	2675
	4	29	2457	171	2116	2675

PSI has provided adhesion efficiency estimates for two types of coal ash. For the Illinois 6 coal ash, it is necessary to cool the particles to below 2200 F in order to minimize adhesion. For the Wyodak-Rochelle coal ash, adhesion efficiencies of 30-50 percent exist even at 1800 F. In any case, the computed results show that particle temperatures remain high in the quench section.

The estimates on adhesion efficiency for the time required to cool the particles were based on a model that assumed that particle velocity lag was large enough such that forced convection was the only important heat transfer mode; that is, free convection was neglected. This model also included conduction within the particle. The model used was derived from a model for a particle in good thermal contact with the surrounding fluid, an assumption that implies high convective heat transfer coefficients as can occur in forced convection However, FLUENT predicts that the velocity lag is small for most of the particle trajectory. Therefore, the only effective heat transfer mechanism is free convection - essentially, the Nusselt number is equal to about two. It is true that turbulent fluctuations will increase the effective Nusselt number (since the particle velocity will always lag that of the fluctuating gas velocity), but these are accounted for in neither the PSI nor the FLUENT calculations. If one considers only free convection to a solid particle of uniform temperature, then it can be shown that the results presented in Exhibit 2.3-38 and -39 are reasonable.

Detailed examination of the results for the 3D flow case suggests the following reasons for the difference between the relatively optimistic results from the simplified model (such as that used by PSI) and the more pessimistic results of the more detailed (3D) calculations. Consider first the larger particles. Here, the trajectories are relatively unaffected by the flow of the cold dilution jet. Particles that are directed initially toward the jet are cooled rapidly initially and then more slowly in the mixing region downstream of the jet. However, since the particles were distributed uniformly across the inlet plane, most of the larger particles flow around the jet and into the relatively unmixed flow just downstream of the jet, thereby cooling more slowly. For the smaller particles,

the trajectories are affected greatly by the presence of the jet. These particles are deflected around the jet and into the relatively warm flow of the mixing zone.

The maximum and minimum temperatures of each particle class are shown in Exhibit 2.3-38 and -39. For the smaller particles, the range of temperatures is quite large. For the larger particles, the range is smaller. In any case, some particles are indeed cooled to the desired temperature range to minimize adhesion. On the other hand, the overall results indicate that the temperatures are not low enough on average.

Assuming that the results for particle temperature provided here are representative of conditions within the quench zone, then it is apparent that much larger dilution flows are required to produce a sufficiently low mixed temperature. Additional length for this section is not generally effective in reducing the temperature of the particles to the desired range - most of the average values in Table 2 remain unchanged from L/D of 2 to L/D of 4. Another possible approach is to accelerate or decelerate the flow rapidly to produce an appreciable velocity lag and thereby increase forced convection effects; for example, the flow from the quench section can be decelerated using a sudden expansion in cross-sectional area, as was done in one of the additional cases run in this series. However, this method will only be effective for the larger particles since small particles accommodate more readily to the local mean gas velocity. In any case, it was found that the overall improvement was only slight.

Use Of Jet Overpenetration

In Exhibit 2.3-40, temperature contours are presented at a location of two quench section diameters downstream of the dilution jets. It can be seen that a relatively warm region of fluid persists on the centerline of the duct. This so-called "hot spot" is a direct consequence of the symmetric arrangement of the dilution jets around the periphery of the duct. The size of the hot spot can be reduced somewhat (but not eliminated) by increasing the penetration of the dilution jets. In Case 5, the momentum flux ratio was increased to 60 and the temperature contours at the same axial location show some decrease in the size of the the hot spot - see Exhibit 2.3-41. For both momentum flux ratios, the temperature distribution is stratified. Particle temperature histories are shown in Exhibit 2.3-42 and -43 and indicate that the temperatures of particles that remain in the flow are somewhat reduced; the temperatures of some trapped particles actually increase due to the larger disturbance of the trajectories caused by the higher momemtum jets.
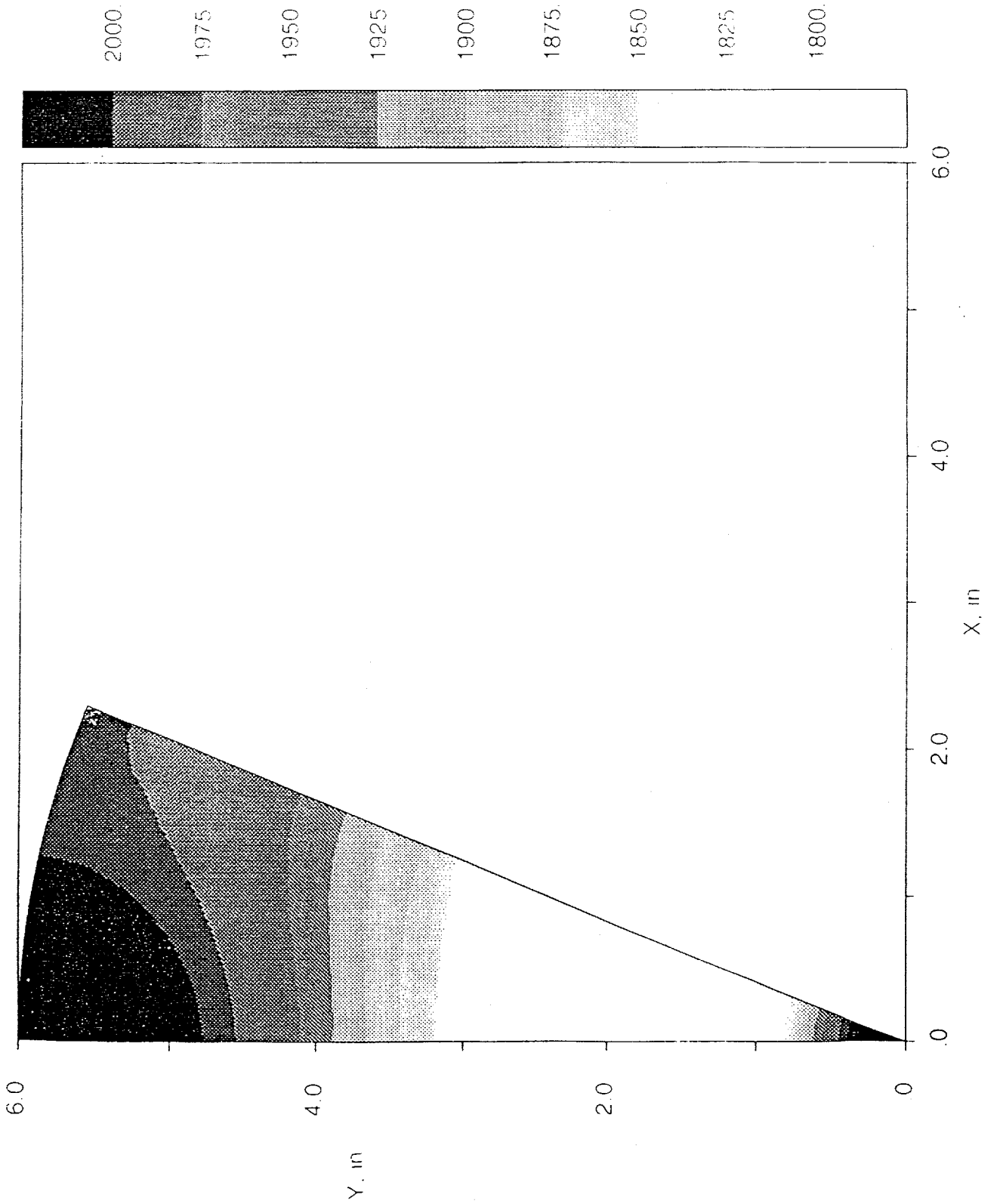
Quench 1 Temperature Contours at Z/D=2 (24 in.)
Exhibit 2.3-40
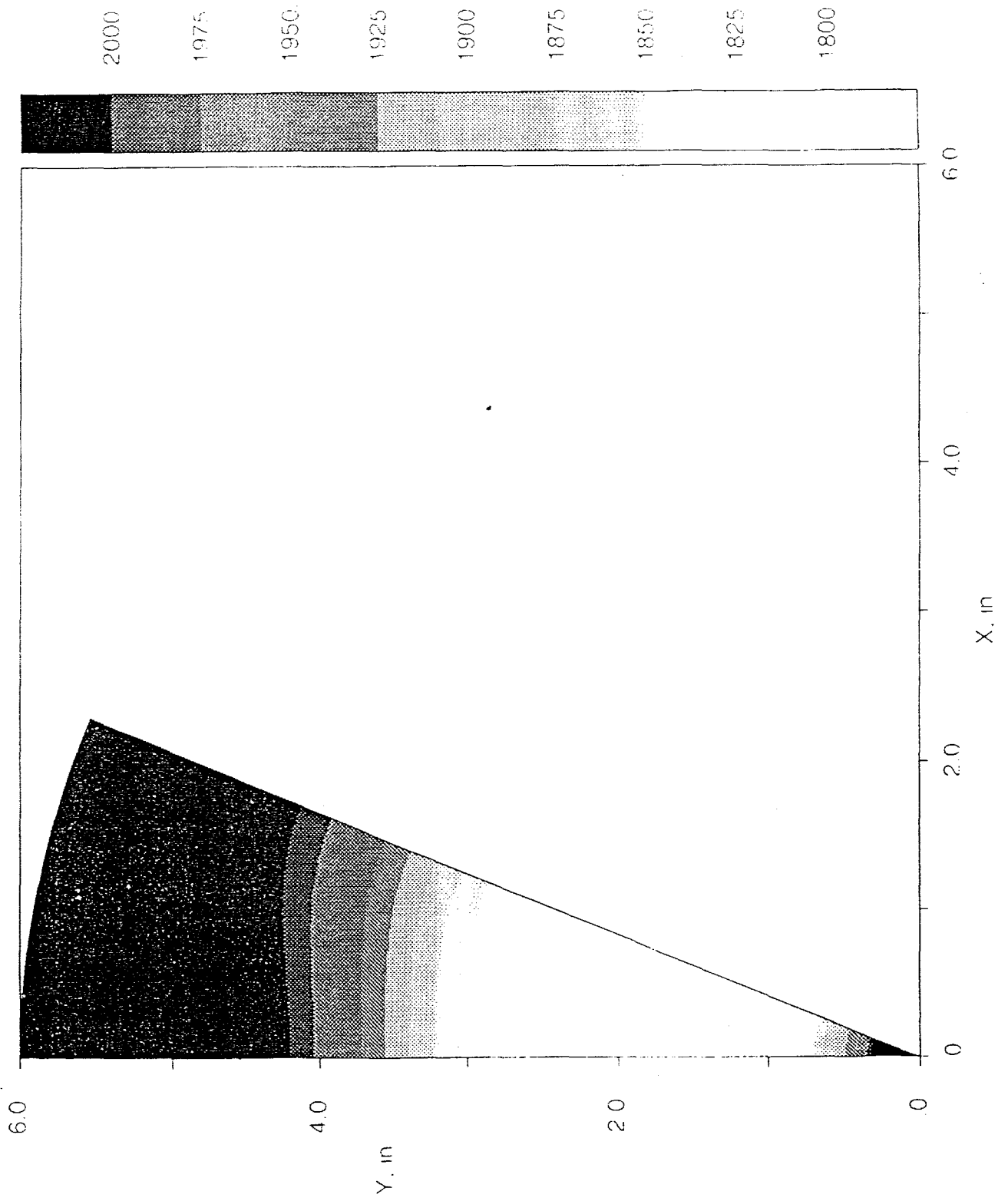
Quench 5 Temperature Contours at Z/D=2 (24 in.)
Exhibit 2.3-41

Exhibit 2.3-42
## Quench 5Temperature Properties of Particles in Flow

Diam, μm	Z/D	Number	Tave, F	Std. Dev., F
2.5	2,4	116	2213	451
5	2,4	112	2246	417
7.5	2,4	109	2216	438
15	2,4	93	2084	462
30	2,4	79	2042	204
50	2	81	2212	122
	4	79	2210	123
75	2	80	2334	92
	4	85	2330	90
100	2	92	2414	76
	4	89	2411	76

Exhibit 2.3-43
Quench 5 Temperature Properties of Trapped Particles

Diam, μm	Z/D	Number	Tave, F	Std. Dev., F
2.5	2,4	2	2411	384
5	2,4	5	2388	207
7.5	2,4	9	2345	200
15	2,4	25	2477	159
30	2,4	39	2505	185
50	2	37	2497	179
	4	39	2477	195
75	2	30	2501	160
	4	33	2473	178
100	2	26	2542	106
	4	29	2512	135

Results for ducts with rectangular geometry

CFD calculations were also made for two designs in which a rectangular duct was used with two dilution hole arrangements. In the first design, the holes in the upper and lower surface of the duct are arranged in a staggered fashion - see Exhibit 2.3-44; this case was designated as Case 6. In Case 7, the holes are aligned on the upper and lower surfaces - see Exhibit 2.3-45; only the upper portion of the duct is shown here, due to the fact that the duct is symmetric in this case. The staggered-hole design can eliminate the hot spot, in principle.
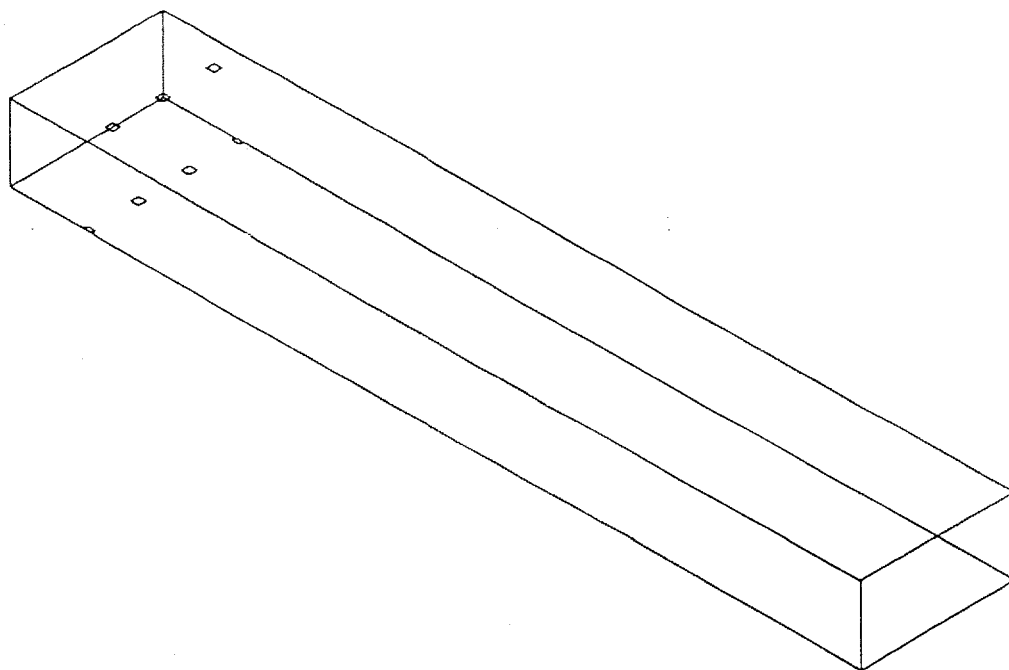
Rectangular Duct with Staggered Dilution Jet Holes
Exhibit 2.3-44
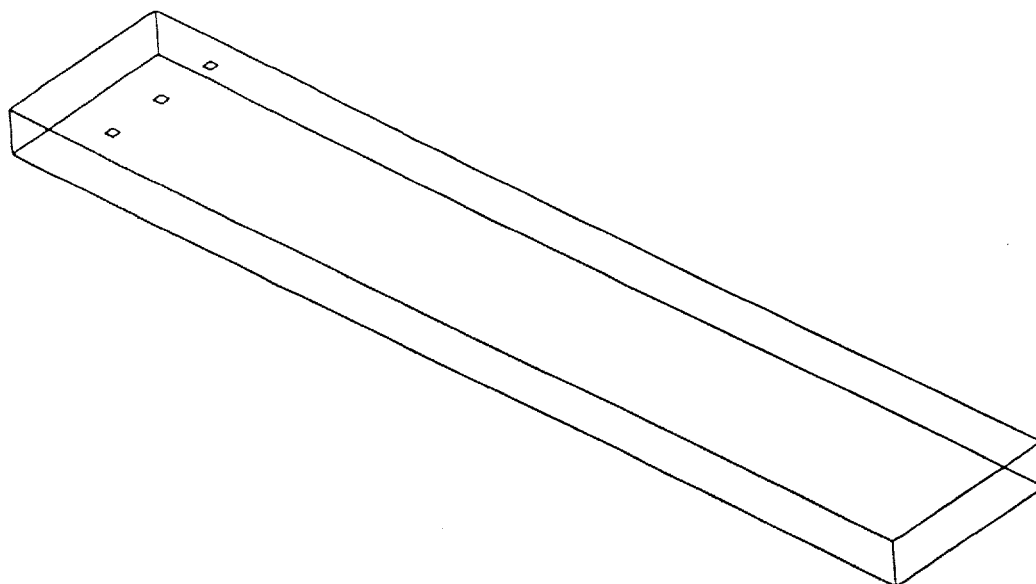
Rectangular Duct with Inline Dilution Jet Holes
Exhibit 2.3-45

Particle temperature results are given inExhibit 2.3-46, -47, -48, and -49 for these two cases. Overall, it can be seen that the staggered-hole arrangement provides better results (lower temperatures) than the in-line design; also, rectangular ducts provide better results than circular ducts do.

Exhibit 2.3-46
Quench 6 Temperature Properties of Particles in Flow

Diam, μm	Z, in.	Number	Tave, F	Std. Dev., F
2.5	24	193	1905	16
5	24	190	1908	56
7.5	24	156	1902	17
15	24	105	1901	15
30	24	· 73	2477	198
50	24	69	2502	91
75	24	69	2515	42
100	24	73	2530	24

Exhibit 2.3-47
Quench 6 Temperature Properties of Trapped Particles

Diam, μm	Z, in.	Number	Tave, F	Std. Dev., F
2.5	24	7	2084	309
5	24	10	2030	291
7.5	24	44	1897	203
15	24	95	1954	198
30	24	127	1968	176
50	24	131	2170	108
75	24	131	2299	91
100	24	127	2363	78

Exhibit 2.3-48
Quench 7 Temperature Properties of Particles in Flow

Diam, μm	Z, in	Number	Tave, F	Std. Dev., F
2.5	24	95	2183	497
5	24	94	2239	465
7.5	24	85	2314	464
15	24	88	2328	451
30	24	54	2420	310
50	24	52	2347	316
75	24	60	2428	178
100	24	63	2470	113

Exhibit 2.3-49
Quench 7 Temperature Properties of Trapped Particles

Diam, μm	Z, in	Number	Tave, F	Std. Dev., F
2.5	24	5	2428	531
5	24	6	2291	583
7.5	24	15	1974	530
15	24	12	1957	563
30	24	46	2190	287
50	24	48	2086	249
75	24	40	2213	167
100	24	37	2319	100

Temperature distributions are shown in Exhibit 2.3-50 and -51. Generally, the flow is mixed better than the flow in the circular geometry cases; the staggered-hole arrangement shows better mixing of the flue gas and dilution jets than does the in-line hole case.
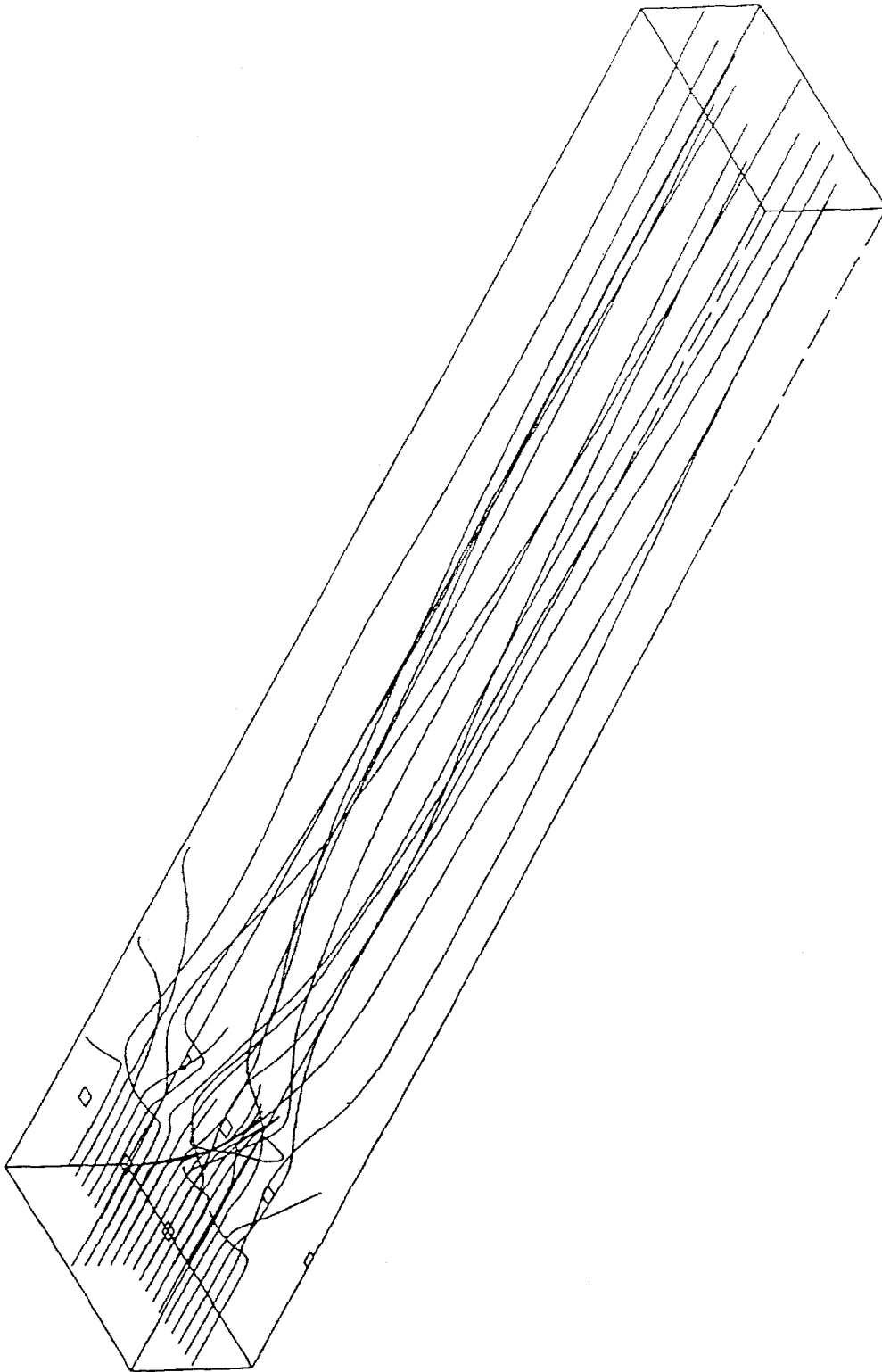
Selected particle trajectories for Case 6 are shown in Exhibit 2.3-52 and -53 for the 15 and 30-micron diameter particles, respectively. As illustrated by the two sets of trajectories located initially along the midplanes, more of the 15-micron diameter particles remain in the flow. Once deflected, the inertia of some of the 30-micron diameter particles transports them to the walls of the duct.
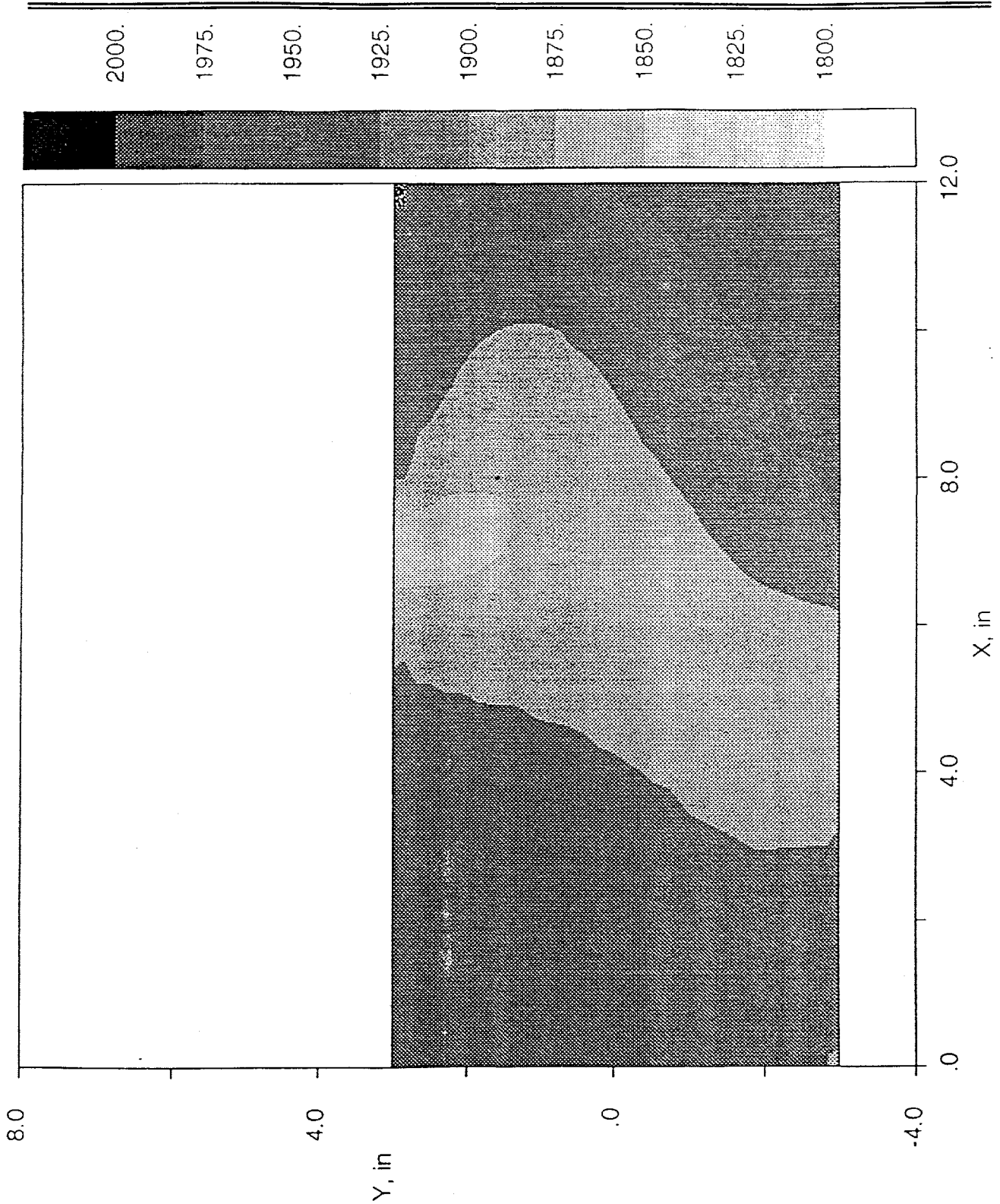
Temperature Contours in Rectangular Duct with Staggered Holes at Z=24In.
Exhibit 2.3-50
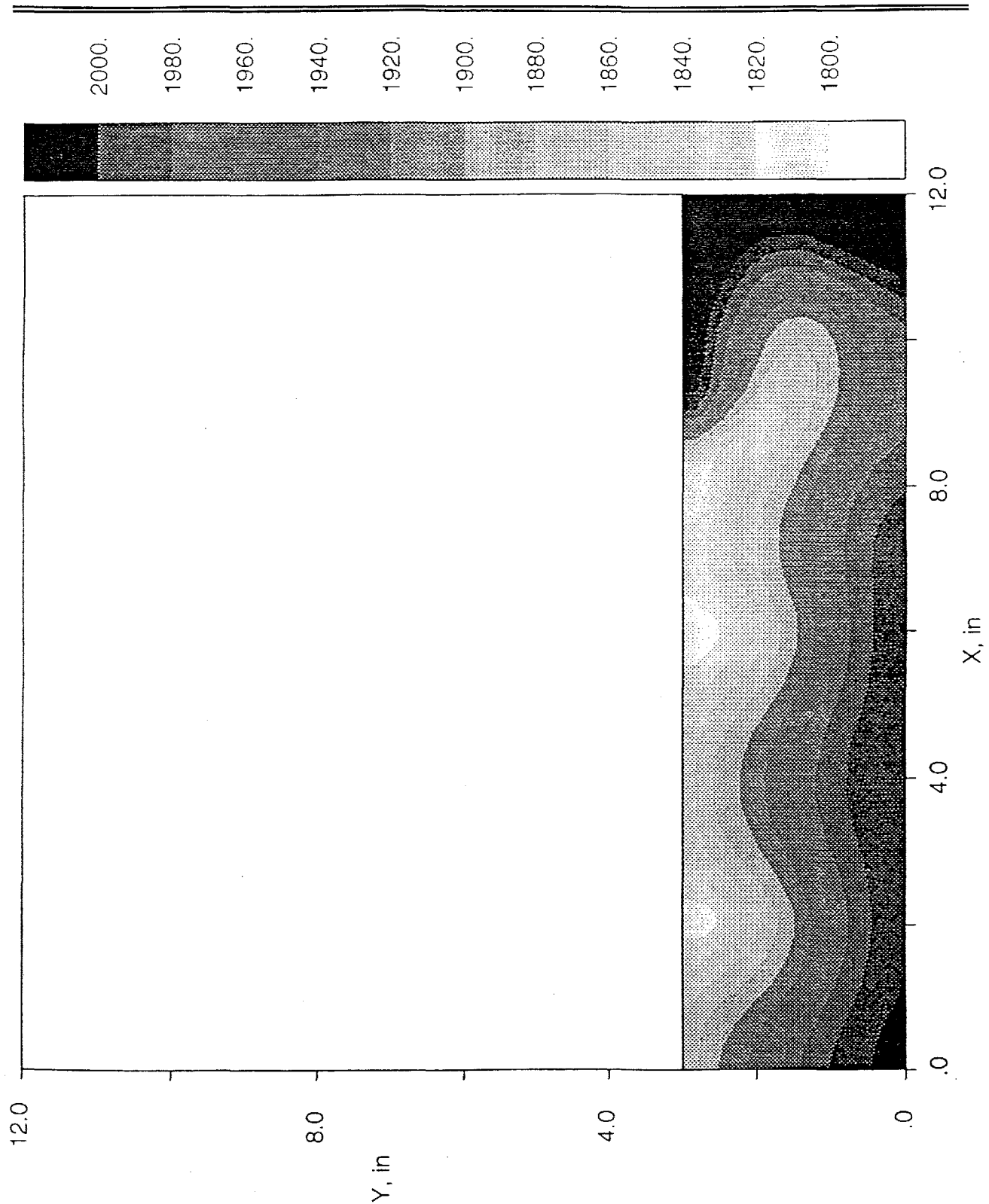
Temperature Contours in Rectangular Duct with
Inline Holes at Z/D=2 (24 in.)
Exhibit 2.3-51

**Selected Tranjectories for quench 6 Case with
15-Micron Diameter Particles
Exhibit 2.3-52**

**Seclected Tranjectories for Quench 6 Case with
30-Micron Diameter Particles
Exhibit 2.3-53**

Concluding Remarks

- The best results are obtained with the staggered-hole arrangement in a rectangular duct.

- Previous calculations show that the slag screen can remove almost all of the larger particles, so the results here may be somewhat pessimistic. Also, no account has been made in the present calculations for the temperature decrease of the flue gases due to the slag screen.

- The results indicate that the temperature reduction may be acceptable for the Illinois No. 6 coal used in the pilot-scale design.

- For the Wyodak-Rochelle coals, no target temperature has been specified, but adhesion results from PSI indicate that it will be necessary to reduce particle temperatures further than those achieved by the designs considered here.

References

1. Kalmanovitch, D.P. and Frank, M. "An effective model of viscosity for ash deposition phenomena," Proc. Engineering Foundation Conference on Mineral Matter and Ash Deposition from Coal, p. 89, 1988.

2. Nowok, J. and Hurley, J., *Energy & Fuels,* 1995.

3. Bool, L.E. and Helble, J.J. "Iron Oxidation State and Its Effect on Ash Particle Stickiness," Proc. Engineering Foundation Conference on Application of Advanced Technology to Ash-Related Problems in Boilers, Henniker, NH, June, 1995.

4. Frenkel, J., "Viscous Flow of Crystalline Bodies Under the Action of Surface Tension" *J.Phys.(Moscow)*, 1945, *9*, 385-391.

5. Hiram, Y. and Nir, A., "A Simulation of Surface Tension Driven Coalescence" *J.Colloid Inter. Sci.* 1983, *95*, 462-470.

6. Mackenzie, J.K. and Shuttleworth, R., "Phenominological Theory of Sintering," *Proc. Phys.Soc.(London)*, 1949 *B62*, 833-852.

7. Scherer, G.W., "Sintering of Low-Density Glasses: I, Theory," *J.Am.Cer.Soc.*, 1977, *60*, 236-239.

8. Raask, E. *Mineral Impurities in Coal Combustion*; Washington, D.C.: Hemisphere Publishing, 1985.

9. Senior, C.L. and Srinivasachar, S. "Viscosity of Ash Particles in Combustion Systems for Prediction of Particle Sticking," *Energy & Fuels* 1995 *9*(2), 277-283.

10. Nowok, J.W. and Benson, S.A. *Inorganic Transformations and Ash Deposition During Combustion*; ASME: New York, NY; 1991, pp. 405-424.

11. Stultz, S. and Kitto, J. *Steam: Its Generation and Use*, 40th Edition; The Babcock & Wilcox Company: Barberton, OH; 1992.

12. Borio, R.W., Levasseur, A.A., Chow, O.K., and Miemiec, L.S., "Ash Deposition: A Boiler Manufacturer's Perspective," *Inorganic Transformations and Ash Deposition During Combustion*; ASME: New York, NY; 1991.

13. Sangiovanni, J.J., Seery, D.J., Chiappetta, L., and Senior, C.L. , "Coal-Fired High Performance Power Generating System," ASME Paper 94-JPGC-PWR-3, 1994.

14. Scherer, G.W. and Bachman, D.L., "Sintering of Low-Density Glasses: II, Experimental Study," *J.Am.Cer.Soc.*, 1977, *60*, 239-243.

15. Nowok, J.W., Benson, S.A., Jones, and Kalmanovitch, D.P., "Sintering behaviour and strength development in various coal ashes," *Fuel*, 1990, *69*, 1020-1027.

Task 2.4 Duct Heater Design

Air Heater Construction

During this reporting period, selection of a supplier for the electric air heater to be used in the UTRC Jet Burner Test Stand (JBTS) was completed. This heater will be used for sub-scale development testing of a low NO_x in-duct boost heater using natural gas to boost the HITAF clean air discharge temperature from 1700° F to 2495° F prior to entry into the gas turbine. This heater system represents a significant capital investment by UTRC (approximately $510k) for this program; consequently every effort was made to ensure that the heater acquired would meet the requirements of this as well as future programs envisioned to be undertaken in the JBTS.

The heater system selected is manufactured by Phoenix Solutions of Minneapolis, MN. This company has had significant experience in development of high temperature, high flow, high pressure resistance heaters for research applications in the U.S. and Japan. Extensive negotiations with Phoenix Solutions were required in order to obtain a heater and control system which would meet the facility requirements of the JBTS, as well as the program requirements, at as low a capital investment cost as possible.

The heater system includes a 4160Vac power supply which provides 210 Vdc to the heater at a 1.5 MW maximum power level. The heater is designed for operation at 600 psig with 900° F inlet air provided by a JBTS natural-gas fired air heater. The flowrate for the heater is nominally 5 lbm/sec.

Located in the test cell will be the water-cooled power supply, the air heater, and the combustor. The air heater as designed by Phoenix Solutions is 5 feet long, vertically mounted, and covers a floor area of 9 square feet. The combustor section and water injection section are estimated to occupy a space 6 feet wide and 14 feet long. Heater controls, and facility interface for monitoring and data acquisition will be provided outside the test cell.

Additional capital items to be provided by UTRC include high temperature piping from the air preheater to the test cell containing the electric air heater, data acquisition equipment for airflow and thermal monitoring, valves for air control, and electrical substation modifications to provide switching and emergency shutoff of the electrical supply (4160Vac at 460 amps).

Negotiations have been completed for final terms and conditions of delivery of the electric air heater and power supply. If the air heater is delivered by September 15, 1996. installation could commence on October 1, 1996, with installation to take an estimated 2-1/2 months. During the interim time period, design of the combustor for the duct heater testing will be initiated and preliminary designs of fuel/air mixers will be evaluated in cold flow per the program described in the original work statement contained within the proposal.

Electrical substation work will be performed during the period prior to delivery of the power supply to provide 4160Vac at 460 amps to the vacuum contact breakers and manual switchgear associated with the JBTS electrical power distribution system. Every effort will be made to have the JBTS facility ready to receive the electrical power supply and air heater when they are delivered and the test cell becomes available for heater installation. It is planned that all outside electrical substation, conduit and trench work will be completed before the onset of winter.

Facility modifications for air piping will be initiated, but final piping interface to the test cell will not be performed until the heater is in place in the test cell due to the critical nature of the high temperature, high pressure piping to be used in this air flow path. However, valving and piping design will have been completed and piping installed up to the test cell prior to this time so that the work can proceed once the electrical air heater is installed in the test cell.

During this period, substantial interaction has taken place between UTRC personnel and Phoenix Solutions to provide optimum integration of the heater and controls with the JBTS facilities. There have been four design reviews and teleconferences in the preceding 2 months with the purpose of finalizing control circuitry and facility controls to protect the integrity of the heater system while in operation. Also, numerous code issues have been addressed and changes made to the interlock systems to enable safe operation and maintenance of the heater once it is in place.

Flue Gas Recirculation Quench Zone

It has been suggested that a rapid quench zone be developed at the discharge of the HITAF heater in order to reduce the gas temperature below the level at which the suspended ash particles would stick to the duct walls. This would prevent slag buildup and facilitate removal of the particulate at regular intervals from the walls through mechanical cleaning without excessive effort. This quench zone has been examined based upon experience in dilution jet mixing as applied to gas turbine combustors, where rapid quenching in very short distances are required. The previous research suggests a quench zone design based on crossflow jets. Recent gas/gas mixing experiments in a cylindrical duct and a limited literature review suggests that quenching can be attained within 2 duct diameters with a crossflow configuration.

In this reporting period, extensive analysis has been performed and it has been proposed that the quench zone be located immediately downstream of the slag screen after transition to a 1 ft diameter (round) duct. The quench section would consist of a row of plenum fed jets injected from the wall of the duct as shown in Exhibit 2.4-1 (end-on view). Based on the flow parameters provided, we calculate that 8 round holes of 1.0" diameter located at 45 degree intervals around the circumference will quench the flue gas within 2 duct diameters. Different duct configurations, including a transition from a round to rectangular duct of various aspect ratios, have been considered. The asymmetry of the rectangular duct would lead, we believe, to recirculation along the walls near the corners and enhance buildup on the wall surface.

Analysis

The correlation of Holdeman[1] and Sowa[2] for optimum mixing of wall injected jets into a cylindrical duct, shown below for reference, has been used as a design guideline. This is an empirical correlation developed for gas phase mixing based on many experimental and numerical investigations. The key to rapid mixing in a crossflow configuration is proper jet penetration, which is optimum at D/4, where D is the duct diameter. The correlation relates the primary variables and provides a guideline for optimum jet penetration.

$$n = \frac{\pi\sqrt{2J}}{C}$$

where, n is the number of orifices, J is jet-to-mainstream momentum-flux ratio, and C is a constant that has been found to be 2.5.
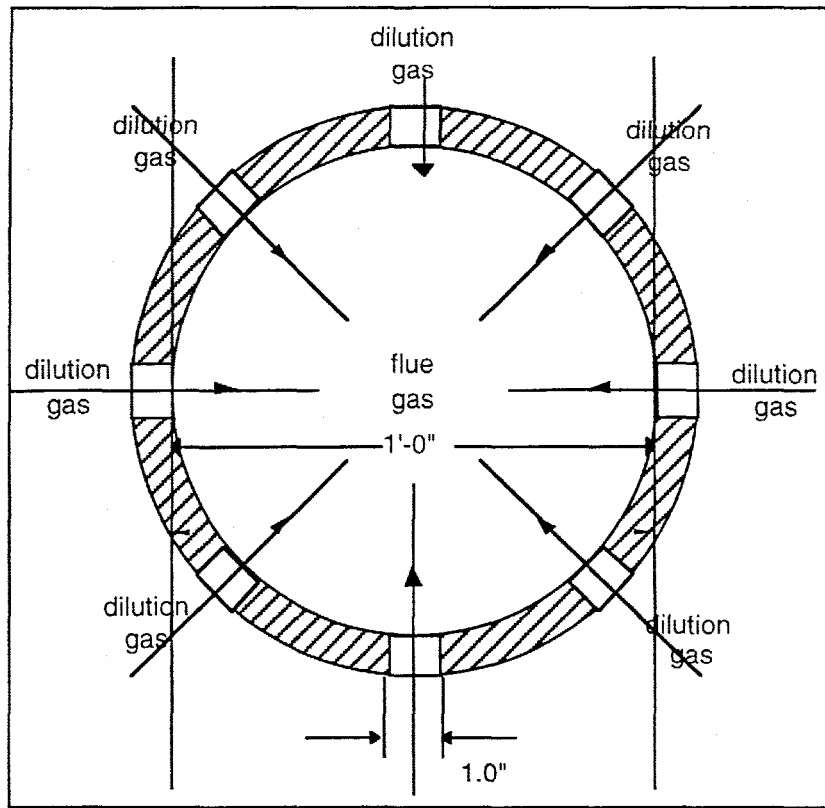
Proposed Quench Zone (end-on view)
Exhibit 2.4-1

To minimize fabrication cost and pressure drop, 8 injection locations have been selected. Although the equation would predict a value for J of 20, as an iteration to the final design, a slightly higher value of J is recommended based on the author's experimental results in a similar mixing configuration (see Appendix A). Furthermore, with the particle laden stream, over-penetration vs. under-penetration would be desired. Using the given flow parameters in Exhibit 2.4-2 and a J of 30 results in a quench jet velocity of 218 ft/s and a quench jet diameter of 1.0" (the discharge coefficient is assumed to be 0.7).

Exhibit 2.4-2
Assumed Flow Parameters for the Quench Zone Design

	mass flow (lbm/s)	temperature (deg F)	density (lbm/ft^3)	velocity (ft/s)
Flue Gas	0.8	2700	0.013	81
Dilution Gas	0.4	300	0.052	218

The quench zone flow field is being examined analytically to determine the particle temperatures and trajectories to determine if sufficient reduction of particle temperature can be achieved prior to the flow encountering any significant turns or obstructions. This effort is still

being pursued; preliminary results suggest that a staggering of dilution jets may provide better quenching of the core flow temperature.

It has not been resolved why the computed particle temperatures do not agree with measured degree of mixing (and hence, temperature) as determined experimentally. However, based on the excellent mixing of the gas flows as determined experimentally (shown in Appendix A), the empirical correlation of the equation will be used for the quench zone design. If it is found that the particle temperatures are not reduced sufficiently in the pilot test facility, distance will be added after the injection of the flue gas and before the HITAF exhaust makes a sharp turn to prevent slag buildup on the piping walls. Resolution of the discrepancy between the analytical predictions of particle temperatures and the flow field temperature profiles will be a goal during the next reporting period.

Exhibit 2.4-3 shows the results of the preliminary modeling effort using the FLUENT® CFD code, which is used extensively at UTRC for analyzing flows which include thermal gradients. In the table, the parameter ΔT is a temperature deviation parameter, defined as a temperature standard deviation; s is the mass-weighted standard deviation from the CFD results. Included in the table is an "unmixedness" parameter (U) from previous experimental research, which is defined as:

$$U = \frac{C_{var}}{C_{avg}(1 - C_{avg})}$$

where,

$$C_{var} = \frac{1}{m}\sum_{i=1}^{m}(\overline{C}_i - C_{avg})^2$$

= spatial concentration variance

$\overline{C}_i$ =   time average concentration at measurement location (an image pixel)

C_{avg} =   fully mixed concentration

By definition, U=0 corresponds to a perfectly mixed system, while U=1 corresponds to a perfectly segregated system.

Exhibit 2.4-3
Comparison of CFD Predictions and Measurements

| Z/D	U	ΔT	σ
1	0.041	161	13
2	0.027	88	10
4	0.026	38	6
6	0.029	25	5

The results tabulated indicate that the measured mixing based upon planar digital imaging of jets in a crossflow is better than that indicated by the temperature deviation ΔT. The low sigma values suggest that there are large regions of essentially uniform flow. In the table, Z is the distance downstream from the dilution jet centerline, and D is the dilution jet hole diameter. In this comparison, ΔT and s are based on a mass-weighted value; the unmixedness parameter (U) does not provide weighting for the boundary layer mass fluxes as is done with the CFD prediction. However, U is based upon c_{avg} which is determined from all the pixels available in the imaging plane and therefore will account for boundary layer flow.

References

1. Holdeman, J.D. (1993). Mixing of Multiple Jets With a Subsonic Crossflow. Prog. Energy Combust. Sci., Vol.19, pp. 31-70 (see also AIAA-91-2458 & NASA TM 104412).

2. Sowa, W.A., Kroll, J.T., Samuelsen, G.S., and Holdeman, J.D. (1994). Optimization of Orifice Geometry for Crossflow Mixing in a Cylindrical Duct. AIAA Paper 94-0219 (also NASA TM 106436).

Appendix Task 2.4

Concentration distributions for a configuration with 8 dilution jets injected perpendicular to a 3.875" diameter duct are shown in Exhibit 2.4-1 as a function of J and downstream position. C_{avg} is the fully mixed jet mixture fraction. Mixture uniformity is seen in general to increase with downstream position and vary as a function of J. The jets tend to under-penetrate with lower values of J and over-penetrate at higher values. Also note that the mixing rate is very rapid as indicated by the small number of contours at the downstream locations.
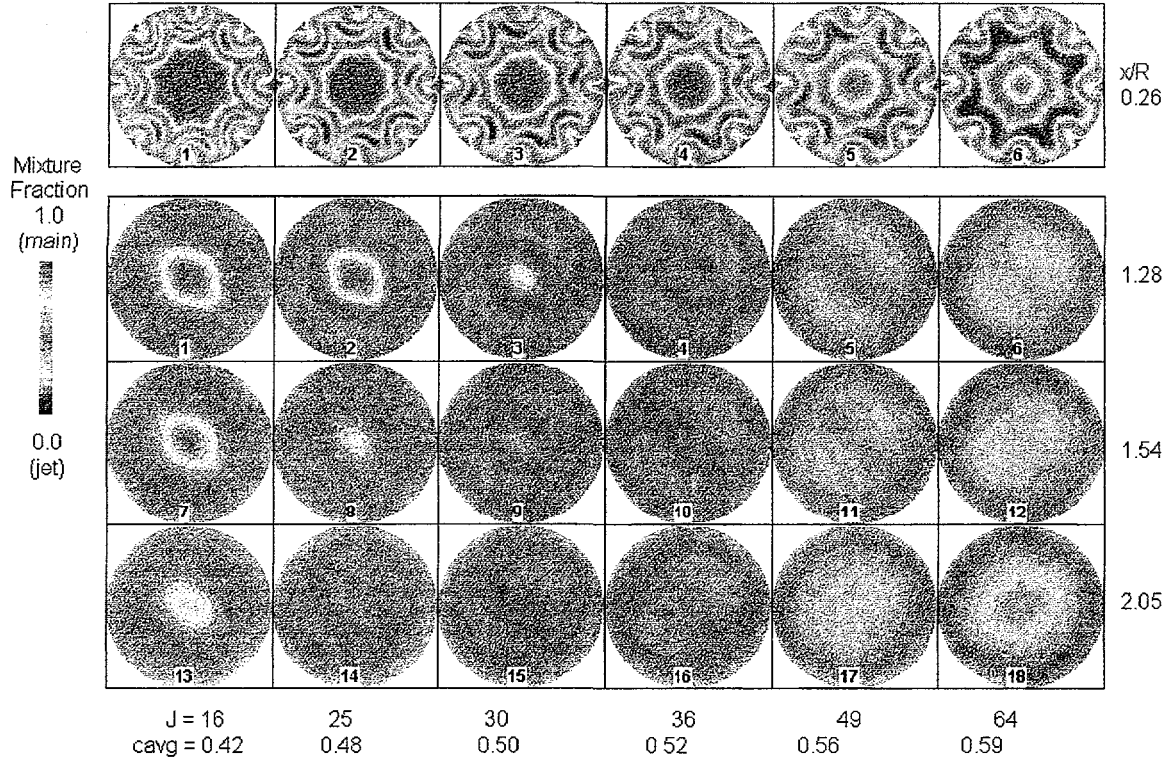
Concentration Distributions of 8 Round Jets Injected Perpendicular to a Cylindrical Mainstream

Exhibit A2.4-1

In Exhibit 2.4-2 the optimum value of J is indicated to be between 20 and 40 based on a plot of spatial unmixedness (a quantitative measurement similar to "percent mixed") at x/R of 1.2, i.e., ~1/2 duct diameter.
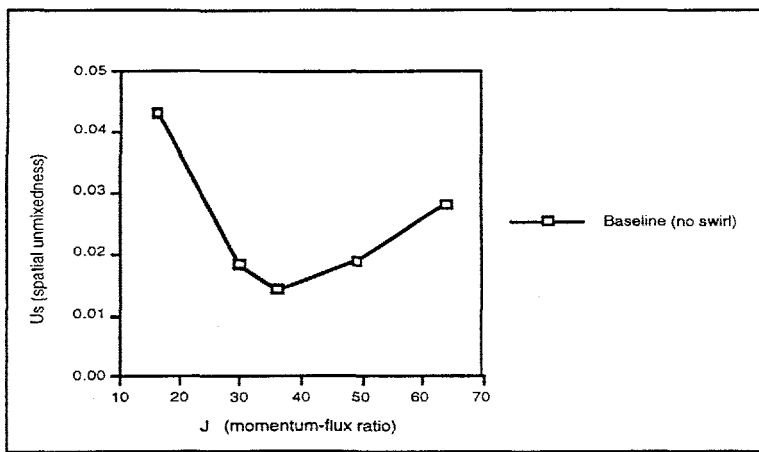
Comparison of Spatial Unmixedness at x/R = 1.2
Exhibit A2.4-2

Task 2.6 Operation and Controls

HIPPS is more complex than a conventional pulverized coal power plant or even a gas turbine-combined cycle due to the coupling of a "slow" (i.e., high thermal inertia) combustor with "fast" gas and steam turbines. The way in which we control HITAF must be determined in the very beginning of the design process because the control philosophy determines what equipment will be needed in the commercial plant and what the performance criteria will be for subsystems. Both affect the capital and operating costs for the commercial plant as well as the Phase III system. The combustor control philosophy is shaped by the need to accommodate following factors:
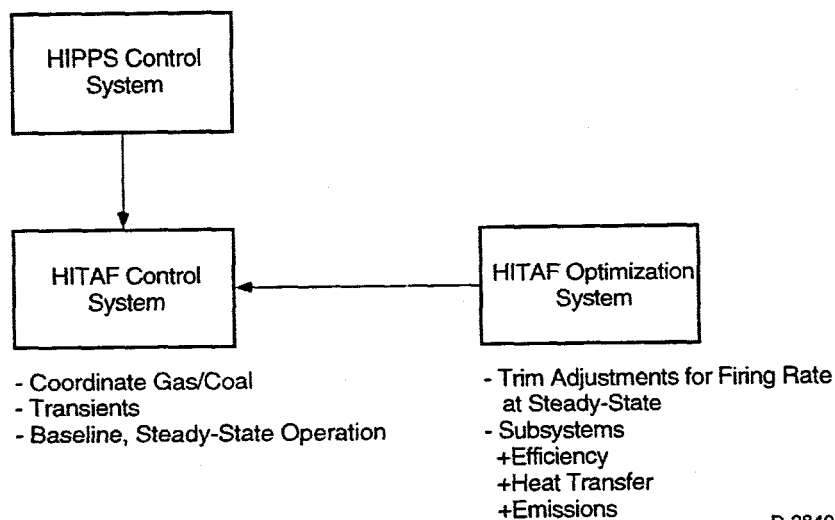
- Rapid load changes (startup, shutdown, equipment failure)
- Load following
- Heat flux distribution in radiant zone
- Integration of NO_x control subsystems

We plan to take advantage of improvements and advances in sensor and control technology in order to maximize the efficiency and availability of the HITAF. This is best implemented as shown in Exhibit 2.6-1. A "baseline" HITAF control system will be responsible for start-up, shut-down and transient operation. Once the steady state condition has been achieved, the HITAF optimization system comes into play. Exhibit 2.6-2 and 2.6-3 outline the HIPPS plant control system and the baseline HITAF control system.
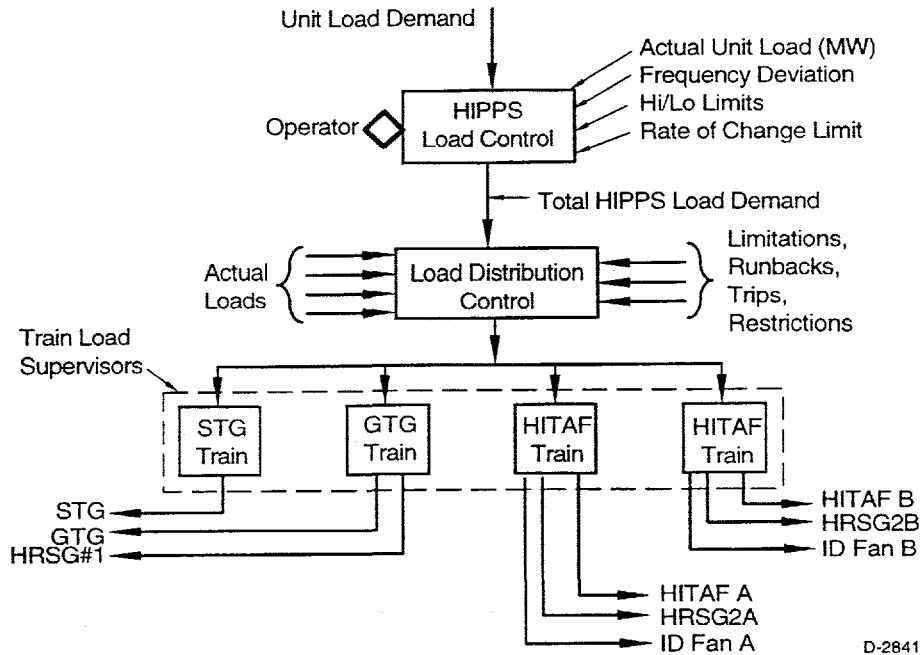
The HITAF optimization system (Exhibit 2.6-4) will provide adjustments in firing rates of individual burners in order to minimize burner NO_x production and maximize efficiency.

Temperature distributions in the radiant and convective air heaters will be needed to maximize heat transfer and to detect incipient tube failures.

Implementation of the HITAF control philosophy will require new control subsystems as well as new sensors. Exhibit 2.6-5 outlines the new subsystems and sensor requirements. New sensors are italicized. Next quarter a survey of the state-of-the-art for these measurements will be started.

HIPPS Control System

HITAF Control System

HITAF Optimization System

- Coordinate Gas/Coal
- Transients
- Baseline, Steady-State Operation

- Trim Adjustments for Firing Rate at Steady-State
- Subsystems
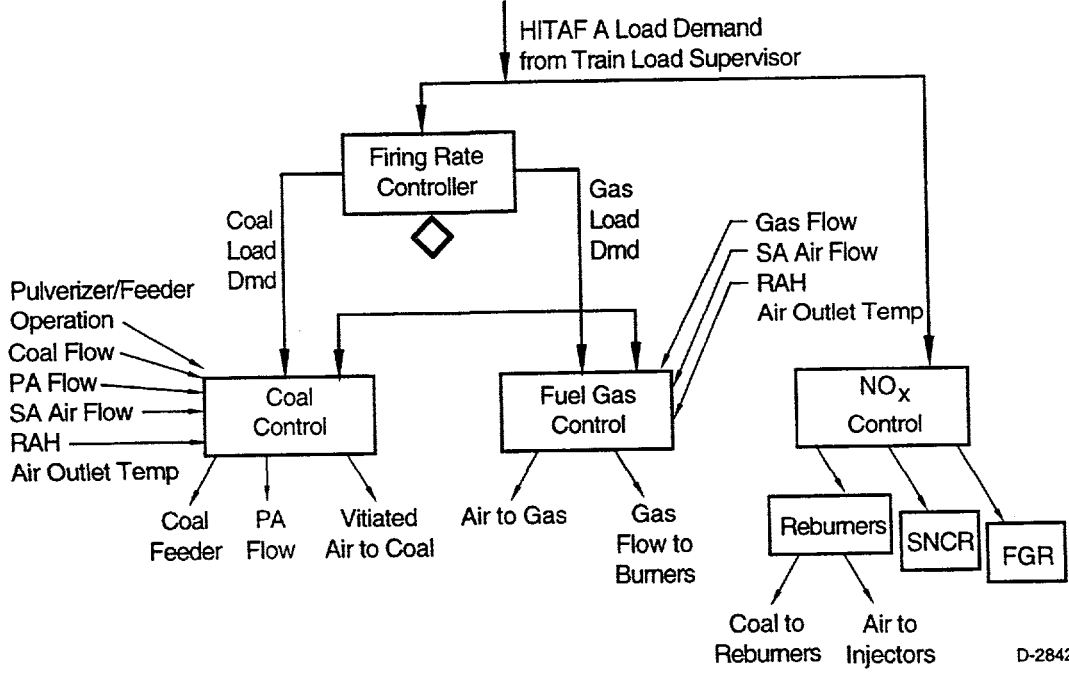 +Efficiency
  +Heat Transfer
  +Emissions

D-2840

HITAF Control Philosophy
Exhibit 2.6-1

HIPPS Control System Overview
Exhibit 2.6-2

HITAF Baseline Control System Overview
Exhibit 2.6-3

HITAF Optimization System Integrated with Baseline Control System
Exhibit 2.6-4

Exhibit 2.6-5
Sensor and Control Needs for HITAF Optimization

<u>Subsystems:</u>	Burner Control	
	Inputs:	Load demand
		Load
		Fuel and Air Flows
		Flame scanner signals
	Outputs:	Individual burner A/F adjustments
<u>New Subsystems</u>	NO_X/Temperature Profile optimization	
Inputs:	Inputs:	Stack gas NO_X
		FGR Flow
		Reburn/Burner coal ratio flow
		Coal/Gas load ratio
		NO_X/CO "in-furnace"
		RAH Temperature Distribution
		Furnace temperature
		SNCR inlet temperature
	Outputs:	NO_X control system adjustment
		Burner control system adjustment
	Burner Balancing	
	Inputs:	Relative Load
		Fuel and Air flows
		RAH temperature distribution
		Flame scanner signals
	Outputs:	A/F adjustment on one or more burners
		Aerodynamic (e.g., swirl) adjustment on one or more burners
	Efficiency Control	
	Inputs:	Stack gases: O_2, CO
		Stack temperatures
		Load
		Fuel and air flows (HITAF and duct burner)
		RAH & CAH air temperatures/flows
		Unburned carbon at furnace exit
		Furnace temperature
		SNCR inlet temperature
	Outputs:	Coal flow adjustment
		Gas flow adjustment
		Soot blower control signal
		Sootblower Control
	Inputs:	Efficiency control adjustment
		Pressure drop across slag screen and CAH
		Furnace temperature
		Furnace/slag screen deposits
		RAH/CAH temperature distributions
	Outputs:	Waterwall sootblowers
		CAH sootblowers